การออกแบบเชิงคำนวณ การสังเคราะห์และการประเมินผลทางชีววิทยาของสารยับยั้งโปรตีนไคเนส

COMPUTATIONAL DESIGN, SYNTHESIS, AND BIOLOGICAL EVALUATION OF INHIBITORS OF PROTEIN KINASES

อัชฎา คนซื่อ

ADCHATA KONSUE

วิทยานิพนธ์นี้เป็นส่วนหนึ่งของการศึกษาตามหลักสูตรปริญญาวิศวกรรมศาสตรดุษฎีบัณฑิต

สาขาวิชาวิศวกรรมชีวการแพทย์

คณะวิศวกรรมศาสตร์

สถาบันเทคโนโลยีพระจอมเกล้าเจ้าคุณทหารลาดกระบัง

พ.ศ.2567

KMITL-2024-EN-D-318-299

This material is reserved for educational use only, not allowed for commercial use.
Forbidden to modify the content, and cite the document when use.

COMPUTATIONAL DESIGN, SYNTHESIS, AND BIOLOGICAL EVALUATION OF INHIBITORS OF PROTEIN KINASES

ADCHATA KONSUE

A THESIS SUBMITTED IN PARTIAL FULFILLMENT

OF THE REQUIREMENT FOR THE DEGREE OF

DOCTOR OF ENGINEERING IN BIOMEDICAL ENGINEERING

SCHOOL OF ENGINEERING

KING MONGKUT'S INSTITUTE OF TECHNOLOGY LADKRABANG

2024

KMITL-2024-EN-D-318-299

This material is reserved for educational use only, not allowed for commercial use.

Forbidden to modify the content, and cite the document when use.

COPYRIGHT 2024

SCHOOL OF ENGINEERING

KING MONGKUT'S INSTITUTE OF TECHNOLOGY LADKRABANG

This material is reserved for educational use only, not allowed for commercial use.

Forbidden to modify the content, and cite the document when use.

หัวข้อวิทยานิพนธ์	การออกแบบเชิงคำนวณ การสังเคราะห์และการประเมินผลทางชีววิทยาของสารยับยั้งโปรตีนไคเนส
นักศึกษา	นายอัชฏา คนซื่อ
รหัสประจำตัว	62601003
ปริญญา	วิศวกรรมศาสตรดุษฎีบัณฑิต
สาขาวิชา	วิศวกรรมชีวการแพทย์
พ.ศ.	2567
อาจารย์ที่ปรึกษาวิทยานิพนธ์	รศ. ดร. แมทธิว พอล กลีสัน
อาจารย์ที่ปรึกษาวิทยานิพนธ์ร่วม	รศ. ดร. ดวงกมล กลีสัน

บทคัดย่อ

Epidermal Growth Factor Receptor (EGFR) ถูกค้นพบเนื่องจากการทำงานที่ปกติของโปรตีนชนิดนี้มีความสัมพันธ์กับการเกิดโรคมะเร็งปอดชนิดที่ไม่ใช่เซลล์เล็ก หรือ NSCLC เนื่องด้วยสาเหตุนี้ทำให้มีการพัฒนาสารยับยั้งเพื่อยับยั้งการทำงานที่ผิดปกติของ EGFR จากการพัฒนาสารยับยั้งตั้งแต่อดีตจนถึงปัจจุบันมีการตรวจพบการดื้อยาของผู้ป่วยเนื่องด้วยปัญหาการกลายพันธุ์ของ EGFR ไม่ว่าจะเป็น EGFR T790M หรือ EGFR T790M&L858R ในงานวิจัยนี้เราได้นำเสนอวิธีการสังเคราะห์ และการตรวจสอบเอกลักษณ์ของสารยับยั้งโปรตีน EGFR ซึ่งถูกออกแบบจากโครงสร้างอนุพันธ์ของ 2,4-diaminopyrimidine โดยรวมทั้งหมด 55 โครงสร้างและทุกสารยับยั้งได้มีการสังเคราะห์หมู่อิเล็กโตรฟิลิค ได้แก่ acrylamide, 2-chloroacetamide และ (2E)-3-phenylprop-2-enamide เพื่อสร้างพันธะกับกรดอะมิโน Cys797 ของโปรตีน EGFR นอกจากนี้ยังได้มีการสังเคราะห์หมู่ที่มีขั้วทางเคมีเพื่อเพิ่มประสิทธิภาพทางด้านการละลายของสารยับยั้ง ทำให้สารยับยั้งดังกล่าวมีคุณสมบัติทางกายภาพที่ดีกว่ายาในท้องตลาดไม่ว่าจะเป็น Rociletinib หรือ Osimertinib ด้านการตรวจสอบคุณสมบัติการยับยั้งตัวโรคในงานวิจัยนี้ได้มีการทดสอบกับโปตีน EGFR ชนิด WT และ T790M&L858R รวมถึงมีการทดสอบประสิทธิภาพการยับยั้งในเซลล์ A431 และ A549 ทั้งนี้ได้ทดสอบความเป็นพิษกับเซลล์ HepG2 และมีการทดสอบคุณสมบัติทางกายภาพของสารยับยั้ง อาทิเช่น LogD และสมบัติการละลาย จากผลการทดสอบที่กล่าวมาข้างต้นงานวิจัยนี้ได้ค้นพบสารยั้งที่ดีที่สุด โดยมีค่าการยับยั้ง กับโปรตีน EGFR T790M&L858R น้อยกว่า 20 nM ได้แก่ สารยับยั้ง **20**, **21**, **23**, **79** และ **80** โดยสารยับยั้งเหล่านี้มีความจำเพาะกับโปรตีน EGFR T790M&L858R เมื่อเทียบกับ EGFR WT และ JAK3 ซึ่งมากกว่า Rociletinib และ Osimertinib ท้ายที่สุดทางเราได้ทำการทดลองเพื่อหาค่าทางไคเนติคเพื่อยืนยันการสร้างพันธะโควาเลนต์ระหว่าง **21** และ **80** กับโปรตีน EGFR ในตำแหน่ง Cys797.

This material is reserved for educational use only, not allowed for commercial use.
Forbidden to modify the content, and cite the document when use.

Thesis	COMPUTATIONAL DESIGN, SYNTHESIS, AND BIOLOGICAL EVALUATION OF INHIBITORS OF PROTEIN KINASES
Student	Mr. Adchata Konsue
Student ID.	62601003
Degree	Doctor of Engineering
Program	Biomedical Engineering
Year	2024
Thesis Advisor	Assoc. Prof. Dr. Matthew Paul Gleeson
Thesis co-advisor	Assoc. Prof. Dr. Duangkamol Gleeson

Abstract

Epidermal growth factor receptor (EGFR) kinase has been implicated in the uncontrolled cell growth associated with non-small cell lung cancer (NSCLC). This has prompted the development of 3 generations of EGFR inhibitors over the last 2 decades due to the rapid development of drug resistance issues caused by clinical mutations, including T790M, L858R, and the double mutant T790M & L858R. In this work, we report the design, preparation, and biological assessment of new irreversible 2,4-diaminopyrimidine-based inhibitors of EGFR kinase. Fifty-five new compounds have been prepared and evaluated which include a range of electrophilic moieties, including acrylamide, 2-chloroacetamide, and (2*E*)-3-phenylprop-2-enamide, to allow reaction with residue Cys797. In addition, more polar groups have been incorporated to provide a better balance of physical properties than clinical candidates Rociletinib and Osimertinib. Inhibitory activities against EGFR wildtype (WT) and EGFR T790M & L858R have been evaluated along with cytotoxicity against EGFR-overexpressing (A549, A431) and normal cell lines (HepG2). Selectivity against JAK3 kinase as well as physicochemical properties determination ($logD_{7.4}$ and phosphate buffer solubility) have been used to profile the compounds. We have identified **20**, **21** **23**, **79,** and **80** as potent mutant EGFR inhibitors (≤20 nM), with comparable or better selectivity over WT EGFR and lower activity at JAK3, than observed for Osimertinib or Rociletinib. Finally, kinetic studies on **21** and **80** were performed, confirming a covalent mechanism of action at EGFR.

This material is reserved for educational use only, not allowed for commercial use.
Forbidden to modify the content, and cite the document when use.

ACKNOWLEDGMENTS

I would like to acknowledge and thank all who helped, supported, and funded my thesis at King Mongkut's Institute of Technology Ladkrabang, National Research Council of Thailand; NRCT, and the University of Leicester.

Firstly, I express my deepest gratitude to my thesis advisor and mentor Assoc. Assoc. Prof. Dr. Mathew Paul Gleeson of the Department of Biomedical Engineering at King Mongkut's Institute of Technology Ladkrabang. He generously encouraged, guided, and pushed me to make the most of my research experience. Moreover, he went beyond the role of thesis advisor by mentoring me through all the years in graduate school. I would like to express my gratitude to Prof. Dr. Donald Jones and Dr. Robert G. Britton, my co-advisor from the Cancer Studies Department at the University of Leicester, UK, for their invaluable help and suggestions throughout the development of this thesis. I would also like to thank Assoc. Prof. Dr. Duangkamol Gleeson, my co-advisor from the School of Science, King Mongkut's Institute of Technology Ladkrabang for having my back during my thesis research

Secondly, I would like to extend my acknowledgment to my fellow students in the CMCL group for their friendship, support, and sincere interest in my study during all these years. I wish to express my thanks for introducing me to the world of pharmaceutical chemistry.

Additionally, this study has received financial support from NRCT, Thailand. AK would like to acknowledge financial support from the NRCT, NRCT5-RGJ63021-171.

Finally, an honorable mention goes to my family for their love and always encourage me to get through challenging times. I really appreciated their genuine support to complete this project.

Adchata Konsue

This material is reserved for educational use only, not allowed for commercial use.

Forbidden to modify the content, and cite the document when use.

Table of Contents

page

This material is reserved for educational use only, not allowed for commercial use.

Forbidden to modify the content, and cite the document when use.

This material is reserved for educational use only, not allowed for commercial use.
Forbidden to modify the content, and cite the document when use.

This material is reserved for educational use only, not allowed for commercial use.

Forbidden to modify the content, and cite the document when use.

This material is reserved for educational use only, not allowed for commercial use.

Forbidden to modify the content, and cite the document when use.

List of Tables

page

This material is reserved for educational use only, not allowed for commercial use.
Forbidden to modify the content, and cite the document when use.

List of schemes

page

This material is reserved for educational use only, not allowed for commercial use.

Forbidden to modify the content, and cite the document when use.

List of Figures

page

This material is reserved for educational use only, not allowed for commercial use.
Forbidden to modify the content, and cite the document when use.

This material is reserved for educational use only, not allowed for commercial use.
Forbidden to modify the content, and cite the document when use.

This material is reserved for educational use only, not allowed for commercial use.
Forbidden to modify the content, and cite the document when use.

This material is reserved for educational use only, not allowed for commercial use.
Forbidden to modify the content, and cite the document when use.

List of Abbreviations

mL	=	milliliter
mg	=	milligram
µM	=	micro molar
nM	=	nano molar
nm	=	nanometer
ns	=	nanosecond
ppm	=	part per million
RMSD	=	Root Mean Square Deviation
SD	=	Standard deviation
NMR	=	Nuclear Magnetic Resonance
HPLC	=	High Performance Liquid Chromatography
TLC	=	Thin layer chromatography
MS	=	Mass Spectroscopy
PBS	=	Phosphate Buffer Solution
PDB	=	Protein Data Bank
H_2	=	Hydrogen
N_2	=	Nitrogen
Pd/C	=	Palladium on activated carbon
SAR	=	Structure Activity Relationships
TEA	=	Triethylamine
TFA	=	Trifluoroacetic acid
THF	=	Tetrahydrofuran
MeOH	=	Methanol
DIPEA	=	N, N-Diisopropylethylamine
EtOAc	=	Ethylacetate
pTSA	=	para-toluene sulfonic acid
DMSO	=	Dimethyl sulfoxide
MD	=	Molecular Dynamic

This material is reserved for educational use only, not allowed for commercial use.
Forbidden to modify the content, and cite the document when use.

DCM	=	Dichloromethane
QM	=	Quantum Mechanic
PDE5	=	Phosphodiesterase type 5
cGMP	=	cyclic Guanosine monophosphate
NO	=	Nitric oxide
PAH	=	Pulmonary Arterial Hypertension
CONF	=	Conformation
HB	=	Hydrogen Bond
%I	=	%Inhibition
IC_{50}	=	half-maximal inhibitory concentration
EGFR	=	Epidermal Growth Factor Receptor
WT	=	Wild-type
DM	=	Double mutant (T790M/L8585R)
JAK3	=	Janus Kinase 3
Cys	=	Cysteine residue

This material is reserved for educational use only, not allowed for commercial use.
Forbidden to modify the content, and cite the document when use.

Chapter 1

Introduction

1.1 Statement and significance of the problems

The foundation of engineering is built on Mathematics, Physics, and Chemistry. Biomedical Engineering is a highly diverse field, traditionally focused on Instrumentation (electronics) and Mechanical aspects (physics). However, its scope has expanded to encompass any technology related to human-use products or even medical chemistry. Drug design involves all stages of drug development connected to chemistry, from the initial design to the final delivery. This process covers a wide range of activities, starting with the rational design of drugs through molecular modelling, based on computational, physical, and organic chemistry principles. Following this, a large number of chemical compounds are synthesized and characterized through various processes to identify potential molecules, known as "hits" [1]. These hit molecules are extensively tested against specific targets and studied for their pharmacokinetic properties within an organism. Parameters such as Absorption, Distribution, Metabolism, and Excretion (ADME) are analysed so that chemists can modify the compounds to enhance these characteristics. Once optimized, a hit molecule is selected as a lead molecule and advanced to human clinical trials, where it undergoes further evaluation to determine its viability as a potential drug.

Receptor tyrosine kinase (RTK) and nonreceptor tyrosine kinase (NRTK) are proteins that act as a receptor to growth factor ligands on a cell's surface. Growth factor ligands bind to (1) the extracellular domain of receptor tyrosine kinases, and the receptor is often activated by ligand-induced dimerization or oligomerization. (2) The transmembrane domain consists of the entirety of the hydrophobic region of amino acids in the cell membrane. (3) intracellular tyrosine kinase domains when tyrosine kinases recruit and activate with phosphorylation. It induces a conformational change to an increase of kinase activity and stimulates signal transduction for disease cell proliferation [2-4].

This material is reserved for educational use only, not allowed for commercial use.
Forbidden to modify the content, and cite the document when use.

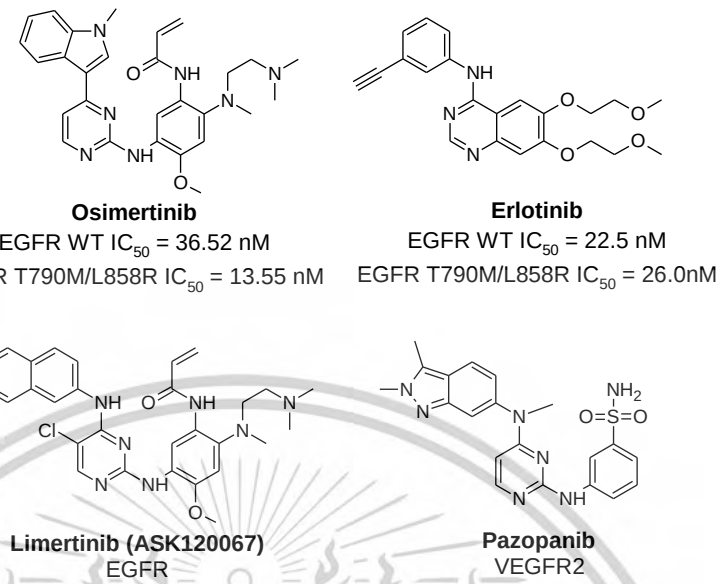

Figure 1. Structures of related drugs and EGFR development compounds:

Osimertinib [5-7], Erlotinib [8], Limertinib [9, 10] and Pazopanib [11].

The epidermal growth factor receptor (EGFR) belongs to the ErbB family of receptor tyrosine kinases. It is a key mediator in cellular signaling related to cell growth, proliferation, survival, and migration. Its aberrant activity plays a pivotal role in the development and growth of tumor cells and is associated with the onset and progression of non-small cell lung cancer (NSCLC) [12, 13]. Recently, selective small-molecule EGFR tyrosine kinase inhibitors (EGFR TKI) are becoming the evidence-based first-line therapy for advanced NSCLC that harbors sensitizing EGFR mutations. Although patients with sensitizing EGFR mutations could achieve good responses to therapy with the first-generation EGFR TKIs, such as Erlotinib (Figure 1), most patients acquired drug resistance to EGFR TKI within a 1-year treatment. From this, a variety of irreversible inhibitors were developed. These inhibitors contain a Michael acceptor moiety designed to form a covalent bond with the conserved cysteine residue (Cys797) at the lip of the EGFR ATP binding site [14]. Osimertinib (Figure 1) is a novel mono-anilino-pyrimidine which is a third-generation of EGFR TKIs. Osimertinib covalently binds the Cys797 of EGFR with its meta-acrylamide group [15-18]. In 2015, the U.S. approved Osimertinib to treat patients whose disease has gotten worse after treatment of EGFR- first-line therapy [19].

This material is reserved for educational use only, not allowed for commercial use.
Forbidden to modify the content, and cite the document when use.

The development of new anti-cancer inhibitors is ongoing due to (i) the ongoing threat of drug resistance due to kinase enzyme mutations and (ii) the desire to develop new inhibitors of related kinase targets that are implicated in other types of cancers. For example, the amino-pyrimidine Limertinib (Figure 1) has been investigated as a new irreversible inhibitor targeting EGFR, while a structurally related Pazopanib which is a VEGFR drug.

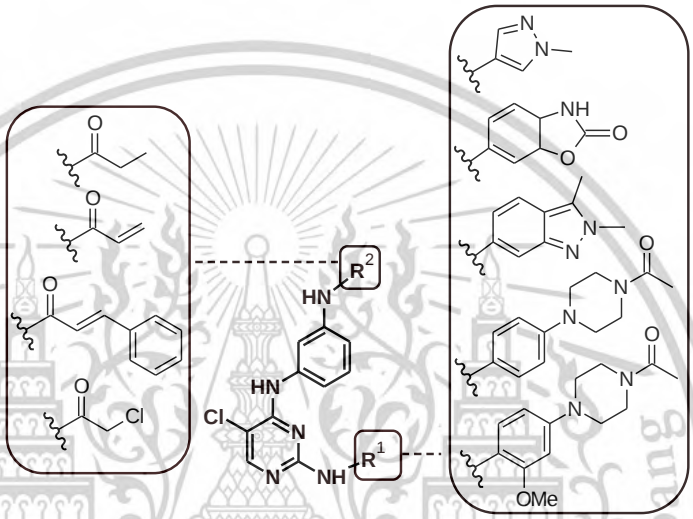

Figure 2. Scope of the scaffold modifications for the first study.

In the first study, we applied a structure-based design to develop new EGFR inhibitors based on the 2,4-diaminopyrimidine scaffold as shown in Figure 2. We have focused on exploring the effect of incorporating different electrophilic groups on WT and mutant EGFR activities, and incorporation of polar moieties to improve physical properties, including lipophilicity and solubility. In total, 20 compounds have been prepared that incorporate new electrophilic groups, smaller, more polar aromatic amines at the 2-position of pyrimidine, as well as the removal of the more lipophilic CF_3 group with the Cl which lies adjacent to the gatekeeper residue. We maintain the 3-substituted aniline linker favored by EGFR inhibitors and modify the electrophilic groups attached, which can affect the suicidal complex formation. The SAR of compounds has then been assessed for EGFR wildtype enzyme, the T790M & L858R mutant, and a selection of EGFR over-expressing cell lines (A549 & A431). A kinetic evaluation of the top compound has been performed to confirm the mechanism of action. In addition, quantum mechanical (QM)

This material is reserved for educational use only, not allowed for commercial use.
Forbidden to modify the content, and cite the document when use.

methods have been used to understand the relative reactivity of the different electrophilic groups which can be related back to their EGFR activity.

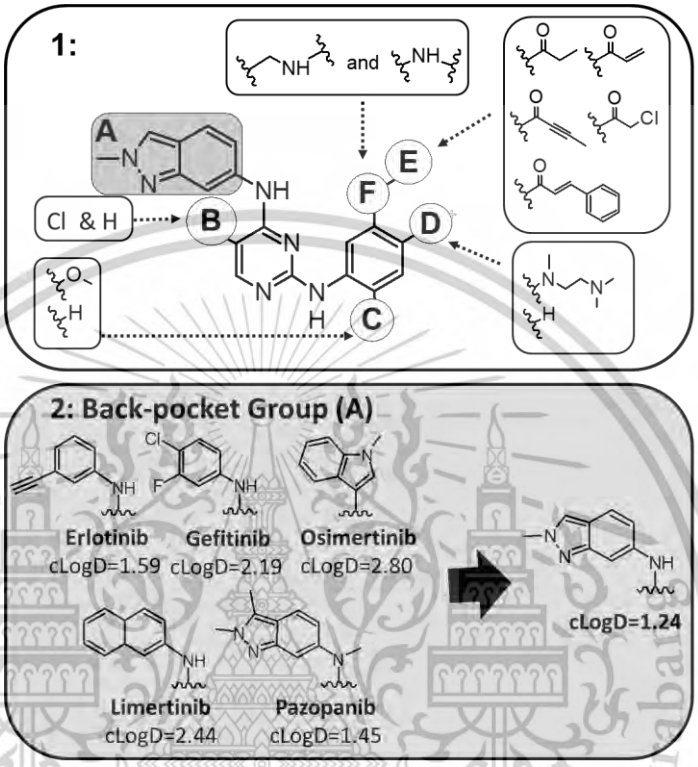

Figure 3. 1: Scope of the scaffold modifications for the second study, 2: Optimization at the back-pocket of EGFR.

In the second study, we applied structure-based design methods to develop new inhibitors of EGFR with good activity at EGFR WT and double mutant T790M & L858R guided by the available SAR data. The scope of the study is shown in Figure 3, 1&2. Starting from Osimertinib, Limertinib, and Pazopanib (Figure 1) incorporated 2-methyl-2*H*-indazol-6-amine at the A-position, as well as added the more lipophilic Cl which lies adjacent to the gatekeeper residue, leading to a general improvement in physicochemical properties. The basic center at the D-position pointed to the solvent region leading to a general improvement in physicochemical properties. We have modified the electrophilic groups at the E-position including acrylamide, but-2-ynamide, 2-chloroacetamide, (2E)-3-phenylprop-2-enamide as well as the non-electrophilic propenamide group for comparison. From this, the length of the bond to form a covalent bond was also

This material is reserved for educational use only, not allowed for commercial use.
Forbidden to modify the content, and cite the document when use.

investigated at the F-position including the benzyl-linker and phenyl groups. The introduction of the benzyl-linker resulted in increased solubility over 3-folded and decreased LogD when compared to the phenyl group. In total, 34 compounds have been prepared and the compound SAR at EGFR wildtype, T790M & L858R mutant, and a selection of EGFR over-expressing cell lines have been undertaken. We have also used molecular dynamics (MD) to predict the binding pose of the 2-methyl-2H-indazol-6-amine with EGFR T790M and EGFR WT similar to the previously reported that MD is used to predict the binding post of Osimertinib [20, 21].

1.2 Scope of the study

This research emphasizes the development of methods for the treatment of EGFR in drug form. The research involves a multi-disciplinary study effort covering. (a) computational inhibitors target analysis, (b) 2,4-diaminopyrimidine based compounds, synthesis, and characterization, and (c) biological assay being performed by established our collaborators in Thailand and the United Kingdom.

This material is reserved for educational use only, not allowed for commercial use.
Forbidden to modify the content, and cite the document when use.

Chapter 2

Theory and Literature Reviews

2.1 Non-small cell lung cancer (NSCLC)

Cancer is characterized by the aberrant alteration of one of several cellular processes including proliferation, survival, and motility. These functions are governed by a complex series of intracellular signaling pathways in which protein kinases play a crucial role [22, 23]. In 2020, the World Health Organization (WHO) reported an estimated 18.1 million new cancer cases and 9.6 million deaths. The most frequently diagnosed type was lung cancer at 11.6%, which accounted for 18.4% of total deaths. The development of improved lung cancer treatments is therefore a continuing goal of the medical community [24].

Non-small Cell Lung Cancer (NSCLC) comprises 85% of all lung cancer types and is classified by the WHO into three main histological types: adenocarcinoma, squamous cell carcinoma, and large cell [25]. Adenocarcinoma is the most prevalent subtype, accounting for around 40% of lung cancers [26]. In lung cancer, epidermal growth factor receptor (EGFR) and its mutations have already been approved for standard therapy. The EGFR (also known as ErbB1 or Her1) is a member of the ErbB family of membrane receptor tyrosine kinases including ErbB2, ErbB3, and ErbB4. The EGFR is a common target that has been used in NSCLC treatment. It is exhibited at high levels on the surface of NSCLC and is activated by a variety of ligands mainly transforming growth factor alpha and epidermal growth factor. High expression of the EGFR has been correlated with poor prognosis and resistance to therapy in NSCLC [27]. Abnormal signaling through the EGFR because of increased expression of receptors on the cell surface increases the production of ligands, or by activating mutations results in activation of intracellular signaling pathways, such as the phosphatidylinositol 3-kinase and the mitogen-activated protein kinase pathways that lead to increased cell survival, proliferation, angiogenesis and propensity for metastasis [28].

In May 2004, researchers reported that the somatic mutations in the kinase domain of EGFR have positively related to the potent response of EGFR Tyrosine Kinase Inhibitors

This material is reserved for educational use only, not allowed for commercial use.
Forbidden to modify the content, and cite the document when use.

(TKIs) against advanced NSCLC [29, 30]. The 2 most encountered EGFR mutations in NSCLC are the L858R mutation in exon 21 as well as the exon 19 deletions. Both of these mutations are drug-sensitizing mutations and represent over 85% of EGFR mutations in lung cancer [31]. L858R and del 19 of EGFR mutations can activate the EGFR signaling pathway in the mutant EGFR-positive cancer-causing cells. The sensitivity of some of the mutations results in a higher level if compared with the cases having wild-type EGFR. Conversely, resistance mutations can also be found either at the start of the mutations or after sustained exposure to TKIs. For examples of EGFR mutations resulting in resistance are PTEN, KRAS, and BRAF mutations [32]. These are commonly involved in developing resistance to EGFR TKIs in cases of NSCLC. In clinical practice, there are two classes of EGFR inhibitors: small molecule tyrosine kinase inhibitors (TKIs) (e.g. gefitinib and erlotinib) and monoclonal antibodies (e.g. cetuximab and panitumumab).

Recently, selective small-molecule EGFR tyrosine kinase inhibitors (EGFR TKI) are becoming the evidence-based first-line therapy for advanced NSCLC that harbors sensitizing EGFR mutations. TKIs are orally administered and inhibit downstream signaling by competing with ATP to bind the intracellular domain of the EGFR, preventing autophosphorylation and activation of the receptor [27]. Although patients with sensitizing EGFR mutations (L858r mutation in exon 21 as well as the exon 19 deletions) showed a significant decrease in the size of tumors with the first-generation EGFR TKIs, such as Erlotinib and Gefitinib (Figure 4), unfortunately, most patients acquired drug resistance to EGFR TKI within a 1-year treatment mostly driven by T790M which is the second mutation of EGFR. From this, a variety of irreversible inhibitors were developed. These inhibitors contain a Michael acceptor moiety designed to form a covalent bond with the conserved cysteine residue (Cys797) at the lip of the EGFR ATP binding site [14]. Osimertinib or AZD9291 (Figure 4) is a novel mono-anilino-pyrimidine which is a third generation of EGFR TKIs. Osimertinib covalently binds the Cys797 of EGFR with its meta-acrylamide group [15-18]. In 2015, the U.S. approved Osimertinib to treat patients whose disease has gotten worse after treatment of EGFR- first-line therapy [19].

This material is reserved for educational use only, not allowed for commercial use.
Forbidden to modify the content, and cite the document when use.

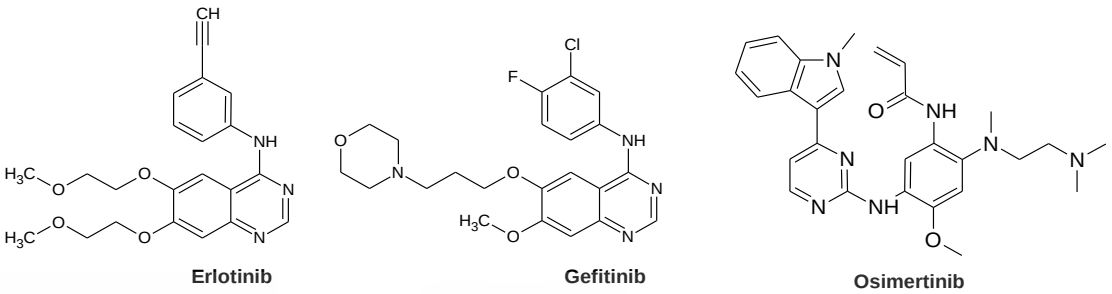

Figure 4. Small molecule TKIs: erlotinib, gefitinib, and Osimertinib.

2.1.1 Kinases in cancer

Kinases can be separated into receptor tyrosine kinase (RTK) and nonreceptor tyrosine kinase (NRTK). Kinases are enzymes involved in transferring a phosphate group to a protein while phosphatases remove a phosphate group from a protein. They act as a receptor to growth factor ligands on a cell's surface growth factor ligands bind to (1) the extracellular domain of receptor tyrosine kinases, and the receptor is often activated by ligand-induced dimerization or oligomerization. (2) The transmembrane domain consists of the entirety of the hydrophobic region of amino acids in the cell membrane. (3) intracellular tyrosine kinase domains when tyrosine kinases recruit and activate with phosphorylation. The enzymatic processes induce a conformational change to an increase of kinase activity and stimulate signal transduction for disease cell proliferation [2-4] and are often in response to an external stimulus to modulate numerous activities of proteins in a cell [33] Because most protein kinases support cell proliferation, survival, and migration, when constitutively overexpressed, or active, they are also associated with oncogenesis [34].

Protein Kinases are an important class of biological targets accounting for >50% of current pharmaceutical industry drug projects by recent estimates [35]. They represent one of the largest and most diverse enzyme classes in nature, with more than 500 members in the human kinome [36]. Deregulation of kinase activity leads to aberrant cellular signaling resulting in diverse pathological conditions. The size of the kinome, coupled with the central roles that kinases have in cell signaling, physiology, and disease have made them important targets in a range of therapeutic areas [37-39]. Approximately 538 kinases are encoded in the human genome, every process of signal transduction is

This material is reserved for educational use only, not allowed for commercial use.
Forbidden to modify the content, and cite the document when use.

wired through a phosphotransfer cascade, suggesting that inhibition of kinase activity can elicit a real physiological response. Therefore, the complete set of protein kinases encoded in its genome (kinome) has been received as an attractive target for the treatment of numerous types of cancer. Single and multiple kinase inhibitors, both synthetic and natural molecules, are now targeted therapeutic strategies for the treatment of human malignancies [40]. Key oncogenic kinase drug targets such as the PIK3CA, BRAF, and EGFR, which activate significant tumor cell signaling pathways and are related to the mutations and/or deletions in phosphatase and tensin homolog (PTEN), a phosphatase that negatively supervises PI3K [41, 42]. Inhibition of the distinct kinase signaling pathways can be less cytotoxic to non-cancerous cells. This presents the selective killing of tumor cells with considerably lower toxic manifestations [43]. In clinical treatments, Imatinib and Dasatinib, which are specific-kinase inhibitors, have produced more favorable outcomes compared to conventional cytotoxic therapy [44]. Besides, these kinase inhibitors include target kinome members such as EGFR, ERBB2, VEGFRs, Kit, PDGFRs, ABL, SRC, and mTOR, all providing improved clinical results and patient health status [45]. The general targeting of these inhibitors is the ATP-binding site, while a few of the non-ATP competitive kinase inhibitors target novel allosteric sites [46, 47]. Currently, 35 drugs have been approved by the U.S. Food and Drug Administration (FDA) including orally effective direct protein kinase inhibitors that target a limited number of enzymes (

Table **1**). Although these provided good results in cancer treatment, the problems with drug resistance, toxicity, and compromised efficacy present critical challenges in both clinical and experimental oncology [48].

2.1.2 Protein kinase ATP-binding site

Protein kinases are identified by their ability to catalyze phosphor transfer reactions from ATP to substrates such as serine, threonine, or tyrosine residue. Generally, in bi-lobal structures, kinases contain β-stranded amino-lobe (N-lobe), which mediates ATP binding, and an α-helical carboxy-lobe (C-lobe), which is important for substrate binding. This two-domain linked together by the hinge region, which is a short and flexible stretch (Figure 5). An ATP molecule is bound to a deep cleft between the lobes [49, 50]. In this ATP binding site, the adenine ring forms hydrogen bonds with the kinase 'hinge' the segment

This material is reserved for educational use only, not allowed for commercial use.
Forbidden to modify the content, and cite the document when use.

that connects the amino and carboxy-terminal kinase domains. The ribose and triphosphate groups of ATP bind in a hydrophilic channel extending to the substrate binding site that features conserved residues that are essential to catalysis.

Table 1. Kinase inhibitors identified by FDA and their drug targets [40].

Drug target	Protein substrate	Drug
ALK	Tyrosine	Crizotinib, Ceritinib, Alectinib, Brigatinib
BCR–Abl	Tyrosine	Bosutinib, Dasatinib, Imatinib, Nilotinib, Ponatinib
B-Raf	Serine/threonine	Vemurafenib, Dabrafenib
BTK	Tyrosine	Ibrutinib
CDK family	Serine/threonine	Palbociclib, Sorafenib, Ribociclib
c-Met	Tyrosine	Crizotinib, Cabozantinib
EGFR family	Tyrosine	Gefitinib, Erlotinib, Lapatinib, Vandetanib, Afatinib, Osimertinib
JAK family	Tyrosine	Ruxolitinib, Tofacitinib
MEK1/2	Dual specificity	Trametinib
PDGFR α/β	Tyrosine	Axitinib, Gefitinib, Imatinib, Lenvatinib, Nintedanib, Pazopanib, Regorafenib, Sorafenib, Sunitinib
RET	Tyrosine	Vandetanib
Src family	Tyrosine	Bosutinib, Dasatinib, Ponatinib, Vandetanib
VEGFR family	Tyrosine	Axitinib, Lenvatinib, Nintedanib, Regorafenib, Pazopanib, Sorafenib, Sunitinib

Commonly, the activation loop, which has a conserved in all kinases is important in regulating kinase activity and is marked by conserved DFG and APE motifs at the start and end of the loop, respectively. The A-loop exists in two conformations: first, catalytically competent and usually phosphorylated (active), and second blocking the active site (inactive) [52]. At present, the development of kinase inhibitors is ATP competitive and shows one to three hydrogen bonds to the amino acids located in the hinge region of the target kinase. These hydrogen bonds are normally formed by the adenine ring of ATP (Figure 6).

This material is reserved for educational use only, not allowed for commercial use.
Forbidden to modify the content, and cite the document when use.

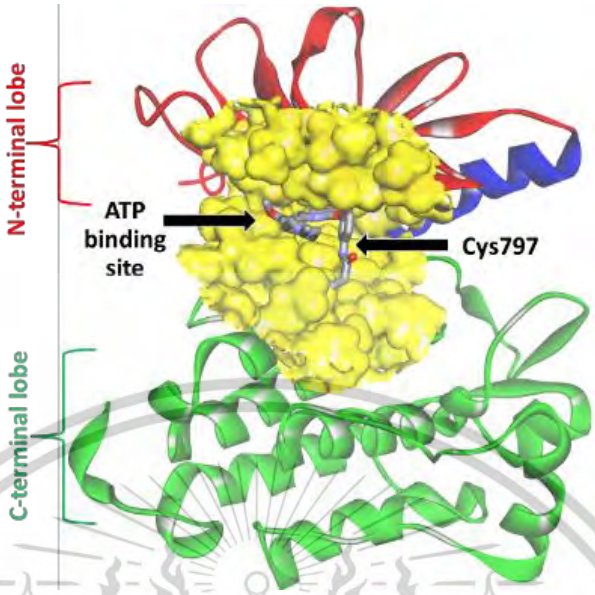

Figure 5. Catalytic domain of protein kinases showed the N-terminal lobe (red) and the C-terminal lobe (green) and binding site (yellow) [51].

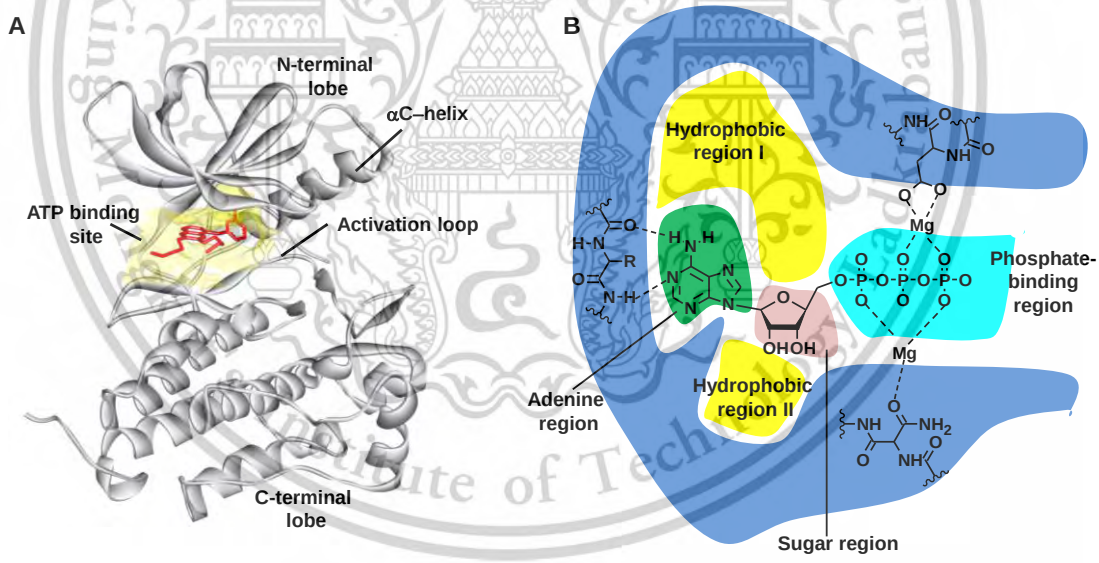

Figure 6. Structure and subregions of a typical protein kinase domain. (A) Structure of a typical protein kinase domain. The protein backbone is shown in cartoon form in gray, and the peptide substrate is shown in red. The ATP binding site is shown in yellow. From PDB structure 1M17. (B) Schematic representation of ATP binding site divided into subregions [52-54].

This material is reserved for educational use only, not allowed for commercial use.
Forbidden to modify the content, and cite the document when use.

2.1.3 Types of kinase inhibitors

In the treatment of cancer, kinase inhibitors show excellent results, especially targeting specific mutations that chiefly drive tumorigenesis. In the past, they categorized types of kinase inhibitors according to their mechanism of action. Initially, small molecule protein kinase inhibitors can be classified into three classes: Type I, Type II, and Type III [55]. Type 1 inhibitors show ATP-competitors that mimic the purine ring of the adenine moiety of ATP. These types interact with the conformational phosphorylated active catalytic site of the kinases and alter the structural conformation otherwise favorable to phosphotransfer [52, 56]. Type I inhibitors generally consist of a heterocyclic ring system that occupies the purine binding site where it serves as a scaffold for side chains that occupy adjacent hydrophobic regions [57]. To date, there are many Types I kinase inhibitors used in the treatment of cancer such as Bosutinib, Crizotinib, Dasatinib, Erlotinib, Gefitinib, Lapatinib, Pazopanib, Ruxolitinib, Sunitinib, and Vemurafenib. However, in the large-scale clinical success, Type I kinase inhibitors also come with adverse side-effects [58].

Type II kinase inhibitors. In contrast, Type II kinase inhibitors accept the inactive conformation of kinases and act with the catalytic site of the unphosphorylated inactive conformation of kinases [59]. Type II kinase inhibitors exploit new interactions inside the lipophilic pocket derived from the change of confirmation of the phenylalanine residue of the “Asp-Phe-Gly (DFG)” N-terminal loop conformation of kinases [40]. Apart from kinase inhibitors of this form hydrogen bonds with the protein in the hinge region, Type II kinase inhibitors also cause extra interactions in the open DFG-out conformation. Type II kinase inhibitors also show high conservation of interactions between the inhibitor and the glutamic and aspartic acids of the kinase (e.g. H-bond pattern) [60]. However, there is considerable overlap of selectivity between type I and type II inhibitors. All these types show together pharmacophore and hydrogen bonds that interact with DFG-out kinase conformational structure as revealed by the discovery of the Type II kinase inhibitor co-crystal structure [61]. This is the advantage of Type II kinase inhibitors that Type I does not have. Therefore, Type II kinase inhibitors demonstrate high selectivity towards kinase

This material is reserved for educational use only, not allowed for commercial use.
Forbidden to modify the content, and cite the document when use.

inhibition as compared to Type I kinase inhibitors along with the profound impact on cellular activity.

Type III or allosteric inhibitors. This class of kinase inhibitors binds outside the ATP-binding site and modulates kinase activity in an allosteric manner. Some researchers have divided Type III into two subtypes: type III-A inhibitors bind to an allosteric site next to the adenine-binding pocket and type III-B inhibitors bind elsewhere [62]. Allosteric inhibitors show promising to exhibit the highest degree of target kinase because they exploit binding sites and physiological mechanisms that are exclusive to a particular kinase. One of the best allosteric inhibitors is CI-1040, an orally active, highly specific, which inhibits MeK1 and MeK2 by occupying a pocket adjacent to the ATP binding site [63]. For other examples such as GnF2, which binds to the myristate binding site of BCR–ABL1, and BMS-345541, which binds to the nuclear factor-**K**B kinase, and RO0281675 and numerous analogues44 that activate glucokinase, as well as AICAR45 and A-769662, which activate AMP-activated protein kinase (Figure 7) [64, 65]. All of these inhibitors are good samples for thought to be a crucial approach for overcoming hurdles in kinase inhibitor research, such as limited selectivity, off-target side effects, and drug resistance [40].

2.1.4 Epidermal growth factor receptor (EGFR)

EGFR is implicated in a variety of cancer types, including NSCLC. EGFR plays a pivotal role in regulating cell proliferation, survival, adhesion, migration, and differentiation [66, 67]. NSCLC accounts for approximately 85% of all lung cancers. In a subset of NSCLC patients, EGFR has gained activating primary mutations, thus the EGFR is a common target that has been used in NSCLC treatment. It is exhibited at high levels on the surface of NSCLC and is activated by a variety of ligands mainly transforming growth factor alpha and epidermal growth factor.

EGFR is a member of the ErbB receptor family and belongs to the super-family of structurally related receptor tyrosine kinases (RTKs). The ErbB receptor family also includes the epidermal growth factor receptor 2 (ErbB2; HER2), as well as HER3 (ErbB3) and HER4 (ErbB4) [68]. EGFR signaling regulates the activation of several intracellular signaling pathways responsible for sustaining physiological cellular processes. These include the

This material is reserved for educational use only, not allowed for commercial use.
Forbidden to modify the content, and cite the document when use.

mitogen-activated protein kinases (MAPK)/ extracellular signal-regulated kinases (ERK), phosphatidylinositol 3-kinase (PI3K)/Akt/mTOR, and the interleukin 6 (IL-6)/Janus kinase (JAK)/signal transducer and activator of transcription 3 (STAT3) pathway [69]. That leads to increased cell survival, proliferation, angiogenesis, and propensity for metastasis [28].

Mutations of the EGFR tyrosine kinase domain have been recently discovered in clinical carcinomas. In NSCLC, EGFR mutations are identified in 10–30% of patients, common EGFR alterations including exon 19 deletions and the L858R point mutation in exon 21 [70-72]. These two frequent primary mutations occur either in the activation loop as a point mutation (L858R) or by a short deletion in exon 19 [70-78]. These mutations promote a dysregulated, ligand-independent activation of EGFR signaling that sustains the proliferation, survival, metabolism, and migration of cancer cells. The activating primary mutations occur in approximately 10–15 % of NSCLC cases in Caucasian patients and approximately 30–40 % in East Asian patients [79, 80]. Recently, selective small-molecule EGFR tyrosine kinase inhibitors (EGFR TKI) are becoming the evidence-based first-line therapy for advanced NSCLC that harbors sensitizing EGFR mutations. Although patients with sensitizing EGFR mutations could achieve good responses to therapy with the first-generation EGFR TKIs, such as Gefitinib and Erlotinib (Figure 4), most patients acquired drug resistance to EGFR TKI within a 1-year treatment. This is mostly driven in about 60% of cases by a second-site EGFR T790M point mutation occurring within exon 20 [73-77]. The second-generation EGFR TKIs such as Afatinib, Neratinib, and Dacomitinib demonstrated promising activity against T790M in preclinical models. They have failed to overcome T790M-mediated resistance in patients due to dose-limiting toxicity resulting from nonselective inhibition of wild-type (WT) EGFR [15, 81]. A variety of irreversible inhibitors were developed. These inhibitors contain a Michael acceptor moiety designed to form a covalent bond with the conserved cysteine residue (Cys797) at the lip of the EGFR ATP binding site [14]. Osimertinib (AZD9291) is a novel mono-anilino-pyrimidine which is a third generation of EGFR TKIs. Osimertinib covalently binds the Cys797 of EGFR with its meta-acrylamide group, and it has been developed to selectively target the T790M mutation EGFR [15-18]. In 2015, the U.S. granted approval for Osimertinib to treat EGFRT790M

This material is reserved for educational use only, not allowed for commercial use.
Forbidden to modify the content, and cite the document when use.

mutated patients whose disease has gotten worse after treatment of EGFR-blocking therapy [19].

As of 2021, three generations of EGFR-TKIs have been developed and are available in the clinic. The fourth generation of EGFR inhibitors is currently undergoing preclinical evaluation. A list of EGFR-TKIs approved for the treatment of EGFR-mutated NSCLC is provided in

Table **1**. Resistance to 3rd generation TKIs can be driven by the gain of secondary EGFR alterations, e.g., substitution at cysteine-797 to serine (C797S) [82]. Real-world evidence shows that in addition to C797S, other EGFR alterations are also acquired upon osimertinib treatment, including kinase domain mutations (e.g., S768I), extracellular domain alterations (e.g., EGFRvIII, A289X), and EGFR amplification [83-85]. 4th generation EGFR inhibitors have been developed to overcome acquired resistance to 3rd generation EGFR-TKIs such as Brigatinib [86], BLU-945 [87], and BI4020 [88].

Most of the available crystal structures of the EGFR kinase domain on the RCSB database, bound to drug inhibitors, originated from ligand-based drug design studies. Haddad et al, [89] analyzed a difference of 110 crystal structures of the EGFR kinase domain, spanning amino acids 714 to 950, in complex with various ligands. This domain comprises the N-lobe (714–795) and C-lobe (796–950), which enclose TKI ligands in a sandwich-like manner, exhibiting nearly planar geometry.

Structure–structure alignment was used to compare 110 3D structures and resulted in two distinct clans that can be divided further into two to three families each. The largest clan of 78 structures was highly similar and divided into family A (22 structures with one or no mutations in EGFR), family B (31 structures with mostly double EGFR mutations), and family C (25 structures with one or two EGFR mutations, divided into subfamily 1 with 21 structures and subfamily 2 with four structures). The other clan was more divergent and was divided into family D (17 structures divided into subfamily 1 with seven wild-type EGFR structures and subfamily 2 with ten triple-mutated EGFR structures) and family E (15 highly divergent structures divided into two subfamilies of ten and five structures). Method: Using the keyword ‘EGFR’, a RCSB protein databank (www.rcsb.org) database search resulted in 260 structures.

This material is reserved for educational use only, not allowed for commercial use.
Forbidden to modify the content, and cite the document when use.

The authors identified eight distinct families, emphasizing the orientation of the C-helix within the N-lobe of the EGFR kinase domain. These families exhibited similar mutational profiles, as well as similarities in the chemical composition, geometry, and charge of the ligand R-groups, particularly those facing the C-helix, mutation sites, and the DFG domain. The superposition of the N-lobe of the epidermal growth factor receptor (EGFR) kinase domain and the bound ligands.

(a) Family A (22 structures with one or no mutations in EGFR) showing the C-helix in proximity to ligands and contacts with Glu762.

(b) Family B (31 structures with mostly double EGFR mutations) showing T790M mutants and the C-helix in proximity to ligands by contacts with Glu762.

(c) Family C1 (21 structures with one or two EGFR mutations) showing T790M mutants and the C-helix in proximity to ligands by contacts with Glu762. Family C2 (four structures) showing shifting of the C-helix away from ligands because of a steric effect.

(d) Family D1 (seven wild-type EGFR structures) showing the steric effect of ligands, and the C-helix is shifting away with no contacts against Glu762. Family D2 in (ten triple-mutated EGFR structures) showing shifting of the C-helix away from ligands possibly because of the effects of mutations.

(e) Family E1 (ten structures) showing the steric effect of ligands and the C-helix shifting away with no contacts against Glu762.

(F) Family E1 and E2 superposed. Family E2 (five highly divergent structures) showing a back-shift in the C-helix with ligand contacts against Glu762 and Ile759.

2.1.5 Reversible and Irreversible Epidermal Growth Factor Receptor - Tyrosine Kinase Inhibitors (EGFR-TKIs)

Mutant EGFR can be inhibited either by small molecule TKI such as gefitinib or erlotinib. These small molecules are the first TKIs developed to work on the EGFR intracellular tyrosine kinase domain that showed a significant decrease in the size of tumors in some patients having EGFR mutations [29]. Then, these inhibitors were to be

This material is reserved for educational use only, not allowed for commercial use.
Forbidden to modify the content, and cite the document when use.

developed and employed in a quinazoline-based scaffold and were reversible in nature. However, the efficacy of those drugs has been limited due to acquired resistance and the rapid development of TKI-resistant mutations such as threonine 790 with methionine (T790M) [73-77]. This has led to the development of covalent irreversible inhibitors in a next-generation targeting Cys797 in EGFR T790M. The second-generation EGFR TKIs, irreversible inhibitors, such as afatinib and dacomitinib (Table 2), prompted the adaptation of the quinazoline scaffold with an electrophilic group allowing a reaction with a cysteine residue (Cys797) at the lip of the active site. They demonstrated promising activity against T790M in preclinical models and have failed to overcome T790M-mediated resistance in patients due to dose-limiting toxicity resulting from nonselective inhibition of wild-type (WT) EGFR [15, 81].

Osimertinib and Olmutinib, novel mono-anilino-pyrimidine third-generation EGFR TKI, have been developed to selectively target the T790M mutation EGFR in a covalent irreversible manner [15-18]. To overcome the T790M mutation-related drug resistance, a variety of irreversible inhibitors were developed. These compounds contain a Michael acceptor moiety designed to form a covalent bond with the conserved cysteine residue (Cys797) at the lip of the EGFR ATP binding site [14]. The U.S. FDA recently granted accelerated approval for Osimertinib to treat EGFR T790M in the clinic [19]. Olmutinib has been approved by the Korean FDA for the same clinical indication [90]. Although EGFR covalent inhibitors have been continuously developed of 3rd generation EGFR TKIs beyond Osimertinib, the detailed mechanism of their reaction with the target cysteine has been a little investigated so far. This includes Rociletinib, Limertinib [10], Lazertinib [91, 92] and Almonertinib [93]. Regrettably, following a year of treatment with 3rd generation EGFR-TKIs, the emergence of the C797S mutation is common, along with other EGFR alterations such as S768I and A289X. To address acquired resistance to 3rd generation EGFR-TKIs, researchers have developed 4th generation EGFR inhibitors [82].

This material is reserved for educational use only, not allowed for commercial use.
Forbidden to modify the content, and cite the document when use.

Table 2. EGFR-TKIs approved for the treatment of EGFR-mutant advanced/metastatic NSCLC.

DRUG	MANUFACTURER	GENERATION	BOND	SPECTRUM OF ACTIVITY	APPROVAL
GEFITINIB (IRESSA®)	AstraZeneca	First	Reversible	Mutated and WT- *EGFR*	FDA, EMA
ERLOTINIB (TARCEVA®)	Roche	First	Reversible	Mutated and WT- *EGFR*	FDA, EMA
ICOTINIB (CONMANA®)	Betta Pharmaceuticals	First	Reversible	Mutated and WT- *EGFR*	CNMPA
AFATINIB (GILOTRIF®)	Boehringer Ingelheim	Second	Irreversible	Pan-ErbB inhibitor	FDA, EMA
DACOMITINIB (VIZIMPRO®)	Pfizer	Second	Irreversible	Pan-ErbB inhibitor	FDA, EMA
OSIMERTINIB (TAGRISSO®)	AstraZeneca	Third	Irreversible	Common and T790 M mutations	FDA, EMA
ALMONERTINIB (AMELIE®)	Hansoh Pharmaceutical	Third	Irreversible	Common and T790 M mutations	CNMPA

Abbreviations: EGFR-TKI (EGFR-Tyrosine Kinase Inhibitors); NSCLC (Non-Small Cell Lung Cancer); WT (Wild-Type); FDA (U.S. Food and Drugs Administration), EMA (European Medicine Agency); CNMPA (China National Medical Product Administration).

2.1.5.1 First-generation EGFR-TKIs

First-generation EGFR-TKIs are low molecular weight, reversible, oral EGFR inhibitors which exert their anticancer activity by inhibiting the intracellular phosphorylation of the EGFR receptor. Of note, the development of first-generation EGFR-TKIs started before the discovery of EGFR-sensitizing mutations [94]. Three first-generation EGFR-TKIs have received approval for the treatment of EGFR-mutant advanced/metastatic NSCLC: gefitinib, erlotinib, and icotinib.

This material is reserved for educational use only, not allowed for commercial use.
Forbidden to modify the content, and cite the document when use.

Gefitinib

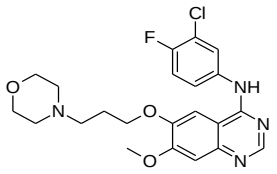

Figure 7. Structure of Gefitinib.

Gefitinib (Iressa™; AstraZeneca, London, United Kingdom) initially received approval by the U.S. Food and Drugs Administration (FDA) as second-line therapy for advanced-stage NSCLC patients who progressed after platinum-based chemotherapy [95]. The pivotal phase III IPASS trial (NCT00322452) demonstrated that first-line treatment with gefitinib improves PFS (9.5 months vs. 6.3 months; $p < 0.001$) compared to carboplatin-paclitaxel in a selected cohort of Asian patients with advanced NSCLC [96]. Similar findings were achieved in several phase III trials (NEJ002, WJTOG-3405, IFUM, first-SIGNAL), leading to gefitinib approval by the FDA and the European Medicine Agency (EMA) as first-line therapy for advanced/metastatic NSCLC patients harboring EGFR-activating mutations [97-100].

Erlotinib

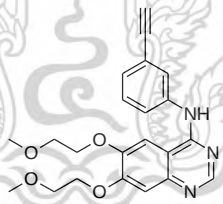

Figure 8. Structure of Erlotinib.

Erlotinib (Tarceva™; F. Hoffman-La Roche, Basel, Switzerland) was initially approved by the FDA for use in unselected advanced/metastatic NSCLC patients who progressed while receiving platinum chemotherapy [101]. Based on results obtained in several randomized phase III clinical trials (EURTAC, OPTIMAL, and ENSURE), the FDA and EMA later extended erlotinib approval to include its use as first-line therapy for EGFR-mutated advanced/metastatic NSCLC. These trials demonstrated erlotinib superiority over

This material is reserved for educational use only, not allowed for commercial use.
Forbidden to modify the content, and cite the document when use.

platinum-containing chemotherapy concerning PFS, along with a more favorable toxicity profile, in NSCLC patients with EGFR mutations [102-104].

Icotinib

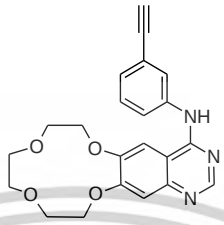

Figure 9. Structure of Icotinib.

Icotinib (Conmana™; Zhejiang Beta Pharmaceutical Co Ltd, Hangzhou, People's Republic of China) is a first-generation EGFR-TKIs that received approval from the Chinese National Medical Products Administration (CNMPA) for the second-line treatment of EGFR-mutant advanced/metastatic NSCLC. Approval was granted after the phase III ICOGEN trial (NCT01040780) established that icotinib is non-inferior to gefitinib in patients who progressed after at least one platinum-based chemotherapy regimen and that treatment with icotinib is associated with fewer adverse events [105]. Based on the positive results obtained in the phase III CONVINCE trial (NCT01719536), the CNMPA later extended icotinib approval to include its use as first-line treatment for EGFR-mutant advanced/metastatic NSCLC [106].

2.1.5.2 Second-generation EGFR-TKIs

Despite the remarkable clinical responses observed in EGFR-mutant advanced/metastatic NSCLC patients treated with first-generation EGFR-TKIs, acquired resistance to these compounds inevitably develops after a median period of 10 – 14 months, principally due to the selection of resistant clones harboring the secondary EGFR-T790M mutation [107]. Consequently, a second-generation of EGFR-TKIs was developed to address the issue of acquired resistance to first-generation EGFR-TKIs.

Second-generation EGFR-TKIs are irreversible pan-ErbB inhibitors [108]. Pros of this generation of EGFR inhibitors include a broader inhibitory profile on the ErbB receptor family and a more robust inhibition of downstream signaling [109]. Second-generation

This material is reserved for educational use only, not allowed for commercial use.
Forbidden to modify the content, and cite the document when use.

EGFR-TKIs approved for the treatment of EGFR-mutant advanced/metastatic NSCLC include afatinib and dacomitinib [110].

Afatinib

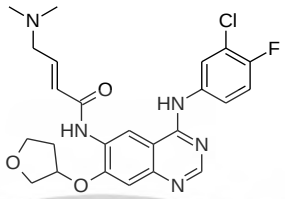

Figure 10. Structure of Afatinib.

Afatinib (Gilotrif™; Boehringer Ingelheim, Ingelheim, Germany) is the first irreversible second-generation EGFR-TKI approved for the treatment of EGFR-mutant advanced/metastatic NSCLC [45]. The efficacy and safety of afatinib as first-line therapy for EGFRmutated advanced/metastatic NSCLC was explored in the phase III LUXLung 3 (NCT00949650) and LUX-Lung 6 (NCT01121393) trials in comparison with cisplatin-pemetrexed chemotherapy and cisplatingemcitabine chemotherapy, respectively [46,47]. In both trials, patients who received afatinib achieved a significantly longer PFS than patients treated with platinum-based chemotherapy, although without substantial improvements in OS [48]. A later subgroup analysis revealed that afatinib-treated patients harboring atypical EGFR mutations (L861Q, G719X, or S768I) had a longer OS than chemotherapy-treated patients. This finding led to the extension of afatinib approval to include patients expressing atypical EGFR mutations [49,50]. The phase IIb LUX-Lung 7 study (NCT01466660) was the first direct comparison between a first- and a second-generation EGFR-TKI for the treatment of EGFR-mutant advanced/metastatic NSCLC in the first-line setting [51]. Clinical results demonstrated that afatinib treatment significantly improves PFS and ORR and has a longer median duration of response (DoR) than gefitinib, although without significant differences in OS between the two treatment arms [52,53].

This material is reserved for educational use only, not allowed for commercial use.
Forbidden to modify the content, and cite the document when use.

Dacomitinib

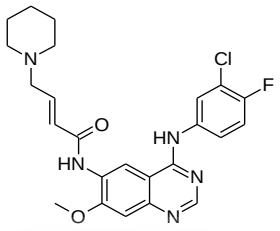

Figure 11. Structure of Dacomitinib.

Dacomitinib (Vizimpro™; Pfizer Inc, New York, USA) is a second-generation EGFR-TKI approved by EMA and FDA for the first-line treatment of patients with EGFR-mutant advanced/metastatic NSCLC [44,54]. Dacomitinib was initially investigated as salvage therapy in phase II/III ARCHER 1028 (NCT00769067) and ARCHER 1009 (NCT01360554) studies in unselected NSCLC patients who progressed while on platinum-based chemotherapy. Results failed to demonstrate the superiority of dacomitinib over erlotinib concerning PFS and OS. However, a subsequent analysis of patient subgroups revealed that dacomitinib has an efficacy comparable to that of erlotinib in patients harboring EGFR-activating mutations [55–57]. Dacomitinib as first-line treatment was assessed in phase III ARCHER 1050 trial (NCT01774721) in a selected population of NSCLC patients harboring EGFR-activating mutations. Dacomitinib showed benefits over gefitinib concerning both PFS and OS, although with a higher incidence of treatment-related adverse events [58–60]. Since the ARCHER 1050 trial excluded patients with brain metastases, evidence regarding the efficacy of dacomitinib in treating CNS lesions is lacking. Clinical studies performed in China and Japan suggest that dacomitinib might be more active against brain metastases than first-generation EGFR-TKIs. Nevertheless, given the small sample size of these studies, the efficacy of dacomitinib for the treatment of CNS lesions remains unclear [61–63].

2.1.5.3 Third-generation EGFR-TKIs

A third generation of EGFR TKI drugs which are irreversible inhibitors is emerging with high potency against T790M-containing mutants and selectivity over WT EGFR. A wealth of preclinical studies has been reported and clinical findings are becoming available. The current review is designed to highlight the novel methodologies developed

This material is reserved for educational use only, not allowed for commercial use.
Forbidden to modify the content, and cite the document when use.

to enable discovery of the third generation EGFR drugs and provide an overview of those currently in clinical trials.

Rociletinib

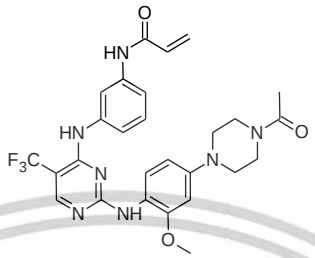

Figure 12. Structure of Rociletinib.

Rociletinib (CO1686) is a 2,4-disubstituted pyrimidine that covalently binds the C797 of EGFR with its meta-acrylamide group. Rociletinib has IC_{50} of 636 and 51.7 nM (Table 2) against EGFR wild-type (WT) and double-mutant EGFR (L858R/T790M EGFR), respectively. In vitro tests comparing the effect of Rociletinib on the double-mutant EGFR with that of EGFR WT showed that it was 16 and 4 times more selective for double-mutant EGFR as compared to Erlotinib and Osimertinib, respectively, but Rociletinib was the potent compound to inhibit JAK3 at a concentration of 4.30 nM (Table 2) and had high LogP and molecular mass. This inclination was also observed by Hao, Y et. Al, [111] The development of Rociletinib was terminated on May 6, 2016, due to a lower efficacy than Osimertinib and incidences of adverse events such as high-grade hyperglycemia and QT interval prolongation [93, 112, 113].

WZ4002

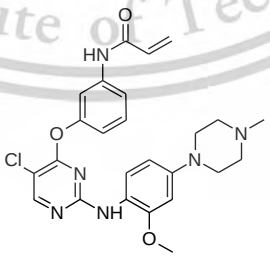

Figure 13. Structure of WZ4002.

This material is reserved for educational use only, not allowed for commercial use.
Forbidden to modify the content, and cite the document when use.

WZ4002 is a chemical compound that has been researched extensively in the context of medical studies, particularly in oncology. It is a selective inhibitor of certain proteins and has shown potential therapeutic applications in preclinical models [114].

Osimertinib (AZD9291)

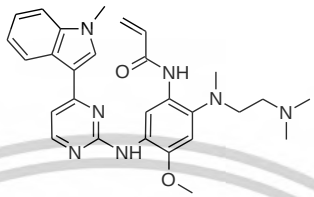

Figure 14. Structure of Osimertinib.

Osimertinib, an oral, novel mono-anilino-pyrimidine third-generation EGFR TKI, has been developed to selectively target the T790M mutation EGFR in a covalent irreversible manner. The tablet formulation of osimertinib has been granted accelerated approval by the United States Food and Drug Administration (FDA) in November 2015, for the therapy of patients with metastatic EGFR T790M mutation-positive NSCLC who have progressed on or after the first and second generation of EGFR TKI therapy. Currently, reports have indicated that osimertinib undergoes extensive metabolism in the body, leading to low levels of the parent compound in feces and urine [19].

Olmutinib

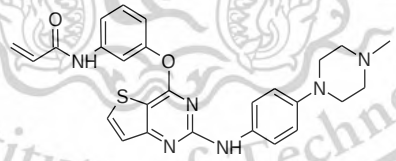

Figure 15. Structure of Olmutinib.

Olmutinib, also known as HM61713, is a third-generation epidermal growth factor receptor (EGFR) tyrosine kinase inhibitor (TKI) used in the treatment of non-small cell lung cancer (NSCLC). It's specifically designed to target EGFR mutations, including the T790M mutation, which is often associated with resistance to first- and second-generation EGFR TKIs. Olmutinib works by blocking the activity of EGFR, thereby inhibiting the growth and spread of cancer cells. Clinical studies have demonstrated its efficacy in patients with

This material is reserved for educational use only, not allowed for commercial use.
Forbidden to modify the content, and cite the document when use.

NSCLC who have developed resistance to other EGFR TKIs, showing promising results in terms of response rates and progression-free survival [113, 115].

Almonertinib

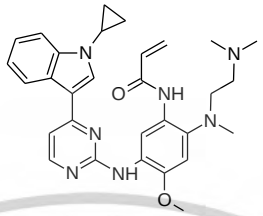

Figure 16. Structure of Almonertinib.

Almonertinib, also known as HS-10296, is a third-generation epidermal growth factor receptor (EGFR) tyrosine kinase inhibitor (TKI) developed for the treatment of non-small cell lung cancer (NSCLC), particularly in patients with EGFR mutations, including the T790M mutation. It works by selectively inhibiting EGFR activity, thereby suppressing the growth and spread of cancer cells. Clinical trials have demonstrated its efficacy in patients who have developed resistance to previous generations of EGFR TKIs [115].

Limertinib

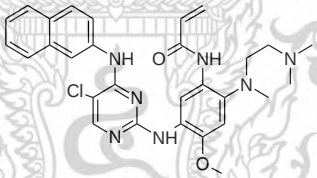

Figure 17. Structure of Limertinib.

Limertinib (ASK120067) is a newly developed third-generation EGFR tyrosine kinase inhibitor targeting both sensitizing EGFR and EGFR Thr790Met (T790M) mutations. It is on phase 2b study conducted at 62 hospitals across China developed by Jiangsu Aosaikang Pharmaceutical Co., Ltd. China. Limertinib demonstrated promising efficacy and an acceptable safety profile for the treatment of patients with locally advanced or metastatic EGFR T790M [10, 116].

This material is reserved for educational use only, not allowed for commercial use.
Forbidden to modify the content, and cite the document when use.

Lazertinib

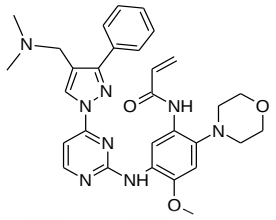

Figure 18. Structure of Lazertinib.

Lazertinib, also known as YH25448, is a third-generation epidermal growth factor receptor (EGFR) tyrosine kinase inhibitor (TKI) used in the treatment of non-small cell lung cancer (NSCLC), particularly in patients with EGFR mutations, including the T790M mutation. It is designed to selectively inhibit EGFR activity, thereby inhibiting the growth and spread of cancer cells. Lazertinib has shown promising results in clinical trials, demonstrating efficacy in patients who have developed resistance to other EGFR TKIs [117, 118].

2.1.5.4 Fourth-generation EGFR-TKIs

Unfortunately, after 1 year of treatment with 3rd generation EGFR-TKIs usually occur C797S mutation other EGFR alterations are also observed, including S768I, and A289X. 4th generation EGFR inhibitors have been developed to overcome acquired resistance to 3rd-generation EGFR-TKIs.

Brigatinib

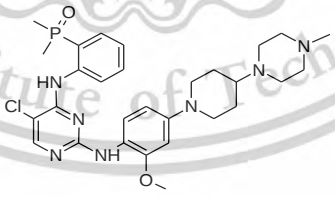

Figure 19. Structure of Brigatinib.

Brigatinib is a tyrosine kinase inhibitor used in the treatment of non-small cell lung cancer (NSCLC), specifically targeting tumors with mutations in the anaplastic lymphoma kinase (ALK) gene. It works by blocking the activity of the ALK protein, as well as other related proteins involved in cancer cell growth. Brigatinib has shown efficacy in both

This material is reserved for educational use only, not allowed for commercial use.
Forbidden to modify the content, and cite the document when use.

treatment-naive patients and those who have developed resistance to other ALK inhibitors. Clinical trials have demonstrated its ability to shrink tumors and improve progression-free survival in patients with ALK-positive NSCLC [119]. Brigantine could overcome EGFR C797S mutation if it is combined with an anti-EGFR antibody such as cetuximab or panitumumab [120]. The U.S. FDA Approves Brigatinib as a First-Line Treatment Option for Patients Diagnosed with Rare and Serious Forms of Lung Cancer [86, 120, 121].

BLU-945

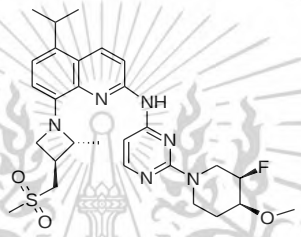

Figure 20. Structure of BLU-945.

BLU-945 is a selective inhibitor of a protein known as KRASG12C, which is implicated in certain types of cancer, particularly non-small cell lung cancer (NSCLC) and colorectal cancer. It works by binding to the KRASG12C protein, thereby inhibiting its activity and disrupting the signaling pathways that promote cancer cell growth. BLU-945 is currently being investigated in clinical trials as a potential treatment for KRASG12C-mutant cancers [87].

BI-4020

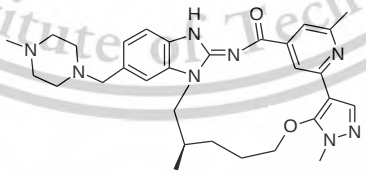

Figure 21. Structure of BI-4020.

BI-4020 is a novel macrocyclic inhibitor of T790M and C797S mutant and has shown promise in pre-clinical. BI-4020 had additional H-bonds to conserved K745 and T845

This material is reserved for educational use only, not allowed for commercial use.
Forbidden to modify the content, and cite the document when use.

residues. Thus, the existence of the catalytic K745 appears viable strategy for improving reversible binding and the ability to inhibit C797S in next-generation EGFR inhibitors [122].

In an effort to comprehend the mechanism of irreversible covalent EGFR inhibitors, Capoferri et al. delved into the mechanism of EGFR inhibition performed by the prototypical covalent inhibitor N-(4-anilinoquinazolin-6-yl)acrylamide, utilizing a quantum mechanics/molecular mechanics (QM/MM) approach [123]. Their findings proposed potential reaction pathways for the addition of Cys797 to the acrylamide of the compound, as illustrated in Figure 22.

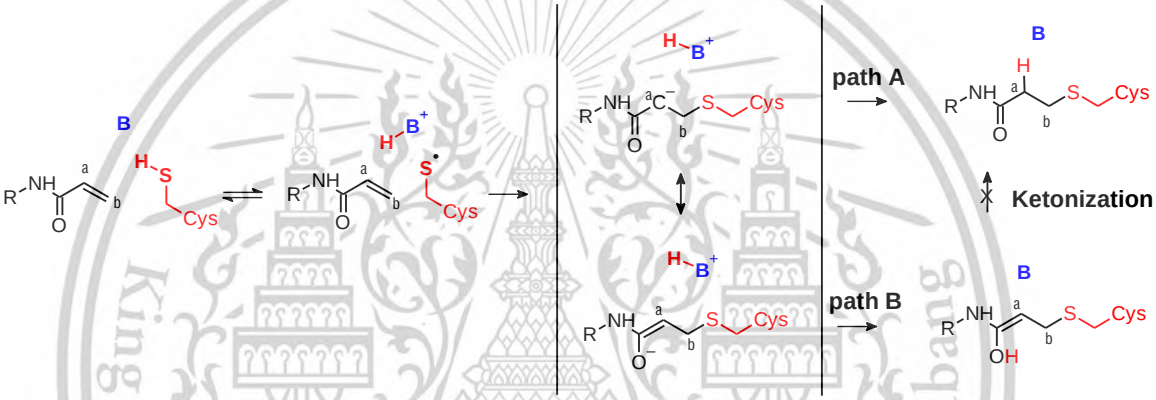

Figure 22. Possible reaction mechanisms for the addition of cysteine to a substituted acrylamide, B represents general base and BH^+ represents general acid [123].

Notably, thiolate could undergo a reaction with acrylamide via one of two alternative mechanisms. Firstly, the direct addition mechanism (Figure 22, path A) involves the thiolate attacking the Cβ of the acrylamide, while a proton is transferred from the protonated base (BH+) at the EGFR active site to the Cα of the acrylamide, resulting in the formation of a beta-substituted amide as the final product. Secondly, the 1,4-addition mechanism (Figure 22, path B) leads to the final product through ketonization following nucleophilic attack and the formation of an enolate intermediate. Here, a proton is transferred from the protonated base to the oxygen atom, leading to the formation of the enolic form of the amide [123]. However, Paasche et al. demonstrated that α,β-unsaturated amides typically undergo preferential direct addition mechanism with thiols, as the ketonization process following 1,4 addition is unlikely due to the high energy content of the enol intermediate [124].

This material is reserved for educational use only, not allowed for commercial use.
Forbidden to modify the content, and cite the document when use.

2.1.6 Pyrimidine core structure for the NSCLC anti-cancer

Pyrimidine is the 6-member ring in a class of heterocyclic aromatic organic compounds, containing 2 nitrogen atoms (Figure 27) at positions 1 and 3 of the ring. It has lots of novel derivatives that possess an effective pyrimidine ring as the central core. Pyrimidine is popular in the field of drug research to design and discover new physiologically and pharmacologically active compounds shown in Figure 23. Pyrimidine derivatives can exhibit a wide range of biological activities such as antibacterial and antifungal activity, antitubercular, antimicrobial, antiplatelet, and antiviral properties [125-127].

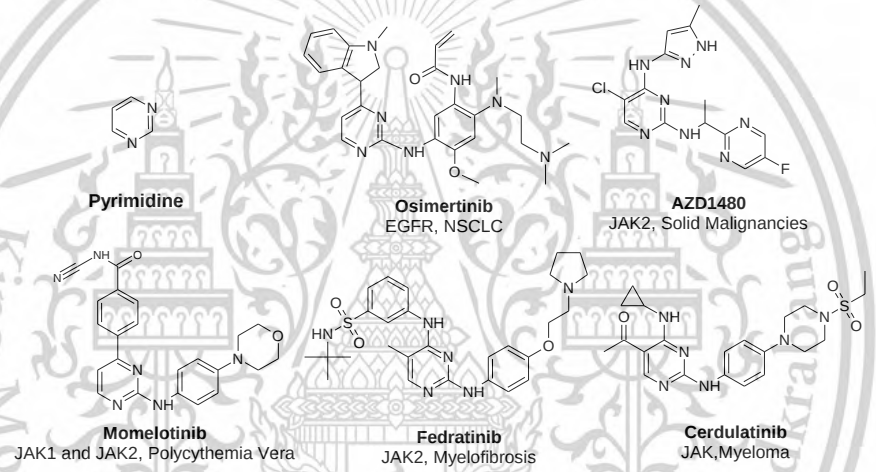

Figure 23. Kinase inhibitors and target Osimertinib[125], AZD1480[126], Fedratinib[127], Momelotinib[126], and Cerdulatinib[126].

The pyrimidine core structure was widely used by the inhibitors of a wide range of kinases such as phosphoinositide 3-kinases (PI3Ks), c-jun-N-terminal kinase (JNK), aurora Kinase, nuclear factor-**K**B (NF-**K**B) family and glycogen synthase kinase 3 (GSK-3). Protein kinases offer great potential due to their role in regulating the majority of cellular pathways, including cellular growth, differentiation, and apoptosis [128]. These inhibitors work on certain patient sub-populations and are sensitive to gene mutations, meaning new treatments are constantly sought [129]. Yang *et al.*, 2014 mentioned that a novel series of pyrimidine core structure derivatives demonstrated the most potent inhibitory activity against PI3K**γ** kinase as well as at the cellular level. This kinase is becoming an important target for cancer treatment. Phosphoinositide 3-kinases (PI3Ks) could catalyze

This material is reserved for educational use only, not allowed for commercial use.
Forbidden to modify the content, and cite the document when use.

phosphorylation of the 3-hydroxyl position of phosphatidylinositol 4,5-diphosphate (PIP2) to generate phosphatidylinositol 3,4,5-triphosphate (PIP3) which had a significant second intracellular messenger in the control of a diverse set of cellular processes, including cell growth, proliferation, differentiation, survival, intracellular trafficking and membrane ruffling [130, 131]. SAR analysis of substituents on the 4-pyrimidine has been studied with various groups of halogen and methyl. Para substituents displayed low binding energy compared with the reference compound (TG100713). The substituents on the 2-pyrimidine ring were observed with a variety of substituted anilines. Among the compounds with a variety of substitutions, compound **C8** as shown in Figure 24 (IC_{50} = 65 nM) demonstrated the most potent inhibitory activity against PI3K**γ** kinase, in which the 4-pyrimidine ring was substituted by 4-chloro, and 2-pyrimidine ring was substituted by 3,4,5-trimethoxy. Apart from inhibitory activities toward PI3K**γ**, compound **C8** also exhibited the best inhibition activity in HepG2, HeLa, A549, and MCF-7 with the IC_{50} values of 0.09 μM, 0.29 μM, 0.36 μM, and 3.15 μM respectively.

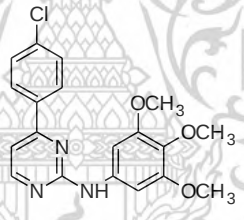

C8

Figure 24. The *N*,4-diphenylpyrimidin-2-amine for PI3K**γ** [130, 131].

Ward et al. reported a novel pyrimidine core of small-molecule inhibitors has been developed to treat NSCLC. The compounds present selectivity for EGFR double-mutant (H1975) over wild-type EGFR (A431). In Figure 25, all compounds showed better in Double mutant cells, particularly in compound **56**, so these compounds show significant activity against the activating mutations [132]. This is supported by Finlay et al. who investigated a similar pyrimidine core to inhibit NSCLC. Compounds **5**, **9**, and **10** in Figure 26 demonstrated strong activity to treat NSCLC and specific to EGFR mutants more than wild-type in terms of inhibition [133].

This material is reserved for educational use only, not allowed for commercial use.
Forbidden to modify the content, and cite the document when use.

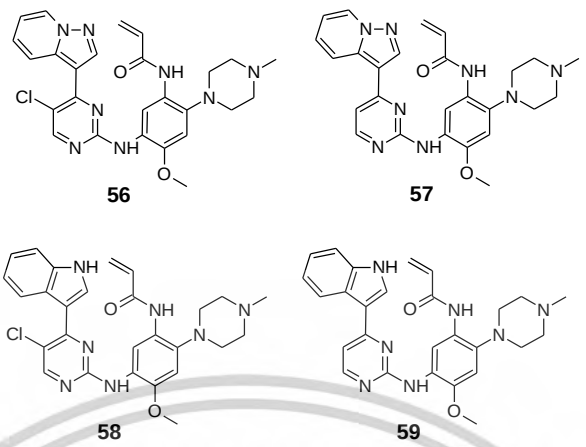

Figure 25. Compounds with the Addition of a Piperazine Group [132].

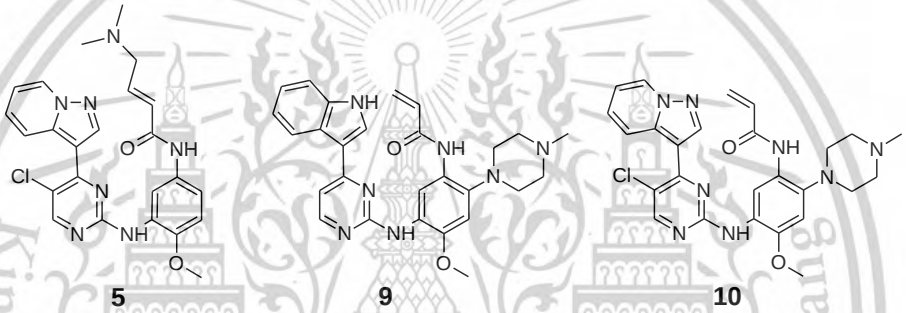

Figure 26. Structures of Lead Optimization Start Points [133].

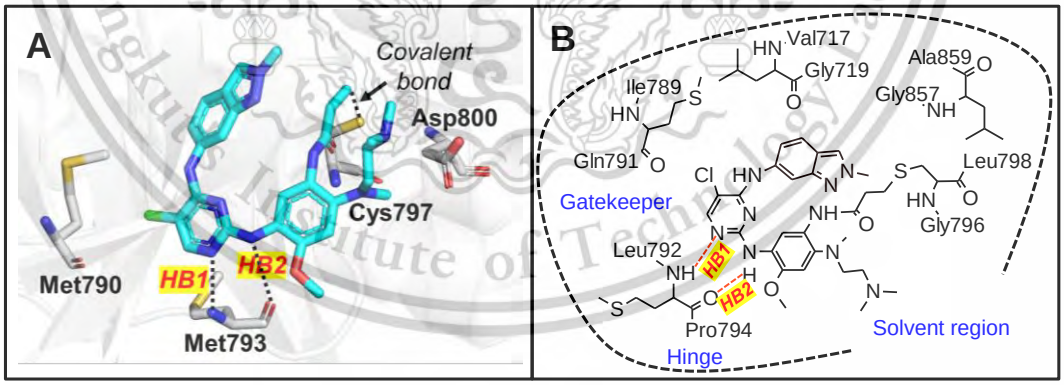

Figure 27. Docking of EGFR TKI to EGFR kinase (PDB ID: 6JX4) shows 2 hydrogen bonds (HB) at the hinge region.

In addition, Pelletier *et al*., 2009 identified 2-aminopyrimidine motif that targeted the glycogen synthase kinase-3β (GSK-3β) [134]. GSK3 is pervasive a ubiquitous serine/threonine kinase that is present in mammals in two isoforms: α and β [135]. GSK3

This material is reserved for educational use only, not allowed for commercial use.
Forbidden to modify the content, and cite the document when use.

is an enzyme involved in the regulation of glycogen metabolism and plays a key role in regulating a diverse range of cellular functions, including cell survival and death. West *et al.*, 2003 demonstrated that nicotine and NNK, two components of cigarette smoke, increased phosphorylation of GSK3 in vitro [136]. Therefore, GSK3 inhibition has been considered an attractive therapeutic strategy for certain diseases such as A549 cells in which GSK3 is highly expressed. In Pelletier's study, SAR of the 2-aminopyrimidine motif showed varied substitutions at the 2 and 4 positions of pyrimidine by thiophenyl and naphthyl have been represented at the 4-position, and benzenesulfonamide and piperidin-1-amine have been represented at 2-position. Compound **1** (Figure 28) also led to enhanced GSK-3β inhibition and substantially reduced solubility. The methylamine in compound **5** (Figure 28) possessed the most potent activity in the primary assay, low kinase inhibition potential, and high solubility.

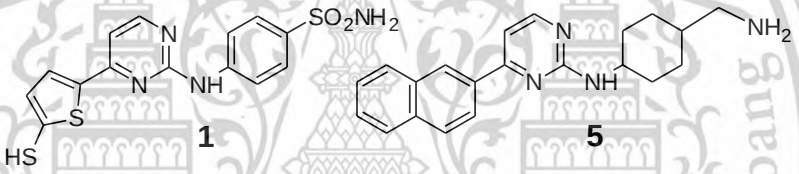

Figure 28. Compounds 1 and 5 for TCF-Luciferase and GSK-3β [134].

Crombie *et al.*, 2010 synthesized and evaluated anilinopyrimidine core for inhibitors of IKKβ. The SAR studies, they investigated compound **1**, this compound had an excellent in vitro IKKβ inhibitory profile [137]. The sulfonamide of compound **1**, water solubilizing groups, showed a compound with similar in vitro IKKb inhibitory activity but improved aqueous solubility and pharmacokinetic properties. In addition, this study found that the substitution of the *para* phenyl on pyrimidine with acylamino groups has excellent enzyme potency and cellular activity such as **11**, **12**, and **13** (Figure 29).

This material is reserved for educational use only, not allowed for commercial use.
Forbidden to modify the content, and cite the document when use.

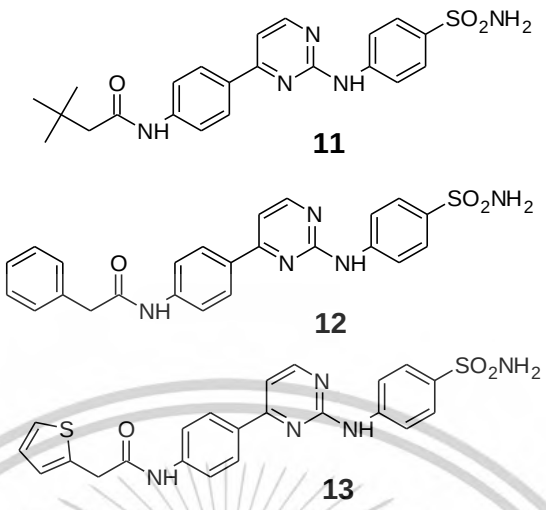

Figure 29. Lead compound from exploratory investigations [137].

Apart from the mentioned protein kinase, the c-Jun NH 2-terminal kinases (JNKs) JNK play a prosurvival role in human lung cancer-derived cell lines, and the enzyme contributes to oncogenic transformation. JNKs are commonly activated in response to stress and hence are also known as stress-activated protein kinases [138]. The c-Jun is a target for JNK study in which phosphorylation of c-Jun at serines 63 and 73 promotes activation of this transcription factor [139]. The c-Jun protein has been implicated in both the induction and prevention of apoptosis [140]. JNK activation of c-Jun is necessary for apoptosis in myeloid and lymphoid cells because the use of a dominant-negative c-Jun mutant blocks programmed cell death in these cells [141]. Therefore, JNK inhibitors can promote apoptosis in A549 cells.

Kamenecka *et al*., 2010 try to develop highly selective JNK inhibitors in the rung of aminopyrimidines [142]. The structure-activity relationships (SAR) of a series of aminopyrimidines. All compounds had biochemical IC_{50} values < 500 nM with JNK3. The two most potent compounds, **9d** and **9e (**Figure 30**)**, had IC_{50} values = 7 and 4 nM, respectively, in which these compounds contained methyl sulfonamide at the R2 position. Replacement of the sulfonamide moiety in the R4 position of compound **9e** by a 1,2,3-triazole had no effect on JNK3 or JNK1 inhibition. Therefore, the class of aminopyrimidines or pyrimidine core represents good candidates for designing, developing, and synthesis as a treatment for non-small cell lung cancer.

This material is reserved for educational use only, not allowed for commercial use.
Forbidden to modify the content, and cite the document when use.

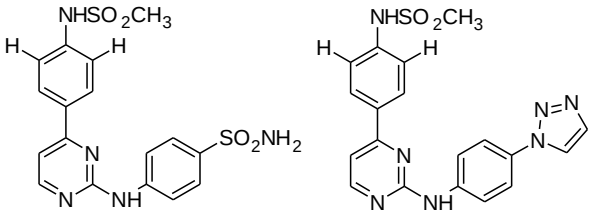

Figure 30. Inhibitors of JNK1, JNK3, and p38 [142].

For kinase inhibitory, Tan et al. report the discovery and optimization of 2,4-substituted pyrimidines as covalent JAK3 inhibitors that exploit a unique cysteine (Cys909) residue in JAK3. Investigation of structure–activity relationship (SAR) utilizing biochemical and transformed Ba/F3 cellular assays resulted in the identification of potent and selective inhibitors such as compounds **9** (Figure 31). A 2.9 Å cocrystal structure of JAK3 in complex with 9 confirms the covalent interaction. Compound **9** exhibited decent pharmacokinetic properties and is suitable for use in vivo. This inhibitor provides a set of useful tools to pharmacologically interrogate JAK3-dependent biology [143].

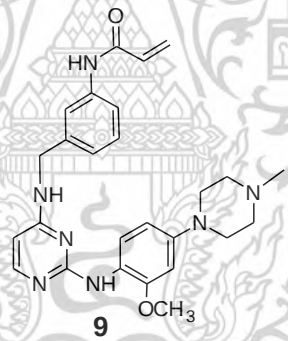

Figure 31. Biochemical IC50s for Inhibition of JAK3 and Cell-Based Inhibition of Ba/F3 [143].

2.2 Covalent kinase inhibitors (CKIs)

Covalent inhibitors, Irreversible inhibitors, are usually small molecules that make bonds to enzymes and then close them temporarily or permanently. In the 19th century, been used small molecules as covalent inhibitors to target functionally critical enzymes in cells [144]. In the 20th century, showed that the electrophilic acetyl within aspirin irreversibly inhibited a nucleophilic serine hydroxyl on cyclooxygenase (COX-1, COX-2)

This material is reserved for educational use only, not allowed for commercial use.
Forbidden to modify the content, and cite the document when use.

enzymes (Figure 32) [145]. Inactivation of COX function prevents Prostaglandin synthesis and an anti-inflammatory effect [146, 147].

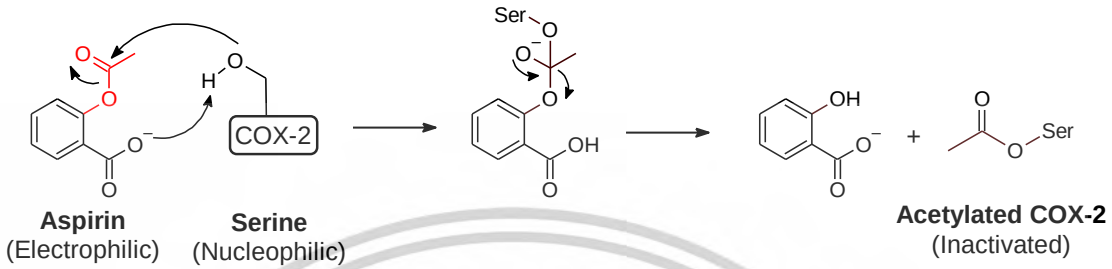

Figure 32. 2D of the covalent mechanism of aspirin irreversibly inhibited cyclooxygenase2 via serine modification [145].

At present, the pharmaceutical industry has interests in the development of covalent drugs as therapeutic agents because covalent drugs were successful covalent drugs like aspirin in the market. Besides, covalent inhibitors display advantages compared to reversible inhibitors such as being non-toxic, having strong target affinity and prolonged acting lives in patients (Figure 33). In EGFR activities, Engle et al, reported the comparison between acrylamide (5l, Figure 34) and propenamide (5m, Figure 34) as an irreversible and reversible inhibitor. The covalent inhibitor or irreversible inhibitor is more potent in EGFR L858R and EGFR T790M&L858R when compared to non-covalent or reversible inhibitors. However, there is no significant effect on EGFR WT between both irreversible and reversible inhibitors but this is well for the future study of covalent inhibitor studies such as Kinetic properties, Mass spectrometry confirmation pharmacokinetics, and pharmacodynamics [148].

This material is reserved for educational use only, not allowed for commercial use.
Forbidden to modify the content, and cite the document when use.

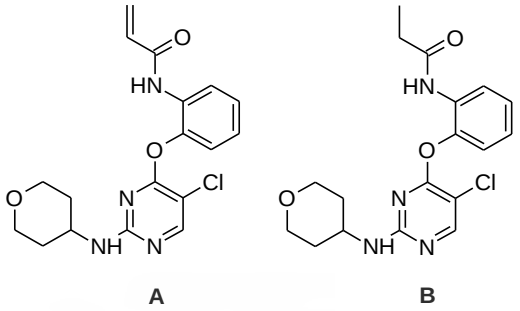

Figure 33. Comparing structures of covalent (A) and non-covalent (B) mitogen-activated protein kinase 1 (MAPK1) inhibitors at varying [ATP] [145].

In general, covalent inhibitors contain electrophiles that react with nucleophilic residues in enzymes. There are several molecules that substituted by electrophilic warheads such as epoxide, ester, aziridine, ketone, α, β-unsaturated carbonyl, nitrile, etc. have been identified as covalent inhibitors [149]. A new type of inhibitors known as "sulfur tethers" have also caught attention because of their ability to covalently conjugate cysteines in enzymes.

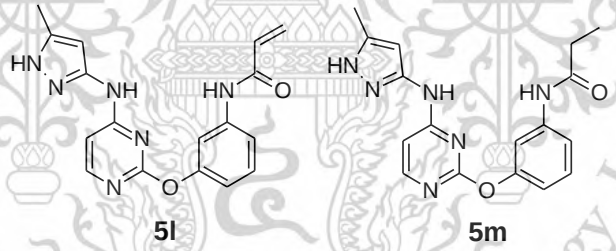

Figure 34. Overview of a Focused Small Molecule Library of Pyrimidine-Based Inhibitors [148].

2.2.1 Covalent Inhibitors of Protein Kinases

Protein kinases represent one of the most important targets in drug discovery. They are important in the regulation of physiological mechanisms, including cell proliferation, differentiation, and metabolism. The difference of kinase inhibitors is defined by the center around the enzyme-ligand complex. Generally, protein kinases contain β-stranded amino-lobe (N-lobe), ATP binding, and a-helical carboxy-lobe (C-lobe). These domains are linked together by the hinge region. A Gly-rich loop within the N-lobe is known as the ATP binding loop (P-loop) and it interacts with ATP a and b phosphates. In addition, the more variable

This material is reserved for educational use only, not allowed for commercial use.
Forbidden to modify the content, and cite the document when use.

region that plays a regulatory role in kinase activity is called the activation loop (A-loop). The A-loop exists in two conformations (open/closed), which characterize an active kinase state, (open A-loop) allowing substrate binding, and an inactive kinase state (closed A-loop), blocking the active site. Besides, the A-loop also contains a conserved Asp-Phe-Gly sequence (DFG motif) which is also important in ATP binding [150].

Dar and Shokat have categorized kinase inhibitors into three classes: I, II, and III. Class I molecules bind the active kinase conformation within the ATP pocket. Class II binds the inactive kinase conformation and class III are non-ATP competitive inhibitors such as allosteric [55]. Subsequently, Gavrin and Saiah have reported class IV inhibitors, which target a pocket distant from the ATP-binding site, a hydrophobic pocket, or a pocket on the surface of the kinase [151]. Active and inactive kinase conformations are defined relative to the positioning of the DFG motif. In the active state (DFG-in), the Phe residue of the DFG motif is buried inwards towards the hydrophobic pocket. Conversely, in the inactive state (DFG-out), a 180°-flip reorients the Phe residue outwards. Zuccotto et al., [152] offer class I 1/2 inhibitors, which bind to a DFG-in but the ATP pocket of inactive kinases. Lamba and Gosh [62] proposed class V inhibitors, which bind two distinct regions within the catalytic domain. Finally, class VI inhibitors bind within permanent/long-lived covalent attachments. Generally, covalent kinase inhibitors have the warhead, which improves the binding affinity and selectivity by forming a covalent interaction with a kinase reactive residue (nucleophilic residues) [144]. The kinome consists of several nucleophilic residues such as cysteines [52], lysines [153], aspartic acids [154], and others [155]. Most frequently, the covalent inhibitors bind to the kinase active site in a covalent form with a nucleophilic cysteine residue, located near the ATP-binding site [156].

2.2.2 Cysteine (nucleophilic residues)

Cysteine displays the most targeted amino acid in the field of covalent kinase inhibitors (CKIs) because of various unique properties such as cysteine residue having a low abundance if compared with the other 19 possible residues, which represents an attractive feature in the context of kinases where selectivity is challenging. Cysteines also show non-catalytic roles in kinases such as stabilizing protein tertiary structure through

This material is reserved for educational use only, not allowed for commercial use.
Forbidden to modify the content, and cite the document when use.

intra- and inter-molecular disulfide bonds. Therefore, the main feature of cysteine is the high reactivity and chemical plasticity of the anionic thiolate (Cys-S^-) [157].

The susceptibility of cysteine is variable across the kinome in covalent modification. This reactivity is relative to the function of pKa and dependent on the location of cysteine within the desired binding pocket. Thiols exposed on protein surfaces that are not directly involved with protein function tend to be more acidic with a lower pKa. A lower pKa improves reactivity relative to their buried counterparts due to the ability to form H-bond interactions with water and other polar residues. However, the existence of basic residues (e.g. lysine, arginine) within the vicinity of buried cysteines can serve to decrease their pKa, increasing the likelihood of having an available nucleophilic thiol [158].

Although buried cysteines are quite rare they can react with a wide range of warheads, particularly Michael acceptors (e.g. α,β-unsaturated carbonyls) [159]. These unique properties have attracted broad interest in this nucleophile making in the development of a wide array of cysteine targeting warheads with diverse chemistries [50]. The current view of covalent kinase inhibitors is heavily biased towards a few major drug targets. These include EGFR, BTK, ITK, and JAK3, all of which have an equivalently positioned cysteine within the hinge region of the catalytic ATP binding pocket.

2.2.3 Electrophilic groups & Michael acceptors

Forming a Michael acceptor is a conjugation of alkenyl motifs to EWGs relaying electrophilicity to the unsaturated b-carbon, which is suitable for attack by soft nucleophiles (Figure 22) [160]. In Figure 35,b nucleophiles can regioselectivity attack at the carbonyl carbon or the β-position.

This material is reserved for educational use only, not allowed for commercial use.
Forbidden to modify the content, and cite the document when use.

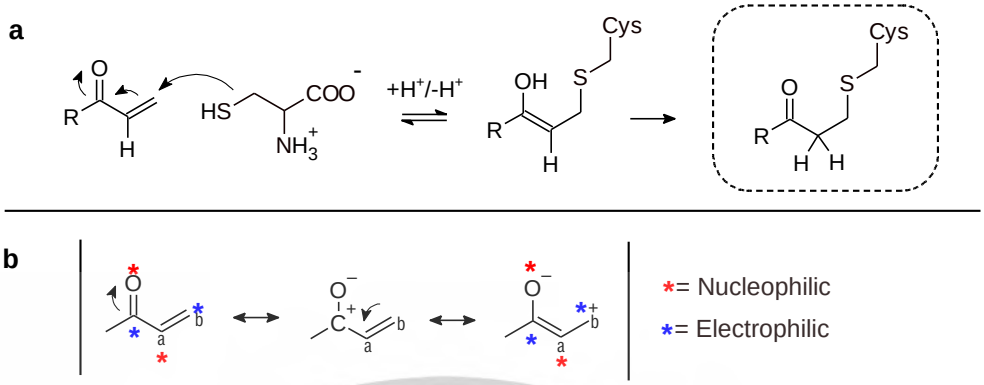

Figure 35. (a) The mechanism of covalent modification by α,β-unsaturated carbonyl, (b) Electron movement in α,β-unsaturated carbonyls through resonance mediated tautomerization, highlighting nucleophilic and electrophilic sites [145].

Nucleophilic addition to acrylamides basically depends on basicity, going through 1,2-addition and weak bases result in 1,4 or conjugate addition. As of current, the unsaturated carbonyls represent acrylamide, the most common electrophile in covalent kinase inhibitor development. Acrylamides are a sub-family of α,β-unsaturated carbonyls characterized by their unique reactivity profile and soft electrophilic nature. Nitrogen heteroatom in acrylamides extends conjugation via resonance, resulting in attenuated reactivity, a desirable feature for covalent inhibitors. Unfunctionalized acrylamides are only minimally reactive towards thiol nucleophiles and virtually non-reactive against amino acids of dissimilar hardness. Therefore, acrylamides are the most suitable utilized electrophiles in CKI development [161]. Recently, several researchers assessed the glutathione GSH reactivity of several aryl-acrylamides with varying ortho, meta, and para substituents. Acrylamides can substitute with *N*-aryl, *N*-alkyl and/or varied substituents at the α or β positions revealing heightened reactivity for *N*-substituted scaffolds relative to carbon-substituted counterparts [162].

Quantum chemistry calculations are the availability of more computational power and in the development of more accurate and efficient methods. This paved the way for quantum chemistry being used to solve problems that arise in a pharmaceutical industrial setting as reported in the literature. Hermann et al, predicted the reactivity of a specific class of covalent drugs using QM calculations. This can be applied in the drug discovery

This material is reserved for educational use only, not allowed for commercial use.
Forbidden to modify the content, and cite the document when use.

process and focus on compounds with a suitable reactivity to be administered to the patient. They also presented the usage of the electrophilicity index on three common warheads, i.e., acrylamides, 2-chloroacetamides, and propargylamides (Figure 36) similar to that seen in the previously reported by Lonsdale et al, (predicted the reactivity of warhead) [163, 164]. Palazzesi et al, estimated the compound's intrinsic reactivity using the QM calculations. The highly intrinsically reactive compound can lead to unwanted and toxic effects [165]. Mihalovits et al, investigated the prediction of covalent ligand selectivity. The results of the calculations are in good agreement with the experimental free energy values derived from the inhibition and kinetic constants (Ki and kinact) of the enzyme-inhibitor binding [166]. There are many ways to study electrophilic groups such as looking into (i) prediction of the reactivity of different molecules from 3 warhead classes: acrylamide, 2-chloroacetamide, and 2*E*)-3-phenylprop-2-enamide (ii) prediction of the insertion at acyl of different molecules from warhead classes and propenamide (iii) comparison of reactivity to find the optimal of warheads.

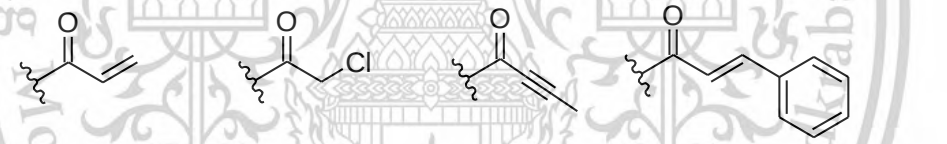

Acrylamide 2-chloroacetamide But-2-ynamide (2*E*)-3-phenylprop-2-enamide

Figure 36. Electrophilic groups for the development of covalent inhibitors.

There are many publications that investigated the efficacy of electrophilic groups such as acrylamide, 2-chloroacetamide, and propenamide as the non-electrophile for comparison. Amaral et al. investigate the effective inhibition for 3 types of EGFR (wildtype, double-mutant, and L858R) by comparing them on the electrophilic groups. The results showed that there was no significant effect between electrophilic groups in the same SAR analysis. Compound **7h** (Figure 37) incorporated with acrylamide showed the strongest inhibition for EGFR WT, L858R, and T790M/L858R with the IC_{50} 25, 18, and 1682 nM, respectively [167].

Furthermore, Castelli et al synthesized a 2-chloroacetamide **8** (Figure 37) an acrylamide derivative on **9** (Figure 37) as a prototype of an EGFR inhibitor potentially able

This material is reserved for educational use only, not allowed for commercial use.
Forbidden to modify the content, and cite the document when use.

to react with Cys797 by nucleophilic substitution. They inhibited both EGFR autophosphorylation and proliferation in H1975 lung cancer cells (expressing EGFR L858R/T790M mutant) at low micromolar concentrations [168].

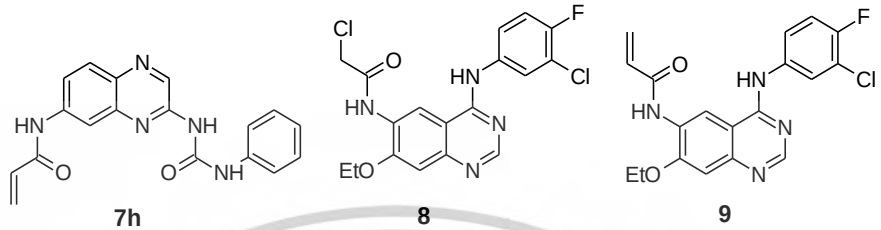

Figure 37. EGFR inhibitors **7h, 8,** and **9** [167, 168].

In other kinase inhibitions, Tan et al. investigated the inhibition of TAK1 (transforming growth factor-b-activated kinase 1) which is an essential intracellular mediator of cytokine and growth factor signaling and a potential therapeutic target for the treatment of immune diseases and cancer. They have developed a series of 2,4-disubstituted pyrimidine covalent TAK1 inhibitors that target Cys174, a residue immediately adjacent to the 'DFG-motif' of the kinase activation loop. Finally, they discovered the Lead compounds such as **2** and **10** on Figure 38 showed greater than 10-fold biochemical selectivity for TAK1 over the closely related kinases MEK1 and ERK1 which possess an equivalently positioned cysteine residue. These compounds are synthesized by incorporating acrylamide, propenamide, and 2-chloroacetamide on the R_1 of compounds **2**, **8**, and **10**, respectively. The results showed that acrylamide and 2-chloroacetamide are strongly inhibition in the same ranges at nanomolar concentration while the propenamide that is non-electrophilic group showed less activity on both TAK1 and MEK1 (IC_{50}>10000 nM) [169].

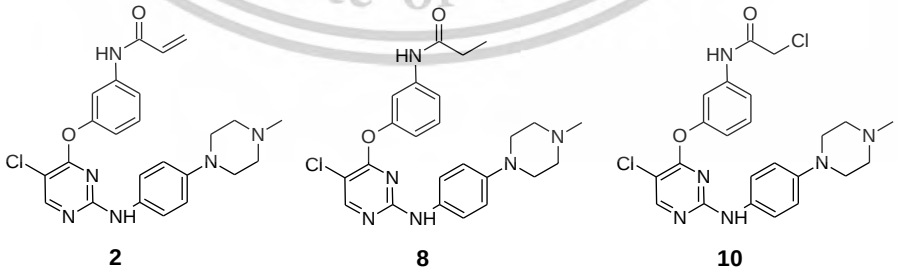

Figure 38. SAR of Lead compounds [169].

This material is reserved for educational use only, not allowed for commercial use.
Forbidden to modify the content, and cite the document when use.

McAulay et al. were interested in covalent drugs and there was a need to identify new moieties capable of cysteine bond formation that are differentiated from commonly employed systems such as acrylamide. They reported on the discovery of new acrylamide and but-2-ynamide moieties capable of covalent reaction with cysteine. Their utility as alternative electrophilic warheads for chemical biological probes and drug molecules is demonstrated through site-selective protein modification and incorporation into kinase drug scaffolds. They investigated the efficacy of these electrophilic groups on JAK kinases. The results showed that **16** with the acrylamide and **17** with the but-2-ynamide (Figure 39) are favorably potent compounds to inhibit JAKs, EGFRT790M, BMX, BLK, and BTK at the low nanomolar concentration, particularly in compound 16 that very specific for JAK3 over JAK1 and JAK2 [170].

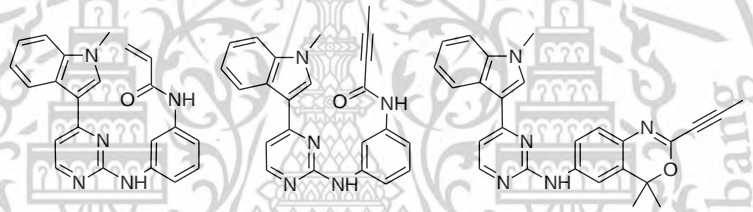

16 **17** **18**

Figure 39. Inhibitors for Selected Cysteine Containing Kinases and JAK Family Members [170].

2.2.4 Covalent bond confirmation using Mass Spectrometry (MS)

Lelais et al. and Engle et al. reported In vitro adducts of compounds with EGFR kinase. The recombinant kinase domain of EGFR L858R and T790M-L858R mutants were incubated with the compounds to confirm the covalent modification of EGFR and the site of adduction. The recombinant enzyme was incubated at room temperature with a 20-fold molar excess of the compound in 40 mM Tris, pH 8, 500 mM NaCl, 1% glycerol, and 5 mM TCEP for 1 h. The reaction was quenched by the addition of dithiothreitol (DTT, 80-fold excess to compound) and transferred to ice. A third of the reaction (10 μL) was processed for intact MS by adding an equal volume of 6 M Guan HCl, 100 mM Tris, pH 8, 20 mM DTT, and 10 mM TCEP and incubating at room temperature for 15 min. Intact MS analysis was performed on the mass spectrometer. The samples were injected into a

This material is reserved for educational use only, not allowed for commercial use.
Forbidden to modify the content, and cite the document when use.

column. The data were analyzed in MassHunter for automatic peak selection, integration, and spectral deconvolution with a mass range of 15,000–75,000 Da.

Reaction solutions were also processed for enzymatic digestion and LC/MSMS. Samples were buffer exchanged to remove excess compound using DTT and incubated at 60 °C for 20 min. Iodoacetamide was added to 25 mM, and the samples were incubated for 45 min at room temperature in the dark prior to dilution to 150 µL. The samples were divided in two, and 1 µL of either 0.5 mg/mL chymotrypsin or sequencing-grade modified trypsin was added and incubated overnight at 37 °C. Samples were acidified to 1% formic acid and analyzed on a Q-Exactive mass spectrometer for accurate mass and MS/MS. The data were converted to Mascot generic format (MGF) using Proteome Discoverer (Thermo) and searched using Mascot against a custom database allowing for variable modification of methionine oxidation, cysteine carbamidomethylation, and the custom modification of Michael addition by the compounds to cysteines. Enzyme specificity was trypsin or no enzyme (chymotrypsin digest), and the peptide and fragment ion tolerances were set to 25 ppm and 50 mmu, respectively. The data were visualized in Scaffold 4.4.3 and filtered for 95% peptide confidence and 99% protein confidence [148, 171].

Li Tan et al. also investigated the covalent formation between JAK3 and inhibitor using Mass Spectrometry. JAK3 protein (5µg) was labeled with a 10-fold excess of inhibitor or DMSO for 30 min at 4°C. After labeling, proteins were desalted using 0.5 mL Zeba spin desalting columns (Thermo Fisher Scientific). After washing to remove salts, the protein was eluted with an HPLC gradient (0%–100% B in 1 min, A = 0.2 M acetic acid in water, B = 0.2 M acetic acid in acetonitrile, flow rate = 10µL/min) into a linear ion trap mass spectrometer (LTQ, Thermo Fisher Scientific, San Jose, CA). Data were acquired in profile mode scanning m/z 300–2000. Mass spectra were deconvoluted using MagTran software. Sites of covalent modification were identified using a “bottom-up” strategy. Desalted proteins were reduced with tris(2-carboxyethyl)phosphine (10 mM, 10min room temperature), alkylated with iodoacetamide (20 mM, 30 min room temperature in dark), and digested with trypsin for 4 hrs. at 37°C. Digests were analyzed by Nano LC-ESI-MS [172].

This material is reserved for educational use only, not allowed for commercial use.
Forbidden to modify the content, and cite the document when use.

2.2.4 Kinetic characterization

Enzyme inhibitors that form covalent bonds with their targets are being increasingly pursued in drug development. Assessing their biochemical activity relies on time-dependent assays, which are distinct and more complex compared with methods commonly employed for reversible-binding inhibitors. To provide general guidance to the covalent inhibitor development community, Hoyt et al. explored methods and reported kinetic values and experimental factors in determining the biochemical activity of various covalent epidermal growth factor receptor (EGFR) inhibitors. They have suggested that 1) The potency and selectivity of covalent enzyme inhibitors can only be determined in time-dependent activity assays (IC_{50} values are inappropriate). 2) Kinetic values for covalent EGFR inhibitors reported in the literature are not consistent, and investigators must include benchmark compounds as important controls. 3) Inhibitor molecular properties, assay reagent concentrations, and dilution protocols can significantly impact potency values.

All drug development campaigns rely on biochemical activity assays to make decisions regarding compound design by assembling structure–activity relationships (SARs) or, more appropriately for covalent inhibitors, structure–kinetic relationships (SKRs). Generally, all irreversible covalent enzyme inhibitors, including the second- and third-generation EGFR inhibitors mentioned above, operate in a two-step mechanism involving initial binding to the target protein in a reversible process, followed by permanent inactivation through covalent bond formation in an irreversible reaction (Figure 40). The reaction of the free enzyme (E) with the inhibitor (I) to form the overall non-covalent E·I complex is described by the dissociation constant Ki (eq 1), which is the classic parameter used to assess the potency of a reversible inhibitor, such as erlotinib or gefitinib [173].

This material is reserved for educational use only, not allowed for commercial use.
Forbidden to modify the content, and cite the document when use.

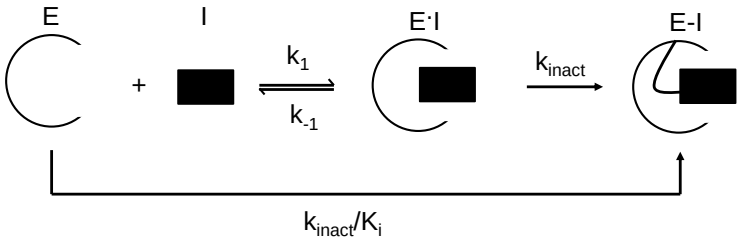

Figure 40. Two-step inactivation of an enzyme target by an irreversible inhibitor [173].

The next step involves the formation of an irreversible covalent adduct (E-I), defined by the first-order rate constant kinact, which is the maximum rate of inactivation achieved at an infinite concentration of an inhibitor (Figure 2). For a particular covalent inhibitor, the potency through the composite second-order rate constant (kinact/KI, eq 2) is a reflection of how quickly the free enzyme (E) is irreversibly inactivated (E-I). The utility of kinact/KI, the inactivation efficiency, in understanding covalent inhibitor potency cannot be overstated as this term contains all of the rate constants that govern target inhibition and is the most important term for assessing the relative covalent inhibitor potency and for SAR/SKR optimizations. Separately, the inactivation constant (KI, eq 3) is the inhibitor concentration required to inactivate the enzyme at ½ kinact. In this way, KI is comparable to KM in Michaelis–Menten enzyme turnover (where the [S] at ½ Vmax is KM); it is a composite of the rate constants describing the fate of the E·I complex and can be utilized in the interpretation of relative reversible affinities of an inhibitor for the target enzyme [173].

$$K_i = \frac{k_{-1}}{k_1} \qquad (1)$$

$$k_{inact}/K_1 = \frac{k_1 k_{inact}}{k_{-1} + k_{inact}} \qquad (2)$$

$$K_1 = \frac{[E][I]}{[\mathrm{E} \cdot \mathrm{I}]} = K_i + \frac{k_{inact}}{k_1} = \frac{k_{-1} + k_{inact}}{k_1} \qquad (3)$$

2.3 Drug Discovery Process

A drug discovery program is initiated because there is a disease or clinical condition without suitable medical products available, and it is this unmet clinical need that is the underlying driving motivation for the project. The initial research, often occurring in

This material is reserved for educational use only, not allowed for commercial use.
Forbidden to modify the content, and cite the document when use.

academia, generates data to develop a hypothesis that the inhibition or activation of a protein or pathway will result in a therapeutic effect in a disease state [174]. Drug discovery is a process that aims at identifying a compound therapeutically useful in curing and treating disease. This process involves the identification of candidates, synthesis, characterization, validation, optimization, screening, and assays for therapeutic efficacy. Once a compound has shown its significance in these investigations, it will initiate the process of drug development earlier to clinical trials. The new drug development process must continue through several stages to make a medicine that is safe, effective, and has approved all regulatory requirements. One overall theme is that the process is sufficiently long, complex, and expensive so that many biological targets must be considered for every new medicine ultimately approved for clinical use and new research tools may be needed to investigate each new target. From initial discovery to marketable medicine is a long, challenging task. It takes about 12 - 15 years from discovery to the approved medicine and requires an investment of about US $1 billion. On average, a million molecules are screened but only a single is explored in late-stage clinical trials and is finally made obtainable for patients [175].

The average cost for research and development for each efficacious drug is likely to be $900 million to $2 billion. This figure includes the cost of the thousands of failures: For every 5,000-10,000 compounds that enter the investigation and development pipeline, ultimately only one attains approval. These statistics challenge the imagination, but a brief understanding of the R&D process can explain why so many compounds don't make it and why it takes such a large, lengthy effort to get one medicine to patients [176]. The success requires immense resources, the best scientific and logical minds, highly sophisticated laboratories and technology, and multifaceted project management. It also takes persistence and good fortune [177]. Eventually, the process of drug discovery brings hope, faith, and relief to billions of patients [175, 178].

2.3.1 Five critical steps in the U.S. drug development process

There are 5 steps in the U.S. drug development process Starting from the first step which is the discovery and development. Today's drug discovery involves screening hits, medicinal chemistry, and optimization of hits to reduce potential drug side effects

This material is reserved for educational use only, not allowed for commercial use.
Forbidden to modify the content, and cite the document when use.

(increasing affinity and selectivity). Efficacy or potency, metabolic stability (half-life), and oral bioavailability are also improved in this step of the drug development process. Figure 47 provides an overall summary of this discovery and development. Then, the next step is preclinical research. Preclinical trials test the new drug on non-human subjects for efficacy, toxicity, and pharmacokinetic (PK) information. These trials are conducted by scientists in vitro and in vivo with unrestricted dosages. Step 3 is Clinical Development Clinical trials are conducted in people (volunteers) and intended to answer specific questions about the safety and efficacy of drugs, vaccines, other therapies, or new methods of using current treatments. Then, they decide:

- Selection criteria for participants.
- Number of people who take part in the study.
- Duration of study.
- Dose and route of administration of dosage.
- Assessment of parameters.
- Data collection and analysis.

The FDA review is the next process. Once the new drug has been formulated for its best efficacy and safety, and the results from clinical trials are available, it's advanced forward for wholistic FDA review. At this time, the FDA reviews and approves, or does not approve, the drug application submitted by the drug development company. Finally, step 5, which is FDA post-market safety monitoring, following drug approval and manufacturing, the FDA requires drug companies to monitor the safety of their drug using the FDA Adverse Event Reporting System (FAERS) database. FAERS helps the FDA implement its post-marketing safety surveillance program. Through this program, manufacturers, health professionals, and consumers report problems with approved drugs.

2.3.2 Drug Discovery Process for Kinase Inhibitors

2.3.2.1 Target Identification and Validation

Protein kinases play a pivotal role in the regulation of a diverse range of cellular functions. It is therefore not surprising that abnormally elevated kinase activity can lead to various pathological conditions including proliferative diseases such as cancer, fibrosis, restenosis, psoriasis, and atherosclerosis as well as diabetes, inflammation, T-cell

This material is reserved for educational use only, not allowed for commercial use.
Forbidden to modify the content, and cite the document when use.

activation, tumor angiogenesis, osteoporosis, and platelet aggregation. The discovery and development of selective protein kinase inhibitors to treat diseases caused by the dysregulation of signaling pathways has become an extremely promising and widespread approach to drug discovery [179].

2.3.1.2 Lead Discovery

Among the various approaches for the modulation of protein kinase activity, inhibition by low-molecular-weight compounds targeting the catalytic site of kinases with ATP competitive inhibitors still appears to be the most promising for drug intervention. In many cases, the start of a new lead-discovery program is achieved by high-throughput screening of large compound collections. O. V. Ahsen and U. Bçmer reviewed the field of high-throughput screening for kinase inhibitors and guided the reader through efficient state-of-the-art assay development and high-throughput screening technologies [179].

2.3.1.3 Lead Optimization

For the medicinal chemist, protein kinases represent both a gold mine and a tremendous challenge of design opportunities. While only a handful of structural scaffolds were known prior to 1990, a very large number of chemical families have emerged in the last decade; this has led to ever more potent and selective inhibitors [179].

2.3.1.4 Preclinical and Clinical Development

Currently 55 kinase inhibitors are under clinical evaluation (compared to only seven five years ago) of which half target tyrosine kinases. Of the 31,000 pharmaceutical patents published in 2002, more than 800 concern kinase inhibitors. It is estimated today that 30–35% of discovery programs target a protein kinase, as many as those targeting GPCRs [179].

The inhibition of protein kinases presents the drug-discovery community with both enormous opportunities and challenges. This special issue of ChemBioChem has been conceived to cover recent and successful kinase-inhibitor discovery and optimization methodologies as well as examples of recent diversified kinase targets. Its aim is not to exhaustively review the past but rather to present state-of-the-art methods in the area of protein kinase inhibition to open new horizons and stimulate discussion in the scientific community.

This material is reserved for educational use only, not allowed for commercial use.
Forbidden to modify the content, and cite the document when use.

2.3.3 Structure-based design

The first method of the drug discovery process is to design the ligand that can selectively bind to specific enzymes like the fitting of a lock and key which includes two main processes. SAR study is the indirect process of finding and making up a novel series of inhibitors via integration of structure-activity relationship (SAR) for compounds derived from chemical properties improvement and given a measurable biological or therapeutic activity without having any details of the image of enzyme target. Structure-base design is the more direct method using the three-dimensional (3D) structure of ligand and target to design the new inhibitors which must have known the detail of each site of enzyme target before attempting to create the ligands in order to confirm to be specific for the target [180]. Structure-based design can also help to significantly reduce the time and cost associated with the drug discovery process.

2.4 Computational chemistry approaches

Computational chemistry is equipment to assist in solving chemical problems. They use computers to create information such as properties of molecules and simulate experimental results. There are several computer software used for computational chemistry such as Gaussian xx, GAMESS, and MOPAC. Currently, there are two main branches of computational chemistry: one is based on classical mechanics, and the other is based on quantum mechanics.

Molecular dynamics is one tool used in a computer simulation that is important for studying the macromolecular structure and dynamics [181]. These simulations can reveal the mechanism of biochemical processes occurring on different scales of length and time. The dynamics of the system (protein in aqueous solution) were calculated by the popular force fields such as AMBER, CHARMM, COMPASS, and GROMOS [182]. They have been developed mainly for molecular dynamics of macromolecules used for energy minimizing. Therefore, computational approaches have become a part of chemistry that is important for finding the structures and properties of molecules such as relative energies, electronic charge density distributions, and dipoles.

.

This material is reserved for educational use only, not allowed for commercial use.
Forbidden to modify the content, and cite the document when use.

Chapter 3

Material and Method

3.1 Material

3.1.1 Instruments

All reagents and solvents were purchased from commercial suppliers and were used without further purification. Thin-layer chromatography (TLC) was performed on a TLC aluminum/silica gel plate (Silicycle UltraPure Silica gels) with UV light visualization. Purification of the compounds by column chromatography was performed using silica gel G60 (60-200 μm). ^{1}H NMR and ^{13}C NMR spectra were recorded on a Jeol spectrometer model: ECZ500/S1 at 500 MHz (^{1}H NMR), 125 MHz (^{13}C NMR). Chemical shifts (δ) and coupling constants are quoted in parts per million (ppm) and Hertz (Hz), respectively, with the residual DMSO-*d6* solvent line acting as the internal standard. Mass spectra were obtained from an LC-MSD-Trap mass spectrometer, ion source type ESI(+) mode. High-resolution mass spectra (HRMS) were determined on Bruker Daltonics - micrOTOF-Q III in source ESI(+) mode. Melting points were determined on a Stuart Digital Melting Point Apparatus (Melting Point SMP10). The purity of compounds was confirmed ≥95% based on a UV absorbance HPLC chromatogram (HITACHI/Chromaster HPLC with a Poroshell 120 EC-C8 2.7 μM column using a mobile phase consisting of (a) 0.1% formic acid in water and (b) acetonitrile: 99:1% to 1:99% gradient run in 8 minutes).

3.1.2 Column and Thin Layer Chromatography

Thin Layer Chromatography (TLC) was used to monitor all reactions and was conducted on an aluminum/silica gel plate. The chromatograms were visualized under UV light 254 nm. Utilizing different solvent systems, depending on the polarity of each compound. In this research methanol in dichloromethane and ethyl acetate in dichloromethane were used mostly.

Column chromatography was performed using SiO_2 (particle size 0.040–0.055 mm, 230–400 mesh, which is the method for purifying all compounds in these series. The silica gel was used to pack the column, eluting by different solvent systems. Mostly, 75%DCM/25%EtOAc and 98%DCM/2%MeOH were used in these series.

This material is reserved for educational use only, not allowed for commercial use.
Forbidden to modify the content, and cite the document when use.

3.1.3 Chemical reagents

The reagents, building blocks, and solvents obtained from commercial suppliers were used without further purification.

3.2 Synthesis

3.2.1 Study 1: Synthesis, in vitro SAR and Computational Evaluation of Rociletinib-derived Covalent Inhibitors for the Treatment of EGFR non-small-cell-lung cancers.

All compounds were prepared according to the synthetic route described in Scheme 1. Briefly, intermediate **1** was prepared from the reaction of 2,4,5-trichloropyrimine and 3-nitroaniline with $NaHCO_3$ in ethanol, at 80 °C, for 6 hrs, with a yield of 82%. **1** was then reacted with anilines under acidic conditions (TFA) in isopropyl alcohol at 90 °C overnight to give intermediates **2-6** with yields ranging from 50-78%. The nitro groups were then reduced using $SnCl_2$ in ethanol at 80 °C for 6 hrs, to give **7-11** with yields ranging from 50-80%. Final compounds **12-31** were prepared by reacting **7-11** with acid chlorides using DIPEA in anhydrous DCM at 0°C for 30 mins, with yields ranging from 24-61%. Overall yields ranged from 7-22%.

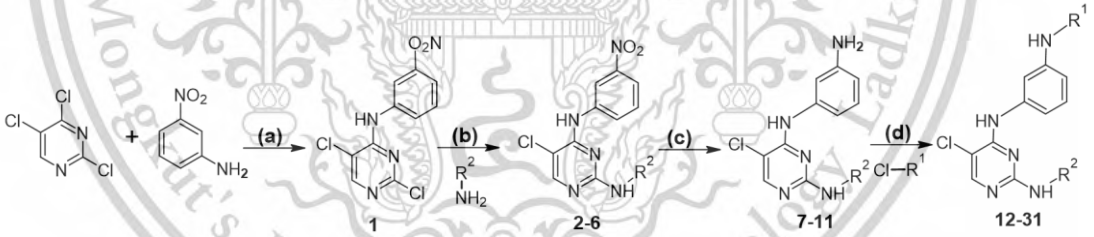

Scheme 1. The general route for the synthesis of compounds (a) $NaHCO_3$, EtOH, 80 °C, 6 hrs, (82%)[183]; (b) TFA, isopropanol, 90 °C, overnight, (50-78%) [183-185]; (c) $SnCl_2$, EtOH, 80 °C, 6hrs, (50-80%)[186]; (d) DIPEA, anhydrous DCM, 0°C, 30 min, (24-61%)[187-190].

3.2.1.1 General procedure A for the preparation of intermediate compound 1.

A solution of 2,4,5-trichloropyrimidine (1.5 equivalent) and 3-nitroaniline (1 equivalent), $NaHCO_3$ (2 equivalent) in EtOH (5 ml for 0.5g) was stirred at 80 °C for 6 hrs. The reaction mixture was filtered through filter paper and washed with EtOAc to obtain a yellow solid.

This material is reserved for educational use only, not allowed for commercial use.
Forbidden to modify the content, and cite the document when use.

3.2.1.2 General procedure B for the preparation of intermediate compounds 2-6.

N^1-(2,5-dichloropyrimidin-4-yl)benzene-1,3-diamine **(1)** and amine (1.5 equivalent) in TFA (0.4 ml) and isopropanol was heated at 90 °C overnight. The reaction mixture was cooled to room temperature and diluted with 1M NaOH to pH 7. The precipitate was filtered, washed with deionized water, isopropanol, EtOAc, and dried under air or purified by silica gel column chromatography (5-10% MeOH/DCM, 1%NH_3) to give the desired product.

3.2.1.3 General procedure C for the preparation of intermediate compounds 7-11.

Compounds **2-5** (1 equivalent) and tin(II)chloride (5 equivalent) were mixed together in ethanol. The reaction was stirred at 80°C for 6 hours. The reaction mixture was filtered through filter paper and the mother liquor was basified with NaOH 6 M and extracted with ethyl acetate. The combined organic extracts were dried over anhydrous Mg_2SO_4 and evaporated to be obtained as a solid. The compound was used in the next step without further purification.

3.2.1.4 General procedure D for the preparation of final compounds 12-31.

Solid from **6-9** (1 equivalent) and DIPEA (2 equivalent) were mixed in anhydrous DCM (10 ml) and DMF (1 ml). The reaction was stirred at 0 °C for 10 mins. The acid chloride (2 equivalent) was added dropwise then the reaction was stirred at 0°C for 30 mins. The crude product was concentrated in vacuo followed by extraction with DCM/DI water. The combined organic extracts were dried over anhydrous Mg_2SO_4 and purified by silica gel column chromatography (MeOH/DCM).

3.2.2 Study 2: Molecular Dynamics Guided Design of *N*^{4}-(2-methyl-2H-indazol-6-yl)-*N*^{2}-phenylpyrimidine-2,4-diamine inhibitors targeting Cys797 and the T790M Gatekeeper Mutation.

All compounds were prepared according to synthetic routes described in Scheme 2. Compounds **1-2** were prepared from the reaction of pyrimidines and 2-Methyl-2H-indazol-6-amine with $NaHCO_3$ as a basic in ethanol, at 80 °C, for 6 hrs, in a yield of 70-90%. Compounds **1-2** were then reacted with amine performed under TFA as the acidic condition in isopropyl alcohol at 90 °C for overnight to give compounds **3-10** with yields

This material is reserved for educational use only, not allowed for commercial use.
Forbidden to modify the content, and cite the document when use.

ranging from 70-90%. Compounds **5-10** were hydrogenated using $SnCl_2$ in ethanol at 80 ℃ for 6 hrs, or Pd/C in methanol at RT for 6 hrs, to give compounds **11-16** with yields ranging from 50-80%. The final compounds **17-50** were achieved using Acid chloride, DIPEA in anhydrous DCM at 0℃ for 30 mins with yields ranging from 20-60% or Carboxylic acid, DCC in anhydrous DCM at RT for 1 hr with yields ranging from 20-41%.

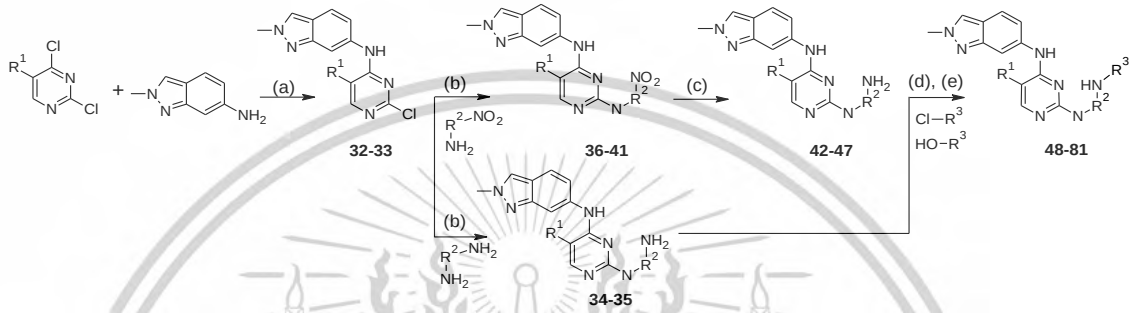

Scheme 2. The general route for the synthesis of compounds: (a) $NaHCO_3$ in EtOH, 80 ℃, 6 hrs (70-90%)[183, 191]; (b) TFA, Isopropanol, 80-120 ℃, overnight (70-90%)[183, 191, 192] (c) $SnCl_2$, EtOH, 80 ℃, 6 hrs,[186] or Pd/C, MeOH, RT, 6 hrs (50-80%)[171]. (d) DIPEA, anhydrous DCM, 0℃, 30 mins (20-41%) [187-190] (e) HATU, DIPEA, anhydrous DCM, 0℃, 30 mins[193, 194] or DCC, anhydrous DCM, RT, 1 hr (20-30%)[170].

3.2.2.1 General procedure A for the preparation of intermediate *N*-(2-chloropyrimidin-4-yl)-2-methyl-2H-indazol-6-amine **(1),** and *N*-(2,5-dichloropyrimidin-4-yl)-2-methyl-2*H*-indazol-6-amine **(2).**

To a solution of 2,4-dichloropyrimidine or 2,4,5-trichloropyrimidine (1.5 equivalent) and 2-Methyl-2H-indazol-6-amine (1 equiv) in EtOH (5 ml for 0.5 g) was added $NaHCO_3$ (2 equivalent). The mixture solution was refluxed for 6 hr. The mixture was cooled to room temperature and concentrated under reduced pressure. The precipitate was filtered, and washed with EtOH, or the resultant was dissolved in water and extracted with ethyl acetate (EtOAc). The organic layers were combined, washed with brine, dried over anhydrous Na_2SO_4, and concentrated in vacuo. The organic layer was purified by silica gel column chromatography to give the desired product.

This material is reserved for educational use only, not allowed for commercial use.
Forbidden to modify the content, and cite the document when use.

3.2.2.2 General procedure B for the preparation of **3-10.**

To a solution of *N*-(2-chloropyrimidin-4-yl)-2-methyl-2H-indazol-6-amine **(1),** *N*-(2,5-dichloropyrimidin-4-yl)-2-methyl-2*H*-indazol-6-amine **(2)** and amine (1.5 equivalent), TFA (3 equivalent) in isopropanol was heated at 150 **℃** for overnight. The reaction mixture was cooled to room temperature and diluted with 1M NaOH until it was neutral. The precipitate was filtered, washed with deionized water, isopropanol, EtOAc, and dried under air or purified by silica gel column chromatography (5-10%MeOH/DCM, 1%NH_3) to give the desired product.

3.2.2.3 General procedure C for the preparation of intermediate compounds **11-13**.

Solid from N^2-[3-(aminomethyl)phenyl]-5-chloro-N^4-(2-methyl-2H-indazol-6-yl)pyrimidine-2,4-diamine **(3)** (1 equivalent) and Pd/C (10%) were mixed together in MeOH. The reaction was flowed hydrogen gas (H_2) at RT for 10 mins. Next, the reaction was stirred at RT for 4 hrs. The crude must be filtered with celite545. The liquid must evaporate out of MeOH and then be extracted with DCM/DI water. The combined organic extracts were over anhydrous Mg_2SO_4 and evaporated to obtain a solid. The compound was used in the next step without further purification.

3.2.3.4 General procedure D for the preparation of compounds **14-16**.

5-chloro-N^4-(2-methyl-2*H*-indazol-6-yl)-N^2-(3-nitrophenyl)pyrimidine-2,4-diamine **(4)** (1 equivalent) and tin(II)chloride (5 equivalent) were mixed together in ethanol. The reaction was stirred at 80°C for 4 hours. The reaction mixture was filtered through filter paper and the mother liquor was basified with NaOH and extracted with Ethyl acetate. The combined organic extracts were over anhydrous Mg_2SO_4 and evaporated to obtain a solid. The compound was used in the next step without further purification.

3.2.2.5 General procedure E for the preparation of final compounds **17-50**.

Solid from **3-4** and **11-16** (1 equivalent) and DIPEA (2 equivalent) were mixed in a little of DMF and anhydrous DCM. The reaction was stirred at 0°C for 10 mins. Next, add dropwise the acid chloride (1.5 equivalent). The reaction was stirred at 0°C for 30 mins. The crude must evaporate out of DMF and then be extracted with DCM/DI water. The

This material is reserved for educational use only, not allowed for commercial use.
Forbidden to modify the content, and cite the document when use.

combined organic extracts were over anhydrous Mg_2SO_4 and purified by silica gel column chromatography (MeOH/DCM).

Solid from **3-4** and **11-16** (1 equivalent) and DCC (2 equivalent) were mixed in DCM. The reaction was stirred at RT for 10 mins. Next, add dropwise the but-2-ynoic acid (1.5 equivalent). The reaction was stirred at RT for 1 hr. The crude must be extracted with DCM/DI water. The combined organic extracts were over anhydrous Mg_2SO_4 and purified by silica gel column chromatography (MeOH/DCM).

3.3 Computational Method

3.3.1 Molecular Docking

The docking protocol used in this study has been described in detail elsewhere.[195] Briefly, **21** was docked to the EGFR WT (1M17, resolution 2.60 Å)[196] and EGFR T790M (5XDK, resolution 2.35 Å)[197]. Proteins were prepared without water molecules or other co-factors and docked using GOLD5.3.[198] Docking solutions enforced a covalent bond between the acrylamide C_b atom of **21** and Cys797.

3.3.2 Quantum Mechanic Calculations (QM Calculations)

All QM calculations were performed in Gaussian 16.[199] All structures were fully optimized using the M06-2x functional [200, 201] and the 6-31G(d) basis set. Minima were confirmed as having no imaginary frequencies and transitions states a single imaginary frequency corresponding to the expected bond breaking/forming process.

3.3.3 Molecular Dynamics (MD) Simulations

MD simulations were performed on the 3 binding poses of **A** docked to EGFR crystal structures. Simulations were carried out using the program GROMACS v. 2019.4 [202] in conjunction with the AMBER99SB forcefield [203, 204]. The restrained electrostatic potential (RESP) charge of the ligand was determined from a Hartree-Fock calculation with the 6-31G(d) basis set. Ligands topology files were created using the ACPYPE script [205] with the GAFF forcefield [206, 207]. The protonation state of amino acid residues was confirmed based on their predicted pK_a calculated using Propka3.1 [208, 209] and a visual assessment of the local interactions. The protein was immersed in a box of TIP3P water molecules with a minimum distance of 12 Å between the protein and the box edge [210].

This material is reserved for educational use only, not allowed for commercial use.
Forbidden to modify the content, and cite the document when use.

NaCl ions were added (0.15 M). The system was minimized to an RMS gradient of 10 kJ mol^{-1} nm^{-1} to relax any steric conflicts. The system was heated from 0 to 300 K over 500 ps using an NVT scheme followed by equilibration for 1 ps. The system underwent production dynamics using an NPT ensemble for 5 ns.

3.4 Kinase Inhibition Assay

All synthesized compounds were tested for their inhibitory activity against EGFR WT, EGFR T790M/L858R, and JAK3 using the ADP-Glo™ Kinase Assay (Promega). The experimental process was performed according to the method described by the manufacturer. The reaction mixture (25 µL) contained 5 µL of kinase buffer (20 mM Tris-HCl (pH 7.5), 20 mM $MgCl_2$, 0.1 mg/mL BSA), 5µL of 25 µM ATP, 5 µL of 12.5 µg/mL poly (Glu:Tyr) substrate, 5 µL of 1 ng/µL HER2-TK or EGFR-TK (diluted in kinase buffer), and 5 µL of various compounds concentrations. Osimertinib and Erlotinib were used as control kinase-inhibitor. The reactions were performed in a 384-well plate (Greiner Bio-One Lumitrac plate, solid white) and incubated at room temperature for 1 hr. Afterward, 5 µL of ADP-Glo reagent was added to terminate the kinase reaction and deplete the remaining ATP at room temperature for 40 min. Next, 10 µL of ADP-Glo detection reagent was added for 30 min to simultaneously convert ADP to ATP and to allow the newly synthesized ATP to be measured using a luciferase/luciferin reaction. Luminescence measurements were made using a microplate spectrophotometer (Synergy HTX Multi-Mode reader, BioTek, VT, USA). The half-maximal inhibitory concentration (IC_{50}) values of inhibitors were determined using the nonlinear regression curve fit in GraphPad Prism (GraphPad Software Inc., San Diego, CA, USA). All assays were done in triplicate. Experiments will be conducted at Kasetsart University, Department of Biochemistry [211].

3.5 Cell-based screening

The in vitro cytotoxicity activity of potent compounds against the A549, A431, and HepG2 cell lines was evaluated using the MTT assay. The first 100 µL of A549 (5000 cells/well), A431 (5000 cells/well), and HepG2 (5000 cells/well) cells suspension was seeded per well in a 96-well microplate and incubated at 37 °C overnight. Then cells were treated with compounds and known drugs (Erlotinib, Osimertinib, and Rociletinib) at different concentrations. Then, incubated for 72 h. Subsequently, the MTT solution (5

This material is reserved for educational use only, not allowed for commercial use.
Forbidden to modify the content, and cite the document when use.

mg/mL) was added to A549, A431, and H1975 cells and incubated at 37 C for 3 h. The medium was removed and 50 µL of DMSO was added to each well to lyse the cells. Finally, the absorbance was measured at 570 nm using a microplate reader (Infinite M200 microplate reader, Tecan, Männedorf, Switzerland) [212].

3.6 Sox-based substrate assay

All reactions were performed with final solutions of 54 mM HEPES pH 7.5, 1 mM ATP, 0.012% Brij-35, 0.5% glycerol, 0.22 mg/ml BSA, 0.55 mM EGTA, 10 mM $MgCl_2$, 10 µM Sox-based substrate. All reactions were run for 240 minutes at 30 °C. Time-dependent fluorescence from the Sox-based substrate was monitored in a 384-well plate, microplate reader with excitation (360 nm) and emission (485 nm) wavelengths in kinetic mode. Inhibitors were dosed between 0 and 1 µM in 12-point curves with 2-fold dilutions. Fluorescence was determined in duplicate, to obtain corrected fluorescence intensity (FI). The global fit model was utilized to obtain kinetic parameters recorded with 125 nM, 250 nM, and 500 nM inhibitor concentrations from the starting point until 100 mins [213].

3.8 Aqueous Solubility

The equilibrium solubility was determined in phosphate buffer (PBS) at pH 7.4 [214]. Approximately 1 mg of each sample was dissolved in 2 mL of 0.02 M PBS at pH7.4 in a 10 mL glass screw top vial, sonicated and shaken for 1 hr and 6 hrs, respectively, to make the saturated solution, and then filtered using a syringe filter (13mm, 0.20 mm, filter, Xiboshi). A standard solution for each sample was prepared by dissolving a known amount of sample in 1 mL of DMSO, pre-diluted 10 times using DMSO. The amount of sample present in the PBS and DMSO solutions was determined by HPLC-UV (HITACHI/Chromaster HPLC with a Poroshell 120 EC-C8 2.7 µM column). A 100 µL injection of the aqueous sample and 10 µL of DMSO solution were used. The solubility was calculated based on the ratio of the area under the curve obtained from the 2 samples, corrected for the dilution factors and injection volume.

3.9 Partition coefficient ($logD_{7.4}$)

The 1-octanol, pre-saturated with 0.02M PBS at $pH_{7.4}$ was determined using the shake flask technique [215]. Roughly 1 mg of the sample was added into a 10 mL glass screw-top vial to which 2 mL of octanol was added. The solution was sonicated for 1 hr.

This material is reserved for educational use only, not allowed for commercial use.
Forbidden to modify the content, and cite the document when use.

Compounds that were incompletely dissolved were diluted in further octanol and sonicated until a completely clear solution resulted. A final volume of 2 mL of octanol solution and 8 mL of 0.02 M of PBS at $pH_{7.4}$ were shaken for 6 hrs. The resulting solutions were centrifuged (4000 rpm for 15 min), and the octanol and aqueous layers were extracted separately. The amount of samples present in the octanol and PBS solutions was determined by HPLC-UV (HITACHI/Chromaster HPLC with a Poroshell 120 EC-C8 2.7 μM column).

This material is reserved for educational use only, not allowed for commercial use.
Forbidden to modify the content, and cite the document when use.

Chapter 4

Result and discussion

4.1 Study 1: Synthesis, in vitro SAR and Computational Evaluation of Rociletinib-derived Covalent Inhibitors for the Treatment of EGFR non-small-cell-lung cancers.

4.1.1 Synthesis Results

All compounds were prepared according to the synthetic route described in Scheme 1. Briefly, intermediate **1** was prepared from the reaction of 2,4,5-trichloropyrimine and 3-nitroaniline with $NaHCO_3$ in ethanol, at 80 °C, for 6 hrs, with a yield of 82%. **1** was then reacted with anilines under acidic conditions (TFA) in isopropyl alcohol at 90 °C overnight to give intermediates **2-6** with yields ranging from 50-78%. The nitro groups were then reduced using $SnCl_2$ in ethanol at 80 °C for 6 hrs, to give **7-11** with yields ranging from 50-80%. Final compounds **12-31** were prepared by reacting **7-11** with acid chlorides using DIPEA in anhydrous DCM at 0°C for 30 mins, with yields ranging from 24-61%. Overall yields ranged from 7-22%.

All of the final compounds (Table 3) were confirmed using ^1H NMR spectroscopy and High-resolution mass spectra (HRMS) accounting for more detail of each compound. In addition, the purity of the compound is investigated by HPLC as more than 95% pure.

This material is reserved for educational use only, not allowed for commercial use.
Forbidden to modify the content, and cite the document when use.

Table 3. 12-31 and standard assessed in this study. Reported are R-groups, physical properties, yields, and EGFR activities (%I at 1 μM and IC_{50}).

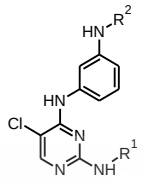

ID	R^1	R^2	MW	cLogD[a]	%Yield	%I at 1 μM	EGFR WT IC_{50} (nM)
12	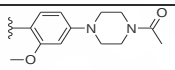		524.0	3.76	17.2	95.3	62.9±3.09
13	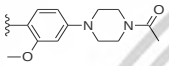		522.0	3.82	8.8	68.7	87.6±3.94
14	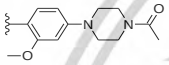	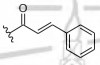	598.1	5.42	9.10	56.9	58.0±4.00
15	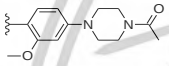		544.4	3.60	15.0	64.2	22.6±3.18
16	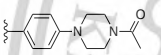		533.0	3.92	13.8	96.4	65.9±4.03
17	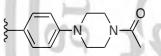		492.0	3.98	9.10	91.7	43.6±4.48
18	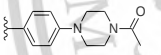	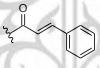	568.1	5.59	8.10	92.7	87.8±3.93
19	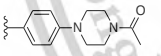		514.4	3.76	6.30	84.6	114±4.02
20			371.8	3.17	16.0	61.4	35.0±3.88
21			369.8	3.23	11.2	79.5	174±6.63
22		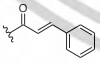	445.9	4.83	7.0	95.2	44.8±2.28
23			392.2	3.00	12.8	112	41.6±5.23
24	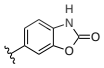		358.8	3.37	17.1	87.3	116±3.80
25	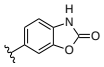		357.8	3.42	8.60	102	63.5±3.19
26	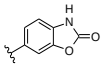	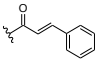	432.9	5.0	21.8	114	76.7±3.41

This material is reserved for educational use only, not allowed for commercial use.
Forbidden to modify the content, and cite the document when use.

27	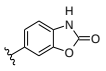		379.2	3.21	11.8	96.4	43.1±3.43
28	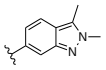		435.9	4.74	8.60	44.4	59.2±3.27
29	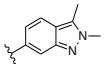		433.9	4.80	12.7	76.6	97.8±5.80
30	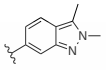	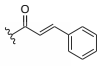	510.0	6.40	7.4	61.3	65.6±3.25
31	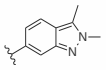		456.3	4.58	8.0	44.5	78.9±5.13
	Erlotinib		393.4	3.20	-	77.6	20.5±3.65
	Osimertinib		499.6	3.00	-	78.2	36.5±4.06
	Rociletinib		555.6	4.10	-	66.7	636±12.8

[a] calculated using ChemAxon JChem for Excel version 21.15.705 [216].

4.1.2 Design

The kinase domain (KD) of receptor tyrosine kinases (RTK) such as EGFR is comprised of two lobes. The smaller N-terminal lobe mainly consists of beta-strands and a single large alpha-helix, and the larger C-terminal lobe is almost exclusively α-helical (Figure 2a). The ATP-binding site is located at the point between the two lobes resulting in an active site that is dynamic in size and shape [217]. The binding mode of the chemotype under investigation is shown to bind to T790M EGFR enzyme (Figure 42). The predicted binding conformation of inhibitor **21** shows the same characteristic interactions with the EGFR active site as seen in Rociletinib (PDB 5XDK) and related ligands [218, 219]. The pyrimidine-2-amine core forms a bidentate H-bond interaction with the hinge residues, while the 5-position chlorine of pyrimidine points toward the mutatable gatekeeper residue at position 790 (Figure 42 b and c).

This material is reserved for educational use only, not allowed for commercial use.
Forbidden to modify the content, and cite the document when use.

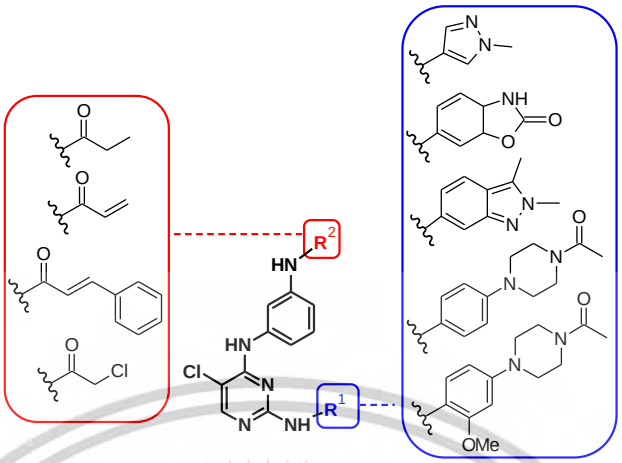

Figure 41. Scope of the scaffold modifications

The first change to the Rociletinib scaffold we undertook was to replace the 5-pyrimidine CF_3 with a smaller, less lipophilic Cl atom. Indeed, Ward et al[132] investigated the effect of -H, -F, -CH_3, -Cl, and -S(=O)CH_3) groups at the 5-pyrimidine position of Osimertinib-like inhibitors of EGFR, finding -Cl led to the most potent and selective EGFR inhibitors. This finding is also consistent with other related EGFR inhibitor scaffolds, [10, 86, 121, 220] as exemplified by compound **A**[221] (Figure 43). A further advantage of this modification is an almost 1 log unit drop in predicted logP [216].

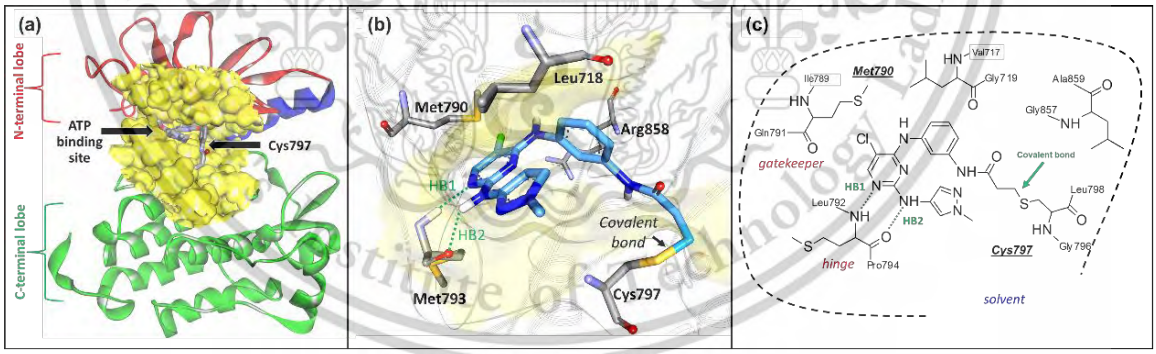

Figure 42. (a) Catalytic domain of protein kinases. showing the N-terminal lobe (red) and the C-terminal lobe (green) and the binding site (yellow),[51] (b) The predicted binding mode of compound 21 to T790M EGFR kinase (PDB ID: 5XDK) and (c) 2D schematic representation.

The effect of modifying the 2-methoxy-4-piperazinylaniline found at the R^1 position of Rociletinib was also undertaken. Several different heterocycles have been studied, each

This material is reserved for educational use only, not allowed for commercial use.
Forbidden to modify the content, and cite the document when use.

varying in terms of their size, shape, H-bonding characteristics, and overall lipophilicity (Figure 3). For example, the small, polar *N*1-methyl-4-aminopyrazole ring has shown to be well tolerated in EGFR [222, 223] (i.e. B, Figure 43) and leads to an overall reduction in logP of ~0.5. Modification to a small ring such as benzoxazol-2-one or 2,3-dimethyl-indazole rings is also expected to be tolerated within the ATP binding site [224-226] although unlike *N*1-methyl-4-aminopyrazole ring, the former modification has a negligible effect on logP, while the latter affords approximately 1 log unit increase. Finally, the effect of replacing the 2-methoxy group with hydrogen (i.e. giving 4-piperazinylaniline) was also investigated.

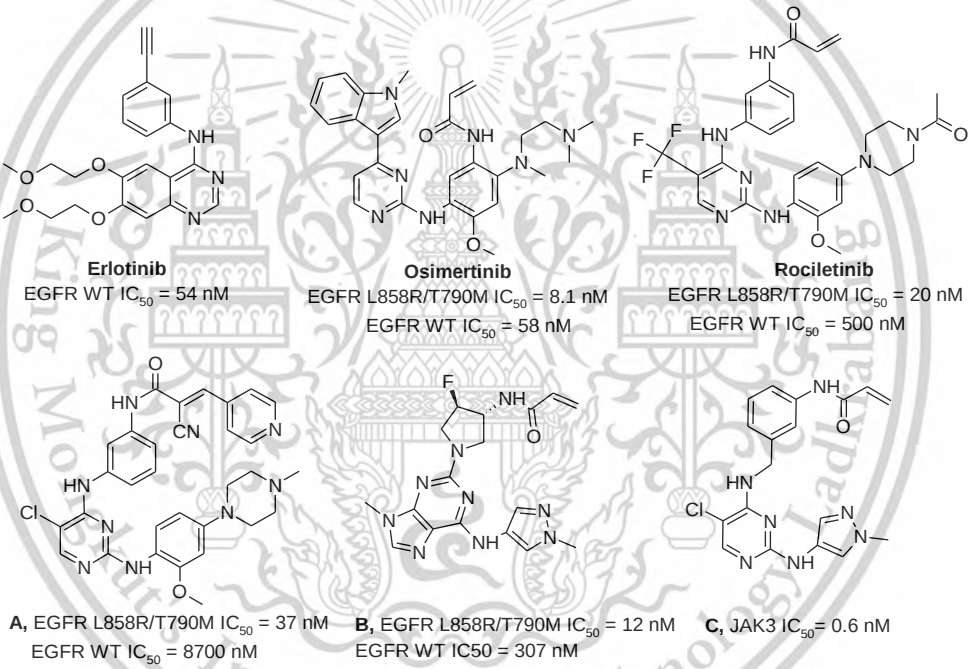

Figure 43. EGFR inhibitors Erlotinib[8, 227], Osimertinib[6, 228], Rociletinib[229, 230], and a selection of early development compounds targeting A: EGFR[221], B: EGFR[222] and C: JAK3[231].

At the R^2 position (Figure 41), we have incorporated different electrophilic groups that can react with the nucleophilic Cys797 residue. This includes acrylamide, one of the most common suicidal inhibitor electrophiles,[167] as well as 2-chloroacetamide[168] and (2*E*)-3-phenylprop-2-enamide. The unreactive propenamide moiety was also prepared for the purpose of comparison.

This material is reserved for educational use only, not allowed for commercial use.
Forbidden to modify the content, and cite the document when use.

4.1.3 EGFR WT Inhibition

All compounds were evaluated for their activity against EGFR WT at a concentration of 1 μM. %inhibition (%I) values ranged from 44.4 to 114% (Table 3). The %I of 18 compounds was shown to be greater than 50%. In addition, the %I values of 11 compounds were found to be greater than those of the EGFR drugs tested, namely Erlotinib, Osimertinib, and Rociletinib.

The IC_{50} of Compounds **12-31** were subsequently tested against EGFR WT with IC_{50} values ranging from 22.6 to 174 nM (Table 3). Compound **15** had the lowest IC_{50} at 22.6 nM, followed by **20** at 35.0 nM and **23** at 41.6 nM. The values obtained for Erlotinib and Osimertinib were 20.5 and 36.5 nM, respectively. In contrast, the value for Rociletinib was 636 nM. This weak activity towards the WT enzyme is in line with other reports,[111] a result of the molecule being specifically designed to selectively target the T790M mutant compared to the WT.

At the R^1 position, the 2-methoxy-4-piperazinylaniline and the *N*1-methyl-4-aminopyrazole ring generally resulted in better activity than other rings. The most potent compound, **15,** has the former ring, and the second most potent compound, **20**, has the latter.

The R^2 position SAR, arising from the electrophilic groups, revealed no significant activity differences overall. Compound **15** with a 2-chloroacetamide electrophile resulted in the best overall EGFR WT activity at 22.6 nM, being 28-fold greater than Rociletinib (636 nM). However, compound **20**, which is incapable of covalent bond formation with Cys797, also displayed good activity at 35.0 nM. The most active acrylamide was **17**, with an IC_{50} of 43.6 nM while the most potent (2*E*)-3-phenylprop-2-enamide was **22** at 44.8 nM.

4.1.4 EGFR T790M/L858R Inhibition

The most potent compounds against WT EGFR were selected for further testing against the T790M/L858R double-mutant (DM). Compounds **15**, **17**, **20**, **21**, **22**, **23,** and **27**, having WT IC_{50} < 50 nM were evaluated along with the 3 EGFR drug standards (Table 4). The IC_{50} of the compounds ranged from 18.9 to 69.7 nM. The most potent compounds, **20**, **21**, **22**, containing a *N*1-methyl-4-aminopyrazole ring, were found to be the most active

This material is reserved for educational use only, not allowed for commercial use.
Forbidden to modify the content, and cite the document when use.

of the compounds against the mutant enzyme, with IC_{50} of 18.9, 20.7 and 22.8 nM, respectively. The compounds were also found to be more active against the mutant than the WT enzyme with SI values (ratio of the IC_{50}) of 1.9, 8.4, and 2.0 respectively (Table **4**).

Osimertinib, Rociletinib, and Erlotinib displayed double mutant IC_{50} of 13.5, 51.7, and 20.5 nM. The SI values of the molecules were 2.7, 52, and 0.78 respectively. These results confirm that compounds **20**, **21,** and **22** have comparable activity levels and selectivity to that of the marketed drug Osimertinib. Interestingly, **20** is essentially equipotent to **21** and **22** despite having no electrophilic group.

In summary, four inhibitors displayed IC_{50} < 25 nM against the T790M/L858R EGFR enzyme including Osimertinib, and three *N*1-methyl-4-aminopyrazole containing derivatives, **20-22**. Rociletinib is a clear outlier, having a distinctly different EGFR inhibition profile,[111] being a very weak inhibitor of the WT enzyme, and only a moderate inhibitor of the double mutant, which might account for issues in clinical development. Despite this, other factors such as selectivity towards related kinases, physical properties, etc, are important for compound progression in drug discovery.

Covalent docking using GOLD5.3[198] was undertaken to try and rationalize the preference of **21** for the mutant EGFR enzyme. The molecule was docked to the active site of the WT enzyme (1M17)[196] and to one containing the active site T790M mutation (5XDK) [197]. Goldscores of 33.2 and 37.3, respectively, were obtained indicating **21** appears to bind preferentially to the T790M, in-line with the experimental observation. Analysis of the docked structures (Figure 44) results in a distinct shift in the ligand position (RMSD ~1.38Å) towards the rear of the ATP binding site due to the interaction with residue 790 which also impacts the trajectory of the electrophile–Cys797 interaction.

This material is reserved for educational use only, not allowed for commercial use.
Forbidden to modify the content, and cite the document when use.

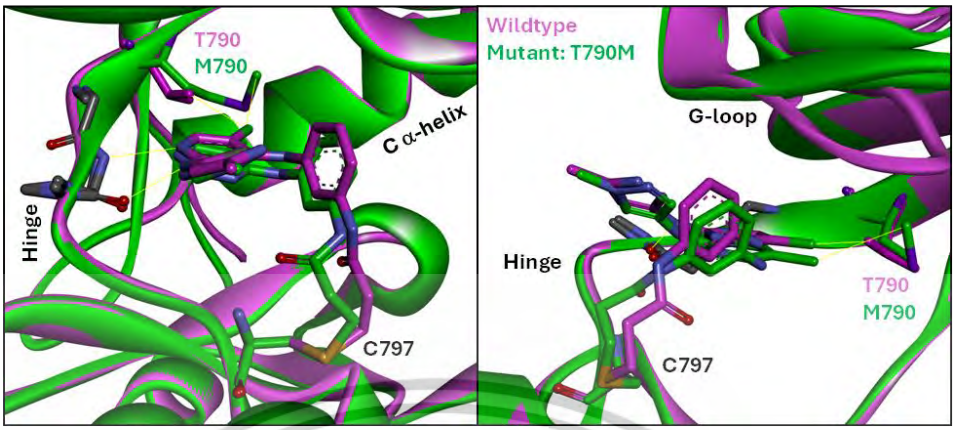

Figure 44. Covalent docking of 21 to wild-type (1M17) and T790M mutant EGFR (5XDK). Goldscores of 33.2 and 37.3, respectively, were obtained indicating **21** appears to bind preferentially to the T790M active site, in-line with our experimental observation.

4.1.5 JAK3 Inhibition

JAK3 is a kinase with approximately 55% KD sequence similarity to EGFR and contains a reactive cysteine residue at the same location on its kinase domain [232]. Indeed, compound **C,** as shown in Figure 43, is structurally related to the majority of compounds identified here against the double mutant EGFR (**20-22**), primarily differing at the 4-position of pyrimidine through the replacement of the 3-substituted aniline in the former with a benzyl equivalent in the latter. This suggested that counter-screening against JAK3 is warranted. To this end, the most potent inhibitors containing the preferred *N*1-methyl-4-aminopyrazole ring (**20-23**) were assessed against JAK3 (Table **4**). We found Erlotinib, Osimertinib, and Rociletinib were also potent inhibitors of JAK3 with IC_{50} values of 14.1, 35.3, and 4.3 nM respectively. This is compared to IC_{50} values of 31.7, 69.5, 8.0, and 911 nM obtained for compounds **20-23**, respectively. The JAK3 inhibitor Tofacitinib displayed an IC_{50} value of 3.7 nM.

The data shows the most selective EGFR inhibitor to be **23**, with an SI of 19, followed by **21,** with a value of 3.4, and Osimertinib with a value of 2.6. The SI value for Rociletinib was found to be just 0.08. The greater selectivity for **23** appears to arise due to the 2-chloroacetamide electrophilic group. Interestingly, this increased selectivity could arise due to its S_N2 reactivity, rather than Michael addition, or be a result of non-bonded

This material is reserved for educational use only, not allowed for commercial use.
Forbidden to modify the content, and cite the document when use.

interactions within the enzyme. This prompted us to investigate the intrinsic reactivity of the different electrophiles which we discuss later.

4.1.6 Cell Cytotoxicity

The cytotoxic activity of compounds with WT EGFR activity < 50 nM was assessed in EGFR overexpressing cell lines (A549, A431) as well as in the non-EGFR over-expressing HepG2 liver cell line. Compounds showed the greatest cytotoxic activity against A549 cells followed by A431, with HepG2 cells being least susceptible to the compounds. Rociletinib, **17** and **21** exhibited sub-micromolar cytotoxic activities in A549 cells with IC_{50} values of 0.20, 0.23 and 0.79 μM, respectively. Only Rociletinib exhibited sub-micromolar activity against the A431 cell line (0.32 μM).

Interestingly, the failed clinical candidate Rociletinib displayed the best selectivity for EGFR-expressing A549 cells compared to HepG2 (SI=36.9). Marketed drugs Osimertinib and Erlotinib displayed no selectivity, 0.35 and 1.2, respectively.

Of the novel compounds reported here, **20**, has the best selectivity, with SI values of 10.2, followed by **17** with an SI of 4.7 and **21** with an SI of 4.1. Interestingly, the most selective compound **20**, possesses a non-reactive propenamide, which might be expected to be more non-specific

4.1.7 Physicochemical properties.

The experimental octanol/phosphate buffer partition coefficient ($logD_{7.4}$) and phosphate buffer solubility were determined using a shake flask technique (Table **4**). Compounds containing a *N*1-methyl-4-aminopyrazole ring (**20**, **21,** and **23**) showed the lowest experimental $logD_{7.4}$ (2.6-2.9), lower than marketed drugs Erlotinib (3.09), Rociletinib (3.2) and Osimertinib (3.4). **22**, which incorporates a large (2*E*)-3-phenylprop-2-enamide electrophile has the highest of all logDs at 4.2. Rociletinib was found to display the best phosphate buffer solubility of all compounds (221 μg/ml), presumably due to the disruption of p-stacking in the crystal lattice by the bulky CF_3 group. Of the compounds prepared here, **23** (183 μg/ml), **21** (109 μg/ml), and **21** (80 μg/ml) were the best, being approximately 2-8 fold more soluble than Osimertinib (30 μg/ml) and Erlotinib (21 μg/ml).

This material is reserved for educational use only, not allowed for commercial use.
Forbidden to modify the content, and cite the document when use.

Table 4. Follow-up profiling of the most promising compounds based on the initial EGFR WT activity.

ID	EGFR WT IC_{50} (nM)	EGFR DM T790M/L858 R IC_{50} (nM)	SI EGFR T790M/ L858R	JAK3 IC_{50} (nM)	SI JAK3 Vs EGFR DM	A549 IC_{50} (μM)	A431 IC_{50} (μM)	HepG2 IC_{50} (μM)	SI A549 vs HepG2	Sol. (μg)	logD $pH_{7.4}$
20	35.0±3.88	18.9±4.28	1.85	31.7±0.70	1.67	2.77±0.04	11.2 ±0.25	28.3 ±1.77	10.2	80.1	2.67
21	174±6.63	20.7±4.16	8.44	69.5±28.3	3.35	0.79 ±0.01	6.39±0.04	3.25 ±0.16	4.11	109	2.86
22	44.8±2.28	22.8±4.13	1.95	8.0±3.50	0.35	1.48±0.01	10.5±1.16	3.65±0.25	2.46	1.35	4.18
23	41.6±5.23	47.8±6.65	0.87	911±416	19.0	2.78±0.13	3.70±0.01	4.30±0.02	1.54	183	2.60
15	22.5±3.18	56.8±3.29	0.39	-	-	5.78±0.35	7.05±0.39	12.6±0.01	2.18	8.65	3.67
17	43.6±4.48	69.7±5.42	0.62	-	-	0.23±0.49	3.47±0.02	1.07±0.01	4.65	13.4	3.18
27	43.1±3.43	63.2±6.11	0.68	-	-	7.29±0.47	7.46±0.30	7.06±1.15	0.96	15.4	3.51
Erlotinib	20.5±3.65	26.0±4.69	0.78	14.1±0.30	0.54	11,1±0.11	12.3±0.14	13.5±0.27	1.21	20.6	3.09
Osimertinib	36.5±4.06	13.5±4.61	2.69	35.3±4.30	2.61	10.2±2.29	7.21±2.66	3.65±0.03	0.35	30.1	3.43
Rociletinib	636±12.8	51.7±8.33	12.9	4.30±2.20	0.08	0.20±0.002	0.32±0.01	7.39±1.11	36.9	221	3.18
Tofacitinib	-	-	-	3.7±0.60	-	-	-	-	-	-	-

DB = Double mutant

4.1.8 Mechanism of Action Studies on 21

Kinase inhibition via covalent bond formation is a two-step process that begins with the compound binding to the kinase, as represented by K_i, and ends with an inactivation step (k_{inact}) (Figure 45). Accordingly, the true potency of covalent inhibitors cannot be determined using only traditional IC_{50} as these do not account for the entirety of the two-step process of covalent bond formation [173, 233, 234]. Traditionally, the ratio of the k_{inact}/Ki is therefore used to distinguish between covalent inhibitors and non-covalent inhibitors against a target [233]. A sox-based substrate method to estimate the K_i and evaluate the inactivation rate for **21**. We also included the non-covalent inhibitor Erlotinib and covalent inhibitor Osimertinib as controls (Figure 45). Fitting of the data using standard kinetic methods led to the kinetic constants in Table 5 [213].

The k_{inact} of Erlotinib possessed was observed to be slow (1.14×10^{-8} s^{-1}) consistent with a reversible inhibitor. In contrast, both **21** and Osimertinib showed much faster rates at 6.16×10^{-1} s^{-1}, and 1.13×10^{-4}, respectively, confirming irreversible inhibition. However, it

This material is reserved for educational use only, not allowed for commercial use.
Forbidden to modify the content, and cite the document when use.

can be noted that the **21** displays an ~1000 fold faster off-rate than Osimertinib (1.13 x 10^{-4}).

The k_{inact}/K_i for Erlotinib was found to be 8.36 x 10^{-7} $M^{-1}s^{-1}$, confirming a covalent bond did not form. In contrast, the k_{inact}/K_i for Osimertinib was 3.04 x 10^3 $M^{-1}s^{-1,}$ and **21** was 1.62 x 10^2 $M^{-1}s^{-1}$, consistent with covalent bond formation. Tomassi et al,[235] previously reported the kinetic parameters of Rociletinib which showed a k_{inact}/K_i ratio of 4.0 x 10^4 $M^{-1}s^{-1}$ broadly in line with the values reported here for **21**.

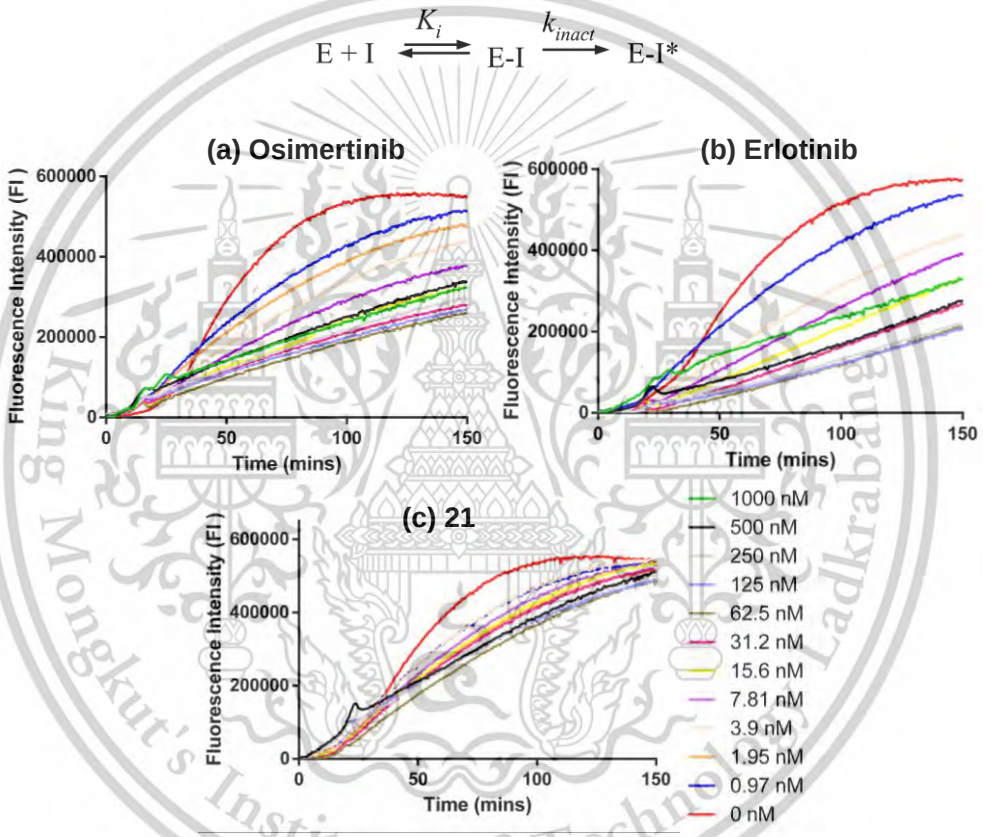

Figure 45. Determination of EGFR inactivation kinetic parameters[213] for (a) Osimertinib, and (b) Erlotinib and (c) 21.

In summary, the kinetic results obtained confirm that **21** displays kinetics consistent with a covalent mode of action.

This material is reserved for educational use only, not allowed for commercial use.
Forbidden to modify the content, and cite the document when use.

Table 5: Kinetic parameters for inactivation of Osimertinib, Erlotinib, and **21** against EGFR WT.

Compound	k_{inact}/Ki ($M^{-1}s^{-1}$)	K_i (M)	k_{inact} (s^{-1})
21	1.62×10^{2}	3.81×10^{-3}	6.16×10^{-1}
Osimertinib	3.04×10^{3}	3.74×10^{-8}	1.13×10^{-4}
Erlotinib	8.36×10^{-7}	1.37×10^{-2}	1.14×10^{-8}

4.1.9 QM Evaluation of Electrophile Reactivity

Finally, we wished to investigate any differences in reactivity between the different electrophiles used and to see if this could explain why the **15** (chloro-acetamide) was nearly 2-fold more active against WT EGFR than other derivatives, while **20** (propenamide) **21** (acrylamide) and **22** ((2*E*)-3-phenylprop-2-enamide) were essentially equipotent against the double mutant. To this end, we employed QM methods to assess the reactivity of the electrophiles used here. Such calculations have been used in the past to study the electrophilicity index on three common warheads [163-166]. A QM model consisting of each electrophile attached to aniline was created, undergoing reaction with methanethiol in the presence of a water molecule to facilitate the nucleophile generation step (Scheme 3).

We simulated 3 potential reactions with the thiol nucleophile, namely Michael addition to acrylamide (i.e. **21**) and (2*E*)-3-phenylprop-2-enamide (i.e. **22**) (Scheme 3,a) and S_N2 reaction for chloro-acetamide (i.e. **23**) (Scheme 3,b). Minima and transition state structures and energies were obtained using the Gaussian 16 program as described in detail elsewhere (Figure 46 and Figure 47) [236, 237].

The electrophile resulting in the lowest activation energy involved the S_N2 reaction of 2-chloroacetamide (28.1 Kcal/mol). The MA reaction that the acrylamide and (2*E*)-3-phenylprop-2-enamide were considerably higher at 38.2 and 42.5 kcal/mol, respectively. The latter result suggests the additional phenyl ring acts to reduce the electrophilicity of the group. The intermediate formed by the acrylamide is found to be the most exothermic at -20.3 kcal/mol, followed by (2*E*)-3-phenylprop-2-enamide at -14.2 kcal/mol. 2-

This material is reserved for educational use only, not allowed for commercial use.
Forbidden to modify the content, and cite the document when use.

chloroacetamide forms the least exothermic intermediate of the electrophiles, with an energy of -10.0 kcal/mol. Alternatively, if we focus on the off-rate of the inhibitors, which is governed by the reverse reaction. In this case, we would predict a reverse barrier to the reaction of 58.5 kcal/mol for acrylamide, 56.7 kcal/mol for (2*E*)-3-phenylprop-2-enamide, and just 38.1 kcal/mol for 2-chloroacetamide.

For comparison, we simulated the nucleophilic attack of the acyl of the propenamide acyl group (i.e. **20**) which leads to a tetrahedral intermediate (Figure 47) with a barrier of only 30.2 kcal/mol. However, the intermediate is highly endothermic and with a reverse barrier of just 15.2 kcal/mol. This confirms reactivity with Cys797 will be negligible compared to the other moieties.

The selection of a suitable electrophile is indeed challenging, being highly selective for a particular enzyme, having a relatively low barrier to forward reaction, and a higher reverse barrier. Indeed, Amaral et al. reported on the differences between acrylamide and 2-chloroacetamide and noted that the greater reactivity of 2-chloroacetamide might make it too non-specific and thus unsuitable for use in selective TKIs [167].

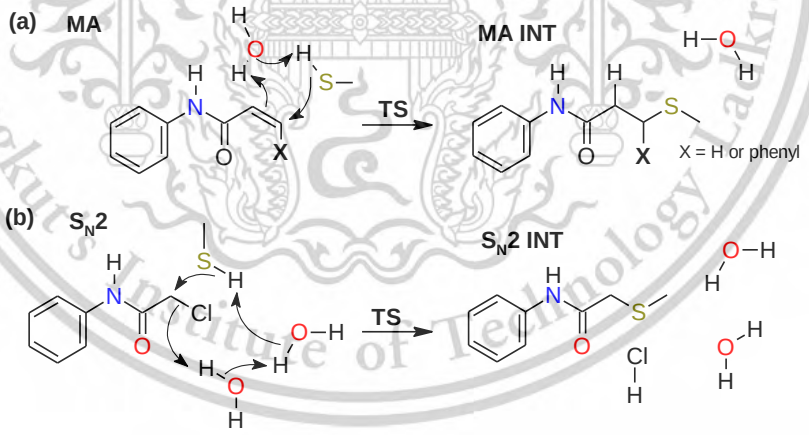

Scheme 3. (a) mechanism of Michael acceptor to form a covalent bond, and (b) mechanism of 2-chloroacetamide to form a covalent bond.

This material is reserved for educational use only, not allowed for commercial use.
Forbidden to modify the content, and cite the document when use.

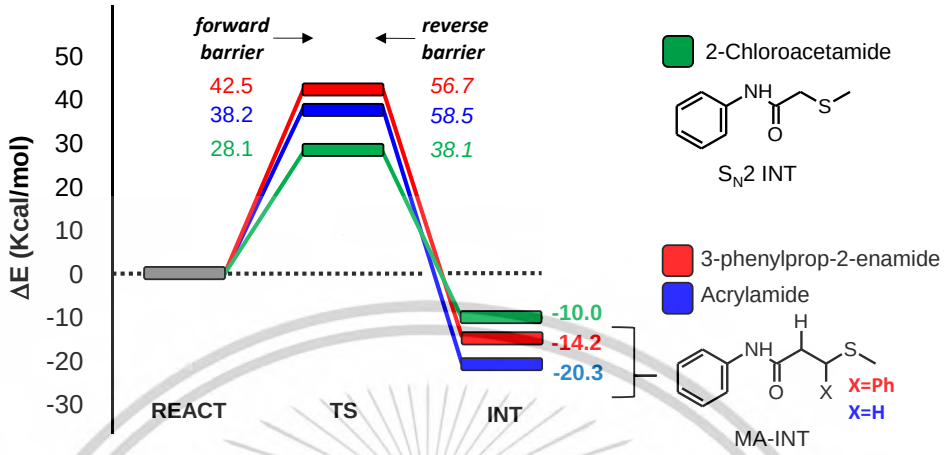

Figure 46. Reaction of a thiol nucleophile with inhibitor electrophilic group.

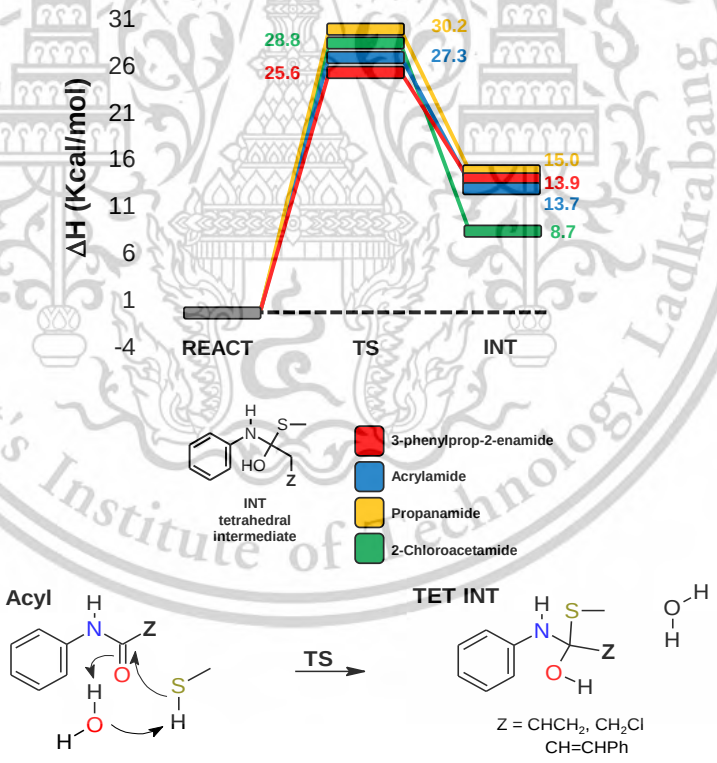

Figure 47. Reaction of a thiol nucleophile with inhibitor carbonyl group.

This material is reserved for educational use only, not allowed for commercial use.
Forbidden to modify the content, and cite the document when use.

4.2 Study 2: Molecular Dynamics Guided Design of N^4-(2-methyl-2H-indazol-6-yl)-N^2-phenylpyrimidine-2,4-diamine inhibitors targeting Cys797 and the T790M Gatekeeper Mutation.

4.2.1 Synthesis Results

All compounds were prepared according to synthetic routes described in Scheme 2. Compounds **32-33** were prepared from the reaction of pyrimidines and 2-Methyl-2H-indazol-6-amine with $NaHCO_3$ as basic in ethanol, at 80 °C, for 6 hrs, in a yield of 70-90%. Compounds **32-33** were then reacted with amine performed under TFA as the acidic condition in isopropyl alcohol at 90 °C for overnight to give compounds **34-41** with yields ranging from 70-90%. Compounds **36-41** were hydrogenated using $SnCl_2$ in ethanol at 80 °C for 6 hrs, or Pd/C in methanol at RT for 6 hrs, to give compounds **42-47** with yields ranging from 50-80%. The final compounds **48-81** were achieved using Acid chloride, DIPEA in anhydrous DCM at 0°C for 30 mins with yields ranging from 20-60% or Carboxylic acid, DCC in anhydrous DCM at RT for 1 hr with yields ranging from 20-41%.

All of the final compounds (Table 6) were confirmed using ^{1}H NMR spectroscopy and High-resolution mass spectra (HRMS) accounting for more detail of each compound. In addition, the purity of the compound is investigated by HPLC as more than 95% pure.

This material is reserved for educational use only, not allowed for commercial use.
Forbidden to modify the content, and cite the document when use.

Table 6. 48-81 and standard assessed in this study. Reported are R-groups, physical properties, and yields.

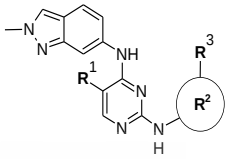

ID	R^1	R^2	R^3	MW	LogD[a]	Yield % overall	%Inh. 1 uM	EGFR WT IC_{50} / nM	EGFR DM IC_{50} / uM	SI for DM ove WT
48	H			401.4	3.65	21	62	45.5 ± 2.94	19.0 ± 3.37	2.3
49	H			399.4	3.70	14	71	6.54 ± 3.21	10.1 ± 2.82	0.6
50	H			475.5	5.31	53	86	3.03 ± 2.70	5.57 ± 3.71	0.5
51	H			421.8	3.48	18	90	15.9 ± 2.90	3.00 ± 2.99	5.3
52	H			411.1	4.19	20	87	12.5 ± 3.27	4.66 ± 2.97	2.6
53	Cl			435.9	4.25	38	94	33.3 ± 2.91	34.3 ± 3.19	0.9
54	Cl			433.9	4.31	13	60	12.7 ± 2.84	4.78 ± 2.76	2.6
55	Cl			510	5.91	16	84	6.69 ± 2.92	10.9 ± 3.06	0.6
56	Cl			456.3	4.09	21	34	49.6 ± 2.71	N/D	N/A
57	Cl			445.9	4.79	22	48	666 ± 3.59	N/D	N/A
58	H			387.5	3.94	15	78	39.7 ± 3.30	760 ± 3.26	0
59	H			385.4	4.00	11	41	89.2 ± 3.25	54.5 ± 3.38	1.6
60	H			461.5	5.60	35	83	32.1 ± 3.48	N/D	N/A
61	H			407.8	3.78	5.1	75	48.6 ± 3.53	N/D	N/A
62	H			397.4	4.48	9.4	84	27.7 ± 3.14	N/D	N/A
63	Cl			421.8	4.54	14	42	631 ± 4.04	111 ± 3.74	5.6

This material is reserved for educational use only, not allowed for commercial use.
Forbidden to modify the content, and cite the document when use.

ID	R^1	R^2	R^3	MW	LogD[a]	Yield % overall	%Inh. 1 uM	EGFR WT IC_{50} / nM	EGFR DM IC_{50} / uM	SI for DM ove WT
64	Cl			419.8	4.60	4.4	94	20.6 ± 3.28	4.72 ± 3.18	4.3
65	Cl			495.9	6.20	11	85	34.4 ± 3.20	N/D	N/A
66	Cl			442.3	4.38	10	88	15.3 ± 3.43	6.37 ± 3.68	2.4
67	Cl			431.8	5.08	2.9	68	18.3 ± 2.39	101 ± 3.43	0.1
68	H			417.4	3.78	4.0	98	12.4 ± 3.59	1471 ± 3.51	0
69	H			415.4	3.84	3.7	87	10.5 ± 2.96	51.0 ± 2.84	0.2
70	H			491.5	5.44	12	55	1534 ± 3.06	N/D	N/A
71	H			427.4	4.33	8.1	63	50.1 ± 2.97	N/D	N/A
72	Cl			451.9	4.39	22	72	14.7 ± 2.65	2.51 ± 2.96	5.8
73	Cl			449.9	4.44	15	66	29.2 ± 3.11	6.35 ± 3.16	4.5
74	Cl			526.0	6.04	14	85	54.7 ± 2.88	N/D	N/A
75	Cl			461.9	4.93	12	47	512 ± 3.46	N/D	N/A
76	H	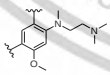		517.6	2.49	7.4	96	22.8 ± 2.58	40.1 ± 2.38	0.5
77	H	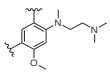		515.6	2.49	3.2	72	58.8 ± 3.36	156 ± 3.19	0.3
78	H	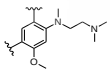		527.6	2.98	2.4	58	19.3 ± 2.94	39.6 ± 3.26	0.4
79	Cl	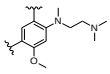		552.0	3.09	3.8	62	53.9 ± 2.64	3.04 ± 2.25	17

This material is reserved for educational use only, not allowed for commercial use.
Forbidden to modify the content, and cite the document when use.

ID	R^1	R^2	R^3	MW	LogD[a]	Yield % overall	%Inh. 1 uM	EGFR WT IC_{50} / nM	EGFR DM IC_{50} / uM	SI for DM ove WT
80	Cl	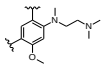		550.0	3.09	5.4	76	40.9 ± 2.56	1.92 ± 2.80	21
81	Cl	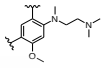		562.0	3.58	4.2	71	48.0 ± 3.44	N/D	N/A
	Erlotinib			393.4	3.20	-	100	5.88 ± 3.15	52.7 ± 2.86	0.1
	Osimertinib			499.6	3.00	-	97	22.1 ± 2.71	9.32 ± 3.91	2.3

[a] calculated using ChemAxon JChem for Excel version 21.15.705 [216].

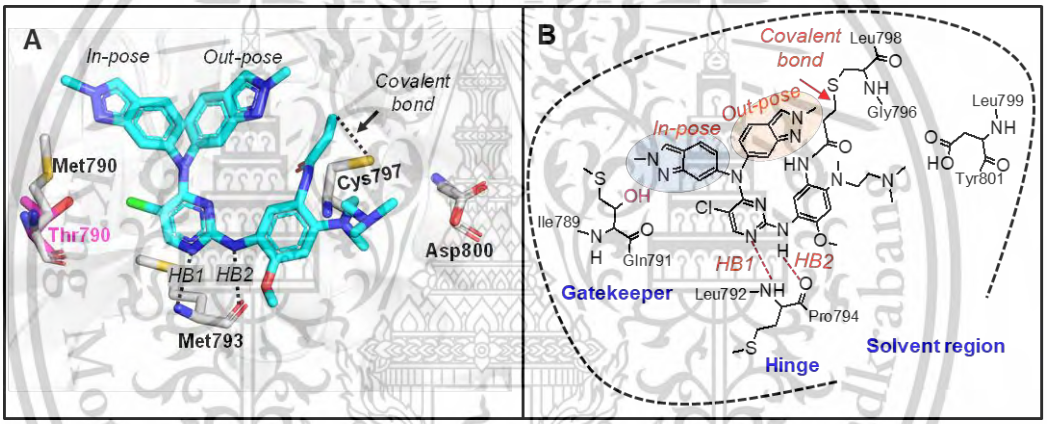

Figure 48. The MD simulation at 10 ns of **80** with in- and out-pose to T790M EGFR kinase (PDB ID: 6JX4) (A) The 3D structure showing interaction in the active site (B) The 2D structure showing interaction in the active site.

4.2.2 Design

In this work, we proposed the development of a novel series of EGFR inhibitors. The new inhibitors of EGFR have been developed based on the 2,4-diaminopyrimidine scaffold exemplified by Osimertinib (Figure 50). The scope of the synthetic modification in this study is shown in Figure 49. Additional alterations have been incorporated into the 2- and 5-position of the pyrimidine ring.

A) The 2-methyl-2*H*-indazol-6-amine on the 2-position of pyrimidine was chosen for this study and it showed the lowest cLogD when compared to Erlotinib, Gefitinib,

This material is reserved for educational use only, not allowed for commercial use.
Forbidden to modify the content, and cite the document when use.

and Osimertinib at the same position (Figure 50). This heterocyclic group possibly forms a hydrogen-bond interaction with the Lys745 residue [238]. Yan et al. reported MD simulations of Osimertinib and suggested an in-pose with T790M EGFR but not with the WT EGFR at the gatekeeper [20]. This is similar to the previously reported complex crystal structure of Osimertinib with the WT EGFR (the phenyl moiety of the indole group points towards the opening/solvent side of the ATP-binding pocket) [21]. Thus, the 2-methyl-2H-indazol-6-amine possibly points to the "in" or "out" pose in the active site of EGFR depending on the gatekeeper residue and the effect of the B position. From this, molecular modeling has been used to predict the binding pose of the 2-methyl-2H-indazol-6-amine with EGFR T790M and EGFR WT.

B) 5-position Cl substitution was also investigated because it could force the 2-methyl-2H-indazol-6-amine (A-position) to out-pose because of its steric effect as well as hydrogen for comparison [192]. We also employed QM calculations to investigate this hypothesis.

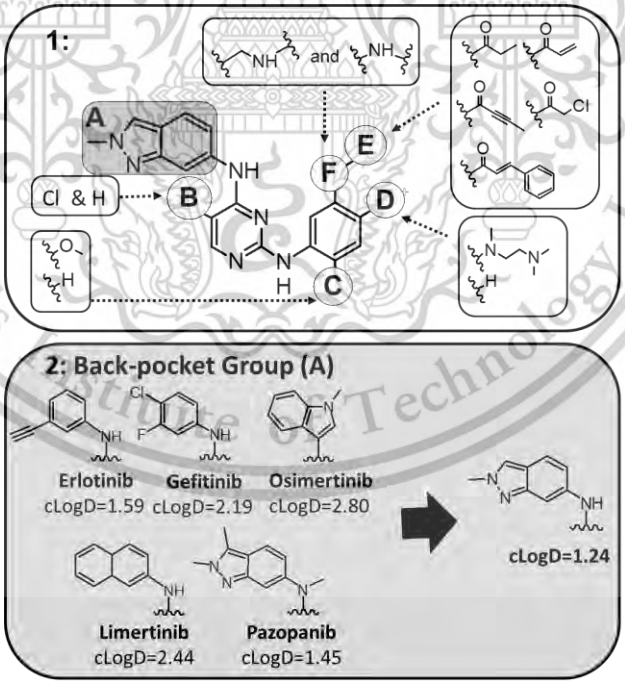

Figure 49. 1: Scope of the scaffold modifications,
2: Optimization at the back-pocket of EGFR.

This material is reserved for educational use only, not allowed for commercial use.
Forbidden to modify the content, and cite the document when use.

C) The effect of replacing the 2-methoxy group with hydrogen was also investigated to investigate the selectivity for EGFR. The bulky OMe forces the aniline ring non-planar to easily form a covalent bond common in many EGFR inhibitors [132, 239].

D) The N^1, N^1, N^2-trimethylethane-1,2-diamine was also synthesized because it was directed toward the solvent region leading to a general improvement in physicochemical properties.

E) The variation of electrophilic groups at the 2-position of the pyrimidine ring was explored by targeting the Cys797 residue in the ATP binding site via the formation of a covalent bond (Figure 51) including acrylamide [167-170], but-2-ynamide [170], 2-chloroacetamide[167-169], (2E)-3-phenylprop-2-enamide as well as the non-electrophilic propenamide[169] group for comparison.

F) Replacement of 2-pyrimidine aniline with benzyl-amine to assess the effect on EGFR WT and T790M activity, the effect on the electrophilicity of warheads, and the effect on physicochemical properties (increased SP3 character). This investigation is novel for EGFR inhibitors.

The Inhibitor design was achieved using SAR data extracted from the ChEMBL database (https://www.ebi.ac.uk/chembl/) and EGFR-inhibitor structural data taken from the RCSB database (www.rcsb.org). In total, 34 compounds have been prepared according to Figure 49. The activity of compounds against EGFR wildtype, T790M & L858R double mutant, and a selection of EGFR over-expressing cell lines have been obtained.

This material is reserved for educational use only, not allowed for commercial use.
Forbidden to modify the content, and cite the document when use.

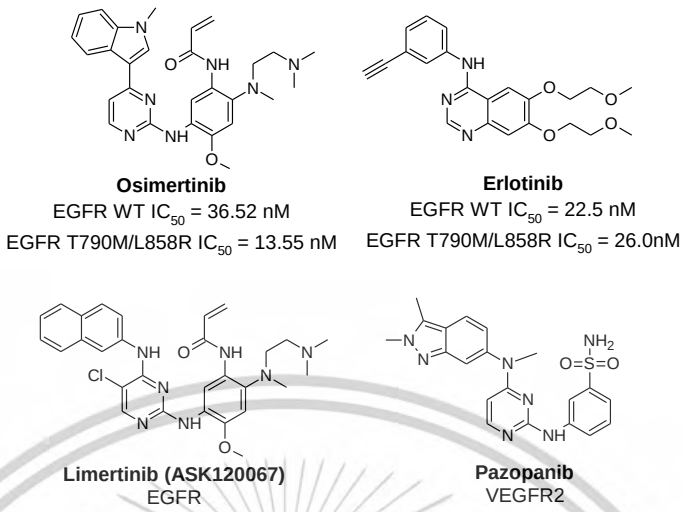

Figure 50. Structures of related drugs and EGFR development compounds: Osimertinib[5-7], Erlotinib[8], Limertinib[9, 10] and Pazopanib[11].

4.2.3 QM simulations

The QM methods employed the M06-2x/6-31G* methods in Gaussian G16 rev. C02 to explore the relative energy of two-low energy conformations of the indazole ring on the 4-position of pyrimidine relative to the 5-pyrimidine with -Cl or -H. Experimental analysis of x-rays shown in Figure 48. that the indazole ring could point "in" or "out" of the pocket and the presence of Cl and H would dramatically influence the relative orientation of the indazole ring. Our results showed that the H substituent showed a marginal preference (Figure 52) to the in-pose and the Cl substituent forced the indazole ring to preferentially adopt to the out-pose due to a steric hindrance. These differences were then compared with those obtained in the EGFR protein using MD.

We have also employed the QM methods to explore the relative reactivity of the different electrophiles and to explore the effect of aniline versus benzyl on the electrophile reactivity (Figure 51 and Scheme 4). 2-chloroacetamide was predicted to have the lowest barrier but formed at the least stable covalent intermediate while the but-2-ynamide formed the lowest energy intermediate and comparable barrier as acrylamide. (2E)-3-phenylprop-2-enamide showed less reactive and less exothermic compared to acrylamide. In terms of the linker, the benzyl had a minor effect on the barrier and intermediate energies that barriers and intermediates were slightly more favorable than

This material is reserved for educational use only, not allowed for commercial use.
Forbidden to modify the content, and cite the document when use.

aniline, except in the case of 2-chloroacetamide. Benzyl with but-2-ynamide formed the lowest energy intermediate and comparable barrier as acrylamide.

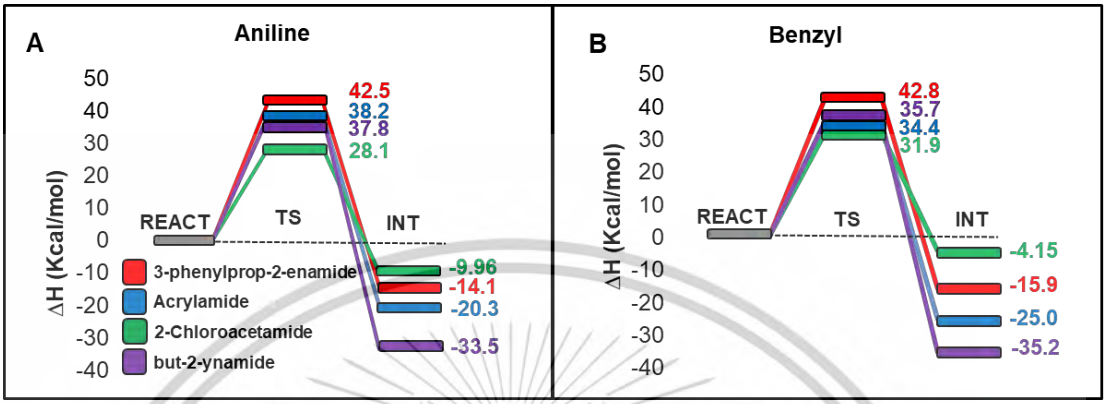

Figure 51. QM calculation results (A) barrier to reaction of aniline, (B) barrier to reaction of benzyl.

4.2.4 MD simulations

MD simulations were undertaken to study the SAR of the designed molecules to both WT and T790M EGFR in terms of A-E.

A. Compare the results with EGFR drugs Erlotinib and Osimertinib.

B. Assess the strength of key H-bond between inhibitor and EGFR.

C. Assess the interaction of indazole, 5-pyrimidine Cl, and H with T790 and M790 EGFR.

D. Determine the nucleophile and electrophile distance between Cys797 and electrophilic groups and the effect of benzyl versus aniline linkers.

E. Assess protein and ligand RMSD as a guide to binding mode stability.

EGFR WT structure was taken from PDB: 1M17[240] which contained Erlotinib with a back-pocket aniline ring in the "in" pose and EGFR T790M structure was taken from PDB: 6JX4[241] which contained Osimertinib with a ring in the "out" pose at the back pocket of EGFR. In these investigations, we have calculated the 2 modules.

1. Erlotinib and Osimertinib simulated the "in" and "out" pose for the comparison.
2. **49**, **54**, **77,** and **80** with indazole simulated the "in" and "out" pose.

This material is reserved for educational use only, not allowed for commercial use.
Forbidden to modify the content, and cite the document when use.

The binding poses of Osimertinib with EGFR WT and T790M remain unclear. The investigation of the spontaneous association with EGFR kinases having WT and T790M mutant gatekeepers was observed by using MD simulations. Yosaatmadja et al. and Yan et al. previously reported the out-pose of the indole group that pointed towards the opening/solvent side of the ATP-binding pocket of EGFR WT [241, 242]. The in-pose of the indole ring from the Osimertinib was suggested in binding with T790M mutation because this brought the warhead of the compound closer to EGFR Cys797 [241]. Our results showed that Osimertinib and Erlotinib bound within the pocket with relatively low ligand and protein RMSD (Figure 53) and formed at least one strong H-bond (Figure 53 and Figure 54) with the hinge regain. The RMSD of ligand (Figure 53 and Figure 54) and a short distance from H-bond (Figure 54) collected with the original inhibitor showed the best results as expected that Erlotinib preferred the in-pose in EGFR WT and Osimertinib preferred the out-pose in EGFR T790M shown in Figure 53 and Figure 54 A&B.

The indazole in 5 H-pyrimidine (**49** and **77**) binds comparably well to the WT and T790M EGFR shown in Figure 54 C&E. There was little difference between the in and out poses of 77 from the RMSD of ligand (Table 7). However, the out-pose was more preferred with the lowest RMSD and strong H-bond (Table 7). In terms of **49** with the benzyl-linker, the in-poses in both proteins were preferred due to the steric interaction of the CH_2-linker with the lowest RMSD. Table 7 revealed that the 5 H-pyrimidine could bind and react with the Cys797 nucleophile in both WT and T790M proteins given the short C-S distances (less than 4.5 Å). The indazole in 5 Cl-pyrimidine (**54** and **80**) showed a clear preference for binding to the T790M protein with the low RMSD of the backbone (Figure 54 D&F), indicating the need for further investigation with respect to EGFR activities for investigation of the stability of Cl at the gatekeeper region in the EGFR kinases. The out-pose in both proteins was preferred due to the steric interaction of Cl with the 790-gatekeeper residue with the lowest RMSD of ligand (Table 7) and the strong H-bond (Table 7) when compared to those of the in-pose. This was also supported by the QM calculation results. In Table 7, it also appeared that the 5 Cl-pyrimidine could only react with the Cys797 nucleophile in T790M proteins given the short C-S distances (less than 4.5 Å).

This material is reserved for educational use only, not allowed for commercial use.
Forbidden to modify the content, and cite the document when use.

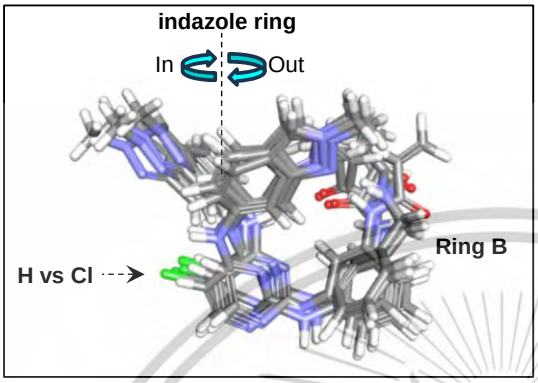

Comp.	Conf.	ΔE / kcal/mol (Aniline)	ΔE / kcal/mol (Benzyl)
-H (49&59)	In	0.00	0.00
	Out	0.69	0.51
-Cl (54&64)	In	5.45	5.77
	Out	0.00	0.00

Figure 52. Computational investigation of QM conformation in the gas phase.

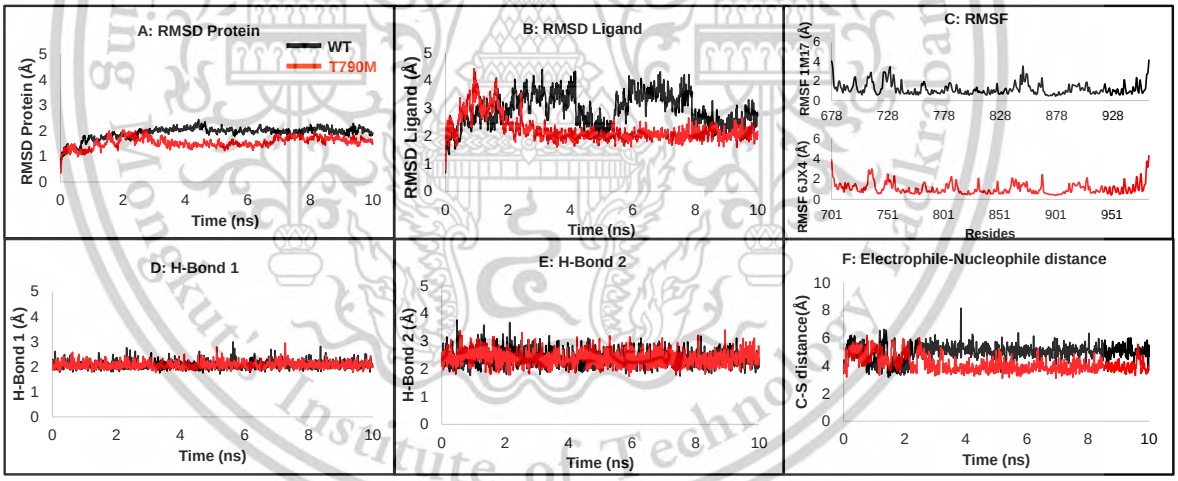

Figure 53. MD results of Osimertinib in the out-pose on EGFR WT vs T790M. (A) RMSD of protein (B) RMSD of Ligand (C) RMSF (D) H-bond 1 distance (E) H-bond 2 distance (F) Electrophile-Nucleophile distance.

This material is reserved for educational use only, not allowed for commercial use.
Forbidden to modify the content, and cite the document when use.

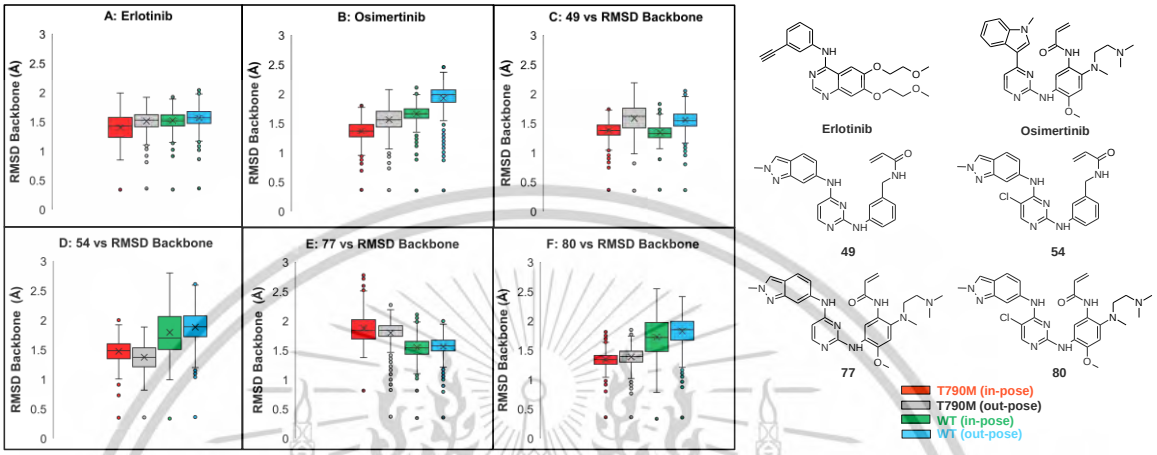

Figure 54. RMSD parameter of the backbone of different binding modes to EGFR T790M (PDB code: 6JX447) and EGFR WT (PDB code: 1M1746). (A) Erlotinib (B) Osimertinib (C) 48 (D) 54 (E) 77 (F) 80.

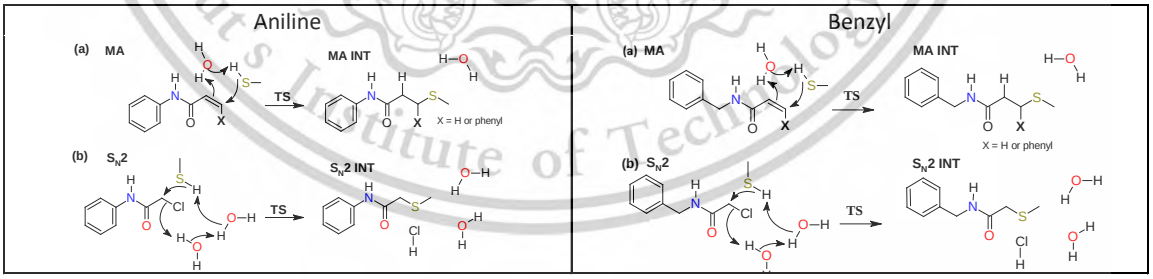

Scheme 4. Mechanism of QM Calculations on Barrier to Reaction.

This material is reserved for educational use only, not allowed for commercial use.
Forbidden to modify the content, and cite the document when use.

Table 7. MD calculation results. * indicated protein/ligand from original PDB

ID	EGFR	Indazole Conf.	HB1 (Å)	HB2 (Å)	C-S (Å)	RMSD ligand (Å)	RMSD protein (Å)
Erlotinib	WT*	in*	2.16	-	-	1.78	1.52
		out	2.21	-	-	2.78	1.57
	T790M	in	2.11	-	-	1.94	1.40
		out	2.20	-	-	2.44	1.51
Osimertinib	WT	in	2.14	2.53	4.41	2.88	1.66
		out	2.08	2.36	4.97	2.94	1.92
	T790M*	in	2.07	2.74	5.15	2.28	1.36
		out*	2.08	2.39	4.11	2.23	1.56
80	WT	in	2.14	3.07	5.19	2.81	1.82
		out	2.23	2.34	5.29	2.66	1.72
	T790M	in	2.11	2.65	4.27	2.69	1.34
		out	2.22	2.40	3.88	2.15	1.38
77	WT	in	2.05	2.59	5.16	2.86	1.54
		out	2.10	2.40	4.80	2.54	1.56
	T790M	in	2.06	2.72	4.36	2.71	1.87
		out	2.12	2.51	3.96	2.43	1.79
54	WT	in	2.12	2.59	6.11	1.96	1.79
		out	2.08	2.21	5.03	2.10	1.87
	T790M	in	2.21	2.37	4.03	2.62	1.47
		out	2.31	2.11	4.72	2.45	1.37
49	WT	in	2.10	2.36	4.62	1.76	1.34
		out	2.10	2.23	6.52	2.74	1.54
	T790M	in	2.08	2.37	5.23	2.05	1.37
		out	2.28	2.84	4.18	3.10	1.58

This material is reserved for educational use only, not allowed for commercial use.
Forbidden to modify the content, and cite the document when use.

4.2.5 EGFR WT Inhibition.

All compounds were evaluated for their activity against EGFR WT at a concentration of 1 μM. %inhibition (%I) values ranged from 34 to 98 (Table 6). The %I of 14 compounds was shown to be greater than 80%. In addition, the %I value of 5 compounds was found to be favorable to the EGFR drugs tested, namely Erlotinib and Osimertinib.

All 34 compounds were evaluated for EGFR WT (Table 6). The compounds displayed good activity against EGFR WT with IC_{50} values ranging from 3.03 and 1534 nM. Erlotinib and Osimertinib were chosen as standard compounds in our kinase assay. Osimertinib and Erlotinib were active against the EGFR WT with IC_{50} values of 22.1 and 5.88 nM, respectively. Compounds **49, 50,** and **55** were found to result in high EGFR WT activity. These compounds were incorporated with the benzyl or CH_2-NH-linker and compared favorably to Erlotinib which was strongly potent on EGFR WT. So, the benzyl-linker rings generally resulted in better activity than that of aniline. Compound **50**, which was incapable of covalent bond formation with Cys797, also displayed good activity at 3.03 nM. The most active acrylamide was **49**, with an IC_{50} of 6.54 nM while the most potent 2-chloroacetamide was **51** and **66** at around 15 nM and the most potent but-2-ynamide was **52** at 12.5 nM. There was no significant effect of Cl and H at the gatekeeper region on EGFR WT. However, Compound **50** was the best incorporated with H on 5-pyrimidine while compound **55** showed the best activity for the substitution with Cl in the same position. The incorporation of the methoxy group and basic center didn't affect increasingly the inhibitory compared to that of H at the same position.

4.2.6 EGFR DM Inhibition.

The 25 compounds (Table 6) were chosen to get the measurement for EGFR DM. Osimertinib was more active against the EGFR DM than Erlotinib (9.32 and 52.7 nM, respectively). From the results, 10 compounds were more potent than drugs compounds **50, 51, 52, 54, 64, 66, 72, 73, 79,** and **80.** These compounds covered all types of electrophilic groups that we were interested in and most of them were synthesized with Cl on the 5-pyrimidine. The substituent of Cl on 5-pyrimidine was more potent than H in contrast to WT activity, this was followed by the MD simulations that 5 Cl-pyrimidine

This material is reserved for educational use only, not allowed for commercial use.
Forbidden to modify the content, and cite the document when use.

preferred binding to the T790M protein with the low RMSD of the backbone. Compound **80,** incorporated with aniline on the linker, was the strongest activity with acrylamide as the electrophile. There was no statistical difference among EGFR activities of electrophilic groups at the 0.05 level of significance. However, the covalent inhibitors generally bind to the target longer and their effects are long-lasting. This could have a benefit in vivo assays in terms of the dose and half-life determination associated with pharmacokinetics (PK) [243]. Compounds that contained both aniline and benzyl linkers showed the same ranges of activity in double-mutant EGFR. Similar to EGFR WT activity, the substituent of the methoxy group and basic center didn't increase the potency compared to that of H at the same position.

The SI values suggested that Osimertinib-like molecules were generally better when compared to other analogs. The introduction of Cl and indazole ring at the back pocket ring gave a 10-fold better selectivity index (SI) for **79** and **80** over a 10-fold better than Osimertinib. From the T-test analysis, we found that the Cl compounds possessed the best SI for EGFR DM over EGFR WT when compared to that of H compounds. Of the best 13 compounds identified (Table 8), most of them showed better SI compared to Osimertinib and contained Cl on 5-pyrimidine which was more specific to EGFR DM. These compounds have been measured in further steps.

4.2.7 JAK3 Inhibition

We aim to develop a more selective EGFR inhibitor. The cysteine residue in EGFR is structurally equivalent to JAK3 which is unique among JAK family members in having a cysteine residue at the gatekeeper-plus-7 (GK+7) position [244]. This residue is Cys909 in JAK3 and Cys797 in EGFR. The cysteine residue has been successfully targeted by covalent kinase inhibitors that are now approved drugs including Osimertinib. The similarity of the whole sequence between EGFR (PDB ID: 5UWD) and JAK3 (PDB ID: 6DUD) is 55.4% while the similarity of the sequence at 8 Å active site is 61.7%.

In this work, 11 compounds were evaluated against JAK3 (Table 2). Compounds **48, 51, 52,** and **54** showed very strong inhibition for JAK3 (less than 10 nM) which was better than the JAK3 activity of Erlotinib and Osimertinib (17.0 and 22.2 nM, respectively).

This material is reserved for educational use only, not allowed for commercial use.
Forbidden to modify the content, and cite the document when use.

Those were synthesized with the benzyl-linker on position F (Figure 49) and compounds that comprised of aniline-linker in the same position displayed moderate activity to JAK3 (20-40 nM). The selectivity of **80** for EGFR DM over JAK3 was 21, which was over 8-fold higher than the selectivity of Erlotinib (SI=0.3), Osimertinib (SI=2.38) and other compounds (SI=0.2-11). Therefore, this compound was very selective to EGFR more than JAK3 when compared to drugs and other compounds.

4.2.8 Mode of Action Studies

Kinase inhibition via covalent bond formation is a two-step process that begins with the compound interacting with the kinase driven by affinity (represented by K_i) and ends with an inactivation step (k_{inact}) shown in Equation 1. Accordingly, the potency of covalent inhibitors cannot be determined using only traditional IC_{50} measurements because this does not account for the entirety of the two-step process of covalent bond formation [173, 233, 234]. Here, we used k_{inact}, which is the preferred metric to distinguish between covalent inhibitors and non-covalent inhibitors against a target [233]. However, the kinetic values for covalent EGFR inhibitors reported in the literature are not consistent, and investigators [173, 245, 246]. From this, we included Erlotinib and Osimertinib which are the benchmark compounds as important controls. To evaluate the inactivation rate, we used the sox-based substrate method to estimate the K_i which was the ratio off rate divided by on rate and the protein-inhibitor reaction rate constant (k_{inact}) shown in Equation 1.

The sox-based assay was performed to obtain the kinetic curves shown in Figure 55 and Figure 56 for both EGFR WT and DM activities. The standard drugs showed the curves that corresponded to their mode of action. Osimertinib showed strong inhibition at high concentrations consistent with covalent inhibitors which were observed in **80**. Erlotinib demonstrated low inhibition curves, indicative of non-covalent inhibitors, consistent with **79**.

This material is reserved for educational use only, not allowed for commercial use.
Forbidden to modify the content, and cite the document when use.

$$E + I \underset{}{\overset{K_i}{\rightleftharpoons}} E\text{-}I \xrightarrow{k_{inact}} E\text{-}I^* \qquad \text{Equation 1}$$

Equation 1. Kinetic parameters for the covalent bond forming.

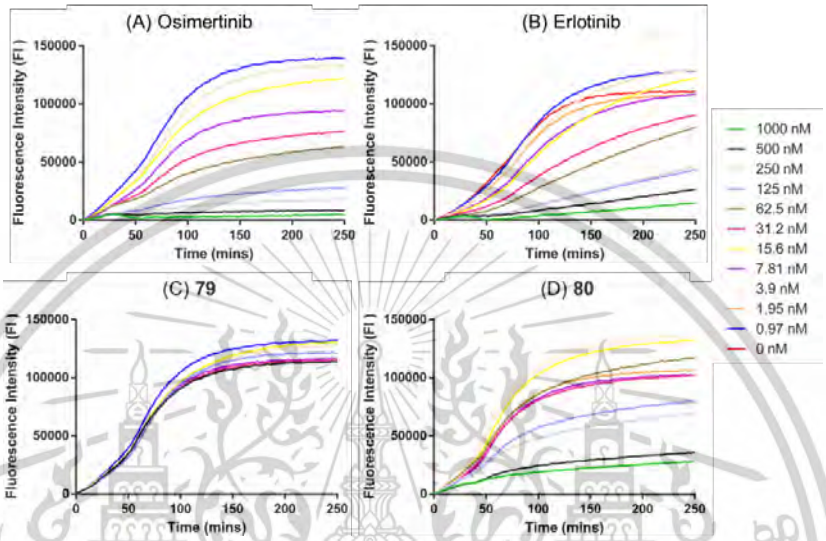

Figure 55. Determination of EGFR WT inactivation kinetic parameters for (A) Osimertinib, and (B) Erlotinib (C) **79** and (D) **80**.

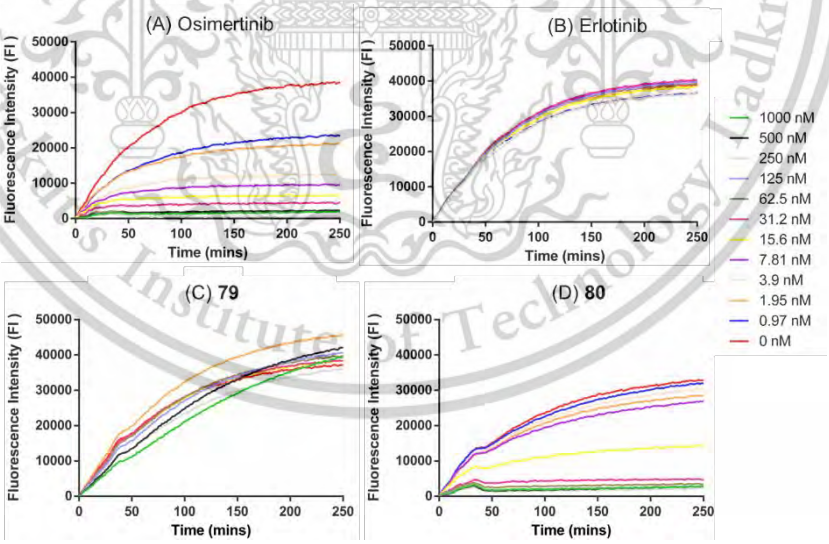

Figure 56. Determination of EGFR T790m/L858R inactivation kinetic parameters for (A) Osimertinib, and (B) Erlotinib (C) **79** and (D) **80**.

This material is reserved for educational use only, not allowed for commercial use.
Forbidden to modify the content, and cite the document when use.

4.2.9 Physicochemical Properties.

The experimental octanol/phosphate buffer partition coefficient ($logD_{7.4}$) and phosphate buffer solubility were determined using a shake flask technique (Table 8). In compounds **48** and **53**, substituted a benzyl-linker on a 2-position of pyrimidine, displayed approximately 1.5-fold improved solubility (96.5 and 57.5 mg/ml, respectively) and decreased LogD when compared to that of phenyl. Compounds **53** and **63,** substituted Cl on the 5-position of pyrimidine, resulted in a decrease in the solubility over 2-fold and increased LogD when compared to that of hydrogen. 2-chloroacetamide of compounds **51** and **66** showed much higher solubility over 8-fold when compared to that of propenamide of compounds **48** and **63**, respectively. Modification of adding the methoxy group trended to increase the solubility over 2-fold. The introduction of basic center compounds **79** and **80** dramatically increased the solubility over 20-fold compared to the market drugs. Thus, **79** and **80** are the best compounds for physicochemical properties.

This material is reserved for educational use only, not allowed for commercial use.
Forbidden to modify the content, and cite the document when use.

Table 8. Investigation of biological and physicochemical properties of selected 13 compounds.

ID	SI EGFR WT Vs WT	JAK3 (nM)	SI JAK3 Vs EGFR DM	Expt. logD	Solubility (μg/mL)
48	2.3	4.79 ± 4.40	0.2	2.81	96.5
51	5.3	1.45 ± 5.19	0.5	2.24	758
52	2.6	10.0 ± 3.09	2.1	2.56	347
53	0.9	ND	ND	3.04	57.5
54	2.6	5.61 ± 2.78	1.2	2.99	61.8
58	0.0	ND	ND	3.01	39.2
63	5.6	35.8 ± 4.34	0.3	3.31	20.0
64	4.3	29.0 ± 3.87	6.1	3.11	28.7
66	2.4	46.4 ± 3.64	7.2	2.78	170
72	5.8	20.7 ± 3.53	8.2	3.16	66.9
73	4.5	23.3 ± 3.25	3.6	3.10	50.7
79	17	36.0 ± 3.58	11	1.56	1451
80	21	40.4 ± 2.84	21	1.20	1519
Erlotinib	0.1	17.0 ± 4.34	0.3	3.09	20.6
Osimertinib	2.3	22.2 ± 2.83	2.38	3.43	30.1

This material is reserved for educational use only, not allowed for commercial use.
Forbidden to modify the content, and cite the document when use.

Chapter 5

Conclusion

5.1 Study 1: Synthesis, in vitro SAR and Computational Evaluation of Rociletinib-derived Covalent Inhibitors for the Treatment of EGFR non-small-cell-lung cancers.

We designed and synthesized twenty new 2,4-diamino-pyrimidine derivatives which were then tested against EGFR WT and T790M/L858R double-mutant. Our goal was to identify new derivatives with improved EGFR double-mutant activity, JAK3 selectivity, solubility, and logD. Compounds showed good to excellent double-mutant EGFR activity with IC_{50} values of 18.93-69.77 nM. Incorporation of *N*1-methyl-4-aminopyrazole ring at R^1 led to molecules **20-23** which demonstrated nM activities against EGFR WT and double mutants, in line with those obtained for marketed drugs Erlotinib and Osimertinib, and better than Rociletinib. The effect of the electrophilic group was less important with the top molecules containing acrylamide 2-chloro-acetamide and propenamide at the R^2.

Compounds **20, 21,** and **23** demonstrated approximately 40 nM activity against EGFR WT and approximately 20 nM activity against the double mutant, comparable to Osimertinib and Erlotinib. The compounds also demonstrated between 2-8 fold better solubility than the marketed drugs, as well as the lowest experimental $logD_{7.4}$ (~2.8). Compounds **20** and **21** demonstrated the best cytotoxic activity in EGFR overexpressing cell lines and selectivity over normal HepG2 liver cells. Finally, compound **23** was the more selective of EGFR over JAK3, with an SI value of 19 compared to just 2.6 for Osimertinib or 0.5 for Erlotinib. Kinetic evaluation of **21** in a SOX-based EGFR inhibition assay confirms that **21** displays K_{inact}/K_i values consistent with a covalent mode of action.

In conclusion, we have identified new derivatives with interesting pharmacological and physical properties. We have identified exemplars with improved or comparable activity, selectivity, and solubility compared to the marketed drugs standards.

This material is reserved for educational use only, not allowed for commercial use.
Forbidden to modify the content, and cite the document when use.

5.2 Study 2: Molecular Dynamics Guided Design of N^4-(2-methyl-2H-indazol-6-yl)-N^2-phenylpyrimidine-2,4-diamine inhibitors targeting Cys797 and the T790M Gatekeeper Mutation.

We designed and synthesized thirty-four novel 2,4-diamino-pyrimidine derivatives which were tested against EGFR WT and the T790M/L858R double-mutant. Our goal was to identify new derivatives with improved EGFR double-mutant activity, JAK3 selectivity, solubility, and logD. We have modified the six positions for this study. Compounds showed good to excellent double-mutant EGFR activity with IC_{50} values of 1.92 – 760 nM and Osimertinib-like molecules were generally better when compared to other analogs. Cl 5-pyrimidine was specific for bidding to EGFR T790M than WT. The introduction of the basic center displayed approximately 50-fold improved solubility compared to Osimertinib and Erlotinib. The effect of the electrophilic group was less important with the top molecules containing acrylamide. 2-chloroacetamide, but-2-ynamide, and propenamide at the E position.

The MD simulations demonstrated that Cl 5-pyrimidine at the B-position preferred binding the out-pose to the T790M protein with the low RMSD. Moreover, the QM calculation revealed that the incorporation of Cl 5-pyrimidine forced the indazole ring on the A-position to be out-pose because of its steric hindrance while that of H preferred both in- and out-poses. These results agreed with the activity that EGFR DM was more potent than EGFR WT of the substituent of Cl on 5-pyrimidine. The compounds that synthesized benzyl-linker on the F position demonstrated potent activity for EGFR WT. The introduction of substitution a basic center on the D position following the scope of the study, displayed approximately 50-fold improved solubility compared to that of Osimertinib and Erlotinib. We also found that the substitution of a benzyl-linker on the F position, methoxy group on the C position, H on the A position, and 2-chloroacetamide on the E position displayed improving solubility and decreasing LogD. Compounds **79** and

This material is reserved for educational use only, not allowed for commercial use.
Forbidden to modify the content, and cite the document when use.

80 were synthesized Cl on 5-pyrimidine demonstrating the best selectivity for double-mutant EGFR over EGFR WT which was 7-fold over than that of Osimertinib. So, the SI values suggested that Osimertinib-like molecules were generally better when compared to other analogs. Furthermore, Compound **80** was very selective for EGFR DM over JAK3 when compared to drugs with over a 5-fold increase. Kinetic evaluation of **80** in a SOX-based EGFR inhibition assay confirms that **80** is consistent with a covalent mode of action.

In conclusion, we have new 2,4 diaminopyrimidine derivatives with improved selectivity and solubility compared to earlier drugs. Nevertheless, the in vitro kinase screening, bioinformatics, and cheminformatics analyses were performed to provide useful SAR and information on potential EGFR targets. This data could be used in future optimization efforts on this chemotype to maintain or improve EGFR activities.

This material is reserved for educational use only, not allowed for commercial use.
Forbidden to modify the content, and cite the document when use.

Reference

1. Barret, R., *1 - Medicines and Drugs*, in *Therapeutical Chemistry*, R. Barret, Editor. 2018, Elsevier. p. 1-20.
2. Sunpaweravong, P., *Tyrosine kinase receptor inhibitor as a molecularly targeted therapy for solid tumors.* 2006, 2006. **24**(1): p. 10.
3. Du, Z. and C.M. Lovly, *Mechanisms of receptor tyrosine kinase activation in cancer.* Mol Cancer, 2018. **17**(1): p. 58.
4. Heldin, C.-H., *Dimerization of cell surface receptors in signal transduction.* Cell, 1995. **80**(2): p. 213-223.
5. Ghafoor, Q., et al., *Epidermal Growth Factor Receptor (EGFR) Kinase Inhibitors and Non-Small Cell Lung Cancer (NSCLC) – Advances in Molecular Diagnostic Techniques to Facilitate Targeted Therapy.* Pathology & Oncology Research, 2018. **24**(4): p. 723-731.
6. Lamb, Y.N., *Osimertinib: A Review in Previously Untreated, EGFR Mutation-Positive, Advanced NSCLC.* Targeted Oncology 2021. **16**(5): p. 687-695.
7. Lee, J.H., et al., *Real-World Study of Osimertinib in Korean Patients with Epidermal Growth Factor Receptor T790M Mutation-Positive Non-Small Cell Lung Cancer.* Cancer Res Treat, 2023. **55**(1): p. 112-122.
8. Truong, D.H., et al., *Delivery of erlotinib for enhanced cancer treatment: An update review on particulate systems.* Journal of Drug Delivery Science and Technology, 2020. **55**: p. 101348.
9. Zhang, T., et al., *Discovery of a novel third-generation EGFR inhibitor and identification of a potential combination strategy to overcome resistance.* Molecular Cancer, 2020. **19**(1): p. 90.
10. Shi, Y., et al., *Efficacy and Safety of Limertinib (ASK120067) in Patients With Locally Advanced or Metastatic EGFR Thr790Met-Mutated NSCLC: A Multicenter, Single-Arm, Phase 2b Study.* Journal of Thoracic Oncology, 2022. **17**(10): p. 1205-1215.
11. Harris, P.A., et al., *Discovery of 5-[[4-[(2,3-Dimethyl-2H-indazol-6-yl)methylamino]-2-pyrimidinyl]amino]-2-methyl-benzenesulfonamide (Pazopanib), a Novel and*

This material is reserved for educational use only, not allowed for commercial use.
Forbidden to modify the content, and cite the document when use.

Potent Vascular Endothelial Growth Factor Receptor Inhibitor. Journal of Medicinal Chemistry, 2008. **51**(15): p. 4632-4640.

12. Wu, J., et al., *Design, Synthesis, and Biological Evaluation of Novel Conformationally Constrained Inhibitors Targeting EGFR.* ACS Med Chem Lett, 2013. **4**(10): p. 974-8.
13. Engel, J., et al., *Targeting Drug Resistance in EGFR with Covalent Inhibitors: A Structure-Based Design Approach.* J Med Chem, 2015. **58**(17): p. 6844-63.
14. Gao, H., et al., *Synthesis and evaluation of osimertinib derivatives as potent EGFR inhibitors.* Bioorg Med Chem, 2017. **25**(17): p. 4553-4559.
15. Zhang, H., *Osimertinib making a breakthrough in lung cancer targeted therapy.* Onco Targets Ther, 2016. **9**: p. 5489-93.
16. Song, Z., et al., *Synthesis and biological evaluation of azole-diphenylpyrimidine derivatives (AzDPPYs) as potent T790M mutant form of epidermal growth factor receptor inhibitors.* Bioorg Med Chem, 2016. **24**(21): p. 5505-5512.
17. Qin, X., et al., *Discovery of new [1,4]dioxino[2,3-f]quinazoline-based inhibitors of EGFR including the T790M/L858R mutant.* Bioorg Med Chem, 2016. **24**(13): p. 2871-2881.
18. Xiao, Q., et al., *Discovery of 5-(methylthio)pyrimidine derivatives as L858R/T790M mutant selective epidermal growth factor receptor (EGFR) inhibitors.* Bioorg Med Chem, 2016. **24**(12): p. 2673-80.
19. Yu, L., et al., *A structure-guided optimization of pyrido[2,3-d]pyrimidin-7-ones as selective inhibitors of EGFR(L858R/T790M) mutant with improved pharmacokinetic properties.* Eur J Med Chem, 2017. **126**: p. 1107-1117.
20. Yan, X.E., et al., *Structural Basis of AZD9291 Selectivity for EGFR T790M.* J Med Chem, 2020. **63**(15): p. 8502-8511.
21. Yosaatmadja, Y., et al., *Binding mode of the breakthrough inhibitor AZD9291 to epidermal growth factor receptor revealed.* J Struct Biol, 2015. **192**(3): p. 539-544.
22. Cicenas, J., et al., *Kinases and Cancer.* Cancers, 2018. **10**(3): p. 63.
23. Brognard, J. and T. Hunter, *Protein kinase signaling networks in cancer.* Current Opinion in Genetics & Development, 2011. **21**(1): p. 4-11.

This material is reserved for educational use only, not allowed for commercial use.
Forbidden to modify the content, and cite the document when use.

24. Waqar, S.N., et al., *Clinician Perspectives on Current Issues in Lung Cancer Drug Development.* Journal of thoracic oncology : official publication of the International Association for the Study of Lung Cancer, 2016. **11**(9): p. 1387-1396.

25. Travis, W.D., et al., *The 2015 World Health Organization Classification of Lung Tumors: Impact of Genetic, Clinical and Radiologic Advances Since the 2004 Classification.* J Thorac Oncol, 2015. **10**(9): p. 1243-1260.

26. Travis, W.D., et al., *Introduction to The 2015 World Health Organization Classification of Tumors of the Lung, Pleura, Thymus, and Heart.* J Thorac Oncol, 2015. **10**(9): p. 1240-1242.

27. Parums, D.V., *Current status of targeted therapy in non-small cell lung cancer.* Drugs Today (Barc), 2014. **50**(7): p. 503-25.

28. Ciardiello, F. and G. Tortora, *EGFR antagonists in cancer treatment.* N Engl J Med, 2008. **358**(11): p. 1160-74.

29. Rasmy, A., et al., *Tyrosine Kinase Inhibitors in Advanced Adenocarcinoma of Lung Cancer: Are able to fight the disease or not?* 2016.

30. Malik, P.S., D. Jain, and L. Kumar, *Epidermal Growth Factor Receptor Tyrosine Kinase Inhibitors in Advanced Non-Small Cell Lung Cancer.* Oncology, 2016. **91(suppl 1)**(Suppl. 1): p. 26-34.

31. Reungwetwattana, T. and G.K. Dy, *Targeted therapies in development for non-small cell lung cancer.* J Carcinog, 2013. **12**: p. 22.

32. Carneiro, J.G., et al., *Spectrum of somatic EGFR, KRAS, BRAF, PTEN mutations and TTF-1 expression in Brazilian lung cancer patients.* Genet Res (Camb), 2014. **96**: p. e002.

33. Coussens, L., et al., *Multiple, distinct forms of bovine and human protein kinase C suggest diversity in cellular signaling pathways.* Science, 1986. **233**(4766): p. 859-66.

34. Maurer, G., B. Tarkowski, and M. Baccarini, *Raf kinases in cancer-roles and therapeutic opportunities.* Oncogene, 2011. **30**(32): p. 3477-88.

35. Zdrazil, B., et al., *Moving targets in drug discovery.* Scientific Reports, 2020. **10**(1): p. 20213.

This material is reserved for educational use only, not allowed for commercial use.

Forbidden to modify the content, and cite the document when use.

36. Manning, G., et al., *The protein kinase complement of the human genome.* Science, 2002. **298**: p. 1912 - 1934.

37. Ferguson, F.M. and N.S. Gray, *Kinase inhibitors: the road ahead.* Nat. Rev. Drug Discov., 2018. **17**: p. 353.

38. Wu, P., T.E. Nielsen, and M.H. Clausen, *Small-molecule kinase inhibitors: an analysis of FDA-approved drugs.* Drug Discov. Today, 2016. **21**(1): p. 5-10.

39. Wu, P., T.E. Nielsen, and M.H. Clausen, *FDA-approved small-molecule kinase inhibitors.* Trends Pharmacol. Sci., 2015. **36**(7): p. 422-439.

40. Bhullar, K.S., et al., *Kinase-targeted cancer therapies: progress, challenges and future directions.* Molecular Cancer, 2018. **17**(1): p. 48.

41. Bardelli, A., et al., *Mutational analysis of the tyrosine kinome in colorectal cancers.* Science, 2003. **300**(5621): p. 949.

42. Chalhoub, N. and S.J. Baker, *PTEN and the PI3-kinase pathway in cancer.* Annu Rev Pathol, 2009. **4**: p. 127-50.

43. Davies, S.P., et al., *Specificity and mechanism of action of some commonly used protein kinase inhibitors.* Biochem J, 2000. **351**(Pt 1): p. 95-105.

44. Lombardo, L.J., et al., *Discovery of N-(2-chloro-6-methyl- phenyl)-2-(6-(4-(2-hydroxyethyl)- piperazin-1-yl)-2-methylpyrimidin-4- ylamino)thiazole-5-carboxamide (BMS-354825), a dual Src/Abl kinase inhibitor with potent antitumor activity in preclinical assays.* J Med Chem, 2004. **47**(27): p. 6658-61.

45. Fabian, M.A., et al., *A small molecule-kinase interaction map for clinical kinase inhibitors.* Nat Biotechnol, 2005. **23**(3): p. 329-36.

46. Shukla, S., et al., *Sunitinib (Sutent, SU11248), a small-molecule receptor tyrosine kinase inhibitor, blocks function of the ATP-binding cassette (ABC) transporters P-glycoprotein (ABCB1) and ABCG2.* Drug Metab Dispos, 2009. **37**(2): p. 359-65.

47. Kirkland, L.O. and C. McInnes, *Non-ATP competitive protein kinase inhibitors as anti-tumor therapeutics.* Biochem Pharmacol, 2009. **77**(10): p. 1561-71.

48. Fabbro, D., S.W. Cowan-Jacob, and H. Moebitz, *Ten things you should know about protein kinases: IUPHAR Review 14.* Br J Pharmacol, 2015. **172**(11): p. 2675-700.

This material is reserved for educational use only, not allowed for commercial use.
Forbidden to modify the content, and cite the document when use.

49. Taylor, S.S. and A.P.J.T.i.b.s. Kornev, *Protein kinases: evolution of dynamic regulatory proteins.* 2011. **36 2**: p. 65-77.

50. Abdeldayem, A., et al., *Advances in covalent kinase inhibitors.* Chemical Society Reviews, 2020. **49**(9): p. 2617-2687.

51. de Oliveira, P.S.L., et al., *Revisiting protein kinase–substrate interactions: Toward therapeutic development.* Science Signaling, 2016. **9**(420): p. re3.

52. Zhang, J., P.L. Yang, and N.S. Gray, *Targeting cancer with small molecule kinase inhibitors.* Nat Rev Cancer, 2009. **9**(1): p. 28-39.

53. Xing, L., et al., *Kinase hinge binding scaffolds and their hydrogen bond patterns.* Bioorganic & Medicinal Chemistry, 2015. **23**(19): p. 6520-6527.

54. Lorente-Macías, Á., *Design synthesis and biological evaluation of 6-alkoxypurine derivatives as kinase inhibitors*. 2019.

55. Dar, A.C. and K.M. Shokat, *The evolution of protein kinase inhibitors from antagonists to agonists of cellular signaling.* Annu Rev Biochem, 2011. **80**: p. 769-95.

56. Liu, Y. and N.S. Gray, *Rational design of inhibitors that bind to inactive kinase conformations.* Nat Chem Biol, 2006. **2**(7): p. 358-64.

57. Davis, M.I., et al., *Comprehensive analysis of kinase inhibitor selectivity.* Nat Biotechnol, 2011. **29**(11): p. 1046-51.

58. Force, T. and K.L. Kolaja, *Cardiotoxicity of kinase inhibitors: the prediction and translation of preclinical models to clinical outcomes.* Nat Rev Drug Discov, 2011. **10**(2): p. 111-26.

59. Kufareva, I. and R. Abagyan, *Type-II kinase inhibitor docking, screening, and profiling using modified structures of active kinase states.* J Med Chem, 2008. **51**(24): p. 7921-32.

60. Wise, D.R. and C.B. Thompson, *Glutamine addiction: a new therapeutic target in cancer.* Trends Biochem Sci, 2010. **35**(8): p. 427-33.

61. Berndt, N., R.M. Karim, and E. Schönbrunn, *Advances of small molecule targeting of kinases.* Curr Opin Chem Biol, 2017. **39**: p. 126-132.

This material is reserved for educational use only, not allowed for commercial use.

Forbidden to modify the content, and cite the document when use.

62. Lamba, V. and I. Ghosh, *New directions in targeting protein kinases: focusing upon true allosteric and bivalent inhibitors.* Curr Pharm Des, 2012. **18**(20): p. 2936-45.

63. Ohren, J.F., et al., *Structures of human MAP kinase kinase 1 (MEK1) and MEK2 describe novel noncompetitive kinase inhibition.* Nat Struct Mol Biol, 2004. **11**(12): p. 1192-7.

64. Grimsby, J., et al., *Allosteric activators of glucokinase: potential role in diabetes therapy.* Science, 2003. **301**(5631): p. 370-3.

65. Sanders, M.J., et al., *Defining the mechanism of activation of AMP-activated protein kinase by the small molecule A-769662, a member of the thienopyridone family.* J Biol Chem, 2007. **282**(45): p. 32539-48.

66. Normanno, N., et al., *Epidermal growth factor receptor (EGFR) signaling in cancer.* Gene, 2006. **366**(1): p. 2-16.

67. Sigismund, S., D. Avanzato, and L. Lanzetti, *Emerging functions of the EGFR in cancer.* Mol Oncol, 2018. **12**(1): p. 3-20.

68. Yun, C.-H., et al., *Structures of Lung Cancer-Derived EGFR Mutants and Inhibitor Complexes: Mechanism of Activation and Insights into Differential Inhibitor Sensitivity.* Cancer Cell, 2007. **11**(3): p. 217-227.

69. Arteaga, Carlos L. and Jeffrey A. Engelman, *ERBB Receptors: From Oncogene Discovery to Basic Science to Mechanism-Based Cancer Therapeutics.* Cancer Cell, 2014. **25**(3): p. 282-303.

70. Maione, P., et al., *Overcoming resistance to targeted therapies in NSCLC: current approaches and clinical application.* Therapeutic advances in medical oncology, 2015. **7**(5): p. 263-273.

71. Hirano, T., et al., *In vitro modeling to determine mutation specificity of EGFR tyrosine kinase inhibitors against clinically relevant EGFR mutants in non-small-cell lung cancer.* Oncotarget, 2015. **6**(36): p. 38789-38803.

72. Sharma, S.V., et al., *Epidermal growth factor receptor mutations in lung cancer.* Nat Rev Cancer, 2007. **7**(3): p. 169-81.

73. Tiseo, M., et al., *Emerging role of gefitinib in the treatment of non-small-cell lung cancer (NSCLC).* Drug design, development and therapy, 2010. **4**: p. 81-98.

This material is reserved for educational use only, not allowed for commercial use.
Forbidden to modify the content, and cite the document when use.

74. Ren, Y., et al., *EGFR gene-mutation status correlated with therapeutic decision making in lung adenocarcinoma.* Onco Targets Ther, 2015. **8**: p. 3017-20.

75. Zhang, Q., et al., *Comparison of single-agent chemotherapy and targeted therapy to first-line treatment in patients aged 80 years and older with advanced non-small-cell lung cancer.* Onco Targets Ther, 2015. **8**: p. 893-8.

76. Villadolid, J., et al., *Management of hyperglycemia from epidermal growth factor receptor (EGFR) tyrosine kinase inhibitors (TKIs) targeting T790M-mediated resistance.* Translational lung cancer research, 2015. **4**(5): p. 576-583.

77. Ercan, D., et al., *EGFR Mutations and Resistance to Irreversible Pyrimidine-Based EGFR Inhibitors.* Clin Cancer Res, 2015. **21**(17): p. 3913-23.

78. Gazdar, A.F., *Activating and resistance mutations of EGFR in non-small-cell lung cancer: role in clinical response to EGFR tyrosine kinase inhibitors.* Oncogene, 2009. **28 Suppl 1**(Suppl 1): p. S24-S31.

79. Sharma, S.V., et al., *Epidermal growth factor receptor mutations in lung cancer.* (1474-175X (Print)).

80. Pao, W. and J. Chmielecki, *Rational, biologically based treatment of EGFR-mutant non-small-cell lung cancer.* (1474-1768 (Electronic)).

81. Ramalingam, S.S., et al., *Randomized phase II study of dacomitinib (PF-00299804), an irreversible pan-human epidermal growth factor receptor inhibitor, versus erlotinib in patients with advanced non-small-cell lung cancer.* J Clin Oncol, 2012. **30**(27): p. 3337-44.

82. Leonetti, A., et al., *Resistance mechanisms to osimertinib in EGFR-mutated non-small cell lung cancer.* British Journal of Cancer, 2019. **121**(9): p. 725-737.

83. Li, R., et al., *Four generations of EGFR TKIs associated with different pathogenic mutations in non-small cell lung carcinoma.* Journal of Drug Targeting, 2020. **28**(9): p. 861-872.

84. Zhang, M., et al., *Design, Synthesis and Biological Evaluation of the Quinazoline Derivatives as L858R/T790M/C797S Triple Mutant Epidermal Growth Factor Receptor Tyrosine Kinase Inhibitors.* Chemical and Pharmaceutical Bulletin, 2020. **68**(10): p. 971-980.

This material is reserved for educational use only, not allowed for commercial use.

Forbidden to modify the content, and cite the document when use.

85. He, J., et al., *The new opportunities in medicinal chemistry of fourth-generation EGFR inhibitors to overcome C797S mutation.* European Journal of Medicinal Chemistry, 2021. **210**: p. 112995.

86. Hoy, S.M., *Brigatinib: A Review in ALK-Inhibitor Naïve Advanced ALK-Positive NSCLC.* Drugs, 2021. **81**(2): p. 267-275.

87. Eno, M.S., et al., *Discovery of BLU-945, a Reversible, Potent, and Wild-Type-Sparing Next-Generation EGFR Mutant Inhibitor for Treatment-Resistant Non-Small-Cell Lung Cancer.* Journal of Medicinal Chemistry, 2022. **65**(14): p. 9662-9677.

88. Tyler, S.B., et al., *Structural analysis of the macrocyclic inhibitor BI-4020 binding to EGFR kinase.* bioRxiv, 2022: p. 2022.08.27.505540.

89. Haddad, Y., et al., *Toward structure-based drug design against the epidermal growth factor receptor (EGFR).* Drug Discovery Today, 2021. **26**(2): p. 289-295.

90. Kim, E.S., *Olmutinib: First Global Approval.* Drugs, 2016. **76**(11): p. 1153-7.

91. Dhillon, S., *Lazertinib: First Approval.* Drugs, 2021. **81**(9): p. 1107-1113.

92. Yang, H., et al., *Design, synthesis and biological evaluation of 2-amino-4-(1,2,4-triazol)pyridine derivatives as potent EGFR inhibitors to overcome TKI-resistance.* European Journal of Medicinal Chemistry, 2020. **187**: p. 111966.

93. Nagasaka, M., et al., *Beyond Osimertinib: The Development of Third-Generation EGFR Tyrosine Kinase Inhibitors For Advanced EGFR+ NSCLC.* Journal of Thoracic Oncology, 2021. **16**(5): p. 740-763.

94. Russo, A., et al., *A decade of EGFR inhibition in EGFR-mutated non small cell lung cancer (NSCLC): Old successes and future perspectives.* Oncotarget; Vol 6, No 29, 2015.

95. Kazandjian, D., et al., *FDA Approval of Gefitinib for the Treatment of Patients with Metastatic EGFR Mutation–Positive Non–Small Cell Lung Cancer.* Clinical Cancer Research, 2016. **22**(6): p. 1307-1312.

96. Mok, T.S., et al., *Gefitinib or Carboplatin–Paclitaxel in Pulmonary Adenocarcinoma.* New England Journal of Medicine, 2009. **361**(10): p. 947-957.

97. Mitsudomi, T., et al., *Gefitinib versus cisplatin plus docetaxel in patients with non-small-cell lung cancer harbouring mutations of the epidermal growth factor*

This material is reserved for educational use only, not allowed for commercial use.
Forbidden to modify the content, and cite the document when use.

receptor (WJTOG3405): an open label, randomised phase 3 trial. (1474-5488 (Electronic)).

98. Maemondo, M., et al., *Gefitinib or Chemotherapy for Non–Small-Cell Lung Cancer with Mutated EGFR.* New England Journal of Medicine, 2010. **362**(25): p. 2380-2388.

99. Douillard, J.Y., et al., *First-line gefitinib in Caucasian EGFR mutation-positive NSCLC patients: a phase-IV, open-label, single-arm study.* British Journal of Cancer, 2014. **110**(1): p. 55-62.

100. Han, J.Y., et al., *First-SIGNAL: first-line single-agent iressa versus gemcitabine and cisplatin trial in never-smokers with adenocarcinoma of the lung.* (1527-7755 (Electronic)).

101. Shepherd, F.A., et al., *Erlotinib in Previously Treated Non–Small-Cell Lung Cancer.* New England Journal of Medicine, 2005. **353**(2): p. 123-132.

102. Rosell, R., et al., *Erlotinib versus standard chemotherapy as first-line treatment for European patients with advanced EGFR mutation-positive non-small-cell lung cancer (EURTAC): a multicentre, open-label, randomised phase 3 trial.* (1474-5488 (Electronic)).

103. Zhou, C., et al., *Erlotinib versus chemotherapy as first-line treatment for patients with advanced EGFR mutation-positive non-small-cell lung cancer (OPTIMAL, CTONG-0802): a multicentre, open-label, randomised, phase 3 study.* (1474-5488 (Electronic)).

104. Wu, Y.L., et al., *First-line erlotinib versus gemcitabine/cisplatin in patients with advanced EGFR mutation-positive non-small-cell lung cancer: analyses from the phase III, randomized, open-label, ENSURE study††Presented in part at the 15th World Congress on Lung Cancer, Sydney, Australia 2013.* Annals of Oncology, 2015. **26**(9): p. 1883-1889.

105. Shi, Y., et al., *Icotinib versus gefitinib in previously treated advanced non-small-cell lung cancer (ICOGEN): a randomised, double-blind phase 3 non-inferiority trial.* (1474-5488 (Electronic)).

106. Shi, Y.K., et al., *First-line icotinib versus cisplatin/pemetrexed plus pemetrexed maintenance therapy for patients with advancedEGFR mutation-positive lung*

This material is reserved for educational use only, not allowed for commercial use.
Forbidden to modify the content, and cite the document when use.

adenocarcinoma (CONVINCE): a phase 3, open-label, randomized study. Annals of Oncology, 2017. **28**(10): p. 2443-2450.

107. Sequist, L.V., et al., *Genotypic and histological evolution of lung cancers acquiring resistance to EGFR inhibitors.* (1946-6242 (Electronic)).

108. Liao, B.-C., C.-C. Lin, and J.C.-H. Yang, *Second and third-generation epidermal growth factor receptor tyrosine kinase inhibitors in advanced nonsmall cell lung cancer.* Current Opinion in Oncology, 2015. **27**(2).

109. Wang, S. and J. Li, *Second-generation EGFR and ErbB tyrosine kinase inhibitors as first-line treatments for non-small cell lung cancer.* (1178-6930 (Print)).

110. Bergonzini, C., et al., *Is there a role for dacomitinib, a second-generation irreversible inhibitor of the epidermal-growth factor receptor tyrosine kinase, in advanced non-small cell lung cancer?* Expert Opinion on Pharmacotherapy, 2020. **21**(11): p. 1287-1298.

111. Hao, Y., et al., *Discovery and Structural Optimization of N5-Substituted 6,7-Dioxo-6,7-dihydropteridines as Potent and Selective Epidermal Growth Factor Receptor (EGFR) Inhibitors against L858R/T790M Resistance Mutation.* Journal of Medicinal Chemistry, 2016. **59**(15): p. 7111-7124.

112. Van Der Steen, N., et al., *New developments in the management of non-small-cell lung cancer, focus on rociletinib: what went wrong?* Onco Targets Ther., 2016. **9**: p. 6065–6074.

113. Tan, C.-S., et al., *Third generation EGFR TKIs: current data and future directions.* Molecular Cancer, 2018. **17**(1): p. 29.

114. Zhou, W., et al., *Novel mutant-selective EGFR kinase inhibitors against EGFR T790M.* Nature, 2009. **462**(7276): p. 1070-1074.

115. Almalki, F.A., et al. *Icotinib, Almonertinib, and Olmutinib: A 2D Similarity/Docking-Based Study to Predict the Potential Binding Modes and Interactions into EGFR*. Molecules, 2021. **26**, DOI: 10.3390/molecules26216423.

116. Lau, S.C.M. and S.-H.I. Ou, *And Still They Come Over Troubled Waters: Can Asia's Third-Generation EGFR Tyrosine Kinase Inhibitors (Furmonertinib, Aumolertinib, Rezivertinib, Limertinib, Befotertinib, SH-1028, and Lazertinib) Affect Global*

This material is reserved for educational use only, not allowed for commercial use.
Forbidden to modify the content, and cite the document when use.

Treatment of EGFR+ NSCLC. Journal of Thoracic Oncology, 2022. **17**(10): p. 1144-1154.

117. Park, K., et al., *Afatinib versus gefitinib as first-line treatment of patients with EGFR mutation-positive non-small-cell lung cancer (LUX-Lung 7): a phase 2B, open-label, randomised controlled trial.* (1474-5488 (Electronic)).

118. Yang, J.C.-H., et al., *Osimertinib in Pretreated T790M-Positive Advanced Non–Small-Cell Lung Cancer: AURA Study Phase II Extension Component.* Journal of Clinical Oncology, 2017. **35**(12): p. 1288-1296.

119. Camidge, D.R., et al., *Brigatinib Versus Crizotinib in ALK Inhibitor-Naive Advanced ALK-Positive NSCLC: Final Results of Phase 3 ALTA-1L Trial.* (1556-1380 (Electronic)).

120. Uchibori, K., et al., *Brigatinib combined with anti-EGFR antibody overcomes osimertinib resistance in EGFR-mutated non-small-cell lung cancer.* Nature Communications, 2017. **8**(1): p. 14768.

121. Fang, H., et al., *Design, synthesis and evaluation of the Brigatinib analogues as potent inhibitors against tertiary EGFR mutants (EGFRdel19/T790M/C797S and EGFRL858R/T790M/C797S).* Bioorganic & Medicinal Chemistry Letters, 2022. **72**: p. 128729.

122. Beyett, T.S., et al., *Structural analysis of the macrocyclic inhibitor BI-4020 binding to EGFR kinase.* (1860-7187 (Electronic)).

123. Capoferri, L., et al., *Quantum Mechanics/Molecular Mechanics Modeling of Covalent Addition between EGFR–Cysteine 797 and N-(4-Anilinoquinazolin-6-yl) Acrylamide.* Journal of Chemical Information and Modeling, 2015. **55**(3): p. 589-599.

124. Paasche, A., et al., *Mechanistic study of the reaction of thiol-containing enzymes with alpha,beta-unsaturated carbonyl substrates by computation and chemoassays.* ChemMedChem, 2010. **5**(6): p. 869-880.

125. Ghafoor, Q.A.-O., et al., *Epidermal Growth Factor Receptor (EGFR) Kinase Inhibitors and Non-Small Cell Lung Cancer (NSCLC) - Advances in Molecular Diagnostic Techniques to Facilitate Targeted Therapy.* (1532-2807 (Electronic)).

This material is reserved for educational use only, not allowed for commercial use.

Forbidden to modify the content, and cite the document when use.

126. Giacomini, M.M., et al., *Interaction of 2,4-Diaminopyrimidine-Containing Drugs Including Fedratinib and Trimethoprim with Thiamine Transporters.* (1521-009X (Electronic)).

127. Talpaz, M.A.-O. and J.A.-O.X. Kiladjian, *Fedratinib, a newly approved treatment for patients with myeloproliferative neoplasm-associated myelofibrosis.* (1476-5551 (Electronic)).

128. Janoueix-Lerosey, I., G. Schleiermacher, and O. Delattre, *Molecular pathogenesis of peripheral neuroblastic tumors.* Oncogene, 2010. **29**(11): p. 1566-1579.

129. Lu, T.-P., E.Y. Chuang, and J.J. Chen, *Identification of reproducible gene expression signatures in lung adenocarcinoma.* BMC Bioinform., 2013. **14**(1): p. 1-10.

130. Giordanetto, F., et al., *Discovery of phosphoinositide 3-kinases (PI3K) p110β isoform inhibitor 4-[2-hydroxyethyl(1-naphthylmethyl)amino]-6-[(2S)-2-methylmorpholin-4-yl]-1H-pyrimidin-2-one, an effective antithrombotic agent without associated bleeding and insulin resistance.* Bioorg Med Chem Lett, 2012. **22**(21): p. 6671-6.

131. Yang, H.-L., et al., *Design and synthesis of a novel series of N,4-diphenylpyrimidin-2-amine derivatives as potent and selective PI3Kγ inhibitors.* MedChemComm, 2014. **5**(2): p. 219-225.

132. Ward, R.A., et al., *Structure- and Reactivity-Based Development of Covalent Inhibitors of the Activating and Gatekeeper Mutant Forms of the Epidermal Growth Factor Receptor (EGFR).* Journal of Medicinal Chemistry, 2013. **56**(17): p. 7025-7048.

133. Finlay, M.R.V., et al., *Discovery of a Potent and Selective EGFR Inhibitor (AZD9291) of Both Sensitizing and T790M Resistance Mutations That Spares the Wild Type Form of the Receptor.* Journal of Medicinal Chemistry, 2014. **57**(20): p. 8249-8267.

134. Pelletier, J.C., et al., *(1-(4-(Naphthalen-2-yl)pyrimidin-2-yl)piperidin-4-yl)methanamine: A Wingless β-Catenin Agonist That Increases Bone Formation Rate.* Journal of Medicinal Chemistry, 2009. **52**(22): p. 6962-6965.

135. Frame, S. and P. Cohen, *GSK3 takes centre stage more than 20 years after its discovery.* Biochem J, 2001. **359**(Pt 1): p. 1-16.

This material is reserved for educational use only, not allowed for commercial use.

Forbidden to modify the content, and cite the document when use.

136. West, K., et al., *West KA, Brognard J, Clark AS, Linnoila IR, Yang X, Swain SM, Harris C, Belinsky S, Dennis PARapid Akt activation by nicotine and a tobacco carcinogen modulates the phenotype of normal human airway epithelial cells. J Clin Invest 111: 81-90.* The Journal of clinical investigation, 2003. **111**: p. 81-90.

137. Crombie, A., et al., *Synthesis and biological evaluation of tricyclic anilinopyrimidines as IKKβ inhibitors.* Bioorganic & medicinal chemistry letters, 2010. **20**: p. 3821-5.

138. Kurinna, S.M., et al., *Ceramide promotes apoptosis in lung cancer-derived A549 cells by a mechanism involving c-Jun NH2-terminal kinase.* Cancer Res, 2004. **64**(21): p. 7852-6.

139. Kyriakis, J.M. and J. Avruch, *Mammalian mitogen-activated protein kinase signal transduction pathways activated by stress and inflammation.* Physiol Rev, 2001. **81**(2): p. 807-69.

140. Shaulian, E. and M. Karin, *AP-1 as a regulator of cell life and death.* Nat Cell Biol, 2002. **4**(5): p. E131-6.

141. Verheij, M., et al., *Requirement for ceramide-initiated SAPK/JNK signalling in stress-induced apoptosis.* Nature, 1996. **380**(6569): p. 75-9.

142. Kamenecka, T., et al., *Synthesis, Biological Evaluation, X-ray Structure, and Pharmacokinetics of Aminopyrimidine c-jun-N-terminal Kinase (JNK) Inhibitors.* Journal of Medicinal Chemistry, 2010. **53**(1): p. 419-431.

143. Tan, L., et al., *Development of Selective Covalent Janus Kinase 3 Inhibitors.* (1520-4804 (Electronic)).

144. Singh, J., et al., *The resurgence of covalent drugs.* Nat Rev Drug Discov, 2011. **10**(4): p. 307-17.

145. Abdeldayem, A., et al., *Advances in covalent kinase inhibitors.* Chemical Society Reviews, 2020. **49**.

146. Vane, J.R. and R.M. Botting, *The mechanism of action of aspirin.* Thromb Res, 2003. **110**(5-6): p. 255-8.

147. Desborough, M.J.R. and D.M. Keeling, *The aspirin story - from willow to wonder drug.* Br J Haematol, 2017. **177**(5): p. 674-683.

This material is reserved for educational use only, not allowed for commercial use.
Forbidden to modify the content, and cite the document when use.

148. Engel, J., et al., *Targeting Drug Resistance in EGFR with Covalent Inhibitors: A Structure-Based Design Approach.* Journal of Medicinal Chemistry, 2015. **58**(17): p. 6844-6863.

149. Bauer, R.A., *Covalent inhibitors in drug discovery: from accidental discoveries to avoided liabilities and designed therapies.* Drug Discov Today, 2015. **20**(9): p. 1061-73.

150. Noble, M.E., J.A. Endicott, and L.N. Johnson, *Protein kinase inhibitors: insights into drug design from structure.* Science, 2004. **303**(5665): p. 1800-5.

151. Gavrin, L.K. and E. Saiah, *Approaches to discover non-ATP site kinase inhibitors.* MedChemComm, 2013. **4**(1): p. 41-51.

152. Zuccotto, F., et al., *Through the "gatekeeper door": exploiting the active kinase conformation.* J Med Chem, 2010. **53**(7): p. 2681-94.

153. Carrera, A.C., K. Alexandrov, and T.M. Roberts, *The conserved lysine of the catalytic domain of protein kinases is actively involved in the phosphotransfer reaction and not required for anchoring ATP.* 1993. **90**(2): p. 442-446.

154. Powis, G., et al., *Wortmannin, a potent and selective inhibitor of phosphatidylinositol-3-kinase.* Cancer Res, 1994. **54**(9): p. 2419-23.

155. Shannon, D.A. and E. Weerapana, *Covalent protein modification: the current landscape of residue-specific electrophiles.* Current opinion in chemical biology, 2015. **24**: p. 18-26.

156. Barf, T. and A. Kaptein, *Irreversible protein kinase inhibitors: balancing the benefits and risks.* J Med Chem, 2012. **55**(14): p. 6243-62.

157. Marino, S.M. and V.N. Gladyshev, *Analysis and functional prediction of reactive cysteine residues.* J Biol Chem, 2012. **287**(7): p. 4419-25.

158. Marino, S.M. and V.N. Gladyshev, *Cysteine function governs its conservation and degeneration and restricts its utilization on protein surfaces.* Journal of molecular biology, 2010. **404**(5): p. 902-916.

159. De Cesco, S., et al., *Covalent inhibitors design and discovery.* Eur J Med Chem, 2017. **138**: p. 96-114.

This material is reserved for educational use only, not allowed for commercial use.

Forbidden to modify the content, and cite the document when use.

160. Casiraghi, G., et al., *The Vinylogous Aldol Reaction: A Valuable, Yet Understated Carbon–Carbon Bond-Forming Maneuver.* Chemical Reviews, 2000. **100**(6): p. 1929-1972.

161. Jackson, P.A., et al., *Covalent Modifiers: A Chemical Perspective on the Reactivity of α,β-Unsaturated Carbonyls with Thiols via Hetero-Michael Addition Reactions.* J Med Chem, 2017. **60**(3): p. 839-885.

162. Cee, V.J., et al., *Systematic Study of the Glutathione (GSH) Reactivity of N-Arylacrylamides: 1. Effects of Aryl Substitution.* J Med Chem, 2015. **58**(23): p. 9171-8.

163. Hermann, M.R., et al., *Covalent inhibitor reactivity prediction by the electrophilicity index—in and out of scope.* Journal of Computer-Aided Molecular Design, 2021. **35**(4): p. 531-539.

164. Lonsdale, R., et al., *Expanding the Armory: Predicting and Tuning Covalent Warhead Reactivity.* Journal of Chemical Information and Modeling, 2017. **57**(12): p. 3124-3137.

165. Palazzesi, F., et al., *BIreactive: A Machine-Learning Model to Estimate Covalent Warhead Reactivity.* Journal of Chemical Information and Modeling, 2020. **60**(6): p. 2915-2923.

166. Mihalovits, L.M., G.G. Ferenczy, and G.M. Keserű, *Affinity and Selectivity Assessment of Covalent Inhibitors by Free Energy Calculations.* Journal of Chemical Information and Modeling, 2020. **60**(12): p. 6579-6594.

167. do Amaral, D.N., et al., *A novel scaffold for EGFR inhibition: Introducing N-(3-(3-phenylureido)quinoxalin-6-yl) acrylamide derivatives.* Scientific Reports, 2019. **9**(1): p. 14.

168. Castelli, R., et al., *Balancing reactivity and antitumor activity: heteroarylthioacetamide derivatives as potent and time-dependent inhibitors of EGFR.* European Journal of Medicinal Chemistry, 2019. **162**: p. 507-524.

169. Tan, L., et al., *Structure-guided development of covalent TAK1 inhibitors.* Bioorganic & Medicinal Chemistry, 2017. **25**(3): p. 838-846.

This material is reserved for educational use only, not allowed for commercial use.
Forbidden to modify the content, and cite the document when use.

170. McAulay, K., et al., *Alkynyl Benzoxazines and Dihydroquinazolines as Cysteine Targeting Covalent Warheads and Their Application in Identification of Selective Irreversible Kinase Inhibitors.* Journal of the American Chemical Society, 2020. **142**(23): p. 10358-10372.

171. Lelais, G., et al., *Discovery of (R,E)-N-(7-Chloro-1-(1-[4-(dimethylamino)but-2-enoyl]azepan-3-yl)-1H-benzo[d]imidazol-2-yl)-2-methylisonicotinamide (EGF816), a Novel, Potent, and WT Sparing Covalent Inhibitor of Oncogenic (L858R, ex19del) and Resistant (T790M) EGFR Mutants for the Treatment of EGFR Mutant Non-Small-Cell Lung Cancers.* J Med Chem, 2016. **59**(14): p. 6671-89.

172. Tan, L., et al., *Development of Selective Covalent Janus Kinase 3 Inhibitors.* Journal of Medicinal Chemistry, 2015. **58**(16): p. 6589-6606.

173. Hoyt, K.W., et al., *Pitfalls and Considerations in Determining the Potency and Mutant Selectivity of Covalent Epidermal Growth Factor Receptor Inhibitors.* Journal of Medicinal Chemistry, 2024. **67**(1): p. 2-16.

174. Hughes, J.P., et al., *Principles of early drug discovery.* (1476-5381 (Electronic)).

175. Deore, A.B., et al., *The Stages of Drug Discovery and Development Process.* Asian Journal of Pharmaceutical Research and Development, 2019. **7**(6): p. 62-67.

176. Moffat, J.G., et al., *Opportunities and challenges in phenotypic drug discovery: an industry perspective.* Nature Reviews Drug Discovery, 2017. **16**(8): p. 531-543.

177. DiMasi, J.A., R.W. Hansen, and H.G. Grabowski, *The price of innovation: new estimates of drug development costs.* Journal of Health Economics, 2003. **22**(2): p. 151-185.

178. Gashaw, I., et al., *What makes a good drug target?* (1878-5832 (Electronic)).

179. Weinmann H Fau - Metternich, R. and R. Metternich, *Drug discovery process for kinase inhibitors.* (1439-4227 (Print)).

180. Craig, S.P., 3rd and A.E. Eakin, *Structure-based inhibitor design.* Vitam Horm, 2000. **58**: p. 149-69.

181. Kar, P. and M. Feig, *Recent advances in transferable coarse-grained modeling of proteins.* Advances in protein chemistry and structural biology, 2014. **96**: p. 143-180.

This material is reserved for educational use only, not allowed for commercial use.
Forbidden to modify the content, and cite the document when use.

182. González, M.A.J.J., *Force fields and molecular dynamics simulations.* 2011. **12**: p. 169-200.

183. Phuangsawai, O., et al., *Evaluation of the anti-malarial activity and cytotoxicity of 2,4-diamino-pyrimidine-based kinase inhibitors.* Eur J Med Chem, 2016. **124**: p. 896-905.

184. Van Horn, K.S., et al., *Antibacterial Activity of a Series of N2,N4-Disubstituted Quinazoline-2,4-diamines.* Journal of Medicinal Chemistry, 2014. **57**(7): p. 3075-3093.

185. Zhu, X., et al., *SAR refinement of antileishmanial N(2),N(4)-disubstituted quinazoline-2,4-diamines.* Bioorganic & medicinal chemistry, 2015. **23**(16): p. 5182-5189.

186. Chen, H., et al., *A safe and convenient synthesis of 4-benzyloxy-3-chloroaniline.* ARKIVOC: archive for organic chemistry, 2008. **2008**: p. 1-6.

187. Xiao, Q., et al., *Discovery of 5-(methylthio)pyrimidine derivatives as L858R/T790M mutant selective Epidermal Growth Factor Receptor (EGFR) inhibitors.* Bioorganic & Medicinal Chemistry, 2016. **24**.

188. Yu, L., et al., *A structure-guided optimization of pyrido[2,3-d]pyrimidin-7-ones as selective inhibitors of EGFRL858R/T790M mutant with improved pharmacokinetic properties.* European Journal of Medicinal Chemistry, 2017. **126**: p. 1107-1117.

189. Finlay, M.R., et al., *Discovery of a potent and selective EGFR inhibitor (AZD9291) of both sensitizing and T790M resistance mutations that spares the wild type form of the receptor.* J Med Chem, 2014. **57**(20): p. 8249-67.

190. Krishnamurthy, V.M., et al., *Dependence of Effective Molarity on Linker Length for an Intramolecular Protein−Ligand System.* Journal of the American Chemical Society, 2007. **129**(5): p. 1312-1320.

191. Chan, S., et al., *2,4-Diarylamino-pyrimidines as kinase inhibitors co-targeting IGF1R and EGFR(L(8)(5)(8)R/T(7)(9)(0)M).* Bioorg Med Chem Lett, 2015. **25**(19): p. 4277-81.

192. Ward, R.A., et al., *Structure- and reactivity-based development of covalent inhibitors of the activating and gatekeeper mutant forms of the epidermal growth factor receptor (EGFR).* J Med Chem, 2013. **56**(17): p. 7025-48.

This material is reserved for educational use only, not allowed for commercial use.

Forbidden to modify the content, and cite the document when use.

193. Shu, L., et al., *Design, synthesis, and pharmacological evaluation of 4- or 6-phenyl-pyrimidine derivatives as novel and selective Janus kinase 3 inhibitors.* European Journal of Medicinal Chemistry, 2020. **191**: p. 112148.

194. Xun, Q., et al., *Design, Synthesis, and Structure–Activity Relationship Study of 2-Oxo-3,4-dihydropyrimido[4,5-d]pyrimidines as New Colony Stimulating Factor 1 Receptor (CSF1R) Kinase Inhibitors.* Journal of Medicinal Chemistry, 2018. **61**(6): p. 2353-2371.

195. Gleeson, M.P. and D. Gleeson, *QM/MM As a Tool in Fragment Based Drug Discovery. A Cross-Docking, Rescoring Study of Kinase Inhibitors.* Journal of Chemical Information and Modeling, 2009. **49**(6): p. 1437-1448.

196. Stamos, J., M.X. Sliwkowski, and C. Eigenbrot, *Structure of the Epidermal Growth Factor Receptor Kinase Domain Alone and in Complex with a 4-Anilinoquinazoline Inhibitor.* Journal of Biological Chemistry, 2002. **277**(48): p. 46265-46272.

197. Yan, X.E., et al., *Structural basis of mutant-selectivity and drug-resistance related to CO-1686.* (1949-2553 (Electronic)).

198. *GOLD5.3:* https://www.ccdc.cam.ac.uk/solutions/csd-discovery/components/gold/.

199. Frisch, M.J., et al., *Gaussian 09, Revision D.01*. 2009, Gaussian Inc.: Wallingford CT.

200. Valero, R., et al., *Good performance of the M06 family of hybrid meta generalized gradient approximation density functionals on a difficult case: CO adsorption on MgO(001).* Journal of Chemical Physics, 2008. **129**(12): p. 124710.

201. Zhao, Y. and D.G. Truhlar, *The M06 Suite of Density Functionals for Main Group Thermochemistry, Thermochemical Kinetics, Noncovalent Interactions, Excited States, and Transition Elements: Two New Functionals and Systematic Testing of Four M06-class Functionals and 12 Other Functionals.* Theor. Chem. Acc., 2008. **120**(1-3): p. 215-241.

202. Abraham, M.J., et al., *GROMACS: High performance molecular simulations through multi-level parallelism from laptops to supercomputers.* SoftwareX, 2015. **1-2**: p. 19-25.

This material is reserved for educational use only, not allowed for commercial use.
Forbidden to modify the content, and cite the document when use.

203. Hornak, V., et al., *Comparison of multiple Amber force fields and development of improved protein backbone parameters.* Proteins: Struct., Funct., Bioinf., 2006. **65**(3): p. 712-725.

204. Thompson, E., et al., *Evaluating Molecular Mechanical Potentials for Helical Peptides and Proteins.* PLoS ONE, 2010. **5**(4): p. e10056.

205. Sousa da Silva, A.W. and W.F. Vranken, *ACPYPE - AnteChamber PYthon Parser interfacE.* BMC Res.Notes, 2012(5): p. 367.

206. Wang, J., et al., *Automatic Atom Type And Bond Type Perception In Molecular Mechanical Calculations.* J. Mol. Graph. Model., 2006. **25**(2): p. 247-260.

207. Wang, J., et al., *Development and testing of a general amber force field.* Journal of Computational Chemistry, 2004. **25**(9): p. 1157-1174.

208. Olsson, M.H.M., et al., *PROPKA3: Consistent Treatment of Internal and Surface Residues in Empirical pKa Predictions.* Journal of Chemical Theory and Computation, 2011. **7**(2): p. 525-537.

209. Søndergaard, C.R., et al., *Improved Treatment of Ligands and Coupling Effects in Empirical Calculation and Rationalization of pKa Values.* Journal of Chemical Theory and Computation, 2011. **7**(7): p. 2284-2295.

210. Price, D.J. and C.L. Brooks, *A modified TIP3P water potential for simulation with Ewald summation.* The Journal of Chemical Physics, 2004. **121**(20): p. 10096-10103.

211. Obounchoey, P., et al., *In silico identification and in vitro validation of nogalamycin N-oxide (NSC116555) as a potent anticancer compound against non–small-cell lung cancer cells.* Journal of Cellular Biochemistry, 2019. **120**(3): p. 3353-3361.

212. Aiebchun, T., et al. *Identification of Vinyl Sulfone Derivatives as EGFR Tyrosine Kinase Inhibitor: In Vitro and In Silico Studies*. Molecules, 2021. **26**, DOI: 10.3390/molecules26082211.

213. Liclican, A., et al., *Biochemical characterization of tirabrutinib and other irreversible inhibitors of Bruton's tyrosine kinase reveals differences in on - and off - target inhibition.* Biochimica et Biophysica Acta (BBA) - General Subjects, 2020. **1864**(4): p. 129531.

This material is reserved for educational use only, not allowed for commercial use.
Forbidden to modify the content, and cite the document when use.

214. Wenlock, M.C., et al., *A Highly Automated Assay for Determining the Aqueous Equilibrium Solubility of Drug Discovery Compounds.* J. Assoc. Lab. Auto., 2011. **16**(4): p. 276-284.

215. Wenlock, M.C., et al., *A Method for Measuring the Lipophilicity of Compounds in Mixtures of 10.* J. Biomol. Screen., 2011. **16**(3): p. 348-355.

216. *ChemAxon JChem: www.chemaxon.com*. ChemAxon JChem: www.chemaxon.com.

217. Niessen, S., et al., *Proteome-wide Map of Targets of T790M-EGFR-Directed Covalent Inhibitors.* Cell Chemical Biology, 2017. **24**(11): p. 1388-1400.e7.

218. Yan, X.-E., et al., *Structural basis of mutant-selectivity and drug-resistance related to CO-1686.* Oncotarget, 2017. **8**(32).

219. Zhou, W., et al., *Novel mutant-selective EGFR kinase inhibitors against EGFR T790M.* Nature, 2009. **462**(7276): p. 1070-4.

220. Sakuma, Y., et al., *WZ4002, a third-generation EGFR inhibitor, can overcome anoikis resistance in EGFR-mutant lung adenocarcinomas more efficiently than Src inhibitors.* Laboratory Investigation, 2012. **92**(3): p. 371-383.

221. Basu, D., A. Richters, and D. Rauh, *Structure-based design and synthesis of covalent-reversible inhibitors to overcome drug resistance in EGFR.* Bioorganic & Medicinal Chemistry, 2015. **23**(12): p. 2767-2780.

222. Planken, S., et al., *Discovery of N-((3R,4R)-4-Fluoro-1-(6-((3-methoxy-1-methyl-1H-pyrazol-4-yl)amino)-9-methyl-9H-purin-2-yl)pyrrolidine-3-yl)acrylamide (PF-06747775) through Structure-Based Drug Design: A High Affinity Irreversible Inhibitor Targeting Oncogenic EGFR Mutants with Selectivity over Wild-Type EGFR.* Journal of Medicinal Chemistry, 2017. **60**(7): p. 3002-3019.

223. Cheng, H., et al., *Discovery of 1-{(3R,4R)-3-[({5-Chloro-2-[(1-methyl-1H-pyrazol-4-yl)amino]-7H-pyrrolo[2,3-d]pyrimidin-4-yl}oxy)methyl]-4-methoxypyrrolidin-1-yl}prop-2-en-1-one (PF-06459988), a Potent, WT Sparing, Irreversible Inhibitor of T790M-Containing EGFR Mutants.* Journal of Medicinal Chemistry, 2016. **59**(5): p. 2005-2024.

This material is reserved for educational use only, not allowed for commercial use.

Forbidden to modify the content, and cite the document when use.

224. Heald, R., et al., *Noncovalent Mutant Selective Epidermal Growth Factor Receptor Inhibitors: A Lead Optimization Case Study.* Journal of Medicinal Chemistry, 2015. **58**(22): p. 8877-8895.

225. Han, S., et al., *Structural Characterization of Proline-rich Tyrosine Kinase 2 (PYK2) Reveals a Unique (DFG-out) Conformation and Enables Inhibitor Design.* Journal of Biological Chemistry, 2009. **284**(19): p. 13193-13201.

226. Liddle, J., et al., *Discovery of GSK143, a highly potent, selective and orally efficacious spleen tyrosine kinase inhibitor.* Bioorganic & Medicinal Chemistry Letters, 2011. **21**(20): p. 6188-6194.

227. Aziz, M.W., et al., *Design, synthesis and assessment of new series of quinazolinone derivatives as EGFR inhibitors along with their cytotoxic evaluation against MCF7 and A549 cancer cell lines.* Bioorganic & Medicinal Chemistry Letters, 2021. **41**: p. 127987.

228. Zhang, B., et al., *Design, synthesis and biological evaluation of sulfamoylphenyl-quinazoline derivatives as potential EGFR/CAIX dual inhibitors.* European Journal of Medicinal Chemistry, 2021. **216**: p. 113300.

229. Van Der Steen, N., et al., *New developments in the management of non-small-cell lung cancer, focus on rociletinib: what went wrong?* Onco Targets Ther, 2016. **9**: p. 6065-6074.

230. Song, Z., et al., *Synthesis and biological evaluation of morpholine-substituted diphenylpyrimidine derivatives (Mor-DPPYs) as potent EGFR T790M inhibitors with improved activity toward the gefitinib-resistant non-small cell lung cancers (NSCLC).* European Journal of Medicinal Chemistry, 2017. **133**: p. 329-339.

231. Tan, L., et al., *Development of Selective Covalent JAK3 Inhibitors.* Journal of medicinal chemistry, 2015. **58**.

232. Liu, Q., et al., *Developing Irreversible Inhibitors of the Protein Kinase Cysteinome.* Chemistry & Biology, 2013. **20**(2): p. 146-159.

233. Bauer, R.A., *Covalent inhibitors in drug discovery: from accidental discoveries to avoided liabilities and designed therapies.* (1878-5832 (Electronic)).

This material is reserved for educational use only, not allowed for commercial use.

Forbidden to modify the content, and cite the document when use.

234. Gurbani, D., et al., *Structure and Characterization of a Covalent Inhibitor of Src Kinase.* (2296-889X (Print)).

235. Tomassi, S., et al., *Indazole-Based Covalent Inhibitors To Target Drug-Resistant Epidermal Growth Factor Receptor.* Journal of Medicinal Chemistry, 2017. **60**(6): p. 2361-2372.

236. Gleeson, D. and M.P. Gleeson, *Theoretical studies to estimate the skin sensitization potential of chemicals of the Schiff base domain.* International Journal of Quantum Chemistry, 2020. **120**(12): p. e26218.

237. Promkatkaew, M., et al., *Skin Sensitization Prediction Using Quantum Chemical Calculations: A Theoretical Model for the SNAr Domain.* Chemical Research in Toxicology, 2014. **27**(1): p. 51-60.

238. Chen, Y., et al., *Discovery of N-(5-((5-chloro-4-((2-(isopropylsulfonyl)phenyl)amino)pyrimidin-2-yl)amino)-4-methoxy-2-(4-methyl-1,4-diazepan-1-yl)phenyl)acrylamide (CHMFL-ALK/EGFR-050) as a potent ALK/EGFR dual kinase inhibitor capable of overcoming a variety of ALK/EGFR associated drug resistant mutants in NSCLC.* Eur J Med Chem, 2017. **139**(20): p. 674-697.

239. Cheng, H., S.K. Nair, and B.W. Murray, *Recent progress on third generation covalent EGFR inhibitors.* Bioorganic & Medicinal Chemistry Letters, 2016. **26**(8): p. 1861-1868.

240. Stamos, J., M.X. Sliwkowski, and C. Eigenbrot, *Structure of the Epidermal Growth Factor Receptor Kinase Domain Alone and in Complex with a 4-Anilinoquinazoline Inhibitor*.* Journal of Biological Chemistry, 2002. **277**(48): p. 46265-46272.

241. Yan, X.-E., et al., *Structural Basis of AZD9291 Selectivity for EGFR T790M.* Journal of Medicinal Chemistry, 2020. **63**(15): p. 8502-8511.

242. Yosaatmadja, Y., et al., *Binding mode of the breakthrough inhibitor AZD9291 to epidermal growth factor receptor revealed.* J. Struct. Biol., 2015. **192**: p. 539.

243. Peters, S., S. Zimmermann, and A.A. Adjei, *Oral epidermal growth factor receptor tyrosine kinase inhibitors for the treatment of non-small cell lung cancer: comparative pharmacokinetics and drug-drug interactions.* Cancer Treatment Reviews, 2014. **40**(8): p. 914-926.

This material is reserved for educational use only, not allowed for commercial use.

Forbidden to modify the content, and cite the document when use.

244. Liu, Q., et al., *Developing irreversible inhibitors of the protein kinase cysteinome.* (1879-1301 (Electronic)).

245. Zhai, X., et al., *Insight into the Therapeutic Selectivity of the Irreversible EGFR Tyrosine Kinase Inhibitor Osimertinib through Enzyme Kinetic Studies.* Biochemistry, 2020. **59**(14): p. 1428-1441.

246. Schwartz, P.A., et al., *Covalent EGFR inhibitor analysis reveals importance of reversible interactions to potency and mechanisms of drug resistance.* Proc. Natl. Acad. Sci. U.S.A., 2014. **111**: p. 173.

This material is reserved for educational use only, not allowed for commercial use.
Forbidden to modify the content, and cite the document when use.

Appendix

This material is reserved for educational use only, not allowed for commercial use.
Forbidden to modify the content, and cite the document when use.

Appendix A: Chemical characterization

Chemical characterization for study 1.

N^1- (2,5- dichloropyrimidin- 4- yl*)* benzene- 1,3- diamine (1), A solution of 2 ,4 ,5-trichloropyrimidine (1 . 5 equivalent) and 3-nitroaniline (1 equivalent), $NaHCO_3$ (2 equivalent) in EtOH (5 ml for 0.5g) was stirred at 80 ℃ for 6 hrs. The reaction mixture was filtered through filter paper and washed with EtOAc to obtain a yellow solid, yield: 67% . ^{1}H NMR (500 MHz, DMSO-d_6) δ 9.85 (s, 1H), 8.57 (t, *J* = 1.7 Hz, 1H), 8.44 (d, *J* = 0.5 Hz, 1H), 8.08 (dd, *J* = 6.5, 1.6 Hz, 1H), 7.97 (dd, *J* = 6.6, 1.8 Hz, 1H), 7.64 (t, *J* = 6.6 Hz, 1H). MS-ESI for $C_{10}H_6Cl_2N_4O_2$ [M], Calcd: 285.1, found: 284.9.

5-chloro-*N^2*-(1-[4-(4-amino-3-methoxyphenyl)piperazin-1-yl]ethan-1-one)-*N^4*-(3-nitrophynyl)pyrimidine-2,4-diamine (2), Following the general procedure A using *N^1*-(2,5-dichloropyrimidin-4-yl)benzene-1,3-diamine (1) (1 equivalent) to substituted 1-[4-(4-amino-3-methoxyphenyl)piperazin-1-yl]ethan-1-one (1.5 equivalent) and TFA (0.4 ml) in isopropanol. yield: 73% . ^{1}H NMR (500 MHz, DMSO-d_6) δ 9.14 (s, 1H), 8.44 (s, 1H), 8.16 (d, J = 6.0 Hz, 1H), 8.08 (s, 1H), 8.01 (s, 1H), 7.83 (dd, J = 6.4, 1.6 Hz, 1H), 7.45 (t, J = 6.6 Hz, 1H), 7.36 (d, J = 6.9 Hz, 1H), 6.60 (d, J = 2.0 Hz, 1H), 6.33 (dd, J = 6.9, 1.8 Hz, 1H), 3.72 (s, 3H), 3.54 (q, J = 5.0 Hz, 4H), 3.08 (t, J = 5.1 Hz, 2H), 3.02 (t, J = 5.2 Hz, 2H), 2.01 (s, 3H). MS-ESI for $C_{23}H_{24}ClN_7O_4$ $[M+H]^+$, Calcd: 498.1, found: 498.1.

5-chloro-*N^2*-(1-[4-(4-aminophenyl)piperazin-1-yl]ethan-1-one)-*N^4*-(3-nitrophynyl)pyrimidine-2,4-diamine **(3),** Following the general procedure A using *N^1*-(2,5-dichloropyrimidin-4-yl)benzene-1,3-diamine **(1)** (1 equivalent) to substituted 1-[4-(4-aminophenyl)piperazin-1-yl]ethan-1-one (1.5 equivalent) and TFA (0.4 ml) in isopropanol. yield: 78%. ^{1}H NMR (500 MHz, DMSO-d_6) δ 9.20 (s, 1H), 9.18 (s, 1H), 8.46 (t, J = 1.5 Hz, 1H), 8.20 (s, 1H), 8.13 (s, 1H), 7.90 (dd, J = 6.5, 1.8 Hz, 1H), 7.56 (t, J = 6.6 Hz, 1H), 7.36 (d, J = 6.9 Hz, 2H), 6.75 (d, J = 7.0 Hz, 2H), 3.53 (q, J = 4.7 Hz, 4H), 3.00 (t, J = 5.0 Hz, 2H), 2.93 (t, J = 5.1 Hz, 2H), 2.00 (s, 3H). MS-ESI for $C_{22}H_{22}ClN_7O_3$ $[M+H]^+$, Calcd: 468.1, found: 468.0.

5-chloro-*N^2*-(1-methyl-1H-pyrazol-4-yl)-*N^4*-(3-nitrophenyl)pyrimidine-2,4-diamine **(4),** Following the general procedure A using *N^1*-(2,5-dichloropyrimidin-4-yl)benzene-1,3-

This material is reserved for educational use only, not allowed for commercial use.
Forbidden to modify the content, and cite the document when use.

diamine **(1)** (1 equivalent) to substituted 1-methyl-1*H*-pyrazol-4-amine (1.5 equivalent) and TFA (0.4 ml) in isopropanol. yield: 50%. ^{1}H NMR (500 MHz, DMSO-d_6) δ 9.22 (s, 3H), 8.46 (s, 1H), 8.13 (s, 2H), 7.94 (s, 1H), 7.61 (t, *J* = 6.5 Hz, 2H), 3.63 (s, 3H). MS-ESI for $C_{14}H_{12}ClN_7O_2$ $[M+H]^+$, Calcd: 346.0, found: 346.0.

5-chloro-N^2-(6-amino-1,3-benzoxazol-2(3H)-one)-N^4-(3-nitrophenyl)pyrimidine-2,4-diamine **(5),** Following the general procedure A using N^1-(2,5-dichloropyrimidin-4-yl)benzene-1,3-diamine **(1)** (1 equivalent) and 6-amino-1,3-benzoxazol-2(3*H*)-one (1.5 equivalent) and TFA (0.4 ml) in isopropanol. yield: 75%. ^{1}H NMR (500 MHz, DMSO-d_6) δ 11.36 (s, 1H), 9.47 (s, 1H), 9.29 (s, 1H), 8.49 (t, J = 1.7 Hz, 1H), 8.19 (s, 1H), 8.14 (d, J = 4.1 Hz, 1H), 8.14 (d, J = 4.1 Hz, 1H), 7.93 (dd, J = 6.6, 1.2 Hz, 1H), 7.61 (s, 1H), 7.58 (t, J = 6.6 Hz, 1H), 7.17 (d, J = 6.0 Hz, 1H), 6.86 (d, J = 6.7 Hz, 1H). MS-ESI for $C_{17}H_{11}ClN_6O_4$ $[M+H]^+$, Calcd: 399.0, found: 399.1.

5-chloro-N^2-(2,3-dimethyl-2H-indazol-6-amine)-N^4-(3-nitrophenyl)pyrimidine-2,4-diamine **(6),** Following the general procedure A using N^1-(2,5-dichloropyrimidin-4-yl)benzene-1,3-diamine **(1)** (1 equivalent) to substituted 2,3-dimethyl-2*H*-indazol-6-amine (1.5 equivalent) and TFA (0.4 ml) in isopropanol. yield: 72%. ^{1}H NMR (500 MHz, DMSO-d_6) δ 9.38 (s, 1H), 9.28 (s, 1H), 8.51 (t, J = 1.7 Hz, 1H), 8.22 (s, 1H), 7.94 (d, J = 1.7 Hz, 1H), 7.92 (dd, J = 1.7, 0.5 Hz, 1H), 7.84 (s, 1H), 7.59 (t, J = 6.5 Hz, 1H), 7.40 (d, J = 7.2 Hz, 1H), 7.03 (dd, J = 7.2, 1.3 Hz, 1H), 3.91 (s, 3H), 2.49 (s, 3H). MS-ESI for $C_{19}H_{16}ClN_7O_2$$[M+H]^+$, Calcd: 410.1, found: 410.2.

5-chloro-N^2-(1-[4-(4-amino-3-methoxyphenyl)piperazin-1-yl]ethan-1-one)-N^4-(3-aminophenyl)pyrimidine-2,4-diamine **(7),** Following the general procedure B using 5-chloro-N^2-(1-[4-(4-amino-3-methoxyphenyl)piperazin-1-yl]ethan-1-one)-N^4-(3-nitrophynyl)pyrimidine-2,4-diamine **(2)**. yield: 67%. ^{1}H NMR (500 MHz, DMSO-d_6) δ 8.36 (s, 1H), 7.97 (s, 1H), 7.66 – 7.63 (m, 2H), 6.90 (t, *J* = 6.3 Hz, 2H), 6.72 (d, *J* = 6.3 Hz, 1H), 6.61 (d, *J* = 2.0 Hz, 1H), 6.40 (dd, *J* = 7.0, 2.0 Hz, 1H), 6.29 (dd, *J* = 6.3, 1.2 Hz, 1H), 4.89 (s, 2H), 3.75 (s, 3H), 3.56 – 3.51 (m, 4H), 3.08 – 3.05 (m, 2H), 3.02 – 2.99 (m, 2H), 2.01(s, 3H). MS-ESI for $C_{23}H_{26}ClN_7O_2$ $[M+H]^+$, Calcd: 468.1, found 468.1.

This material is reserved for educational use only, not allowed for commercial use.
Forbidden to modify the content, and cite the document when use.

5-chloro-N^2-(1-[4-(4-aminophenyl)piperazin-1-yl]ethan-1-one)-N^4-(3-aminophenyl)pyrimidine-2,4-diamine **(8),** Following the general procedure B using 5-chloro-N^2-(1-[4-(4-aminophenyl)piperazin-1-yl]ethan-1-one)-N^4-(3-nitrophynyl)pyrimidine-2,4-diamine **(3)**. yield: 50%. ^{1}H NMR (500 MHz, DMSO-d_6) δ 8.99 (s, 1H), 8.42 (s, 1H), 8.00 (s, 1H), 7.46 (d, J = 7.2 Hz, 2H), 6.94 (t, J = 6.4 Hz, 1H), 6.82 (s, 1H), 6.79 (d, J = 7.3 Hz, 2H), 6.74 (t, J = 5.2 Hz, 1H), 6.33 (dd, J = 6.3, 1.1 Hz, 1H), 4.97 (s, 2H), 3.52 (q, J = 4.3 Hz, 4H), 2.99 (t, J = 5.1 Hz, 2H), 2.92 (t, J = 5.2 Hz, 2H), 1.53 (s, 3H). MS-ESI for $C_{22}H_{24}ClN_7O$ $[M+H]^+$, Calcd: 438.1, found 438.1.

5-chloro-N^2-(1-methyl-1H-pyrazol-4-yl)-N^4-(3-aminophenyl)pyrimidine-2,4-diamine **(9),** Following the general procedure B using 5-chloro-N^2-(1-methyl-1*H*-pyrazol-4-yl)-N^4-(3-nitrophenyl)pyrimidine-2,4-diamine **(4)**. yield: 80%. ^{1}H NMR (500 MHz, DMSO-d_6) δ 9.13 (s, 1H), 8.59 (s, 1H), 7.97 (s, 1H), 7.49 (s, 1H), 7.19 (s, 1H), 7.01 (s, 1H), 6.67 (s, 1H), 6.52 (s, 1H), 6.42 (s, 1H), 5.12 (s, 2H), 3.63 (s, 3H). MS-ESI for $C_{14}H_{14}ClN_7$ $[M+H]^+$, Calcd: 316.1 found, 316.0.

5-chloro-N^2-(6-amino-1,3-benzoxazol-2(3H)-one)-N^4-(3-aminophenyl)pyrimidine-2,4-diamine **(10),** Following the general procedure B using 5-chloro-N^2-(6-amino-1,3-benzoxazol-2(3*H*)-one)-N^4-(3-nitrophynyl)pyrimidine-2,4-diamine **(5).** yield: 59%. ^{1}H NMR (500 MHz, DMSO-d_6) δ 11.33 (s, 1H), 9.26 (s, 1H), 8.54 (s, 1H), 8.05 (s, 1H), 7.67 (d, J = 1.0 Hz, 1H), 7.31 (dd, J = 6.8, 1.6 Hz, 1H), 6.96 (t, J = 6.3 Hz, 1H), 6.86 (d, J = 6.8 Hz, 1H), 6.75 (d, J = 6.7 Hz, 1H), 6.74 (s, 1H), 6.35 (dd, J = 6.4, 0.8 Hz, 1H), 5.01 (s, 2H). MS-ESI for $C_{17}H_{13}ClN_6O_2$ $[M+H]^+$, Calcd: 369.0 found, 369.2.

5-chloro-N^2-(2,3-dimethyl-2H-indazol-6-amine)-N^4-(3-aminophenyl)pyrimidine-2,4-diamine **(11),** Following the general procedure B using 5-chloro-N^2-(2,3-dimethyl-2*H*-indazol-6-amine)-N^4-(3-nitrophynyl)pyrimidine-2,4-diamine **(6)**. yield: 74%. ^{1}H NMR (500 MHz, DMSO-d_6) δ 9.17 (s, 1H), 8.36 (s, 1H), 8.10 (s, 1H), 7.94 (s, 1H), 7.44 (d, J = 7.1 Hz, 1H), 7.11 (dd, J = 7.2, 1.4 Hz, 1H), 7.04 (t, J = 1.6 Hz, 1H), 6.96 (t, J = 6.3 Hz, 1H), 6.82 (dd, J = 6.5, 0.7 Hz, 1H), 6.31 (ddd, J = 6.4, 1.5, 0.5 Hz, 1H), 5.03 (s, 2H), 3.93 (s, 3H), 2.50 (s, 3H). MS-ESI for $C_{19}H_{18}ClN_7$ $[M+H]^+$, Calcd: 380.1, found: 380.2.

This material is reserved for educational use only, not allowed for commercial use.
Forbidden to modify the content, and cite the document when use.

5-chloro-N^2-(1-[4-(4-amino-3-methoxyphenyl)piperazin-1-yl]ethan-1-one)-N^4-(N-(3-aminophenyl)propanamide)pyrimidine-2,4-diamine **(12),** Following the general procedure C using 5-chloro-N^2-(1-[4-(4-amino-3-methoxyphenyl)piperazin-1-yl]ethan-1-one)-N^4-(3-aminophenyl)pyrimidine-2,4-diamine **(7)** and propionyl chloride. yield: 53%, mp =186 ℃, HPLC analysis: retention time = 2.473 min, 97.1% purity. ^{1}H NMR (500 MHz, DMSO-d_6) **δ** 9.90 (s, 1H), 9.57 (s, 1H), 8.13 (s, 1H), 7.82 (s, 1H), 7.45 (d, J = 6.6 Hz, 1H), 7.34 (d, J = 6.2 Hz, 1H), 7.23 (t, J = 6.3 Hz, 1H), 7.19 (d, J = 6.4 Hz, 1H), 6.62 (d, J = 2.0 Hz, 1H), 6.32 (d, J = 5.3 Hz, 1H), 3.76 (s, 3H), 3.54 (q, J = 4.6 Hz, 4H), 3.10 (t, J = 4.9 Hz, 2H), 3.04 (t, J = 5.0 Hz, 2H), 2.28 (q, J = 6.0 Hz, 2H), 2.01 (s, 3H), 1.03 (t, J = 6.0 Hz, 3H). ^{13}C NMR (125 MHz, DMSO-d_6) **δ** 172.57, 168.81, 158.98, 158.71, 157.56, 154.49, 140.07, 138.08, 129.09, 119.58, 117.97, 116.70, 115.79, 115.63, 107.72, 104.40, 101.06, 56.21, 49.73, 49.37, 45.95, 41.16, 30.06, 21.71, 10.18. HRMS (ESI) for $C_{26}H_{30}ClN_7O_3$ $[M+H]^+$, Calcd: 524.2171, found 524.2181.

5-chloro-N^2-(1-[4-(4-amino-3-methoxyphenyl)piperazin-1-yl]ethan-1-one)-N^4-(N-(3-aminophenyl)acrylamide)pyrimidine-2,4-diamine **(13),** Following the general procedure C using 5-chloro-N^2-(1-[4-(4-amino-3-methoxyphenyl)piperazin-1-yl]ethan-1-one)-N^4-(3-aminophenyl)pyrimidine-2,4-diamine **(7)** and Acryloyl chloride. yield: 27%, mp = 168 ℃, HPLC analysis: RT = 3.313 min, 98.5% purity. ^{1}H NMR (500 MHz, DMSO-d_6) **δ** 10.10 (s, 1H), 8.80 (s, 1H), 8.03 (s, 1H), 7.90 (s, 1H), 7.65 (d, J = 7.0 Hz, 1H), 7.63 (s, 1H), 7.41 (d, J = 6.3 Hz, 1H), 7.26 (d, J = 6.6 Hz, 1H), 7.21 (t, J = 6.4 Hz, 1H), 6.59 (d, J = 2.0 Hz, 1H), 6.41 (dd, J = 13.6, 8.1 Hz, 1H), 6.26 (d, J = 7.3 Hz, 1H), 6.22 (dd, J = 13.6, 1.5 Hz, 1H), 5.72 (dd, J = 6.6, 1.4 Hz, 1H), 3.75 (s, 3H), 3.52 (q, J = 5.5 Hz, 4H), 3.02 (t, J = 5.0 Hz, 2H), 2.96 (t, J = 5.1 Hz, 2H), 2.01 (s, 3H). ^{13}C NMR (125 MHz, DMSO-d_6) **δ** 168.71, 163.54, 158.44, 156.42, 155.25, 150.74, 147.92, 139.39, 139.35, 132.41, 128.98, 127.36, 122.43, 121.67, 118.94, 115.62, 115.08, 107.69, 103.90, 101.25, 56.10, 50.06, 49.69, 46.01, 41.20, 21.66. HRMS (ESI) for $C_{26}H_{28}ClN_7O_3$ $[M+Na]^+$, Calcd: 544.1834, found 544.1818.

5-chloro-N^2-(1-[4-(4-amino-3-methoxyphenyl)piperazin-1-yl]ethan-1-one)-N^4-((2E)-N-(3-aminophenyl)-3-phenylprop-2-enamide)pyrimidine-2,4-diamine **(14),** Following the general procedure C using 5-chloro-N^2-(1-[4-(4-amino-3-methoxyphenyl)piperazin-1-yl]ethan-1-one)-N^4-(3-aminophenyl)pyrimidine-2,4-diamine **(7)** and cinnamoyl chloride.

This material is reserved for educational use only, not allowed for commercial use.
Forbidden to modify the content, and cite the document when use.

yield: 28%, mp = 182 °C, HPLC analysis: retention time = 3.660 min, 95.1% purity. ^{1}H NMR (500 MHz, DMSO-d_6) **δ** 10.27 (s, 1H), 8.14 (s, 1H), 7.95 (s, 1H), 7.59 (d, J = 5.6 Hz, 4H), 7.55 (d, J = 12.6 Hz, 2H), 7.49 (d, J = 6.5 Hz, 1H), 7.43 – 7.37 (m, 4H), 7.28 (t, J = 6.4 Hz, 1H), 7.20 (d, J = 5.8 Hz, 1H), 6.84 (d, J = 12.6 Hz, 1H), 6.60 (s, 1H), 3.76 (s, 3H), 3.44 (q, J = 5.5 Hz, 4H), 3.02 (t, J = 5.0 Hz, 2H), 2.98 (t, J = 5.1 Hz, 2H), 1.94 (s, 3H). ^{13}C NMR (125 MHz, DMSO-d_6) **δ** 168.77, 164.20, 157.98, 152.50, 140.69, 140.12, 137.59, 135.18, 130.40, 129.57, 129.34, 128.25, 122.88, 120.28, 117.46, 116.39, 107.95, 104.56, 101.21, 56.32, 49.82, 49.46, 45.69, 40.90, 21.67. HRMS (ESI) for $C_{32}H_{32}ClN_7O_3$ $[M+Na]^+$, Calcd: 620.2147, found 620.2136.

5-chloro-N^2-(1-[4-(4-amino-3-methoxyphenyl)piperazin-1-yl]ethan-1-one)-N^4-(N-(3-aminophenyl)2-chloroacetamide)pyrimidine-2,4-diamine **(15),** Following the general procedure C using 5-chloro-N^2-(1-[4-(4-amino-3-methoxyphenyl)piperazin-1-yl]ethan-1-one)-N^4-(3-aminophenyl)pyrimidine-2,4-diamine **(7)** and chloroacetyl chloride. yield: 46%, mp = 168 °C, HPLC analysis: H_2O-ACN retention time = 3.340 min, 97.1% purity. ^{1}H NMR (500 MHz, DMSO-d_6) **δ** 10.25 (s, 1H), 8.82 (s, 1H), 8.03 (s, 1H), 7.87 (s, 1H), 7.67 (s, 1H), 7.62 (d, J = 6.9 Hz, 1H), 7.33 (d, J = 6.4 Hz, 1H), 7.28 (d, J = 6.9 Hz, 1H), 7.21 (t, J = 6.4 Hz, 1H), 6.60 (d, J = 2.0 Hz, 1H), 6.31 (d, J = 6.0 Hz, 1H), 4.22 (s, 2H), 3.76 (s, 3H), 3.54 (q, J = 5.4 Hz, 4H), 3.05 (t, J = 5.0 Hz, 2H), 3.00 (t, J = 5.2 Hz, 2H), 2.01 (s, 3H). ^{13}C NMR (125 MHz, DMSO-d_6) **δ** 168.71, 165.01, 158.46, 156.34, 155.15, 150.95, 148.07, 139.55, 138.88, 128.99, 122.70, 121.61, 119.09, 115.44, 114.70, 107.77, 101.20, 56.02, 50.04, 49.70, 46.00, 44.04, 41.24, 21.63. HRMS (ESI) for $C_{25}H_{27}Cl_2N_7O_3$ $[M+H]^+$, Calcd: 544.1625, found 544.1633.

5-chloro-N^2-(1-[4-(4-aminophenyl)piperazin-1-yl]ethan-1-one)-N^4-(N-(3-aminophenyl)propanamide)pyrimidine-2,4-diamine **(16),** Following the general procedure C using 5-chloro-N^2-(1-[4-(4-aminophenyl)piperazin-1-yl]ethan-1-one)-N^4-(3-aminophenyl)pyrimidine-2,4-diamine **(8)** and propionyl chloride. yield: 53%, mp = 164 °C, HPLC analysis: retention time = 3.247 min, 95.2% purity. ^{1}H NMR (500 MHz, DMSO-d_6) **δ** 9.84 (s, 1H), 9.06 (s, 1H), 8.79 (s, 1H), 8.04 (s, 1H), 7.75 (s, 1H), 7.42 (d, J = 6.8 Hz, 2H), 7.37 (s, 1H), 7.23 (d, J = 3.4 Hz, 2H), 6.71 (d, J = 6.9 Hz, 2H), 3.51 (q, J = 6.1 Hz, 4H), 2.96 (t, J = 4.9 Hz, 2H), 2.90 (t, J = 5.0 Hz, 2H), 2.28 (q, J = 6.0 Hz, 2H), 1.99 (s, 3H), 1.03 (t, J = 6.0 Hz, 3H). ^{13}C NMR (125 MHz, DMSO-d_6) **δ** 172.47, 168.82, 158.17, 156.58, 155.07, 146.11, 139.78,

This material is reserved for educational use only, not allowed for commercial use.
Forbidden to modify the content, and cite the document when use.

139.22, 133.62, 128.92, 120.60, 118.99, 116.87, 115.67, 115.48, 50.19, 49.76, 46.06, 41.25, 29.99, 21.62, 10.12. HRMS (ESI) for $C_{25}H_{28}ClN_7O_2$ $[M+Na]^+$, Calcd: 516.1885, found 516.1887.

5-chloro-N^2-(1-[4-(4-aminophenyl)piperazin-1-yl]ethan-1-one)-N^4-(N-(3-aminophenyl)acrylamide)pyrimidine-2,4-diamine **(17),** Following the general procedure C using 5-chloro-N^2-(1-[4-(4-aminophenyl)piperazin-1-yl]ethan-1-one)-N^4-(3-aminophenyl)pyrimidine-2,4-diamine **(8)** and Acryloyl chloride. yield: 35%, mp = 186 °C, HPLC analysis: retention time = 3.253 min, 96.8% purity. ^{1}H NMR (500 MHz, DMSO-d_6) δ 10.15 (s, 1H), 9.07 (s, 1H), 8.84 (s, 1H), 8.05 (s, 1H), 7.81 (s, 1H), 7.50 (d, J = 5.8 Hz, 1H), 7.42 (d, J = 7.1 Hz, 2H), 7.27 (t, J = 6.2 Hz, 2H), 6.69 (d, J = 6.8 Hz, 2H), 6.42 (dd, J = 13.6, 8.1 Hz, 1H), 6.23 (dd, J = 13.6, 1.5 Hz, 1H), 5.72 (dd, J = 8.1, 1.5 Hz, 1H), 3.50 (m, J = 4.8 Hz, 1H), 2.94 (t, J = 4.8 Hz, 2H), 2.87 (t, J = 5.0 Hz, 2H), 1.99 (s, 3H). ^{13}C NMR (125 MHz, DMSO-d_6) δ 168.74, 163.62, 158.29, 156.62, 155.32, 146.22, 139.49, 139.36, 133.69, 132.44, 129.12, 127.49, 120.58, 119.64, 116.94, 116.00, 50.25, 49.81, 46.09, 41.24, 21.72. HRMS (ESI) for $C_{25}H_{26}ClN_7O_2$ $[M+Na]^+$, Calcd: 514.1729, found 514.1734.

5-chloro-N^2-(1-[4-(4-aminophenyl)piperazin-1-yl]ethan-1-one)-N^4-((2E)-N-(3-aminophenyl)-3-phenylprop-2-enamide)pyrimidine-2,4-diamine **(18),** Following the general procedure C using 5-chloro-N^2-(1-[4-(4-aminophenyl)piperazin-1-yl]ethan-1-one)-N^4-(3-aminophenyl)pyrimidine-2,4-diamine **(8)** and cinnamoyl chloride. yield: 31%, mp = 162 °C, HPLC analysis: retention time = 3.620 min, 97.9% purity. ^{1}H NMR (500 MHz, DMSO-d_6) δ 10.23 (s, 1H), 9.09 (s, 1H), 8.85 (s, 1H), 8.06 (s, 1H), 7.88 (s, 1H), 7.59 (s, 1H), 7.56 (d, J = 12.7 Hz, 2H), 7.53 (d, J = 6.5 Hz, 1H), 7.46 – 7.38 (m, 5H), 7.29 (t, J = 6.4 Hz, 1H), 7.22 (s, 1H), 6.83 (d, J = 12.6 Hz, 1H), 6.69 (d, J = 6.9 Hz, 2H), 3.42 (m, 4H), 3.35 (m, 2H), 2.87 (m, 2H), 2.83 (m, 2H), 1.89 (s, 3H). ^{13}C NMR (125 MHz, DMSO-d_6) δ 168.54, 163.93, 158.23, 156.59, 155.30, 146.11, 143.92, 140.72, 139.65, 139.29, 135.10, 133.68, 130.33, 129.54, 129.10, 128.17, 125.20, 122.69, 120.41, 119.42, 116.92, 115.87, 50.25, 49.68, 45.95, 41.11, 21.57. HRMS (ESI) for $C_{31}H_{30}ClN_7O_2$ $[M+Na]^+$, Calcd: 590.2042, found 590.2054.

5-chloro-N^2-(1-[4-(4-aminophenyl)piperazin-1-yl]ethan-1-one)-N^4-(N-(3-aminophenyl)-2-chloroacetamide)pyrimidine-2,4-diamine **(19),** Following the general procedure C using 5-chloro-N^2-(1-[4-(4-aminophenyl)piperazin-1-yl]ethan-1-one)-N^4-(3-

This material is reserved for educational use only, not allowed for commercial use.
Forbidden to modify the content, and cite the document when use.

aminophenyl)pyrimidine-2,4-diamine **(8)** and chloroacetyl chloride. yield: 24%, mp = 198 °C, HPLC analysis: retention time = 3.320 min, 97.8% purity. ^{1}H NMR (500 MHz, DMSO-d_6) **δ** 10.27 (s, 1H), 9.06 (s, 1H), 8.84 (s, 1H), 8.05 (s, 1H), 7.74 (s, 1H), 7.41 (d, J = 7.1 Hz, 2H), 7.34 (dd, J = 6.5, 5.1 Hz, 2H), 7.27 (t, J = 6.4 Hz, 1H), 6.72 (d, J = 7.1 Hz, 2H), 4.21 (s, 2H), 3.52 (q, J = 5.4 Hz, 4H), 2.98 (t, J = 5.1 Hz, 2H), 2.91 (t, J = 5.1 Hz, 2H), 2.00 (s, 3H). ^{13}C NMR (125 MHz, DMSO-d_6) **δ** 168.68, 165.09, 160.21, 158.12, 156.43, 154.98, 146.16, 139.43, 138.97, 133.65, 129.04, 120.63, 116.90, 115.62, 50.18, 49.83, 46.03, 44.01, 41.22, 21.61. HRMS (ESI) for $C_{24}H_{25}Cl_2N_7O_2$ $[M+Na]^+$, Calcd: 536.1339, found 536.1329.

5-chloro-N^2-(1-methyl-1H-pyrazol-4-yl)-N^4-(N-(3-aminophenyl)propanamide)pyrimidine-2,4-diamine **(20),** Following the general procedure C using 5-chloro-N^2-(1-methyl-1H-pyrazol-4-yl)-N^4-(3-aminophenyl)pyrimidine-2,4-diamine **(9)** and propionyl chloride. yield: 60%, mp = 204 °C, HPLC analysis: retention time = 3.147 min, 98.1% purity. ^{1}H NMR (500 MHz, DMSO-d_6) **δ** 9.89 (s, 1H), 9.17 (s, 1H), 8.86 (s, 1H), 8.01 (s, 1H), 7.70 (s, 1H), 7.44 (d, J = 3.7 Hz, 1H), 7.29 (d, J = 1.2 Hz, 2H), 7.18 (s, 1H), 7.08 (s, 1H), 3.53 (s, 3H), 2.28 (q, J = 6.0 Hz, 2H), 1.03 (t, J = 6.0 Hz, 3H). ^{13}C NMR (125 MHz, DMSO-d_6) **δ** 177.21, 173.76, 163.56, 139.59, 139.09, 129.46, 123.38, 49.07, 31.09, 10.08. HRMS (ESI) for $C_{17}H_{18}ClN_7O$ $[M+Na]^+$, Calcd: 394.1154, found: 394.1143. HRMS (ESI) for $C_{17}H_{18}ClN_7O$ $[M+K]^+$, Calcd: 410.0893, found: 410.0876.

5-chloro-N^2-(1-methyl-1H-pyrazol-4-yl)-N^4-(N-(3-aminophenyl)acrylamide)pyrimidine-2,4-diamine **(21),** Following the general procedure C using 5-chloro-N^2-(1-methyl-1H-pyrazol-4-yl)-N^4-(3-aminophenyl)pyrimidine-2,4-diamine **(9)** and Acryloyl chloride. yield: 42%, mp = 204 °C, HPLC analysis: retention time = 3.147 min, 98.7% purity. ^{1}H NMR (500 MHz, DMSO-d_6) **δ** 10.20 (s, 1H), 9.20 (s, 1H), 8.91 (s, 1H), 8.02 (s, 1H), 7.79 (s, 1H), 7.54 (s, 1H), 7.33 (s, 2H), 7.18 (s, 1H), 7.14 (s, 1H), 6.41 (dd, *J* = 13.6, 8.1 Hz, 1H), 6.22 (dd, *J* = 13.6, 1.5 Hz, 1H), 5.72 (dd, *J* = 8.1, 1.5 Hz, 1H), 3.51 (s, 3H). ^{13}C NMR (125 MHz, DMSO-d_6) **δ** 163.71, 157.59, 139.65, 139.44, 132.18, 129.29, 127.59, 123.65, 120.80, 49.06. HRMS (ESI) for $C_{17}H_{17}ClN_7O$ $[M+Na]^+$, Calcd: 392.0997, found: 392.0990.

5-chloro-N^2-(1-methyl-1H-pyrazol-4-yl)-N^4-((2E)-N-(3-aminophenyl)-3-phenylprop-2-enamide)pyrimidine-2,4-diamine **(22),** Following the general procedure C using 5-chloro-

This material is reserved for educational use only, not allowed for commercial use.
Forbidden to modify the content, and cite the document when use.

N^2-(1-methyl-1H-pyrazol-4-yl)-N^4-(3-aminophenyl)pyrimidine-2,4-diamine **(9)** and cinnamoyl chloride. yield: 26%, mp = 206 ℃, HPLC analysis: retention time = 3.593 min, 99.8% purity. ^{1}H NMR (500 MHz, DMSO-d_6) **δ** 10.27 (s, 1H), 9.21 (s, 1H), 8.93 (s, 1H), 8.03 (s, 1H), 7.82 (s, 1H), 7.59 (d, *J* = 5.7 Hz, 3H), 7.55 (d, *J* = 12.6 Hz, 2H), 7.43 – 7.34 (m, 5H), 7.19 (s, 1H), 6.82 (d, *J* = 12.6 Hz, 1H), 3.53 (s, 3H). ^{13}C NMR (125 MHz, DMSO-d_6) **δ** 164.95, 163.78, 141.75, 141.19, 139.33, 139.08, 134.57, 129.51, 128.25, 123.29, 121.64, 121.58, 112.73, 109.60, 36.65. HRMS (ESI) for $C_{23}H_{20}ClN_7O$ $[M+Na]^+$, Calcd: 468.1310, found: 468.1303.

5-chloro-N^2-(1-methyl-1H-pyrazol-4-yl)-N^4-(N-(3-aminophenyl)-2-chloroacetamide)pyrimidine-2,4-diamine **(23),** Following the general procedure C using 5-chloro-N^2-(1-methyl-1H-pyrazol-4-yl)-N^4-(3-aminophenyl)pyrimidine-2,4-diamine **(9)** and chloroacetyl chloride. yield: 48%, mp = 214 ℃, HPLC analysis: retention time = 3.187 min, 95.9% purity. ^{1}H NMR (500 MHz, DMSO-d_6) **δ** 10.40 (s, 1H), 9.23 (s, 1H), 8.98 (s, 1H), 8.03 (s, 1H), 7.71 (s, 1H), 7.44 (s, 1H), 7.33 (s, 2H), 7.19 (s, 2H), 4.23 (s, 2H), 3.54 (s, 3H). ^{13}C NMR (125 MHz, DMSO-d_6) **δ** 165.18, 156.82, 154.07, 139.39, 130.10, 129.35, 123.24, 121.01, 116.37, 44.02. HRMS (ESI) for $C_{16}H_{15}Cl_2N_7O$ $[M+Na]^+$, Calcd: 414.0607, found: 414.0605.

5-chloro-N^2-(6-amino-1,3-benzoxazol-2(3H)-one)-N^4-(N-(3-aminophenyl)propanamide)pyrimidine-2,4-diamine **(24),** Following the general procedure C using 5-chloro-N^2-(6-amino-1,3-benzoxazol-2(3H)-one)-N^4-(3-aminophenyl)pyrimidine-2,4-diamine **(10)** and propionyl chloride. yield: 48%, mp = 218 ℃, HPLC analysis: retention time = 3.300 min, 98.9% purity. ^{1}H NMR (500 MHz, DMSO-d_6) **δ** 11.44 (s, 1H), 9.93 (s, 1H), 9.79 (s, 1H), 9.37 (s, 1H), 8.17 (s, 1H), 7.89 (s, 1H), 7.59 (s, 1H), 7.36 (d, J = 6.2 Hz, 1H), 7.24 (t, J = 6.4 Hz, 1H), 7.18 (d, J = 6.9 Hz, 2H), 6.85 (d, J = 6.7 Hz, 1H), 2.28 (q, J = 6.0 Hz, 2H), 1.01 (t, J = 6.0 Hz, 3H). ^{13}C NMR (125 MHz, DMSO-d_6) **δ** 172.76, 157.93, 155.09, 143.77, 140.43, 137.58, 132.51, 129.13, 127.07, 119.91, 116.98, 115.78, 109.90, 104.76, 104.02, 30.05, 10.14. HRMS (ESI) for $C_{20}H_{17}ClN_6O_3$ $[M+H]^+$, Calcd: 425.1123, found: 425.1104.

5-chloro-N^2-(6-amino-1,3-benzoxazol-2(3H)-one)-N^4-(N-(3-aminophenyl)acrylamide)pyrimidine-2,4-diamine **(25),** Following the general procedure C using 5-chloro-N^2-(6-amino-1,3-benzoxazol-2(3H)-one)-N^4-(3-aminophenyl)pyrimidine-2,4-diamine **(10)** and Acryloyl chloride. yield: 24%, mp = 240 ℃, HPLC analysis: retention time

This material is reserved for educational use only, not allowed for commercial use.
Forbidden to modify the content, and cite the document when use.

= 3.207 min, 95.8% purity. ^{1}H NMR (500 MHz, DMSO-d$_6$) δ 11.32 (s, 1H), 10.14 (s, 1H), 9.33 (s, 1H), 8.90 (s, 1H), 8.10 (s, 1H), 7.91 (s, 1H), 7.67 (s, 1H), 7.42 (d, *J* = 5.8 Hz, 1H), 7.30 – 7.23 (m, 3H), 6.81 (d, *J* = 6.7 Hz, 1H), 6.40 (dd, *J* = 13.6, 8.1 Hz, 1H), 6.19 (dd, *J* = 13.5, 1.5 Hz, 1H), 5.69 (dd, *J* = 8.1, 1.5 Hz, 1H). ^{13}C NMR (125 MHz, DMSO-d$_6$) δ 163.68, 158.12, 156.63, 155.25, 143.85, 139.78, 139.34, 135.93, 132.43, 129.13, 127.27, 124.70, 119.60, 115.85, 115.35, 114.92, 109.55, 101.98. HRMS (ESI) for $C_{20}H_{15}ClN_6O_3$ $[M+Na]^+$, Calcd: 445.0786, found: 445.0802.

5-chloro-*N*^{2}-(6-amino-1,3-benzoxazol-2(3H)-one)-*N*^{4}-((2E)-N-(3-aminophenyl)-3-phenylprop-2-enamide)pyrimidine-2,4-diamine **(26),** Following the general procedure C using 5-chloro-*N*^{2}-(6-amino-1,3-benzoxazol-2(3H)-one)-*N*^{4}-(3-aminophenyl)pyrimidine-2,4-diamine **(10)** and cinnamoyl chloride. yield: 61%, mp = 230 °C, HPLC analysis: retention time = 3.673 min, 99.4% purity.^{1}H NMR (500 MHz, DMSO-d$_6$) δ 11.44 (s, 1H), 10.40 (s, 1H), 9.90 (s, 1H), 9.48 (s, 1H), 8.20 (s, 1H), 8.05 (s, 1H), 7.61 – 7.57 (m, 3H), 7.54 – 7.49 (m, 2H), 7.40 (m, 3H), 7.29 (t, *J* = 6.4 Hz, 1H), 7.25 (d, *J* = 6.3 Hz, 1H), 7.20 (d, *J* = 6.5 Hz, 1H), 6.89 (d, *J* = 7.2 Hz, 1H), 6.86 (s, 1H). ^{13}C NMR (125 MHz, DMSO-d$_6$) δ 164.25, 157.62, 155.13, 143.79, 140.63, 140.22, 138.14, 135.22, 133.25, 130.33, 130.18, 129.54, 129.27, 128.28, 126.64, 122.86, 116.87, 109.85, 104.81, 103.86. HRMS (ESI) for $C_{26}H_{19}ClN_6O_3$ $[M+Na]^+$, Calcd: 521.1099, found: 521.1119.

5-chloro-*N*^{2}-(6-amino-1,3-benzoxazol-2(3H)-one)-*N*^{4}-(N-(3-aminophenyl)-2-chloroacetamide)pyrimidine-2,4-diamine **(27),** Following the general procedure C using 5-chloro-*N*^{2}-(6-amino-1,3-benzoxazol-2(3H)-one)-*N*^{4}-(3-aminophenyl)pyrimidine-2,4-diamine **(10)** and chloroacetyl chloride. yield: 33%, mp = 222 °C HPLC analysis: retention time = 3.333 min, 97.8% purity. ^{1}H NMR (500 MHz, DMSO-d$_6$) δ 11.33 (s, 1H), 10.28 (s, 1H), 9.34 (s, 1H), 8.92 (s, 1H), 8.11 (s, 1H), 7.83 (s, 1H), 7.69 (s, 1H), 7.32 (dd, *J* = 8.0, 6.7 Hz, 2H), 7.28 (d, *J* = 6.2 Hz, 1H), 7.20 (dd, *J* = 6.8, 1.2 Hz, 1H), 6.82 (d, *J* = 6.8 Hz, , 1H), 4.21 (s, 2H). ^{13}C NMR (125 MHz, DMSO-d$_6$) δ 165.06, 158.00, 156.56, 155.23, 155.17, 143.80, 139.34, 139.16, 135.81, 129.18, 124.66, 119.83, 115.72, 115.19, 114.87, 109.58, 104.22, 101.93, 44.06. HRMS (ESI) for $C_{19}H_{14}Cl_2N_6O_3$ $[M+H]^+$, Calcd: 445.0577, found: 445.0591.

This material is reserved for educational use only, not allowed for commercial use.
Forbidden to modify the content, and cite the document when use.

5-chloro-N^2-(2,3-dimethyl-2H-indazol-6-amine)-N^4-(N-(3-aminophenyl)propanamide)pyrimidine-2,4-diamine **(28),** Following the general procedure C using compound **11** and propionyl chloride. yield: 29%, mp = 218 °C, HPLC analysis: retention time = 3.340 min, 98.2% purity. ^{1}H NMR (500 MHz, DMSO-d_6) δ 9.79 (s, 1H), 9.17 (s, 1H), 8.80 (s, 1H), 8.13 (s, 1H), 7.84 (s, 1H), 7.80 (s, 1H), 7.38 (d, *J* = 7.1 Hz, 1H), 7.35 (d, *J* = 8.0 Hz, 2H), 7.23 (t, *J* = 6.4 Hz, 1H), 7.14 (dd, *J* = 7.2, 1.2 Hz, 1H), 3.92 (s, 3H), 2.49 (s, 3H), 2.25 (q, *J* = 6.0 Hz, 2H), 1.01 (t, *J* = 6.0 Hz, 3H). ^{13}C NMR (125 MHz, DMSO-d_6) δ 172.40, 158.31, 156.37, 155.01, 147.90, 139.87, 139.28, 138.11, 131.46, 129.04, 119.90, 118.45, 117.38, 116.52, 115.63, 114.78, 104.46, 103.27, 37.42, 29.99, 10.12, 9.82. HRMS (ESI) for $C_{22}H_{22}ClN_7O$ $[M+Na]^+$, Calcd: 458.1467, found: 458.1436.

5-chloro-N^2-(2,3-dimethyl-2H-indazol-6-amine)-N^4-(N-(3-aminophenyl)acrylamide)pyrimidine-2,4-diamine **(29),** Following the general procedure C using compound **11** and Acryloyl chloride. yield: 43%, mp = 210 °C, HPLC analysis: retention time = 3.307 min, 99.5% purity. ^{1}H NMR (500 MHz, DMSO-d_6) δ 10.10 (s, 1H), 9.22 (s, 1H), 8.87 (s, 1H), 8.18 (s, 1H), 7.90 (d, J = 9.2 Hz, 2H), 7.52 (d, J = 8.2 Hz, 1H), 7.46 (d, J = 8.6 Hz, 1H), 7.42 (d, J = 9.0 Hz, 1H), 7.32 (t, J = 8.1 Hz, 1H), 7.19 (dd, J = 9.0, 1.6 Hz, 1H), 6.43 (dd, J = 17.0, 10.1 Hz, 1H), 6.25 (dd, J = 17.0, 2.0 Hz, 1H), 5.74 (dd, J = 10.1, 2.0 Hz, 1H), 3.96 (s, 3H), 2.50 (s, 3H). ^{13}C NMR (125 MHz, DMSO-d_6) δ 163.60, 158.33, 156.36, 155.08, 147.89, 139.52, 139.36, 138.08, 132.47, 131.45, 129.18, 127.13, 119.91, 118.98, 117.40, 116.53, 115.86, 115.05, 104.46, 103.38, 37.40, 9.81. HRMS (ESI) for $C_{22}H_{20}ClN_7O$ $[M+Na]^+$, Calcd: 456.1310, found: 456.1308.

5-chloro-N^2-(2,3-dimethyl-2H-indazol-6-amine)-N^4-((2E)-N-(3-aminophenyl)-3-phenylprop-2-enamide)pyrimidine-2,4-diamine **(30),** Following the general procedure C using compound **11** and cinnamoyl chloride. yield: 25%, mp = 214 °C, HPLC analysis: retention time = 3.687 min, 97.9% purity. ^{1}H NMR (500 MHz, DMSO-d_6) δ 10.10 (s, 1H), 9.19 (s, 1H), 8.84 (s, 1H), 8.14 (s, 1H), 7.89 (t, *J* = 1.5 Hz, 1H), 7.84 (s, 1H), 7.56 (d, *J* = 5.7 Hz, 2H), 7.50 (d, *J* = 12.7 Hz, 2H), 7.43 – 7.36 (m, 5H), 7.29 (t, *J* = 6.4 Hz, 1H), 7.15 (dd, *J* = 7.2, 1.4 Hz, 1H), 6.76 (d, *J* = 12.6 Hz, 1H), 3.87 (s, 3H), 2.41 (s, 3H). ^{13}C NMR (125 MHz, DMSO-d_6) δ 163.95, 158.33, 156.36, 155.11, 147.88, 140.37, 139.77, 139.37, 138.08, 135.20, 131.39,

This material is reserved for educational use only, not allowed for commercial use.
Forbidden to modify the content, and cite the document when use.

130.22, 129.50, 129.19, 128.14, 122.90, 119.90, 118.83, 117.40, 116.55, 115.74, 114.88, 103.41, 37.34, 9.74. HRMS (ESI) for $C_{28}H_{24}ClN_7O$ $[M+Na]^+$, Calcd: 532.1623, found: 532.1589.

5-chloro-N^2-(2,3-dimethyl-2H-indazol-6-amine)-N^4-(N-(3-aminophenyl)-2-chloroacetamide)pyrimidine-2,4-diamine **(31),** Following the general procedure C using compound **11** and chloroacetyl chloride. yield: 27%, mp = 206 ℃, HPLC analysis: retention time = 3.393 min, 95.1% purity. ^{1}H NMR (500 MHz, DMSO-d_6) δ 10.30 (s, 1H), 9.25 (s, 1H), 8.90 (s, 1H), 8.19 (s, 1H), 7.90 (d, J = 7.6 Hz, 2H), 7.49 (d, J = 7.9 Hz, 1H), 7.45 – 7.39 (m, 2H), 7.32 (t, J = 8.0 Hz, 1H), 7.16 (dd, J = 9.0, 1.3 Hz, 1H), 4.23 (s, 2H), 3.97 (s, 3H), 2.53 (s, 3H). ^{13}C NMR (125 MHz, DMSO-d_6) δ 165.01, 158.23, 156.32, 155.03, 147.82, 139.43, 138.98, 138.05, 131.58, 129.25, 119.96, 119.18, 117.36, 116.53, 115.77, 114.94, 104.46, 103.31, 44.08, 37.42, 9.83. HRMS (ESI) for $C_{21}H_{19}Cl_2N_7O$ $[M+Na]^+$, Calcd: 478.0920, found: 478.0886.

Chemical characterization for study 2.

N-(2-chloropyrimidin-4-yl)-2-methyl-2H-indazol-6-amine **(32)**, Following the general procedure using 2,4-dichloropyrimidine and 2-Methyl-2H-indazol-6-amine. The precipitate was filtered and washed with EtOH to give the desired product as a light yellow, 82% yield. ^{1}H NMR (500 MHz, DMSO-d_6) δ 10.00 (s, 1H), 8.24 (s, 1H), 8.12 (d, *J* = 4.7 Hz, 1H), 8.00 (s, 1H), 7.63 (d, 1H), 7.01 (dd, *J* = 7.1, 1.4 Hz, 1H), 6.75 (d, *J* = 4.7 Hz, 1H), 4.09 (s, 3H). MS-ESI for $C_{12}H_{10}ClN_5$ $[M+H]^+$, Calcd: 260.0, found: 260.0.

N-(2,5-dichloropyrimidin-4-yl)-2-methyl-2*H*-indazol-6-amine **(33)**, Following the general procedure using 2,4,5-trichloropyrimidine and 2-Methyl-2H-indazol-6-amine. The precipitate was filtered and washed with EtOH to give the desired product a light yellow, 73% yield. ^{1}H NMR (500 MHz, DMSO-d_6) δ 9.49 (s, 1H), 8.33 (d, *J* = 4.2 Hz, 1H), 8.27, 7.79 – 7.76 (m, 1H), 7.64 (dd, *J* = 7.2, 1.7 Hz, 1H), 7.15 (dd, *J* = 7.1, 1.5 Hz, 1H), 4.11 (s, 3H).MS-ESI for $C_{12}H_9Cl_2N_5$ $[M+H]^+$, Calcd: 294.0, found: 294.0.

N^2-[3-(aminomethyl)phenyl]-5-chloro-N^4-(2-methyl-2H-indazol-6-yl)pyrimidine-2,4-diamine (**34**), Following the general procedure using N-(2-chloropyrimidin-4-yl)-2-methyl-2H-indazol-6-amine **(1)** and 3-(aminomethyl)aniline. 89% yield. ^{1}H NMR (500 MHz, DMSO-d_6) δ 9.47 (s, 1H), 9.21 (s, 1H), 8.20 (s, 1H), 8.18 (s, 1H), 7.98 (d, J = 3.4 Hz, 1H), 7.81 (t, J =

This material is reserved for educational use only, not allowed for commercial use.
Forbidden to modify the content, and cite the document when use.

1.3 Hz, 1H), 7.57 (d, J = 5.3 Hz, 1H), 7.54 (dd, J = 4.9, 1.5 Hz, 1H), 7.20 (t, J = 4.7 Hz, 1H), 7.08 (dd, J = 5.3, 1.1 Hz, 1H), 6.96 (d, J = 2.3 Hz, 1H), 6.26 (d, J = 3.4 Hz, 1H), 4.08 (s, 3H), 3.98 (d, J = 4.1 Hz, 2H), 1.12 (t, J = 4.2 Hz, 2H). LCQTOF for $C_{19}H_{19}N_7$ $[M+H]^+$, Calcd: 346.1774, found: 346.1746.

N^2-[3-(aminomethyl)phenyl]-5-chloro-*N*^{4}-(2-methyl-2H-indazol-6-yl)pyrimidine-2,4-diamine **(35)**, Following the general procedure using N-(2,5-dichloropyrimidin-4-yl)-2-methyl-2H-indazol-6-amine **(2)** and 3-(aminomethyl)aniline. 75% yield. ^{1}H NMR (500 MHz, DMSO-*d*$_6$) **δ** 9.28 (s, 1H), 8.78 (s, 1H), 8.25 (s, 1H), 8.10 (s, 1H), 7.87 (s, 1H), 7.61 (d, J = 5.3 Hz, 1H), 7.52 (s, 1H), 7.41 (dd, J = 4.8, 1.6 Hz, 1H), 7.23 (dd, J = 5.3, 1.1 Hz, 1H), 7.03 (t, J = 4.7 Hz, 1H), 6.84 (d, J = 4.8 Hz, 1H), 4.11 (s, 3H), 3.44 (s, 2H). LCQTOF for $C_{19}H_{18}ClN_7$ $[M+H]^+$, Calcd: 380.1385, found: 380.1404.

N^4-(2-methyl-2H-indazol-6-yl)-*N*^{2}-(3-nitrophenyl)pyrimidine-2,4-diamine **(36),** Following the general procedure using *N*-(2-chloropyrimidin-4-yl)-2-methyl-2H-indazol-6-amine **(1)** and 3-nitroaniline. 72% yield. ^{1}H NMR (500 MHz, DMSO-*d*$_6$) **δ** 10.28 (s, 1H), 10.12 (s, 1H), 8.58 (s, 1H), 8.22 (s, 1H), 8.05 (s, 2H), 8.03 (d, *J* = 3.9 Hz, 1H), 7.86 (d, *J* = 6.4 Hz, 1H), 7.59 (d, *J* = 5.3 Hz, 1H), 7.54 (t, *J* = 4.9 Hz, 1H), 7.06 (dd, *J* = 5.3, 1.1 Hz, 1H), 6.40 (d, *J* = 3.9 Hz, 1H), 4.08 (s, 3H). LCQTOF for $C_{18}H_{15}N_7O_2$ $[M+H]^+$, Calcd: 362.1360, found: 362.1353.

5-chloro-*N*^{4}-(2-methyl-2*H*-indazol-6-yl)-*N*^{2}-(3-nitrophenyl)pyrimidine-2,4-diamine **(37),** Following the general procedure using *N*-(2,5-dichloropyrimidin-4-yl)-2-methyl-2*H*-indazol-6-amine **(33)** and 3-nitroaniline. 67% yield. ^{1}H NMR (500 MHz, DMSO-*d*$_6$) **δ** 9.79 (s, 1H), 8.93 (s, 1H), 8.49 (s, 1H), 8.24 (s, 1H), 8.19 (s, 1H), 8.05 (dd, *J* = 6.6, 1.6 Hz, 1H), 7.86 (s, 1H), 7.66 (dd, *J* = 6.5, 1.7 Hz, 1H), 7.60 (d, *J* = 7.1 Hz, 1H), 7.32 (t, *J* = 6.6 Hz, 1H), 7.21 (dd, *J* = 7.1, 1.4 Hz, 1H), 4.10 (s, 3H). MS-ESI for $C_{18}H_{14}ClN_7O_2$ $[M+H]^+$, Calcd: 396.0, found: 396.0.

N^2-(2-methoxy-5-nitrophenyl)-*N*^{4}-(2-methyl-2*H*-indazol-6-yl)pyrimidine-2,4-diamine **(38),** Following the general procedure using *N*-(2-chloropyrimidin-4-yl)-2-methyl-2H-indazol-6-amine **(32)** and 2-methoxy-5-nitroaniline. 71% yield. ^{1}H NMR (500 MHz, DMSO-*d*$_6$) **δ** 10.87 (s, 1H), 9.92 (s, 1H), 8.61 (s, 1H), 8.23 (s, 1H), 8.15 (dd, *J* = 5.5, 1.6 Hz, 1H), 8.00 (d, *J* = 4.3 Hz, 1H), 7.92 (s, 1H), 7.56 (d, *J* = 5.3 Hz, 1H), 7.33 (d, *J* = 5.5 Hz, 1H), 7.06 (d, *J* =

This material is reserved for educational use only, not allowed for commercial use.
Forbidden to modify the content, and cite the document when use.

5.3 Hz, 1H), 6.55 – 6.49 (m, 1H), 4.06 (s, 3H), 3.97 (s, 3H). LCQTOF for $C_{19}H_{17}N_7O_3$ $[M+H]^+$, Calcd: 392.1465, found: 392.1431.

5-chloro-*N*^{2}-(2-methoxy-5-nitrophenyl)-*N*^{4}-(2-methyl-2*H*-indazol-6-yl)pyrimidine-2,4-diamine **(39)**, Following the general procedure using *N*-(2,5-dichloropyrimidin-4-yl)-2-methyl-2*H*-indazol-6-amine **(33)** and 2-methoxy-5-nitroaniline. 69% yield. ^{1}H NMR (500 MHz, DMSO-d_6) δ 9.47 (s ,H), 8.81 (s, 1H), 8.64 (d, J = 1.8 Hz, 1H), 8.29 (s, 1H), 8.23 (s, 1H), 7.94 (dd, J = 5.5, 1.8 Hz, 1H), 7.76 (s, 1H), 7.53 (d, J = 5.5 Hz, 1H), 7.21 (d, J = 5.5 Hz, 1H), 7.16 (dd, J = 5.4, 1.3 Hz, 1H), 4.07 (s, 3H), 3.93 (s, 3H). LCQTOF for $C_{19}H_{16}ClN_7O_3$ $[M+H]^+$, Calcd: 426.1075, found: 426.1052.

N^2-[4-((dimethylamino)ethyl)-2-methoxy-5-nitrophenyl]-*N*^{4}-(2-methyl-2H-indazol-6-yl)pyrimidine-2,4-diamine **(40),** Following the general procedure using *N*-(2,5-dichloropyrimidin-4-yl)-2-methyl-2*H*-indazol-6-amine **(32)** and *N*^{1}-[2-(dimethylamino)ethyl]-5-methoxy-*N*^{1}-methyl-2-nitrobenzene-1,4-diamine. 60% yield. ^{1}H NMR (500 MHz, DMSO-d_6) δ 9.38 (s, 1H), 8.39 (s, 1H), 8.15 (s, 1H), 8.00 (s, 1H), 7.95 (d, *J* = 3.4 Hz, 1H), 7.84 (s, 1H), 7.50 (d, *J* = 5.3 Hz, 1H), 7.04 (dd, *J* = 5.5, 1.1 Hz, 1H), 6.81 (s, 1H), 6.22 (d, *J* = 3.7 Hz, 1H), 4.06 (s, 3H), 3.91 (s, 3H), 3.22 (t, *J* = 4.2 Hz, 2H), 2.83 (s, 3H), 2.43 – 2.40 (m, 2H), 2.10 (s, 6H). LCQTOF for $C_{24}H_{29}N_9O_3$ $[M+H]^+$, Calcd: 492.2466, found: 492.2453.

5-chloro-*N*^{2}-[4-((dimethylamino)ethyl)-2-methoxy-5-nitrophenyl]-*N*^{4}-(2-methyl-2H-indazol-6-yl)pyrimidine-2,4-diamine **(41),** Following the general procedure using *N*-(2,5-dichloropyrimidin-4-yl)-2-methyl-2*H*-indazol-6-amine **(33)** and *N*^{1}-[2-(dimethylamino)ethyl]-5-methoxy-*N*^{1}-methyl-2-nitrobenzene-1,4-diamine. 58% yield. ^{1}H NMR (500 MHz, DMSO-d_6) δ 8.76 (s, 1H), 8.24 (s, 1H), 8.22 (s, 1H), 8.20 (s, 1H), 8.09 (s, 1H), 7.82 (s, 1H), 7.50 (d, *J* = 5.5 Hz, 1H), 7.19 (dd, *J* = 5.4, 1.3 Hz, 1H), 6.84 (s, 1H), 4.08 (s, 3H), 3.90 (s, 3H), 3.68 – 3.60 (m, 2H), 2.95 (d, *J* = 3.4 Hz, 2H), 2.77 (s, 3H), 2.52 (s, 6H). LCQTOF for $C_{24}H_{28}ClN_9O_3$ $[M+H]^+$, Calcd: 526.2076, found: 526.2105.

N^2-(3-aminophenyl)-*N*^{4}-(2-methyl-2*H*-indazol-6-yl)pyrimidine-2,4-diamine **(42)**, Following the general procedure using *N*^{4}-(2-methyl-2H-indazol-6-yl)-*N*^{2}-(3-nitrophenyl)pyrimidine-2,4-diamine **(36)**. 73% yield. ^{1}H NMR (500 MHz, DMSO-d_6) δ 9.26 (s, 1H), 8.89 (s, 1H), 8.23 (s, 1H), 8.19 (s, 1H), 7.95 (d, J = 3.4 Hz, 1H), 7.57 (d, J = 5.3 Hz, 1H),

This material is reserved for educational use only, not allowed for commercial use.
Forbidden to modify the content, and cite the document when use.

7.18 (t, J = 1.3 Hz, 1H), 7.06 (dd, J = 5.5, 1.1 Hz, 1H), 6.84 (t, J = 4.7 Hz, 1H), 6.79 (dt, J = 4.8, 0.9 Hz, 1H), 6.18 (d, J = 3.4 Hz, 1H), 6.12 (dt, J = 4.6, 1.1 Hz, 1H), 4.91 (s, 2H), 4.08 (s, 3H). LCQTOF for $C_{18}H_{17}N_7$ $[M+H]^+$, Calcd: 332.1618, found: 332.1620.

N^2-(5-amino-2-methoxyphenyl)-*N*^{4}-(2-methyl-2*H*-indazol-6-yl)pyrimidine-2,4-diamine **(43),** Following the general procedure using *N*^{2}-(2-methoxy-5-nitrophenyl)-*N*^{4}-(2-methyl-2*H*-indazol-6-yl)pyrimidine-2,4-diamine **(38)**. 51% yield. ^{1}H NMR (500 MHz, DMSO-d_6) δ 9.40 (s, 1H), 8.22 (s, 1H), 8.17 (s, 1H), 7.96 (d, J = 3.4 Hz, 1H), 7.70 (d, J = 1.6 Hz, 1H), 7.60 (d, J = 5.3 Hz, 1H), 7.45 (s, 1H), 7.00 (dd, J = 5.3, 1.1 Hz, 1H), 6.70 (d, J = 5.3 Hz, 1H), 6.23 (d, J = 3.4 Hz, 1H), 6.14 (dd, J = 5.0, 1.6 Hz, 1H), 4.64 (s, 2H), 4.08 (s, 3H), 3.72 (s, 3H). LCQTOF for $C_{19}H_{19}N_7O$ $[M+H]^+$, Calcd: 362.1723, found: 362.1687.

N^2-[5-amino-4-((dimethylamino)ethyl)-2-methoxyphenyl]-*N*^{4}-(2-methyl-2H-indazol-6-yl)pyrimidine-2,4-diamine **(44),** Following the general procedure using **40.** 56% yield. ^{1}H NMR (500 MHz, DMSO-d_6) δ 9.30 (s, 1H), 8.17 (s, 1H), 8.08 (s, 1H), 7.91 (d, *J* = 3.4 Hz, 1H), 7.76 (s, 1H), 7.52 (d, *J* = 5.3 Hz, 1H), 7.03 (d, *J* = 6.6 Hz, 1H), 6.94 (s, 1H), 6.18 (d, *J* = 3.4 Hz, 1H), 4.08 (s, 3H), 3.80 (s, 3H), 2.67 (s, 3H), 2.60 (q, *J* = 1.1 Hz, 2H), 2.33 – 2.32 (m, 2H), 1.99 (s, 6H). LCQTOF for $C_{24}H_{31}N_9O$ $[M+H]^+$, Calcd: 462.2724, found: 462.2704.

N^2-(3-aminophenyl)-5-chloro-*N*^{4}-(2-methyl-2*H*-indazol-6-yl)pyrimidine-2,4-diamine **(45),** Following the general procedure using. 5-chloro-*N*^{4}-(2-methyl-2*H*-indazol-6-yl)-*N*^{2}-(3-nitrophenyl)pyrimidine-2,4-diamine **(37).** 75% yield. ^{1}H NMR (500 MHz, DMSO-d_6) δ 9.02 (s, 1H), 8.72 (s, 1H), 8.25 (s, 1H), 8.06 (s, 1H), 7.93 (s, 1H), 7.62 (d, J = 7.1 Hz, 1H), 7.23 (dd, J = 7.1, 1.4 Hz, 1H), 6.94 (t, J = 1.5 Hz, 1H), 6.75 – 6.67 (m, 2H), 6.07 (dt, J = 6.1, 1.6 Hz, 1H), 4.69 (s, 2H), 4.11 (s, 3H). MS-ESI for $C_{18}H_{16}ClN_7$ $[M+H]^+$, Calcd: 366.1, found: 366.1.

N^2-(5-amino-2-methoxyphenyl)-5-chloro-*N*^{4}-(2-methyl-2H-indazol-6-yl)pyrimidine-2,4-diamine **(46)**, Following the general procedure using 5-chloro-*N*^{2}-(2-methoxy-5-nitrophenyl)-*N*^{4}-(2-methyl-2*H*-indazol-6-yl)pyrimidine-2,4-diamine **(39).** 95% yield. ^{1}H NMR (500 MHz, DMSO-d_6) δ 8.86 (s, 1H), 8.28 (s, 1H), 8.08 (s, 1H), 7.90 (d, *J* = 1.1 Hz, 1H), 7.64 (d, *J* = 5.3 Hz, 1H), 7.56, 7.36 (d, *J* = 1.6 Hz, 1H), 7.21 – 7.19 (m, 1H), 6.66 (d, *J* = 5.3 Hz, 1H), 6.10 (dd, *J* = 5.3, 1.6 Hz, 1H), 4.33 (s, 2H), 4.11 (s, 3H), 3.67 (s, 3H). LCQTOF for $C_{19}H_{18}ClN_7O$ $[M+H]^+$, Calcd: 396.1334, found: 396.1313.

This material is reserved for educational use only, not allowed for commercial use.
Forbidden to modify the content, and cite the document when use.

N^2-[5-amino-4-((dimethylamino)ethyl)-2-methoxyphenyl]-5-chloro-N^4-(2-methyl-2H-indazol-6-yl)pyrimidine-2,4-diamine **(47),** Following the general procedure using 5-chloro-N^2-[4-((dimethylamino)ethyl)-2-methoxy-5-nitrophenyl]-N^4-(2-methyl-2H-indazol-6-yl)pyrimidine-2,4-diamine **(41)**. 54% yield. ^{1}H NMR (500 MHz, DMSO-d_6) δ 8.77 (s, 1H), 8.25 (s, 1H), 8.05 (s, 1H), 7.92 (s, 1H), 7.65 (s, 1H), 7.61 (d, *J* = 5.5 Hz, 1H), 7.31 (s, 1H), 7.21 (dd, *J* = 5.3, 1.4 Hz, 1H), 6.72 (s, 1H), 4.12 (s, 3H), 3.69 (s, 3H), 3.03 (s, 3H), 2.62 (s, 6H), 2.61 – 2.59 (m, 2H), 2.44 – 2.43 (m, 2H). LCQTOF for $C_{24}H_{30}ClN_9O$ $[M+H]^+$, Calcd: 496.2334, found: 496.2305.

N^2-[3-*N*-benzylpropanamide]-N^4-(2-methyl-2H-indazol-6-yl)pyrimidine-2,4-diamine **(48),** Following the general procedure using N^2-[3-(aminomethyl)phenyl]-5-chloro-N^4-(2-methyl-2H-indazol-6-yl)pyrimidine-2,4-diamine **(34)** and propionyl chloride. 30%, HPLC analysis: retention time = 2.733 min, 96.7% purity. ^{1}H NMR (500 MHz, DMSO-d_6) δ 9.46 (s, 1H), 9.33 (s, 1H), 8.17 (d, *J* = 10.5 Hz, 3H), 7.96 (d, *J* = 3.4 Hz, 1H), 7.61 – 7.57 (m, 3H), 7.17 (t, *J* = 4.6 Hz, 1H), 7.08 (dd, *J* = 5.3, 1.1 Hz, 1H), 6.79 (d, *J* = 4.6 Hz, 1H), 6.24 (d, *J* = 3.7 Hz, 1H), 4.17 (d, *J* = 3.7 Hz, 2H), 4.09 (s, 3H), 2.08 (q, *J* = 4.6 Hz, 2H), 0.98 (t, *J* = 4.6 Hz, 3H). ^{13}C NMR (125 MHz, DMSO-d_6) δ 173.41, 161.22, 159.31, 149.24, 140.94, 140.48, 137.37, 128.92, 124.90, 121.02, 120.74, 118.69, 118.63, 118.42, 118.03, 105.51, 99.63, 42.71, 29.02, 10.53. HRMS (ESI) for $C_{22}H_{23}N_7O$ $[M+H]^+$, Calcd: 402.2037, found: 402.2049.

N^2-[3-*N*-acrylamidebenzyl]-N^4-(2-methyl-2H-indazol-6-yl)pyrimidine-2,4-diamine **(49),** Following the general procedure using N^2-[3-(aminomethyl)phenyl]-5-chloro-N^4-(2-methyl-2H-indazol-6-yl)pyrimidine-2,4-diamine **(34)** and acryloyl chloride. 20%, HPLC analysis: retention time = 2.793 min, 96.9% purity. ^{1}H NMR (500 MHz, DMSO-d_6) δ 9.29 (s, 1H), 9.21 (s, 1H), 8.52 (t, *J* = 3.5 Hz, 1H), 8.18 (s, 2H), 7.97 (d, *J* = 3.4 Hz, 1H), 7.66 (t, *J* = 1.3 Hz, 1H), 7.63 (d, *J* = 4.8 Hz, 1H), 7.57 (d, *J* = 5.5 Hz, 1H), 7.16 (t, *J* = 4.7 Hz, 1H), 7.08 (dd, *J* = 5.4, 1.3 Hz, 1H), 6.78 (d, *J* = 4.6 Hz, 1H), 6.26 – 6.20 (m, 2H), 6.08 (dd, *J* = 10.1, 1.4 Hz, 1H), 5.57 (dd, *J* = 5.9, 1.4 Hz, 1H), 4.26 (d, *J* = 3.4 Hz, 2H), 4.08 (s, 3H). ^{13}C NMR (125 MHz, DMSO-d_6) δ 165.04, 161.16, 160.10, 156.22, 149.34, 141.52, 139.88, 137.63, 132.26, 128.91, 125.83, 124.82, 120.92, 120.45, 118.53, 118.49, 118.19, 118.02, 105.16, 99.55, 43.01. HRMS (ESI) for $C_{22}H_{21}N_7O$ $[M+H]^+$, Calcd: 400.1880, found: 400.1860.

This material is reserved for educational use only, not allowed for commercial use.
Forbidden to modify the content, and cite the document when use.

N^2-[3-(2*E*)-*N*-benzyl-3-phenylprop-2-enamide]-N^4-(2-methyl-2H-indazol-6-yl)pyrimidine-2,4-diamine **(50)**, Following the general procedure using N^2-[3-(aminomethyl)phenyl]-5-chloro-N^4-(2-methyl-2H-indazol-6-yl)pyrimidine-2,4-diamine **(34)** and cinnamoyl chloride. 73%, HPLC analysis: retention time = 2.840 min, 98.7% purity. ^{1}H NMR (500 MHz, DMSO-d_6) **δ** 9.81 (s, 1H), 9.67 (s, 1H), 8.56 (t, *J* = 3.5 Hz, 1H), 8.22 (s, 1H), 8.12 (s, 1H), 7.95 (d, *J* = 3.7 Hz, 1H), 7.61 (d, *J* = 5.3 Hz, 1H), 7.59 (s, 1H), 7.56 (d, *J* = 6.2 Hz, 1H), 7.50 (d, *J* = 4.1 Hz, 2H), 7.42 (d, *J* = 9.4 Hz, 1H), 7.36 (ddd, *J* = 7.6, 4.7, 3.5 Hz, 3H), 7.22 (t, *J* = 4.7 Hz, 1H), 7.09 (dd, *J* = 5.5, 1.1 Hz, 1H), 6.92 (d, *J* = 4.6 Hz, 1H), 6.62 (d, *J* = 9.4 Hz, 1H), 6.29 (d, *J* = 3.7 Hz, 1H), 4.33 (d, *J* = 3.4 Hz, 2H), 4.09 (s, 3H). ^{13}C NMR (125 MHz, DMSO-d_6) **δ** 165.45, 161.41, 159.22, 148.97, 140.52, 139.47, 136.46, 135.40, 130.01, 129.47, 129.26, 128.05, 125.09, 122.58, 122.31, 121.26, 119.92, 119.66, 119.12, 118.10, 106.83, 99.90, 42.96. HRMS (ESI) for $C_{28}H_{25}N_7O$ $[M+H]^+$, Calcd: 476.2193, found: 476.2228.

N^2-[3-*N*-benzyl-2-chloroacetamide]-N^4-(2-methyl-2H-indazol-6-yl)pyrimidine-2,4-diamine **(51)**, Following the general procedure using N^2-[3-(aminomethyl)phenyl]-5-chloro-N^4-(2-methyl-2H-indazol-6-yl)pyrimidine-2,4-diamine **(34)** and chloroacetyl chloride. 25%, HPLC analysis: retention time = 2.793 min, 98.7% purity. ^{1}H NMR (500 MHz, DMSO-d_6) **δ** 8.65 (t, *J* = 3.5 Hz, 1H), 8.20 (s, 1H), 8.14 (s, 1H), 7.96 (d, *J* = 3.7 Hz, 1H), 7.59 (d, *J* = 5.5 Hz, 2H), 7.56 (d, *J* = 4.1 Hz, 1H), 7.20 (t, *J* = 4.8 Hz, 1H), 7.07 (dd, *J* = 5.5, 1.1 Hz, 1H), 6.85 (d, *J* = 4.1 Hz, 1H), 6.26 (d, *J* = 3.7 Hz, 1H), 4.24 (s, 2H), 4.22 (d, *J* = 3.7 Hz, 2H), 4.09 (s, 3H). ^{13}C NMR (125 MHz, DMSO-d_6) **δ** 169.17, 166.48, 161.38, 148.99, 139.89, 136.57, 129.22, 125.05, 121.21, 119.03, 118.07, 99.89, 54.02, 43.16, 42.04. HRMS (ESI) for $C_{21}H_{20}ClN_7O$ $[M+H]^+$, Calcd: 422.1490, found: 422.1472.

N^2-[3-N-benzylbut-2-ynamide]-N^4-(2-methyl-2H-indazol-6-yl)pyrimidine-2,4-diamine **(52)**, Following the general procedure using N^2-[3-(aminomethyl)phenyl]-5-chloro-N^4-(2-methyl-2H-indazol-6-yl)pyrimidine-2,4-diamine **(34)** and but-2-ynoic acid. 28%, HPLC analysis: retention time = 2.667 min, 97.1% purity. ^{1}H NMR (500 MHz, DMSO-d_6) **δ** 9.30 (s, 1H), 9.22 (s, 1H), 8.94 (t, *J* = 3.8 Hz, 1H), 8.19 (s, 2H), 7.97 (d, *J* = 3.4 Hz, 1H), 7.64 (s, 1H), 7.60 (d, *J* = 4.8 Hz, 1H), 7.57 (d, *J* = 5.3 Hz, 1H), 7.15 (t, *J* = 4.7 Hz, 1H), 7.07 (d, *J* = 5.3 Hz, 1H), 6.75 (d, *J* = 4.3 Hz, 1H), 6.22 (d, *J* = 3.4 Hz, 1H), 4.17 (d, *J* = 3.7 Hz, 2H), 4.09 (s, 3H),

This material is reserved for educational use only, not allowed for commercial use.
Forbidden to modify the content, and cite the document when use.

1.90 (s, 3H). ^{13}C NMR (125 MHz, DMSO-d_6) **δ** 161.15, 160.12, 156.25, 153.06, 149.37, 141.45, 139.57, 137.67, 128.90, 124.85, 120.95, 120.29, 118.47, 118.42, 118.23, 117.99, 105.06, 99.57, 83.27, 76.13, 43.02, 3.56. HRMS (ESI) for $C_{23}H_{21}N_7O$ $[M+H]^+$, Calcd: 412.1885, found: 412.1869.

5-chloro-*N*^{2}-[3-N-benzylpropanamide]-*N*^{4}-(2-methyl-2H-indazol-6-yl)pyrimidine-2,4-diamine **(53),** Following the general procedure using *N*^{2}-[3-(aminomethyl)phenyl]-5-chloro-*N*^{4}-(2-methyl-2H-indazol-6-yl)pyrimidine-2,4-diamine **(35)** and propionyl chloride. 70%, HPLC analysis: retention time = 2.680 min, 99.1% purity. ^{1}H NMR (500 MHz, DMSO-d_6) **δ** 9.32 (s, 1H), 8.80 (s, 1H), 8.24 (s, 1H), 8.10 (s, 1H), 8.07 (t, *J* = 3.5 Hz, 1H), 7.87 (s, 1H), 7.62 (d, *J* = 5.3 Hz, 1H), 7.49 (d, *J* = 6.4 Hz, 1H), 7.43 (1H), 7.23 (dd, *J* = 5.5, 1.1 Hz, 1H), 7.01 (t, *J* = 4.7 Hz, 1H), 6.69 (d, *J* = 4.6 Hz, 1H), 4.11 (s, 3H), 3.97 (d, *J* = 3.7 Hz, 2H), 2.07 (q, *J* = 4.5 Hz, 2H), 0.98 (t, *J* = 4.5 Hz, 3H). ^{13}C NMR (125 MHz, DMSO-d_6) **δ** 173.28, 158.29, 156.69, 154.92, 148.90, 140.93, 140.33, 136.36, 128.77, 124.94, 120.55, 120.41, 120.29, 119.51, 118.13, 117.95, 109.56, 104.53, 42.53, 28.98, 10.54. HRMS (ESI) for $C_{22}H_{22}ClN_7O$ $[M+H]^+$, Calcd: 436.1652, found: 436.1635.

5-chloro-*N*^{2}-[3-*N*-acrylamidebenzyl]-*N*^{4}-(2-methyl-2H-indazol-6-yl)pyrimidine-2,4-diamine **(54)**, Following the general procedure using *N*^{2}-[3-(aminomethyl)phenyl]-5-chloro-*N*^{4}-(2-methyl-2H-indazol-6-yl)pyrimidine-2,4-diamine **(35)** and acryloyl chloride. 24%, HPLC analysis: retention time = 2.660 min, 95.8% purity. ^{1}H NMR (500 MHz, DMSO-d_6) **δ** 9.34 (s, 1H), 8.81 (s, 1H), 8.41 (t, *J* = 3.5 Hz, 1H), 8.23 (s, 1H), 8.10 (s, 1H), 7.86 (s, 1H), 7.62 (d, *J* = 5.3 Hz, 1H), 7.49 (d, *J* = 4.8 Hz, 1H), 7.47 (s, 1H), 7.23 (dd, *J* = 5.3, 1.1 Hz, 1H), 7.02 (t, *J* = 4.7 Hz, 1H), 6.70 (d, *J* = 4.6 Hz, 1H), 6.21 (dd, *J* = 10.3, 5.9 Hz, 1H), 6.07 (dd, *J* = 10.3, 1.4 Hz, 1H), 5.56 (dd, *J* = 6.2, 1.4 Hz, 1H), 4.10 (s, 3H), 4.04 (d, *J* = 3.4 Hz, 2H). ^{13}C NMR (125 MHz, DMSO-d_6) **δ** 164.98, 158.26, 156.69, 154.93, 148.89, 140.99, 139.83, 136.34, 132.22, 128.85, 125.84, 124.94, 120.57, 120.30, 119.51, 118.31, 118.10, 109.61, 104.53, 42.76. HRMS (ESI) for $C_{22}H_{20}ClN_7O$ $[M+H]^+$, Calcd: 434.1496, found: 434.1480.

5-chloro-*N*^{2}-[3-(2*E*)-*N*-benzyl-3-phenylprop-2-enamide]-*N*^{4}-(2-methyl-2H-indazol-6-yl)pyrimidine-2,4-diamine **(55)**, Following the general procedure using *N*^{2}-[3-(aminomethyl)phenyl]-5-chloro-*N*^{4}-(2-methyl-2H-indazol-6-yl)pyrimidine-2,4-diamine **(35)**

This material is reserved for educational use only, not allowed for commercial use.
Forbidden to modify the content, and cite the document when use.

and cinnamoyl chloride. 30%, HPLC analysis: retention time = 2.827 min, 98.8% purity. ^{1}H NMR (500 MHz, DMSO-d_6) **δ** 9.35 (s, 1H), 8.81 (s, 1H), 8.42 (t, *J* = 3.5 Hz, 1H), 8.23 (s, 1H), 8.10 (s, 1H), 7.87 (s, 1H), 7.63 (d, *J* = 5.5 Hz, 1H), 7.53 – 7.49 (m, 4H), 7.42 (d, *J* = 9.6 Hz, 1H), 7.39 – 7.33 (m, 3H), 7.23 (dd, *J* = 5.3, 1.1 Hz, 1H), 7.04 (t, *J* = 4.9 Hz, 1H), 6.75 (d, *J* = 4.6 Hz, 1H), 6.63 (d, *J* = 9.4 Hz, 1H), 4.10 (d, *J* = 2.3 Hz, 5H). ^{13}C NMR (125 MHz, DMSO-d_6) **δ** 165.34, 158.27, 156.69, 154.94, 148.90, 141.02, 139.95, 139.36, 136.35, 135.44, 129.99, 129.48, 128.86, 128.03, 124.95, 122.66, 120.57, 120.31, 119.51, 118.30, 118.10, 109.61, 104.53, 42.91. HRMS (ESI) for $C_{28}H_{24}ClN_7O$ $[M+H]^+$, Calcd: 510.1809, found: 510.1792.

5-chloro-N^2-[3-*N*-benzyl-2-chloroacetamide]-N^4-(2-methyl-2H-indazol-6-yl)pyrimidine-2,4-diamine **(56)**, Following the general procedure using N^2-[3-(aminomethyl)phenyl]-5-chloro-N^4-(2-methyl-2H-indazol-6-yl)pyrimidine-2,4-diamine **(35)** and chloroacetyl chloride. 39%, HPLC analysis: retention time = 2.687 min, 95.0% purity. ^{1}H NMR (500 MHz, DMSO-d_6) **δ** 9.33 (s, 1H), 8.81 (s, 1H), 8.54 (t, *J* = 3.5 Hz, 1H), 8.24 (s, 1H), 8.11 (s, 1H), 7.86 (s, 1H), 7.62 (d, *J* = 5.5 Hz, 1H), 7.48 (s, 1H), 7.47 (s, 1H), 7.22 (dd, *J* = 5.3, 1.1 Hz, 1H), 7.03 (t, *J* = 4.8 Hz, 1H), 6.71 (d, *J* = 4.6 Hz, 1H), 4.11 (s, 3H), 4.05 (s, 2H), 3.99 (d, *J* = 3.4 Hz, 2H). ^{13}C NMR (125 MHz, DMSO-d_6) **δ** 166.34, 158.25, 156.70, 154.94, 148.88, 140.99, 139.39, 136.34, 128.86, 120.57, 120.44, 120.32, 119.52, 118.23, 118.15, 109.65, 104.54, 43.16, 42.02. HRMS (ESI) for $C_{21}H_{19}Cl_2N_7O$ $[M+H]^+$, Calcd: 456.1106, found: 456.1088.

5-chloro-N^2-[3-*N*-benzylbut-2-ynamide]-N^4-(2-methyl-2H-indazol-6-yl)pyrimidine-2,4-diamine **(57)**, Following the general procedure using N^2-[3-(aminomethyl)phenyl]-5-chloro-N^4-(2-methyl-2H-indazol-6-yl)pyrimidine-2,4-diamine **(35)** and but-2-ynoic acid. 41%, HPLC analysis: retention time = 2.707 min, 98.7% purity. ^{1}H NMR (500 MHz, DMSO-d_6) **δ** 9.34 (s, 1H), 8.82 (t, *J* = 3.8 Hz, 1H), 8.80 (s, 1H), 8.24 (s, 1H), 8.10 (s, 1H), 7.87 (s, 1H), 7.62 (d, *J* = 5.5 Hz, 1H), 7.48 (dd, *J* = 4.8, 1.4 Hz, 1H), 7.44 (t, *J* = 1.1 Hz, 1H), 7.23 (dd, *J* = 5.3, 1.1 Hz, 1H), 7.02 (t, *J* = 4.7 Hz, 1H), 6.68 (d, *J* = 4.6 Hz, 1H), 4.11 (s, 3H), 3.96 (d, *J* = 3.7 Hz, 2H), 1.91 (s, 3H). ^{13}C NMR (125 MHz, DMSO-d_6) **δ** 158.27, 156.67, 154.94, 153.00, 148.91, 140.95, 139.49, 136.36, 128.82, 124.94, 120.57, 120.27, 119.50, 118.15, 109.52, 104.53, 83.24, 76.09, 42.73, 33.89, 3.57. HRMS (ESI) for $C_{23}H_{20}ClN_7O$ $[M+H]^+$, Calcd: 446.1496, found: 446.1479.

This material is reserved for educational use only, not allowed for commercial use.
Forbidden to modify the content, and cite the document when use.

N^2-[3-*N*-phenylpropanamide]-*N*^{4}-(2-methyl-2H-indazol-6-yl)pyrimidine-2,4-diamine **(58),** Following the general procedure using *N*^{2}-(3-aminophenyl)-*N*^{4}-(2-methyl-2*H*-indazol-6-yl)pyrimidine-2,4-diamine **(42)** and propionyl chloride. yield: 35% , HPLC analysis: retention time = 2.773 min, 98.8% purity. ^{1}H NMR (500 MHz, DMSO-d_6) **δ** 10.48 (s, 1H), 10.40 (s, 1H), 9.88 (s, 1H), 8.26 (s, 1H), 8.01 (s, 1H), 7.92 (d, *J* = 4.1 Hz, 1H), 7.75 (s, 1H), 7.61 (d, *J* = 5.3 Hz, 1H), 7.32 (dd, *J* = 4.7, 1.0 Hz, 2H), 7.22 (t, *J* = 4.8 Hz, 1H), 7.15 (dd, *J* = 5.4, 1.3 Hz, 1H), 6.39 (d, *J* = 4.1 Hz, 1H), 4.11 (s, 3H), 2.26 (q, *J* = 4.5 Hz, 2H), 1.01 (t, *J* = 4.5 Hz, 3H). ^{13}C NMR (125 MHz, DMSO-d_6) **δ** 172.60, 161.53, 160.20, 159.29, 158.97, 148.56, 140.47, 139.20, 137.59, 135.26, 129.66, 125.11, 121.33, 119.63, 118.08, 113.52, 108.36, 100.18, 40.44, 29.98, 10.06. HRMS (ESI) for $C_{21}H_{21}N_7O$ $[M+H]^+$, Calcd: 388.1880, found: 388.1851.

N^2-[3-*N*-acrylamidephenyl]-*N*^{4}-(2-methyl-2H-indazol-6-yl)pyrimidine-2,4-diamine **(59)**, Following the general procedure using *N*^{2}-(3-aminophenyl)-*N*^{4}-(2-methyl-2*H*-indazol-6-yl)pyrimidine-2,4-diamine **(42)** and acryloyl chloride. yield: 27%, HPLC analysis: retention time = 2.773 min, 99.8% purity. ^{1}H NMR (500 MHz, DMSO-d_6) **δ** 9.97 (s, 1H), 9.28 (s, 1H), 9.22 (s, 1H), 8.19 (s, 1H), 8.17 (s, 1H), 7.98 (d, *J* = 3.4 Hz, 1H), 7.92 (t, *J* = 1.3 Hz, 1H), 7.55 (d, *J* = 5.3 Hz, 1H), 7.49 – 7.44 (m, 1H), 7.31 (dd, *J* = 4.7, 1.7 Hz, 1H), 7.13 (d, *J* = 5.0 Hz, 1H), 7.12 – 7.10 (m, 1H), 6.41 (dd, *J* = 10.1, 6.2 Hz, 1H), 6.23 (d, *J* = 3.4 Hz, 1H), 6.19 (dd, *J* = 10.2, 1.3 Hz, 1H), 5.68 (dd, *J* = 6.1, 1.3 Hz, 1H), 4.07 (s, 3H). ^{13}C NMR (125 MHz, DMSO-d_6) **δ** 163.52, 161.15, 160.09, 156.10, 149.36, 141.79, 139.47, 137.66, 132.62, 129.02, 127.00, 124.73, 120.83, 118.47, 117.95, 115.45, 113.32, 111.20, 105.10, 99.77. HRMS (ESI) for $C_{21}H_{19}N_7O$ $[M+H]^+$, Calcd: 386.1724, found: 386.1751.

N^2-[3-*N*-(2*E*)-3-diphenylprop-2-enamide]-*N*^{4}-(2-methyl-2H-indazol-6-yl)pyrimidine-2,4-diamine **(60)**, Following the general procedure using *N*^{2}-(3-aminophenyl)-*N*^{4}-(2-methyl-2*H*-indazol-6-yl)pyrimidine-2,4-diamine **(42)** and cinnamoyl chloride. yield: 82%, HPLC analysis: retention time = 3.573 min, 98.1% purity. ^{1}H NMR (500 MHz, DMSO-d_6) **δ** 10.15 (s, 1H), 8.19 (s, 1H), 8.09 (s, 1H), 7.93 (d, *J* = 5.2 Hz, 1H), 7.90 (s, 1H), 7.60 (s, 1H), 7.57 (d, *J* = 6.0 Hz, 3H), 7.52 (d, *J* = 12.6 Hz, 1H), 7.43 – 7.37 (m, 6H), 7.24 (t, *J* = 6.3 Hz, 1H), 7.13 (d, *J* = 7.0 Hz, 1H), 6.80 (d, *J* = 12.6 Hz, 1H), 6.34 (d, *J* = 4.0 Hz, 1H), 4.07 (s, 3H). ^{13}C NMR (125 MHz, DMSO-d_6) **δ** 164.15, 161.56, 159.41, 154.23, 148.67, 140.60, 140.37, 138.16, 135.48,

This material is reserved for educational use only, not allowed for commercial use.
Forbidden to modify the content, and cite the document when use.

135.24, 130.33, 129.77, 129.56, 128.24, 125.10, 122.86, 121.29, 119.61, 118.68, 118.18, 117.68, 116.30, 116.09, 113.34, 108.24, 100.21. HRMS (ESI) for $C_{27}H_{23}N_7O$ $[M+H]^+$, Calcd: 462.2037, found: 462.2019.

N^2-[3-*N*-2-chloroacetamidephenyl]-*N*^{4}-(2-methyl-2H-indazol-6-yl)pyrimidine-2,4-diamine **(61)**, Following the general procedure using *N*^{2}-(3-aminophenyl)-*N*^{4}-(2-methyl-2*H*-indazol-6-yl)pyrimidine-2,4-diamine **(42)** and chloroacetyl chloride. yield: 12%, HPLC analysis: retention time = 2.773 min, 99.2% purity. ^{1}H NMR (500 MHz, DMSO-*d*$_6$) **δ** 10.15 (s, 1H), 9.31 (s, 1H), 9.26 (s, 1H), 8.19 (s, 1H), 8.18 (s, 1H), 7.98 (d, *J* = 3.4 Hz, 1H), 7.89 (s, 1H), 7.56 (d, *J* = 5.3 Hz, 1H), 7.49 (d, *J* = 5.0 Hz, 1H), 7.21 (d, *J* = 5.0 Hz, 1H), 7.15 (t, *J* = 4.9 Hz, 1H), 7.10 (dd, *J* = 5.4, 1.3 Hz, 1H), 6.24 (d, *J* = 3.4 Hz, 1H), 4.18 (s, 2H), 4.08 (s, 3H). ^{13}C NMR (125 MHz, DMSO-*d*$_6$) **δ** 164.95, 161.17, 159.74, 149.34, 141.68, 139.01, 129.14, 124.76, 120.87, 118.54, 117.97, 117.56, 115.76, 111.23, 105.30, 99.85, 44.16. HRMS (ESI) for $C_{20}H_{18}ClN_7O$ $[M+H]^+$, Calcd: 408.1334, found: 408.1370.

N^2-[3-*N*-phenylbut-2-ynamide]-*N*^{4}-(2-methyl-2H-indazol-6-yl)pyrimidine-2,4-diamine **(62)**, Following the general procedure using *N*^{2}-(3-aminophenyl)-*N*^{4}-(2-methyl-2*H*-indazol-6-yl)pyrimidine-2,4-diamine **(42)** and but-2-ynoic acid. 22%, HPLC analysis: retention time = 2.600 min, 95.0% purity. ^{1}H NMR (500 MHz, DMSO-*d*$_6$) **δ** 10.60 (s, 1H), 10.43 (s, 1H), 10.25 (s, 1H), 8.26 (s, 1H), 8.03 (s, 1H), 7.90 (d, *J* = 4.1 Hz, 1H), 7.75 (s, 1H), 7.62 (d, *J* = 5.3 Hz, 1H), 7.36 (d, *J* = 4.8 Hz, 1H), 7.30 – 7.22 (m, 2H), 7.12 (d, *J* = 5.9 Hz, 1H), 6.38 (d, *J* = 4.1 Hz, 1H), 4.12 (s, 1H), 2.00 (s, 1H). ^{13}C NMR (125 MHz, DMSO-*d*$_6$) **δ** 161.56, 151.14, 148.61, 139.65, 135.30, 129.79, 125.16, 121.36, 119.66, 118.11, 116.63, 114.04, 108.40, 100.28, 84.74, 76.41, 46.23, 3.73. LCQTOF for $C_{22}H_{19}N_7O$ $[M+H]^+$, Calcd: 398.1729, found: 398.1726.

5-chloro-*N*^{2}-[3-*N*-phenylpropanamide]-*N*^{4}-(2-methyl-2H-indazol-6-yl)pyrimidine-2,4-diamine **(63)**, Following the general procedure using *N*^{2}-(3-aminophenyl)-5-chloro-*N*^{4}-(2-methyl-2*H*-indazol-6-yl)pyrimidine-2,4-diamine **(42)** and propionyl chloride. yield: 38%, HPLC analysis: retention time = 2.840 min, 99.1% purity. ^{1}H NMR (500 MHz, DMSO-*d*$_6$) **δ** 9.66 (s, 1H), 9.45 (s, 1H), 8.96 (s, 1H), 8.25 (s, 1H), 8.12 (s, 1H), 7.89 (s, 1H), 7.66 (s, 1H), 7.60 (d, *J* = 5.5 Hz, 1H), 7.35 (dd, *J* = 4.9, 1.5 Hz, 1H), 7.27 (dd, *J* = 5.4, 1.3 Hz, 1H), 7.14 (d, *J* =

This material is reserved for educational use only, not allowed for commercial use.
Forbidden to modify the content, and cite the document when use.

6.2 Hz, 1H), 6.97 (t, *J* = 4.9 Hz, 1H), 4.11 (s, 3H), 2.23 (q, *J* = 4.5 Hz, 2H), 1.01 (t, *J* = 4.6 Hz, 3H). ^{13}C NMR (125 MHz, DMSO-d_6) **δ** 172.31, 156.84, 152.26, 148.72, 140.29, 139.82, 135.94, 128.91, 124.90, 120.43, 120.09, 119.55, 115.39, 114.95, 113.98, 111.45, 109.66, 104.80, 29.89, 10.13. HRMS (ESI) for $C_{21}H_{20}ClN_7O$ $[M+Na]^+$, Calcd: 444.1310, found: 444.1312.

5-chloro-*N*^{2}-[3-*N*-phenylpropanamide]-*N*^{4}-(2-methyl-2H-indazol-6-yl)pyrimidine-2,4-diamine **(64),** Following the general procedure using *N*^{2}-(3-aminophenyl)-5-chloro-*N*^{4}-(2-methyl-2*H*-indazol-6-yl)pyrimidine-2,4-diamine **(45)** and acryloyl chloride. yield: 12%, HPLC analysis: retention time = 3.260 min, 96.2% purity. ^{1}H NMR (500 MHz, DMSO-d_6) **δ** 9.92 (s, 1H), 9.34 (s, 1H), 8.76 (s, 1H), 8.22 (s, 1H), 8.10 (s, 1H), 7.90 (s, 1H), 7.73 (s, 1H), 7.58 (d, *J* = 7.1 Hz, 1H), 7.41 (dd, *J* = 6.6, 2.0 Hz, 1H), 7.27 (dd, *J* = 7.2, 1.4 Hz, 1H), 7.23 (d, *J* = 5.8 Hz, 1H), 7.00 (t, *J* = 6.5 Hz, 1H), 6.37 (dd, *J* = 13.6, 8.1 Hz, 1H), 6.17 (dd, *J* = 13.6, 1.6 Hz, 1H), 5.68 (dd, *J* = 8.1, 1.6 Hz, 1H), 4.10 (s, 3H). ^{13}C NMR (125 MHz, DMSO-d_6) **δ** 163.42, 158.26, 156.49, 154.71, 148.88, 141.19, 139.34, 136.32, 132.52, 128.91, 126.94, 124.77, 120.32, 120.03, 119.35, 115.42, 113.61, 111.21, 109.07, 104.75. HRMS (ESI) for $C_{21}H_{18}ClN_7O$ $[M+H]^+$, Calcd: 420.1334, found: 420.1332.

5-chloro-*N*^{2}-[3-*N*-(2*E*)-3-diphenylprop-2-enamide]-*N*^{4}-(2-methyl-2H-indazol-6-yl)pyrimidine-2,4-diamine **(65)**, Following the general procedure using *N*^{2}-(3-aminophenyl)-5-chloro-*N*^{4}-(2-methyl-2*H*-indazol-6-yl)pyrimidine-2,4-diamine **(45)** and cinnamoyl chloride. yield: 32%, HPLC analysis: retention time = 3.833 min, 99.5% purity. ^{1}H NMR (500 MHz, DMSO-d_6) **δ** 10.03 (s, 1H), 9.55 (s, 1H), 9.02 (s, 1H), 8.20 (s, 1H), 8.14 (s, 1H), 7.89 (1H), 7.75 (s, 1H), 7.64 – 7.54 (m, 3H), 7.51 (d, *J* = 9.4 Hz, 1H), 7.44 – 7.36 (m, 4H), 7.30 (d, *J* = 3.4 Hz, 1H), 7.27 (dd, *J* = 5.5, 1.1 Hz, 1H), 7.02 (t, *J* = 4.9 Hz, 1H), 6.79 (d, *J* = 9.4 Hz, 1H), 4.08 (s, 3H). ^{13}C NMR (125 MHz, DMSO-d_6) **δ** 163.92, 156.85, 148.78, 140.41, 139.74, 136.07, 135.31, 130.27, 129.57, 129.13, 128.22, 124.93, 122.98, 120.49, 120.15, 119.58, 115.75, 114.04, 111.47, 109.65, 104.89. HRMS (ESI) for $C_{27}H_{22}ClN_7O$ $[M+H]^+$, Calcd: 496.1647, found: 496.1657.

5-chloro-*N*^{2}-[3-*N*-2-chloroacetamidephenyl]-*N*^{4}-(2-methyl-2H-indazol-6-yl)pyrimidine-2,4-diamine **(66)**, Following the general procedure using *N*^{2}-(3-aminophenyl)-5-chloro-*N*^{4}-(2-methyl-2*H*-indazol-6-yl)pyrimidine-2,4-diamine **(45)** and chloroacetyl

This material is reserved for educational use only, not allowed for commercial use.
Forbidden to modify the content, and cite the document when use.

chloride. yield: 28%, HPLC analysis: retention time = 3.400 min, 95.1% purity. ^{1}H NMR (500 MHz, DMSO-d_6) **δ** 10.14 (s, 1H), 9.53 (s, 1H), 9.02 (s, 1H), 8.25 (s, 1H), 8.13 (s, 1H), 7.87 (1H), 7.67 (1H), 7.60 (d, *J* = 7.1 Hz, 1H), 7.40 (d, *J* = 6.2 Hz, 1H), 7.24 (dd, *J* = 7.1, 1.2 Hz, 1H), 7.14 (d, *J* = 6.8 Hz, 1H), 7.00 (t, *J* = 6.5 Hz, 1H), 4.16 (s, 2H), 4.11 (s, 3H). ^{13}C NMR (125 MHz, DMSO-d_6) **δ** 169.06, 164.91, 156.77, 148.76, 138.93, 136.00, 129.09, 124.88, 120.43, 119.52, 115.88, 113.86, 111.35, 109.62, 104.87, 53.85, 44.05. HRMS (ESI) for $C_{20}H_{17}Cl_2N_7O$ $[M+H]^+$, Calcd: 442.0944, found: 442.0963.

5-chloro-*N*^{2}-[3-*N*-phenylbut-2-ynamide]-*N*^{4}-(2-methyl-2H-indazol-6-yl)pyrimidine-2,4-diamine **(67),** Following the general procedure using *N*^{2}-(3-aminophenyl)-5-chloro-*N*^{4}-(2-methyl-2*H*-indazol-6-yl)pyrimidine-2,4-diamine **(45)** and but-2-ynoic acid. yield: 8.8%, HPLC analysis: retention time = 2.967 min, 95.6% purity. ^{1}H NMR (500 MHz, DMSO-d_6) **δ** 11.01 (s, 1H), 9.67 (s, 1H), 8.84 (s, 1H), 8.26 (s, 1H), 8.15 (s, 1H), 8.05 (s, 1H), 7.62 (d, *J* = 5.5 Hz, 2H), 7.49 – 7.41 (m, 2H), 7.23 (dd, *J* = 5.3, 1.1 Hz, 1H), 6.15 (s, 1H), 4.15 (s, 3H), 2.32 (s. 3H). ^{13}C NMR (125 MHz, DMSO-d_6) **δ** 162.59, 158.00, 156.58, 154.83, 148.89, 148.23, 142.94, 139.88, 136.22, 125.42, 125.15, 120.65, 119.94, 119.41, 118.45, 114.79, 109.22, 105.54, 104.18, 55.43, 18.90. LCQTOF for $C_{22}H_{18}ClN_7O$ $[M+H]^+$, Calcd: 432.1334, found: 432.1301.

N^2-(2-methoxy-5-(*N*-propanamide)phenyl)-*N*^{4}-(2-methyl-2*H*-indazol-6-yl)pyrimidine-2,4-diamine **(68)**, Following the general procedure using *N*^{2}-(5-amino-2-methoxyphenyl)-*N*^{4}-(2-methyl-2*H*-indazol-6-yl)pyrimidine-2,4-diamine **(43)** and propionyl chloride. yield: 13%, HPLC analysis: retention time = 2.813 min, 97.8% purity. ^{1}H NMR (500 MHz, DMSO-d_6) **δ** 9.57 (s, 1H), 9.34 (s, 1H), 8.21 (d, *J* = 1.6 Hz, 1H), 8.19 (s, 1H), 8.04 (s, 1H), 7.98 (d, *J* = 3.4 Hz, 1H), 7.61 (s, 1H), 7.55 (d, *J* = 5.3 Hz, 1H), 7.32 (dd, *J* = 5.3, 1.6 Hz, 1H), 7.09 (dd, *J* = 5.4, 1.3 Hz, 1H), 6.91 (d, *J* = 5.3 Hz, 1H), 6.25 (d, *J* = 3.4 Hz, 1H), 4.08 (s, 3H), 3.80 (s, 3H), 2.21 (q, *J* = 4.6 Hz, 2H), 1.00 (t, *J* = 4.6 Hz, 3H). ^{13}C NMR (125 MHz, DMSO-d_6) **δ** 171.94, 161.18, 159.81, 156.17, 149.17, 145.44, 137.57, 132.62, 129.21, 124.82, 120.91, 118.46, 117.86, 114.34, 113.46, 110.93, 104.85, 99.97, 56.50, 55.37, 29.74, 10.19. HRMS (ESI) for $C_{22}H_{23}N_7O_2$ $[M+H]^+$, Calcd: 418.1986, found: 418.2010.

N^2-(2-methoxy-5-(*N*-acrylamide)phenyl)-*N*^{4}-(2-methyl-2*H*-indazol-6-yl)pyrimidine-2,4-diamine **(69),** Following the general procedure using *N*^{2}-(5-amino-2-methoxyphenyl)-

This material is reserved for educational use only, not allowed for commercial use.
Forbidden to modify the content, and cite the document when use.

N^4-(2-methyl-2*H*-indazol-6-yl)pyrimidine-2,4-diamine **(43)** and acryloyl chloride. yield: 12%, HPLC analysis: retention time = 2.800 min, 97.9% purity. ^{1}H NMR (500 MHz, DMSO-d_6) **δ** 9.88 (s, 1H), 9.35 (s, 1H), 8.29 (d, *J* = 1.6 Hz, 1H), 8.17 (s, 1H), 8.03 (s, 1H), 7.99 (d, *J* = 3.4 Hz, 1H), 7.63 (s, 1H), 7.54 (d, *J* = 5.3 Hz, 1H), 7.45 (dd, *J* = 5.3, 1.4 Hz, 1H), 7.09 (dd, *J* = 5.4, 1.3 Hz, 1H), 6.95 (d, *J* = 5.5 Hz, 1H), 6.36 (dd, *J* = 10.2, 6.1 Hz, 1H), 6.26 (d, *J* = 3.4 Hz, 1H), 6.15 (dd, *J* = 10.3, 1.4 Hz, 1H), 5.65 (dd, *J* = 6.1, 1.3 Hz, 1H), 4.07 (s, 3H), 3.82 (s, 3H). ^{13}C NMR (125 MHz, DMSO-d_6) **δ** 163.24, 161.20, 159.77, 156.16, 149.14, 145.74, 137.52, 132.60, 132.27, 129.33, 126.48, 124.80, 120.92, 118.47, 117.86, 114.35, 113.34, 111.00, 104.95, 100.04, 56.42, 31.16. HRMS (ESI) for $C_{22}H_{21}N_7O_2$ $[M+H]^+$, Calcd: 416.1829, found: 416.1825.

N^2-[2-methoxy-5-(*N*-(2*E*)-3-diphenylprop-2-enamide)phenyl]-N^4-(2-methyl-2*H*-indazol-6-yl)pyrimidine-2,4-diamine **(70)**, Following the general procedure using N^2-(5-amino-2-methoxyphenyl)-N^4-(2-methyl-2*H*-indazol-6-yl)pyrimidine-2,4-diamine **(43)** and cinnamoyl chloride. 43%, HPLC analysis: retention time = 2.980 min, 96.8% purity. ^{1}H NMR (500 MHz, DMSO-d_6) **δ** 9.96 (s, 1H), 9.37 (s, 1H), 8.34 (d, *J* = 1.4 Hz, 1H), 8.12 (s, 1H), 8.04 (s, 1H), 8.00 (d, *J* = 3.4 Hz, 1H), 7.65 (s, 1H), 7.55 (dd, *J* = 4.8, 3.2 Hz, 3H), 7.51 – 7.47 (m, 2H), 7.41 (q, *J* = 5.3 Hz, 3H), 7.10 (dd, *J* = 5.4, 1.3 Hz, 1H), 6.97 (d, *J* = 5.3 Hz, 1H), 6.76 (d, *J* = 9.4 Hz, 1H), 6.27 (d, *J* = 3.4 Hz, 1H), 4.03 (s, 3H), 3.83 (s, 3H). ^{13}C NMR (125 MHz, DMSO-d_6) **δ** 163.57, 161.20, 159.79, 156.16, 149.16, 145.63, 139.79, 137.53, 135.39, 132.59, 130.06, 129.49, 129.39, 128.06, 124.75, 123.17, 120.91, 118.48, 117.88, 114.13, 113.15, 111.04, 104.96, 100.07, 56.45. HRMS (ESI) for $C_{28}H_{25}N_7O_2$ $[M+Na]^+$, Calcd: 514.1962, found: 514.1970.

N^2-(2-methoxy-5-(*N*-but-2-ynamide)phenyl)-N^4-(2-methyl-2*H*-indazol-6-yl)pyrimidine-2,4-diamine **(71),** Following the general procedure using N^2-(5-amino-2-methoxyphenyl)-N^4-(2-methyl-2*H*-indazol-6-yl)pyrimidine-2,4-diamine **(43)** and but-2-ynoic acid. 27%, HPLC analysis: retention time = 2.640 min, 95.8% purity. ^{1}H NMR (500 MHz, DMSO-d_6) **δ** 10.82 (s, 1H), 10.48 (s, 1H), 8.26 (s, 1H), 7.85 (s, 1H), 7.76 (s, 1H), 7.68 – 7.49 (m, 2H), 7.47 (dd, *J* = 5.4, 1.7 Hz, 1H), 7.15 (d, *J* = 5.7 Hz, 1H), 7.10 (d, *J* = 5.5 Hz, 1H), 6.47 (d, *J* = 4.3 Hz, 1H), 4.12 (s, 3H), 3.77 (s, 3H), 1.99 (s, 3H). ^{13}C NMR (500 MHz, DMSO-d_6)

This material is reserved for educational use only, not allowed for commercial use.
Forbidden to modify the content, and cite the document when use.

δ 153.36, 150.90, 148.53, 135.34, 132.15, 125.15, 121.28, 119.61, 117.67, 112.75, 84.33, 76.45, 56.43, 29.55, 3.72. LCQTOF for $C_{23}H_{21}N_7O_2$ $[M+H]^+$, Calcd: 428.1829, found: 428.1798.

5-chloro-*N*^{2}-(2-methoxy-5-(*N*-propanamide)phenyl)-*N*^{4}-(2-methyl-2*H*-indazol-6-yl)pyrimidine-2,4-diamine **(72),** Following the general procedure using *N*^{2}-(5-amino-2-methoxyphenyl)-5-chloro-*N*^{4}-(2-methyl-2H-indazol-6-yl)pyrimidine-2,4-diamine **(46)** and propionyl chloride. 46%, HPLC analysis: retention time = 3.060 min, 97.1% purity. ^{1}H NMR (500 MHz, DMSO-*d*$_6$) **δ** 9.50 (s, 1H), 8.73 (s, 1H), 8.21 (s, 1H), 8.08 (s, 1H), 7.94 (d, *J* = 1.6 Hz, 1H), 7.85 (s, 2H), 7.53 (d, *J* = 5.5 Hz, 1H), 7.29 (dt, *J* = 5.5, 1.5 Hz, 2H), 6.90 (d, *J* = 5.3 Hz, 1H), 4.10 (s, 3H), 3.74 (s, 3H), 2.19 (q, *J* = 4.6 Hz, 2H), 0.99 (t, *J* = 4.5 Hz, 3H). ^{13}C NMR (125 MHz, DMSO-*d*$_6$) **δ** 171.95, 158.43, 156.39, 154.76, 148.86, 146.51, 136.39, 132.60, 128.65, 124.86, 120.33, 119.61, 119.25, 115.30, 114.65, 111.23, 108.31, 105.13, 56.30, 49.02, 29.54, 10.24. LCQTOF for $C_{22}H_{22}ClN_7O_2$ $[M+H]^+$, Calcd: 452.1596, found: 452.1567.

5-chloro-*N*^{2}-(2-methoxy-5-(*N*-acrylamide)phenyl)-*N*^{4}-(2-methyl-2*H*-indazol-6-yl)pyrimidine-2,4-diamine **(73),** Following the general procedure using *N*^{2}-(5-amino-2-methoxyphenyl)-5-chloro-*N*^{4}-(2-methyl-2H-indazol-6-yl)pyrimidine-2,4-diamine **(46)** and acryloyl chloride. 32%, HPLC analysis: retention time = 2.680 min, 98.5% purity. ^{1}H NMR (500 MHz, DMSO-*d*$_6$) **δ** 9.82 (s, 1H), 8.75 (s, 1H), 8.18 (s, 1H), 8.09 (s, 1H), 8.02 (d, *J* = 1.6 Hz, 1H), 7.85 (d, *J* = 5.0 Hz, 2H), 7.52 (d, *J* = 5.5 Hz, 1H), 7.40 (dd, *J* = 5.3, 1.6 Hz, 1H), 7.27 (dd, *J* = 5.4, 1.3 Hz, 1H), 6.93 (d, *J* = 5.3 Hz, 1H), 6.33 (dd, *J* = 10.2, 6.1 Hz, 1H), 6.15 (dd, *J* = 10.3, 1.4 Hz, 1H), 5.66 (dd, *J* = 5.9, 1.4 Hz, 1H), 4.08 (s, 3H), 3.76 (s, 3H). ^{13}C NMR (125 MHz, DMSO-*d*$_6$) **δ** 163.21, 158.38, 156.44, 154.76, 148.83, 146.77, 136.32, 132.61, 132.24, 128.79, 126.56, 124.84, 120.34, 119.64, 119.27, 115.37, 114.58, 111.31, 108.47, 105.23, 56.34. LCQTOF for $C_{22}H_{20}ClN_7O_2$ $[M+H]^+$, Calcd: 450.1439, found: 450.1449.

5-chloro-*N*^{2}-(2-methoxy-5-(*N*-(2*E*)-3-diphenylprop-2-enamide)phenyl)-*N*^{4}-(2-methyl-2*H*-indazol-6-yl)pyrimidine-2,4-diamine **(74),** Following the general procedure using *N*^{2}-(5-amino-2-methoxyphenyl)-5-chloro-*N*^{4}-(2-methyl-2H-indazol-6-yl)pyrimidine-2,4-diamine **(46)** and cinnamoyl chloride. 31%, HPLC analysis: retention time = 2.867 min, 98.1% purity. ^{1}H NMR (500 MHz, DMSO-*d*$_6$) **δ** 9.93 (s, 1H), 8.99 (s, 1H), 8.12 (s, 1H), 8.11 (s, 1H), 8.01 (d, *J* = 1.6 Hz, 1H), 7.84 (s, 1H), 7.57 (d, *J* = 4.6 Hz, 2H), 7.52 (d, *J* = 5.3 Hz, 1H),

This material is reserved for educational use only, not allowed for commercial use.
Forbidden to modify the content, and cite the document when use.

7.47 – 7.36 (m, 6H), 7.27 (dd, *J* = 5.3, 1.1 Hz, 1H), 6.98 (d, *J* = 5.3 Hz, 1H), 6.72 (d, *J* = 9.4 Hz, 1H), 4.01 (s, 3H), 3.77 (s, 3H). ^{13}C NMR (125 MHz, DMSO-d_6) **δ** 163.59, 156.69, 148.73, 147.22, 139.94, 135.97, 135.39, 132.58, 130.17, 129.57, 128.16, 124.85, 123.05, 120.39, 119.67, 119.46, 116.00, 111.62, 109.02, 105.26, 56.36, 29.24. LCQTOF for $C_{28}H_{24}ClN_7O_2$ $[M+H]^+$, Calcd: 526.1758, found: 526.1752.

5-chloro-N^2-(2-methoxy-5-(*N*-but-2-ynamide)phenyl)-N^4-(2-methyl-2*H*-indazol-6-yl)pyrimidine-2,4-diamine **(75),** Following the general procedure using N^2-(5-amino-2-methoxyphenyl)-5-chloro-N^4-(2-methyl-2H-indazol-6-yl)pyrimidine-2,4-diamine **(46)** and but-2-ynoic acid. 25%, HPLC analysis: retention time = 2.731 min, 97.2% purity. ^{1}H NMR (500 MHz, DMSO-d_6) **δ** 10.24 (s, 1H), 8.72 (s, 1H), , 8.20 (s, 1H), 8.07 (s, 1H), 7.93 (d, *J* = 1.6 Hz, 1H), 7.90 (s, 1H), 7.86 (s, 1H), 7.54 (d, *J* = 5.5 Hz, 1H), 7.27 (dd, *J* = 5.3, 1.1 Hz, 1H), 7.23 (dd, *J* = 5.4, 1.5 Hz, 1H), 6.91 (d, *J* = 5.3 Hz, 1H), 4.11 (s, 3H), 3.75 (s, 3H), 1.99 (s, 3H). ^{13}C NMR (125 MHz, DMSO-d_6) **δ** 158.40, 156.37, 154.78, 150.84, 148.83, 147.38, 136.36, 131.55, 128.65, 124.91, 120.39, 119.53, 119.23, 116.23, 115.51, 111.31, 108.21, 105.07, 84.01, 76.53, 56.32, 29.54, 3.71. LCQTOF for $C_{23}H_{20}ClN_7O_2$ $[M+H]^+$, Calcd: 462.1439, found: 462.1424.

N^2-[4-((dimethylamino)ethyl)-2-methoxy-5-(*N*-propanamide)phenyl]-N^4-(2-methyl-2H-indazol-6-yl)pyrimidine-2,4-diamine **(76)**, Following the general procedure using N^2-[5-amino-4-((dimethylamino)ethyl)-2-methoxyphenyl]-N^4-(2-methyl-2H-indazol-6-yl)pyrimidine-2,4-diamine **(44)** and propionyl chloride. 26%, HPLC analysis: retention time = 2.560 min, 98.9% purity. ^{1}H NMR (500 MHz, DMSO-d_6) **δ** 9.64 (s, 1H), 8.24 (s, 1H), 8.00 (s, 1H), 7.89 (s, 1H), 7.59 (d, *J* = 5.3 Hz, 1H), 7.09 (d, *J* = 5.3 Hz, 1H), 6.92 (s, 1H), 6.38 (d, *J* = 3.9 Hz, 1H), 5.72 (s, 1H), 4.11 (s, 3H), 3.82 (s, 3H), 2.69 (s, 6H), 2.61 (s, 3H), 2.49 (dd, *J* = 2.3, 1.1 Hz, 2H), 2.43 (dt, *J* = 2.5, 1.3 Hz, 2H), 1.00 (t, *J* = 4.5 Hz, 3H). ^{13}C NMR (125 MHz, DMSO-d_6) **δ** 171.97, 159.81, 147.62, 135.49, 124.43, 123.68, 119.61, 117.38, 116.34, 104.38, 103.68, 98.51, 55.03, 52.48, 47.54, 42.12, 41.20, 28.33, 9.08. LCQTOF for $C_{27}H_{35}N_9O_2$ $[M+H]^+$, Calcd: 518.2986, found: 518.2955.

N^2-[4-((dimethylamino)ethyl)-2-methoxy-5-(*N*-acrylamide)phenyl]-N^4-(2-methyl-2H-indazol-6-yl)pyrimidine-2,4-diamine **(77)**, Following the general procedure using N^2-[5-amino-4-((dimethylamino)ethyl)-2-methoxyphenyl]-N^4-(2-methyl-2H-indazol-

This material is reserved for educational use only, not allowed for commercial use.
Forbidden to modify the content, and cite the document when use.

6yl)pyrimidine-2,4-diamine **(44)** and acryloyl chloride. 11%, HPLC analysis: retention time = 3.027 min, 95.9% purity. ^{1}H NMR (500 MHz, DMSO-d_6) **δ** 10.03 (s, 1H), 9.24 (s, 1H), 8.58 (s, 1H), 8.13 (s, 1H), 8.00 (s, 1H), 7.92 (d, *J* = 3.4 Hz, 1H), 7.75 (s, 1H), 7.49 (d, *J* = 5.3 Hz, 1H), 7.06 (dd, *J* = 5.5, 1.1 Hz, 1H), 6.95 (s, 1H), 6.32 (dd, *J* = 10.2, 6.1 Hz, 1H), 6.17 (d, *J* = 3.4 Hz, 1H), 6.13 (d, *J* = 10.1 Hz, 1H), 5.67 (d, *J* = 5.9 Hz, 1H), 4.06 (s, 3H), 3.79 (s, 3H), 2.68 (s, 3H), 2.59 (tt, *J* = 2.6, 1.0 Hz, 2H), 2.32 (p, *J* = 1.1 Hz, 2H), 2.17 (s, 6H). ^{13}C NMR (125 MHz, DMSO-d_6) **δ** 161.19, 160.52, 156.26, 149.28, 137.77, 132.67, 130.18, 125.30, 120.74, 117.82, 104.55, 99.45, 56.31, 45.56, 42.94, 40.58, 40.42, 40.26. LCQTOF for $C_{27}H_{33}N_9O_2$ $[M+H]^+$, Calcd: 516.2830, found: 516.2814.

N^2-[4-((dimethylamino)ethyl)-2-methoxy-5-(*N*-but-2-ynamide)phenyl]-*N*^{4}-(2-methyl-2H-indazol-6-yl)pyrimidine-2,4-diamine **(78)**, Following the general procedure using *N*^{2}-[5-amino-4-((dimethylamino)ethyl)-2-methoxyphenyl]-*N*^{4}-(2-methyl-2H-indazol-6-yl)pyrimidine-2,4-diamine **(44)** and but-2-ynoic acid. 9%, HPLC analysis: retention time = 2.567 min, 97.9% purity. ^{1}H NMR (500 MHz, DMSO-d_6) **δ** 9.35 (s, 1H), 8.21 (s, 1H), 8.19 (s, 1H), 7.93 (d, *J* = 3.4 Hz), 7.61 (s, 1H), 7.60 – 7.57 (m, 1H), 7.44 (s, 1H), 7.00 (dd, *J* = 5.4, 1.3 Hz, 1H), 6.71 (s, 1H), 6.20 (d, *J* = 3.4 Hz, 1H), 4.09 (s, 3H), 3.72 (s, 3H), 2.83 (t, *J* = 4.0 Hz, 2H), 2.55 (s, 3H), 2.36 (t, *J* = 3.9 Hz, 2H), 2.17 (s, 6H). ^{13}C NMR (125 MHz, DMSO-d_6) **δ** 174.91, 161.16, 160.43, 156.23, 149.29, 137.82, 130.18, 124.90, 120.81, 118.27, 117.75, 105.73, 99.57, 76.64, 56.35, 44.83, 29.09, 22.62, 14.48, 3.49. LCQTOF for $C_{28}H_{33}N_9O_2$ $[M+H]^+$, Calcd: 528.2835, found: 528.2802.

5-chloro-*N*^{2}-[4-((dimethylamino)ethyl)-2-methoxy-5-(*N*-propanamide)phenyl]-*N*^{4}-(2-methyl-2H-indazol-6-yl)pyrimidine-2,4-diamine **(79),** Following the general procedure using *N*^{2}-[5-amino-4-((dimethylamino)ethyl)-2-methoxyphenyl]-5-chloro-*N*^{4}-(2-methyl-2H-indazol-6-yl)pyrimidine-2,4-diamine **(47)** and propionyl chloride. 16%, HPLC analysis: retention time = 2.600 min, 97.0% purity. ^{1}H NMR (500 MHz, DMSO-d_6) **δ** 9.65 (s, 1H), 8.57 (s, 1H), 8.17 (s, 1H), 8.06 (s, 1H), 8.02 (s, 1H), 7.86 (s, 1H), 7.47 (d, *J* = 5.3 Hz, 1H), 7.24 (dd, *J* = 5.4, 1.3 Hz, 1H), 6.90 (s, 1H), 5.72 (s, 1H), 4.08 (s, 3H), 3.74 (s, 3H), 2.64 (s, 3H), 2.49 (q, *J* = 1.1 Hz, 2H), 2.43 (p, *J* = 1.1 Hz, 2H), 2.25 – 2.15 (m, 8H), 0.99 (t, *J* = 4.6 Hz, 3H). ^{13}C NMR (125 MHz, DMSO-d_6) **δ** 171.72, 159.16, 156.17, 154.93, 148.92, 140.07, 136.51, 127.59,

This material is reserved for educational use only, not allowed for commercial use.
Forbidden to modify the content, and cite the document when use.

124.71, 120.13, 119.18 (d, *J* = 100.0 Hz), 118.19, 107.58, 105.80, 104.29, 57.24, 56.16, 45.67, 42.81, 29.89, 10.29. LCQTOF for $C_{27}H_{34}ClN_9O_2$ $[M+H]^+$, Calcd: 552.2596, found: 552.2555.

5-chloro-N^2-[4-((dimethylamino)ethyl)-2-methoxy-5-(*N*-acrylamide)phenyl]-N^4-(2-methyl-2H-indazol-6-yl)pyrimidine-2,4-diamine **(80),** Following the general procedure using N^2-[5-amino-4-((dimethylamino)ethyl)-2-methoxyphenyl]-5-chloro-N^4-(2-methyl-2H-indazol-6-yl)pyrimidine-2,4-diamine **(47)** and acryloyl chloride. 24%, HPLC analysis: retention time = 2.533 min, 98.7% purity. ^{1}H NMR (500 MHz, DMSO-d_6) **δ** 9.93 (s, 1H), 8.61 (s, 1H), 8.16 (s, 1H), 8.05 (s, 1H), 8.04 (s, 1H), 7.85 (s, 1H), 7.47 (d, *J* = 5.4 Hz, 1H), 7.24 (d, *J* = 5.4 Hz, 1H), 6.92 (s, 1H), 6.38 (s, 1H), 6.15 (d, *J* = 10.3 Hz, 1H), 5.72 (s, 1H), 5.69 (d, *J* = 6.6 Hz, 1H), 4.08 (s, 3H), 3.77 (s, 3H), 3.04 – 2.84 (m, 2H), 2.63 (s, 3H), 2.27 (s, 6H). ^{13}C NMR (125 MHz, DMSO-d_6) **δ** 159.03, 156.24, 154.92, 149.07, 148.89, 140.46, 136.48, 132.59, 126.71, 124.79, 124.6, 120.20, 119.41, 119.05, 107.76, 105.69, 104.42, 56.23, 44.88, 42.97, 40.51, 40.43, 40.26. LCQTOF for $C_{27}H_{32}ClN_9O_2$ $[M+H]^+$, Calcd: 550.2440, found: 550.2409.

5-chloro-N^2-[4-((dimethylamino)ethyl)-2-methoxy-5-(*N*-but-2-ynamide)phenyl]-N^4-(2-methyl-2H-indazol-6-yl)pyrimidine-2,4-diamine (81), Following the general procedure using N^2-[5-amino-4-((dimethylamino)ethyl)-2-methoxyphenyl]-5-chloro-N^4-(2-methyl-2H-indazol-6-yl)pyrimidine-2,4-diamine (47) and but-2-ynoic acid. 18%, HPLC analysis: retention time = 2.607 min, 96.1% purity. ^{1}H NMR (500 MHz, DMSO-d_6) **δ** 8.59 (s, 1H), 8.19 (d, *J* = 11.0 Hz, 2H), 8.07 (s, 1H), 8.03 (s, 1H), 7.85 (s, 1H), 7.49 (d, *J* = 5.3 Hz, 1H), 7.24 – 7.22 (m, 1H), 6.94 (s, 1H), 4.09 (s, 3H), 3.75 (s, 3H), 2.66 (s, 3H), 2.50 – 2.49 (m, 2H), 2.44 – 2.43 (m, 2H), 2.21 (s, 2H), 2.00 (s, 2H). ^{13}C NMR (125 MHz, DMSO-d_6) **δ** 159.06, 156.21, 154.93, 150.79, 149.27, 148.90, 140.16, 136.50, 124.78, 120.19, 119.35, 119.03, 107.59, 106.23, 104.40, 83.49, 76.75, 56.94, 56.20, 45.36, 42.96, 3.67. LCQTOF for $C_{28}H_{32}ClN_9O_2$ $[M+H]^+$, Calcd: 562.2440, found: 562.2406.

This material is reserved for educational use only, not allowed for commercial use.

Forbidden to modify the content, and cite the document when use.

Appendix B: Chemical characterization spectra

Characterization spectra for compounds 15, 17, 20, 21, 22, 23, and 27 on study 1.

The ^{1}H-NMR, ^{13}C-NMR, MS, and HPLC UV data for the most potent exemplars are shown for the purpose of illustration.

15:5-chloro-*N*^{2}-(1-[4-(4-amino-3-methoxyphenyl)piperazin-1-yl]ethan-1-one)-*N*^{4}-(*N*-(3-aminophenyl)2-chloroacetamide)pyrimidine-2,4-diamine.

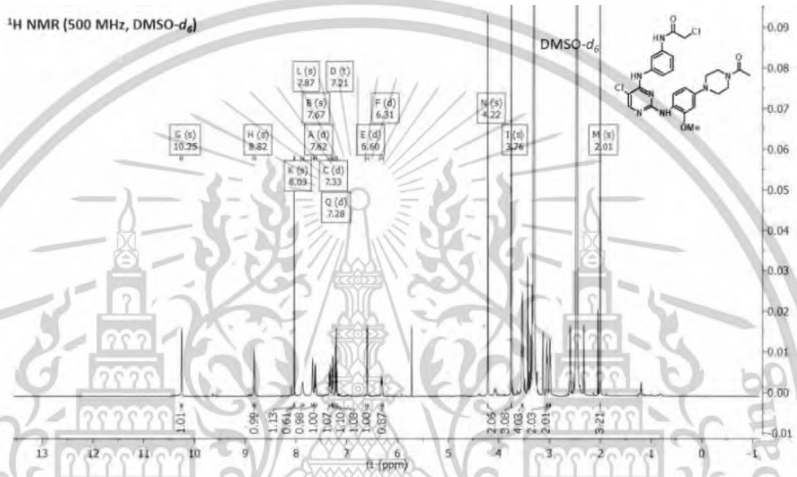

^{1}H NMR spectra of compound **15**.

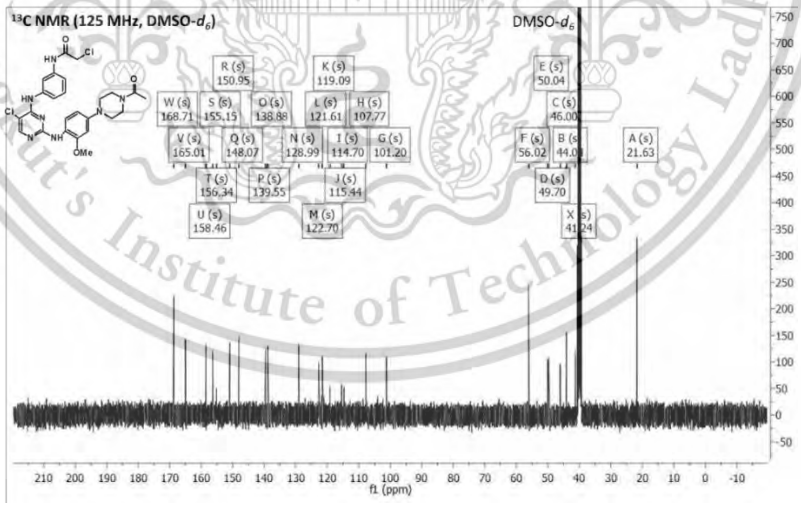

^{13}C NMR spectra of compound **15**.

This material is reserved for educational use only, not allowed for commercial use.
Forbidden to modify the content, and cite the document when use.

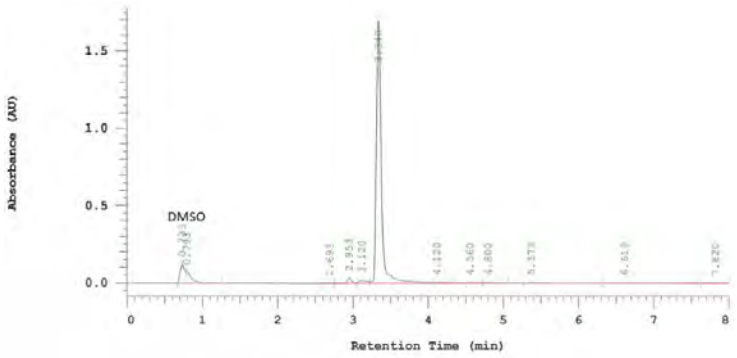

HPLC spectra of compound **15**.

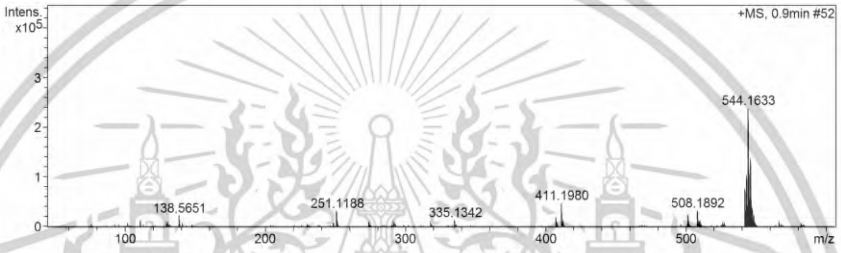

Meas. m/z	#	Ion Formula	m/z	err [mDa]	mSigma	# Sigma	Score	rdb	e⁻ Conf	N-Rule
544.1633	1	C25H28Cl2N7O3	544.1625	-0.8	82.0	1	100.00	14.5	even	ok
	1	C25H28Cl2N7O3	544.1625	-0.8	82.0	1	100.00	14.5	even	ok

HRMS spectra of compound **15.**

17:5-chloro-N^2-(1-[4-(4-aminophenyl)piperazin-1-yl]ethan-1-one)-N^4-(*N*-(3-aminophenyl)acrylamide)pyrimidine-2,4-diamine.

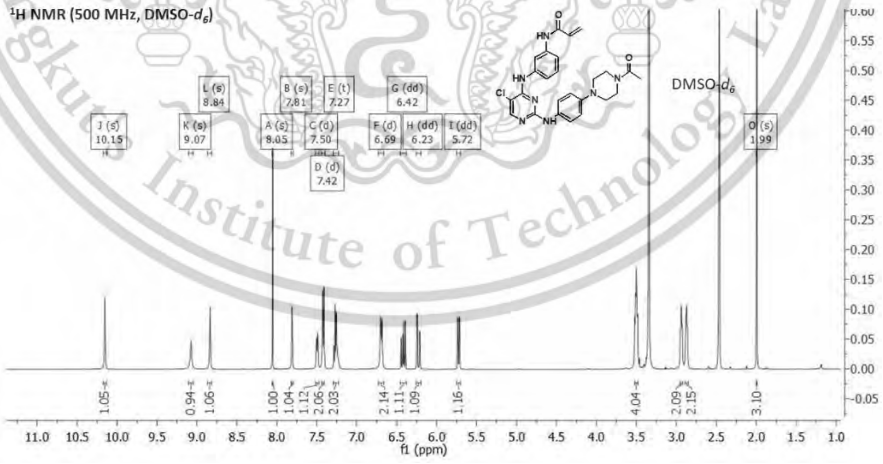

^{1}H NMR spectra of compound **17**.

This material is reserved for educational use only, not allowed for commercial use.
Forbidden to modify the content, and cite the document when use.

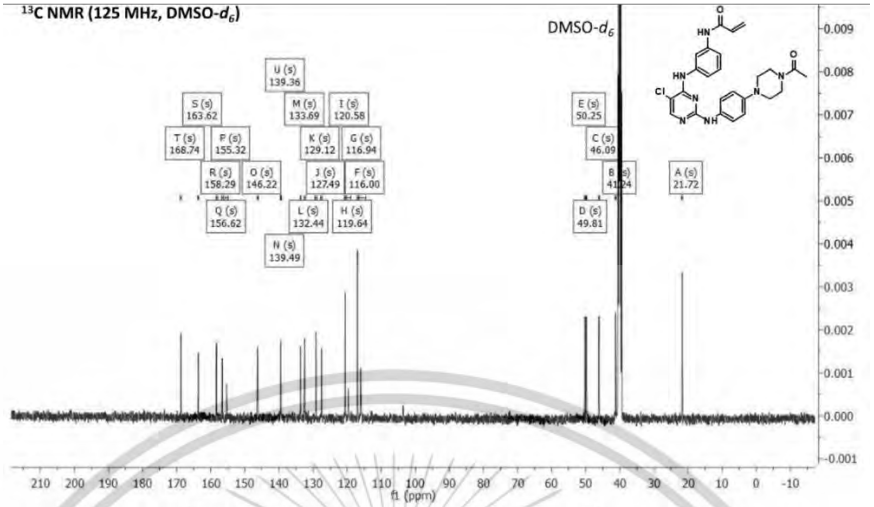

^{13}C NMR spectra of compound **17**.

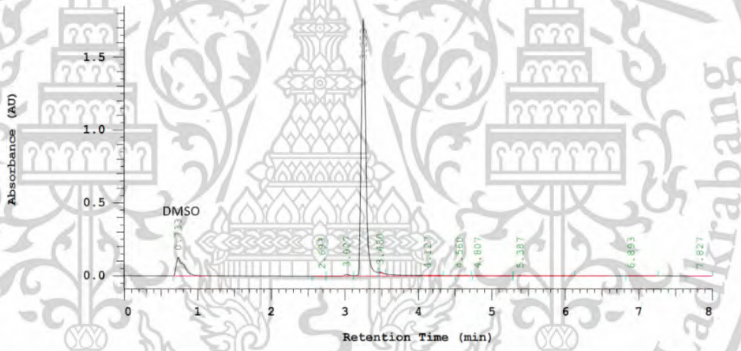

HPLC spectra of compound **17.**

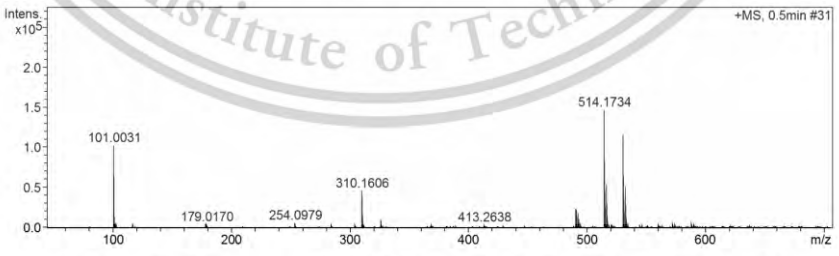

Meas. m/z	#	Ion Formula	m/z	err [mDa]	mSigma	# Sigma	Score	rdb	e¯ Conf	N-Rule
490.1742	1	C23H26ClN7NaO2	490.1729	1.3	385.2	1	100.00	13.5	even	ok
514.1734	1	C25H26ClN7NaO2	514.1729	0.5	6.8	1	100.00	15.5	even	ok

HRMS spectra of compound **17.**

This material is reserved for educational use only, not allowed for commercial use.
Forbidden to modify the content, and cite the document when use.

20:5-chloro-N^2-(1-methyl-1H-pyrazol-4-yl)-N^4-(*N*-(3-aminophenyl)propanamide)pyrimidine-2,4-diamine.

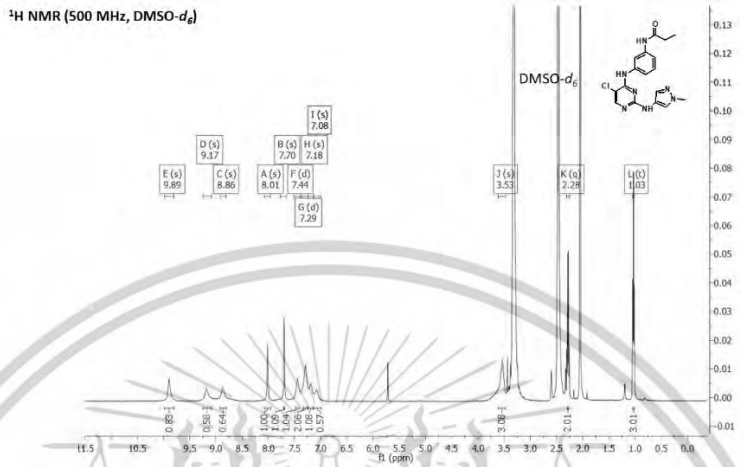

^{1}H NMR spectra of compound **20**.

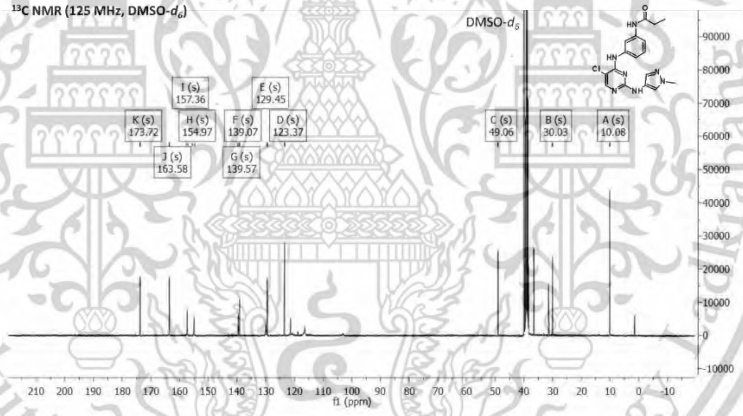

^{13}C NMR spectra of compound **20**.

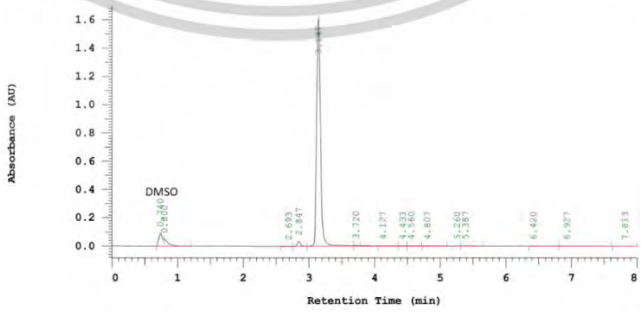

HPLC spectra of compound **20.**

This material is reserved for educational use only, not allowed for commercial use.
Forbidden to modify the content, and cite the document when use.

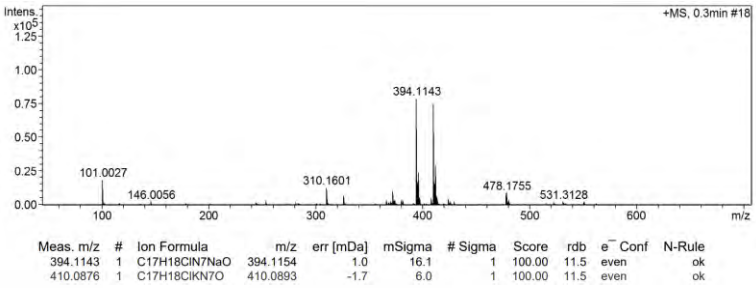

Meas. m/z	#	Ion Formula	m/z	err [mDa]	mSigma	# Sigma	Score	rdb	e⁻ Conf	N-Rule
394.1143	1	C17H18ClN7NaO	394.1154	1.0	16.1	1	100.00	11.5	even	ok
410.0876	1	C17H18ClKN7O	410.0893	-1.7	6.0	1	100.00	11.5	even	ok

HRMS spectra of compound **20.**

21: 5-chloro-*N*^{2}-(1-methyl-1H-pyrazol-4-yl)-*N*^{4}-(*N*-(3-aminophenyl)acrylamide)pyrimidine-2,4-diamine.

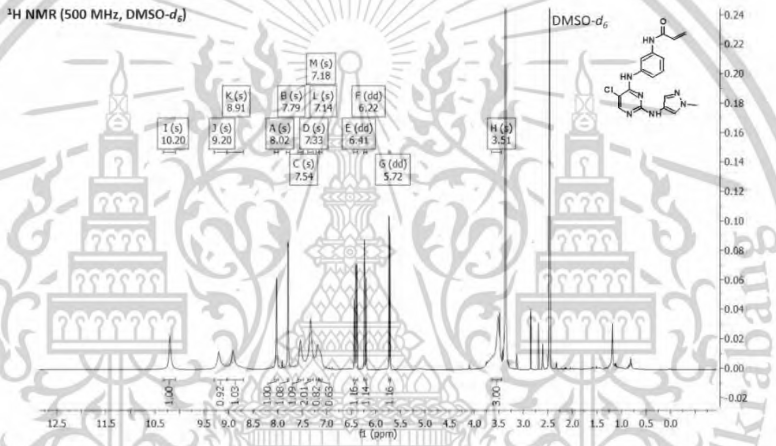

^{1}H NMR spectra of compound **21**.

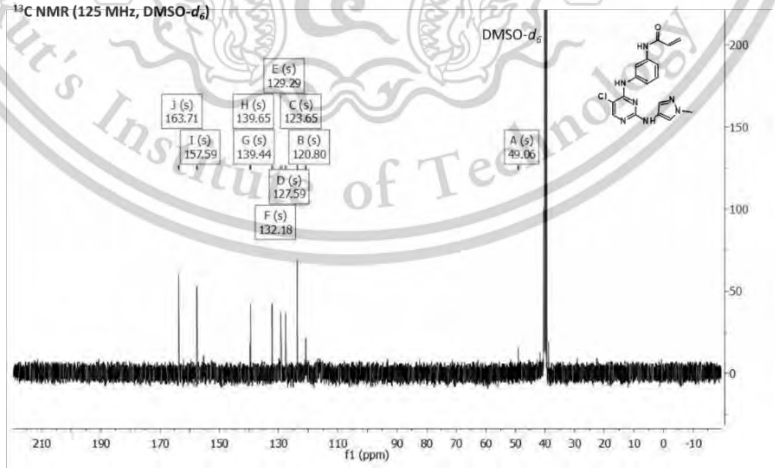

^{13}C NMR spectra of compound **21**.

This material is reserved for educational use only, not allowed for commercial use.
Forbidden to modify the content, and cite the document when use.

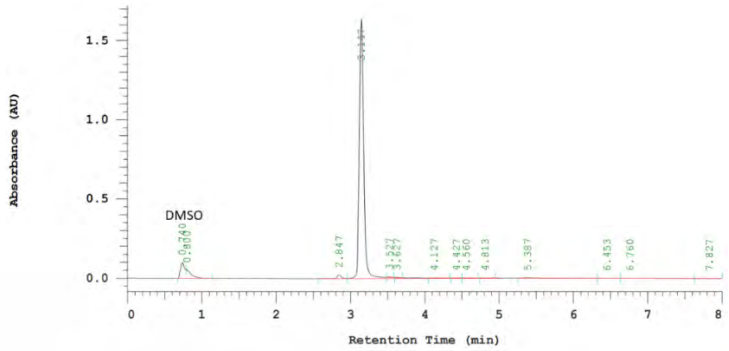

HPLC spectra of compound **21.**

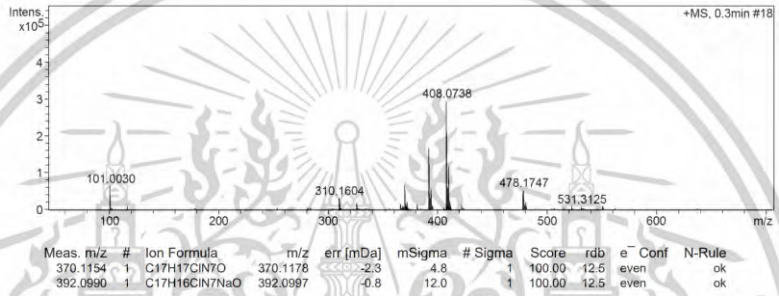

Meas. m/z	#	Ion Formula	m/z	err [mDa]	mSigma	# Sigma	Score	rdb	e⁻ Conf	N-Rule
370.1154	1	C17H17ClN7O	370.1178	-2.3	4.8	1	100.00	12.5	even	ok
392.0990	1	C17H16ClN7NaO	392.0997	-0.8	12.0	1	100.00	12.5	even	ok

HRMS spectra of compound **21.**

22: 5-chloro-*N*^{2}-(1-methyl-1H-pyrazol-4-yl)-*N*^{4}-((2E)-*N*-(3-aminophenyl)-3-phenylprop-2-enamide)pyrimidine-2,4-diamine.

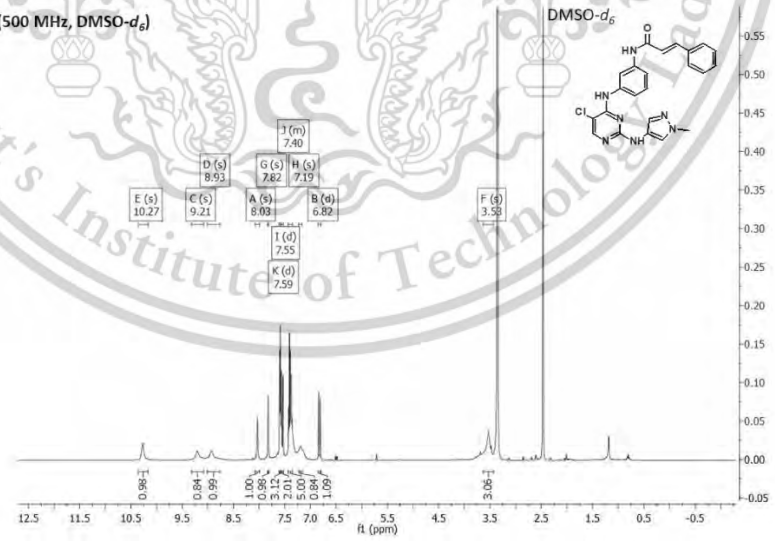

^{1}H NMR spectra of compound **22**.

This material is reserved for educational use only, not allowed for commercial use.
Forbidden to modify the content, and cite the document when use.

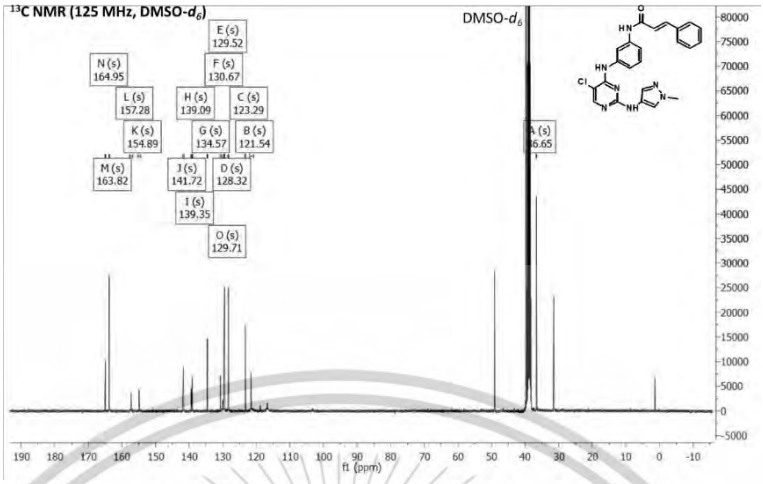

^{13}C NMR spectra of compound **22**.

HPLC spectra of compound **22.**

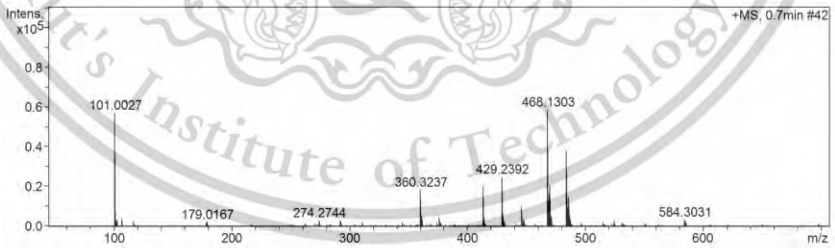

Meas. m/z	#	Ion Formula	m/z	err [mDa]	mSigma	# Sigma	Score	rdb	e⁻ Conf	N-Rule
468.1303	1	C23H20ClN7NaO	468.1310	0.7	3.3	1	100.00	16.5	even	ok
484.1041	1	C23H20ClKN7O	484.1049	0.9	13.3	1	100.00	16.5	even	ok

HRMS spectra of compound **22.**

This material is reserved for educational use only, not allowed for commercial use.
Forbidden to modify the content, and cite the document when use.

23: 5-chloro-N^2-(1-methyl-1H-pyrazol-4-yl)-N^4-(*N*-(3-aminophenyl)-2-chloroacetamide)pyrimidine-2,4-diamine.

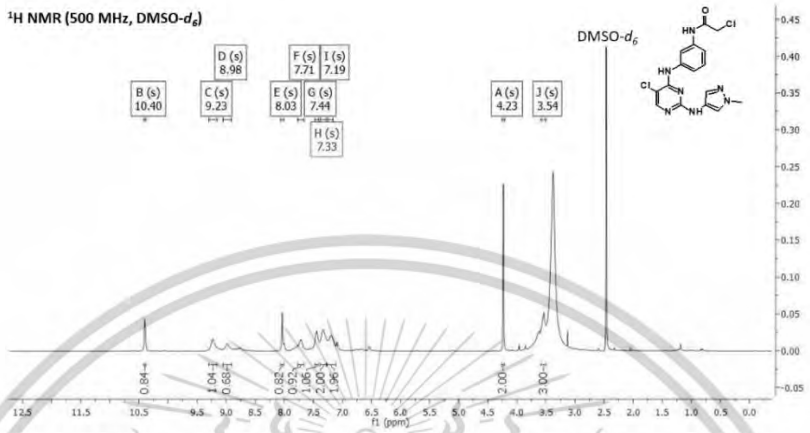

^{1}H NMR spectra of compound **23**.

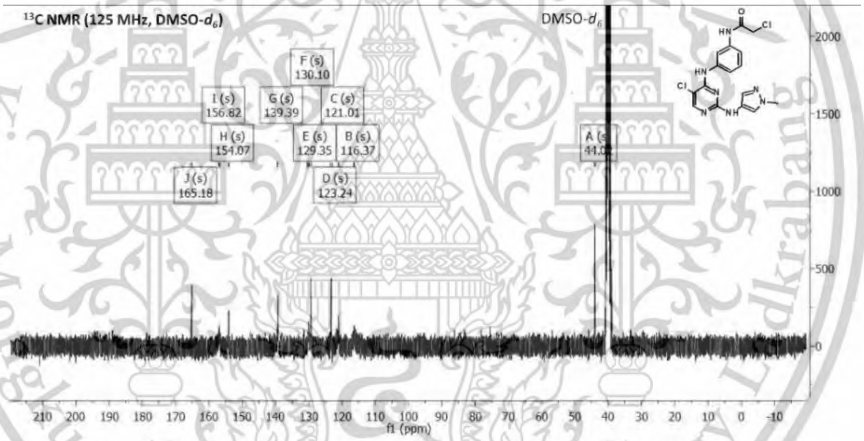

^{13}C NMR spectra of compound **23**.

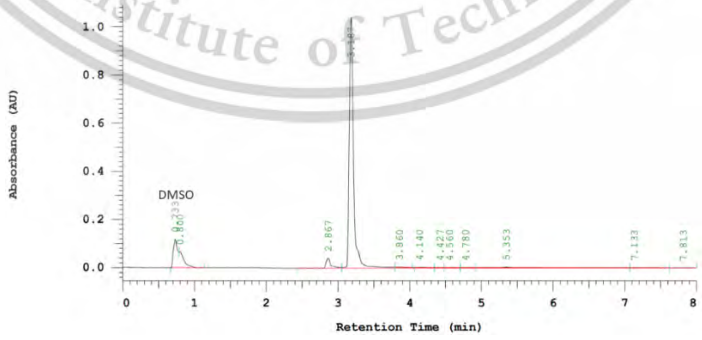

HPLC spectra of compound **23.**

This material is reserved for educational use only, not allowed for commercial use.
Forbidden to modify the content, and cite the document when use.

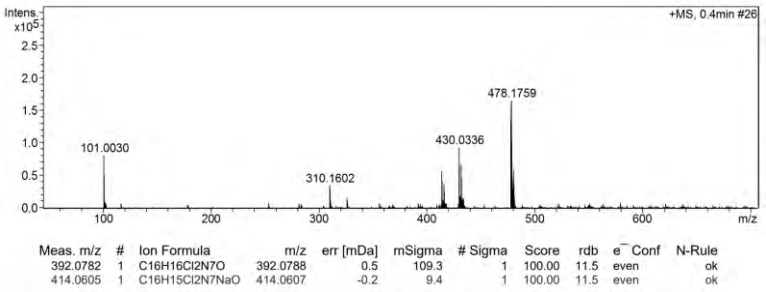

Meas. m/z	#	Ion Formula	m/z	err [mDa]	mSigma	# Sigma	Score	rdb	e⁻ Conf	N-Rule
392.0782	1	C16H16Cl2N7O	392.0788	0.5	109.3	1	100.00	11.5	even	ok
414.0605	1	C16H15Cl2N7NaO	414.0607	-0.2	9.4	1	100.00	11.5	even	ok

HRMS spectra of compound **23.**

27: 5-chloro-N^2-(6-amino-1,3-benzoxazol-2(3H)-one)-N^4-(*N*-(3-aminophenyl)-2-chloroacetamide)pyrimidine-2,4-diamine.

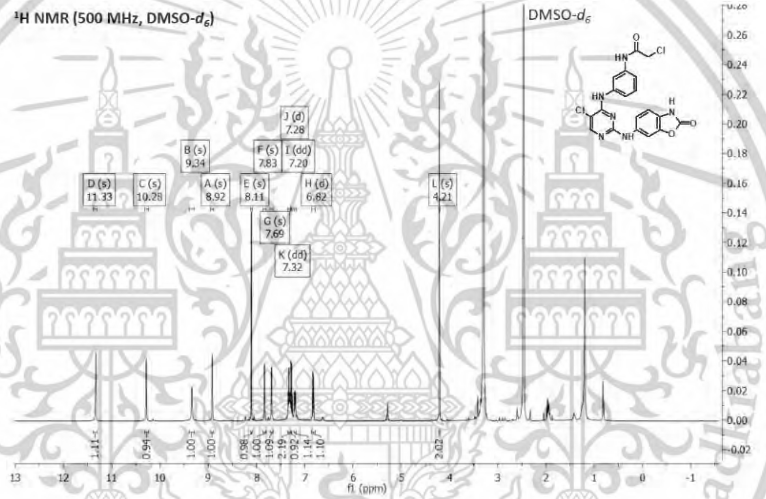

^{1}H NMR spectra of compound **27**.

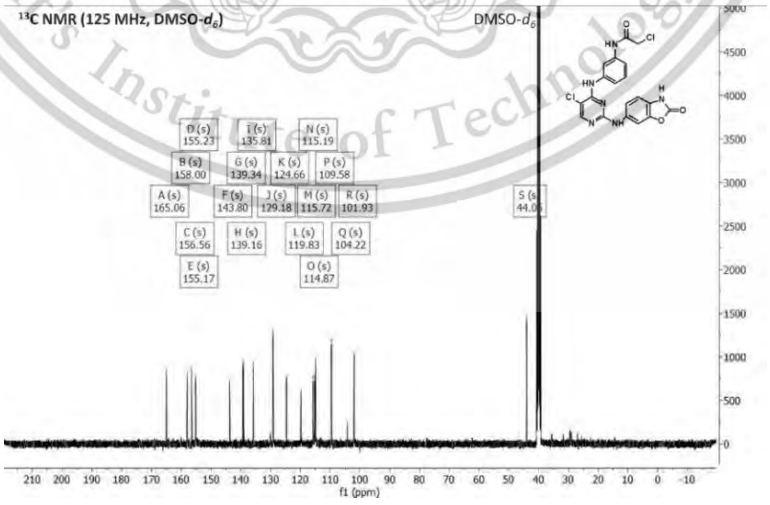

^{13}C NMR spectra of compound **27**.

This material is reserved for educational use only, not allowed for commercial use.
Forbidden to modify the content, and cite the document when use.

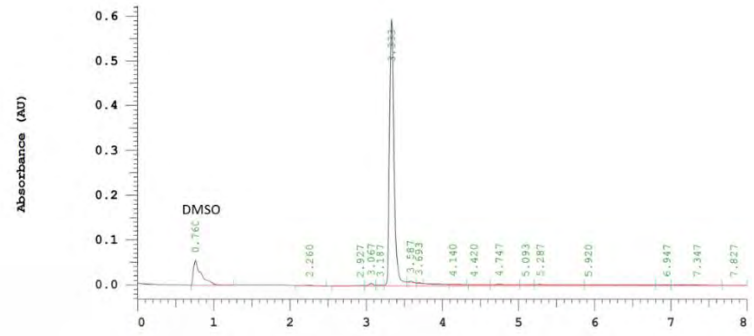

HPLC spectra of compound **27.**

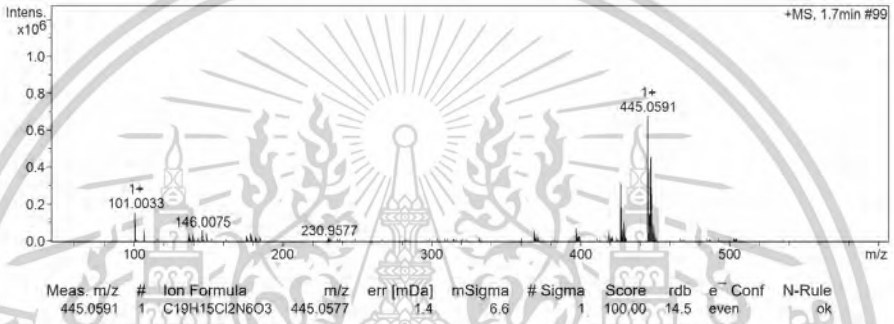

HRMS spectra of compound **27.**

This material is reserved for educational use only, not allowed for commercial use.
Forbidden to modify the content, and cite the document when use.

Characterization spectra for compounds 48, 49, 51, 52, 79, and 80 on study 2. The ^{1}H-NMR, ^{13}C-NMR, MS, and HPLC UV data for the most potent exemplars are shown for the purpose of illustration.

48: *N*^{2}-[3-*N*-benzylpropanamide]-*N*^{4}-(2-methyl-2H-indazol-6-yl)pyrimidine-2,4-diamine.

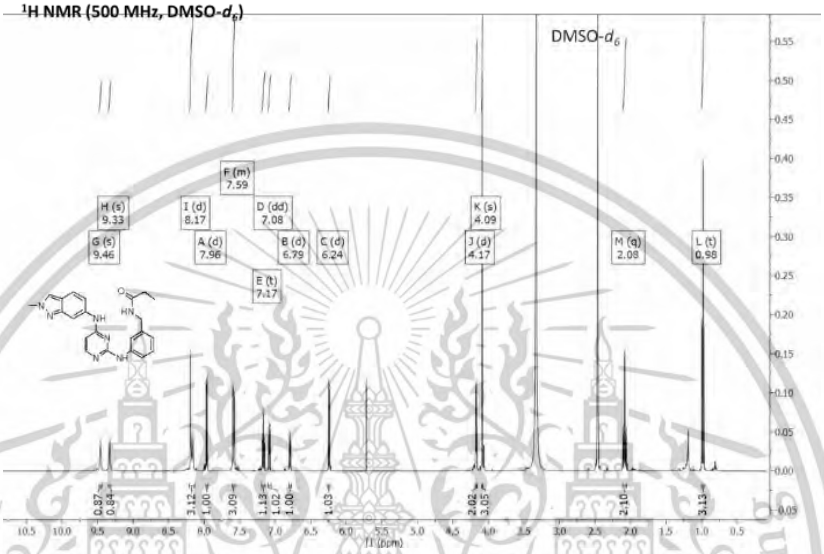

^{1}H NMR spectra of compound **48.**

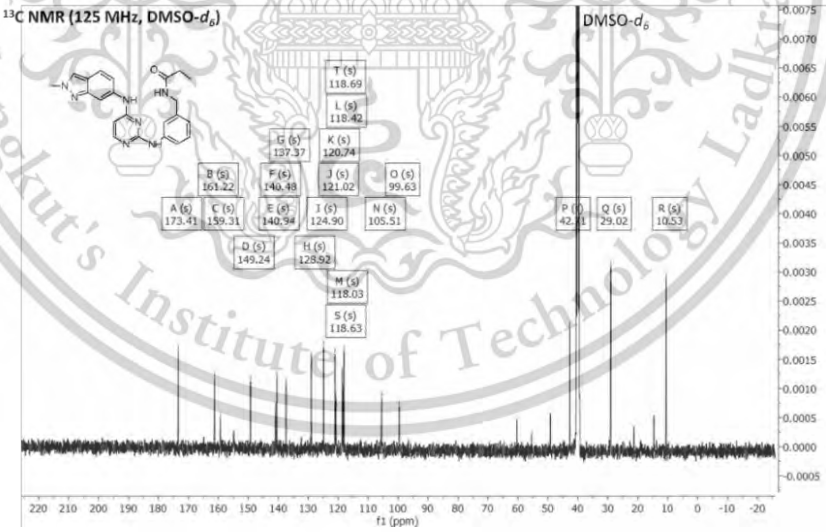

^{13}C NMR spectra of compound **48**.

This material is reserved for educational use only, not allowed for commercial use.
Forbidden to modify the content, and cite the document when use.

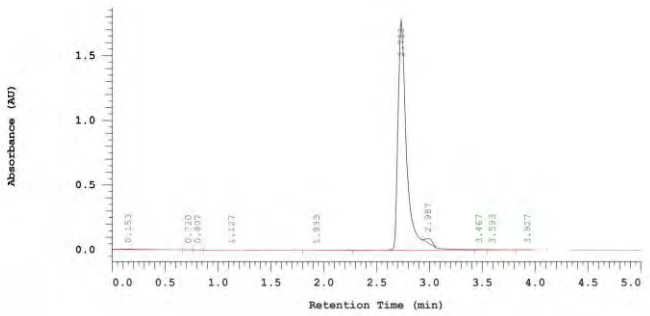

HPLC spectra of compound **48**.

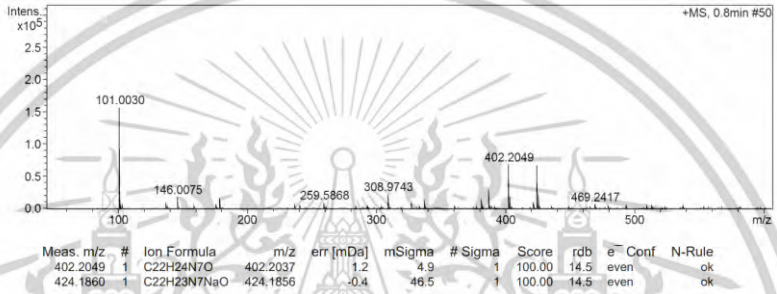

Meas. m/z	#	Ion Formula	m/z	err [mDa]	mSigma	# Sigma	Score	rdb	e⁻ Conf	N-Rule
402.2049	1	C22H24N7O	402.2037	1.2	4.9	1	100.00	14.5	even	ok
424.1860	1	C22H23N7NaO	424.1856	-0.4	46.5	1	100.00	14.5	even	ok

HRMS spectra of compound **48**.

49: N^2-[3-*N*-acrylamidebenzyl]-N^4-(2-methyl-2H-indazol-6-yl)pyrimidine-2,4-diamine.

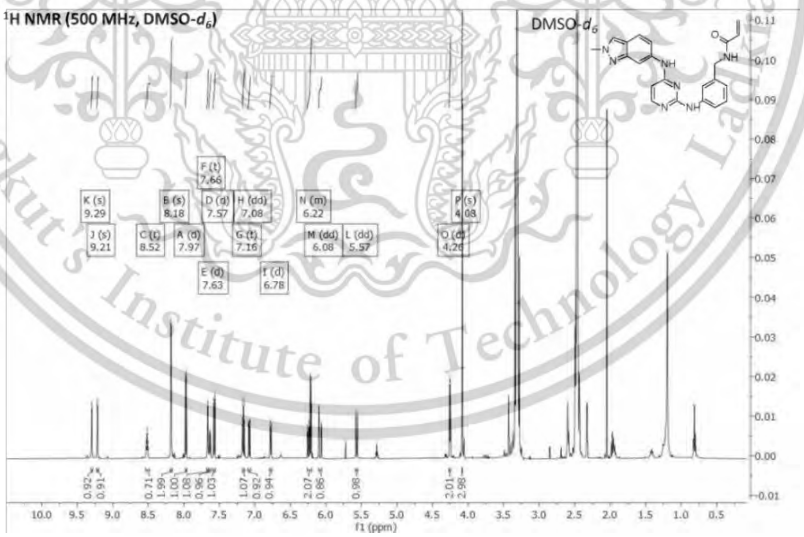

^{1}H NMR spectra of compound **49**.

This material is reserved for educational use only, not allowed for commercial use.
Forbidden to modify the content, and cite the document when use.

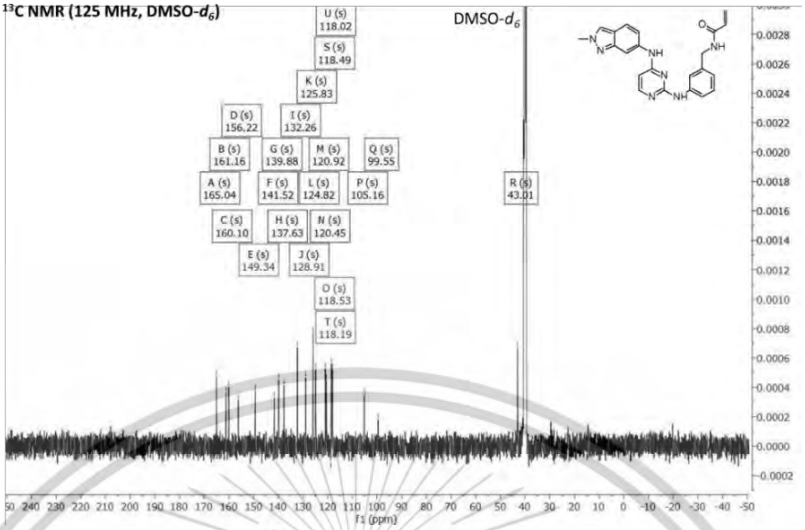

^{13}C NMR spectra of compound **49**.

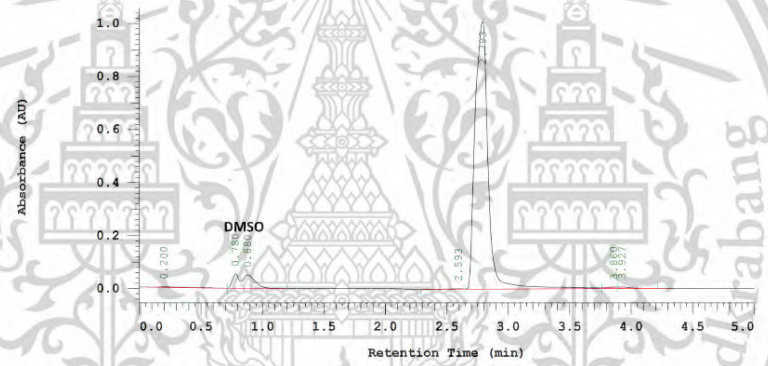

HPLC spectra of compound **49.**

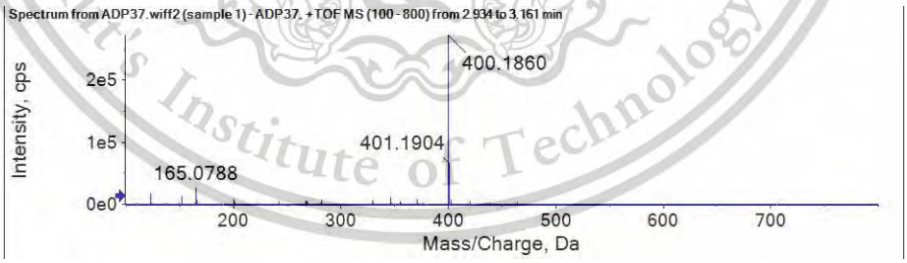

LCQTOF spectra of compound **49**.

This material is reserved for educational use only, not allowed for commercial use.
Forbidden to modify the content, and cite the document when use.

51:N^2-[3-*N*-benzyl-2-chloroacetamide]-N^4-(2-methyl-2H-indazol-6-yl)pyrimidine-2,4 diamine.

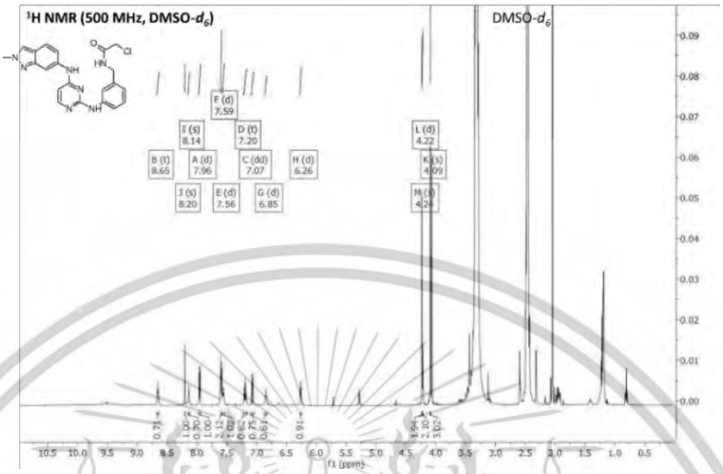

^{1}H NMR spectra of compound **51**.

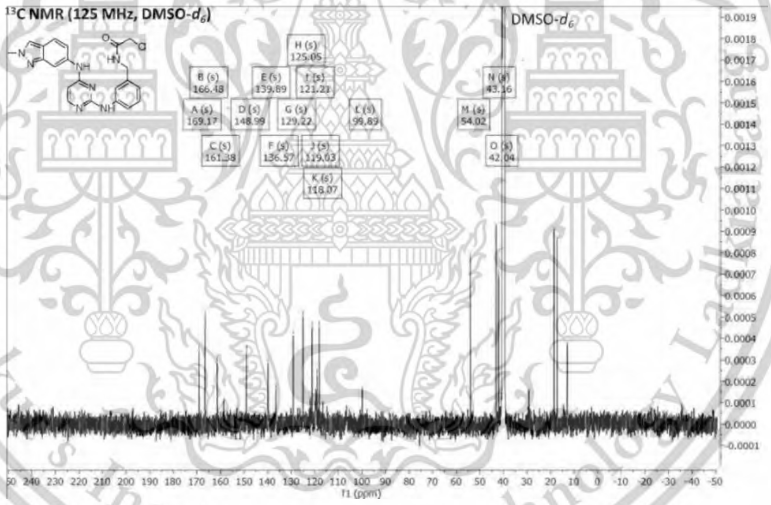

^{13}C NMR spectra of compound **51.**

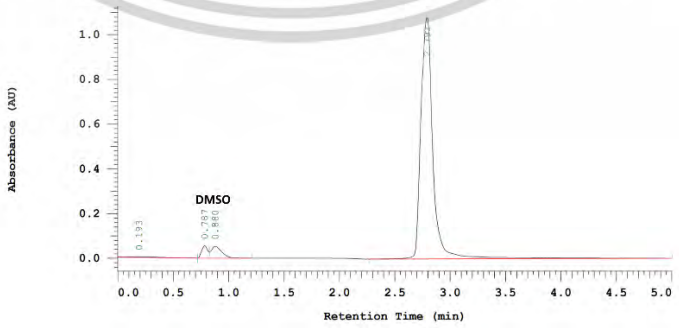

HPLC spectra of compound **51.**

This material is reserved for educational use only, not allowed for commercial use.
Forbidden to modify the content, and cite the document when use.

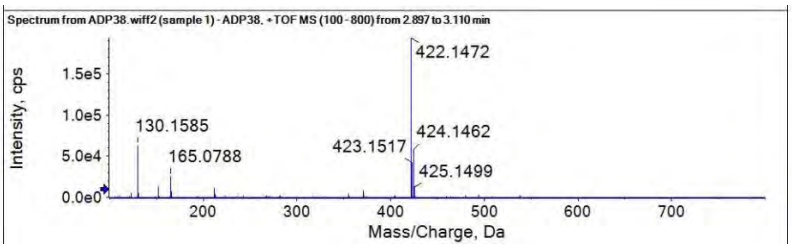

LCQTOF spectra of compound **51.**

52: N^2-[3-N-benzylbut-2-ynamide]-N^4-(2-methyl-2H-indazol-6-yl)pyrimidine-2,4-diamine.

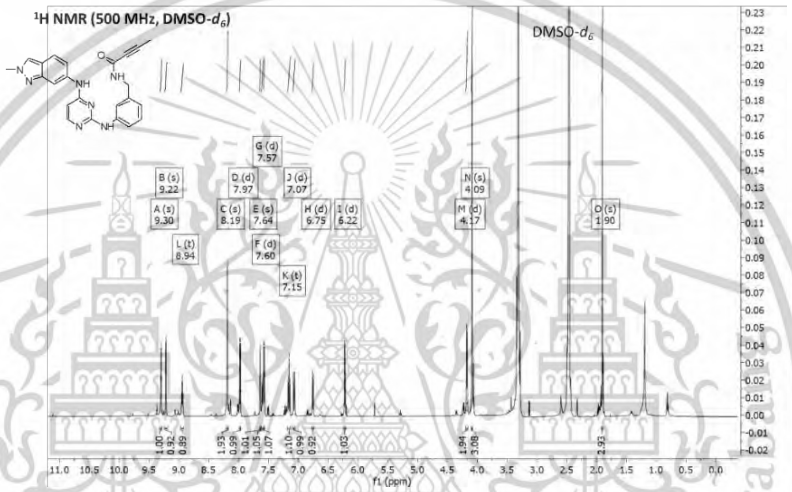

^{1}H NMR spectra of compound **52.**

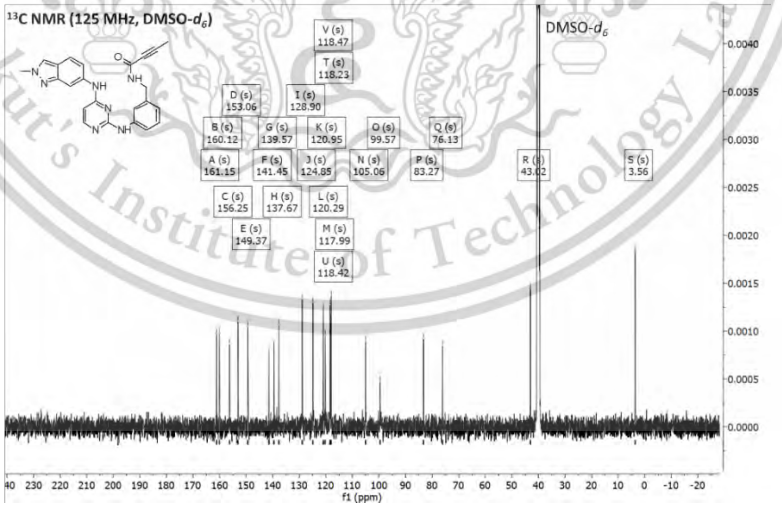

^{13}C NMR spectra of compound **52**.

This material is reserved for educational use only, not allowed for commercial use.
Forbidden to modify the content, and cite the document when use.

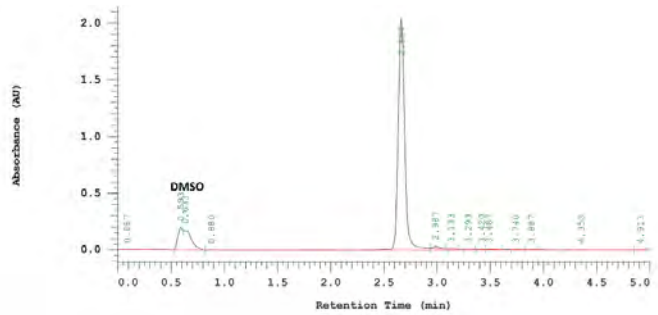

HPLC spectra of compound **52.**

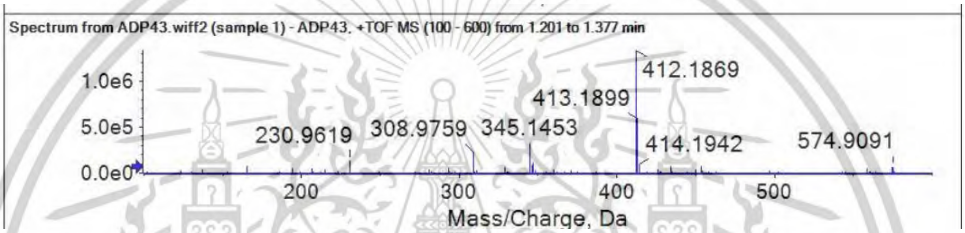

LCQTOF spectra of compound **52.**

79: 5-chloro-N^2-[4-((dimethylamino)ethyl)-2-methoxy-5-(*N*-propanamide)phenyl]-N^4-(2-methyl-2H-indazol-6-yl)pyrimidine-2,4-diamine.

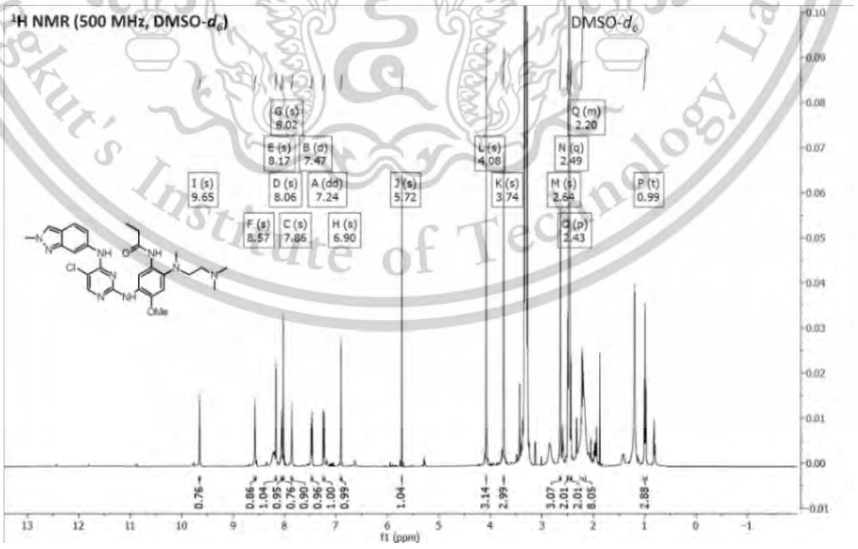

^{1}H NMR spectra of compound **79.**

This material is reserved for educational use only, not allowed for commercial use.
Forbidden to modify the content, and cite the document when use.

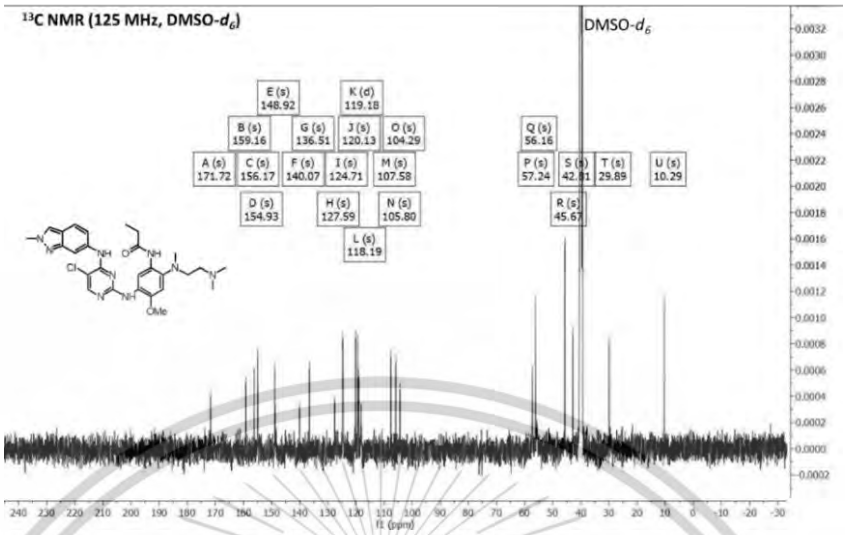

^{13}C NMR spectra of compound **79.**

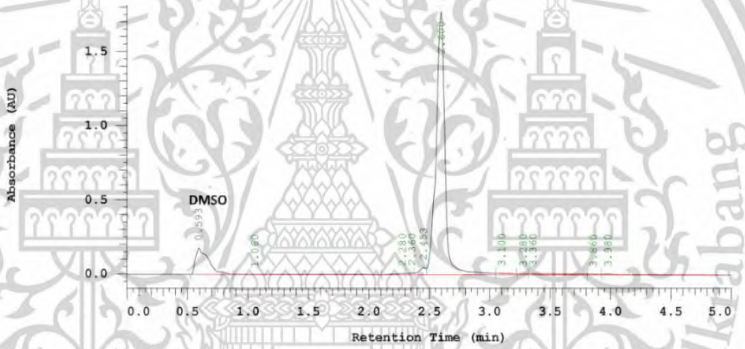

HPLC spectra of compound **79.**

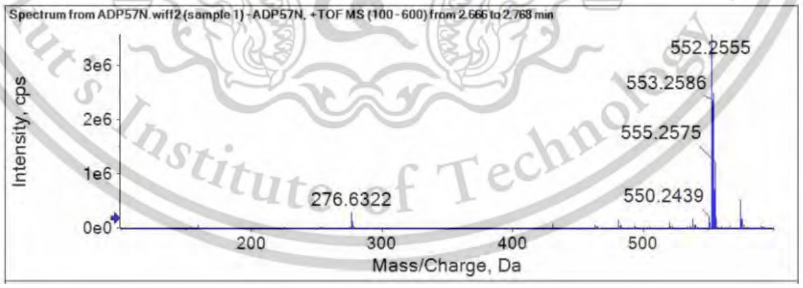

LCQTOF spectra of compound **79.**

This material is reserved for educational use only, not allowed for commercial use.
Forbidden to modify the content, and cite the document when use.

80: 5-chloro-*N*^{2}-[4-((dimethylamino)ethyl)-2-methoxy-5-(*N*-acrylamide)phenyl]-*N*^{4}-(2-methyl-2H-indazol-6-yl)pyrimidine-2,4-diamine.

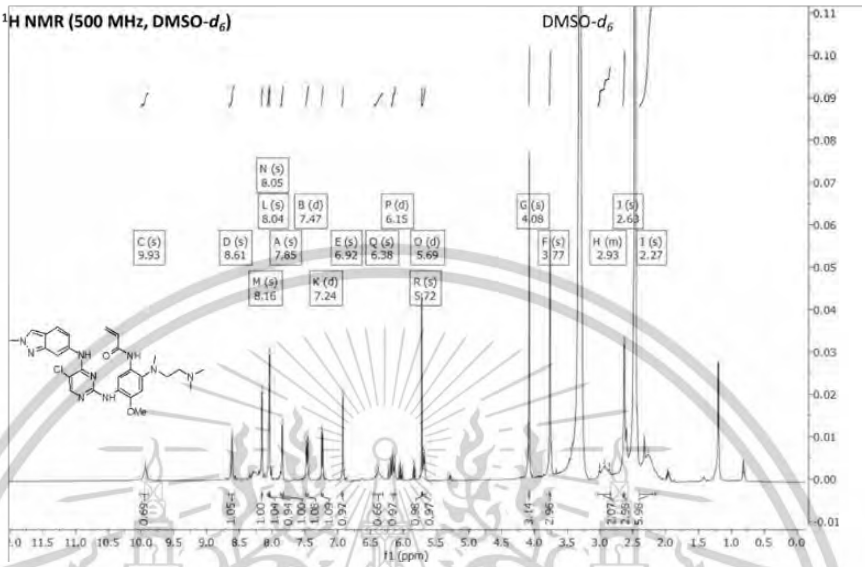

^{1}H NMR spectra of compound **80**.

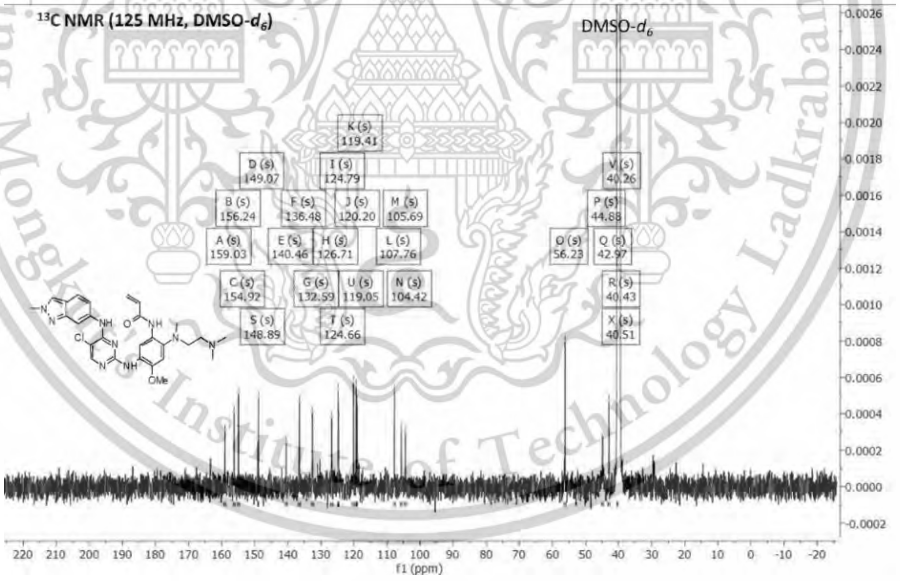

^{13}C NMR spectra of compound **80.**

This material is reserved for educational use only, not allowed for commercial use.
Forbidden to modify the content, and cite the document when use.

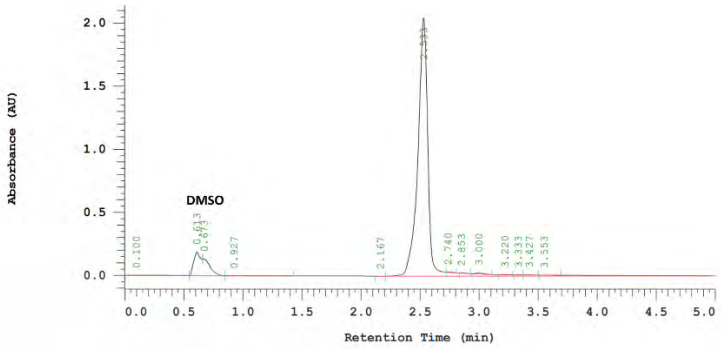

HPLC spectra of compound **80.**

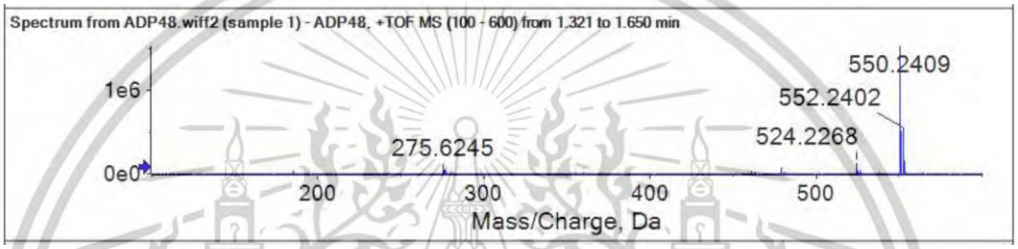

LCQTOF spectra of compound **80.**

This material is reserved for educational use only, not allowed for commercial use.
Forbidden to modify the content, and cite the document when use.